Layer-by-layer assembly of organic films and their application to multichannel surface plasmon resonance sensing

Marco Palumbo, Dott

Layer-by-layer assembly of organic films and their application to multichannel surface plasmon resonance sensing

by

Marco Palumbo, Dott. Ing.

Ustinov College

A thesis submitted in partial fulfilment

of the requirements for the degree of PhD

School of Engineering and Centre for Molecular and Nanoscale Electronics

University of Durham

19 March 2004

Declaration

I hereby declare that the work carried out in this thesis has not been previously submitted for any degree and is not currently being submitted in candidature for any other degree.

Signed.....
Candidate

The work of this thesis was carried out by the candidate.

Signed.....
Director of Studies

Signed.....
Candidate

...this is not a banana.

Shilpa V., Bombay

This thesis is dedicated to Raffaele, Lena, Alessandro and Giampiero.

Acknowledgments

The work carried out in this thesis has been possible because of the help and assistance of many people. Without them, most probably this project would not have been completed at all. To my supervisor, Prof. Michael C. Petty, I am profoundly indebted. My research has greatly benefited from his dedication and accuracy. It has been a long way to walk, but surely a rewarding one. To Dr. Jürgen Nagel in Dresden goes my gratitude for introducing me to the fascinating world of polyelectrolytes and for the developing of a data acquisition program. Moreover, his support in the discussion over the results obtained is also acknowledged. Dr. Christopher Pearson has endured with my inexperience with some of the experimental techniques used for this work and has contributed to the atomic force microscope characterization of the polymeric films. Towards the Mechanical and Electronic Workshop of the School of Engineering I have a big obligation for all the effort they have put in realizing various "bits and pieces" needed for the realization of my project. Finally, thanks to Prof. Ludovico Valli and Dr. Roberto Rella in Lecce and Dr. Ritu Kataky in Durham for some useful discussions. Ultimately however, I take full responsibility for the content, and mistakes, of this thesis.

To all the colleagues and friends of the Centre for Molecular and Nanoscale Electronics goes my gratitude for the stimulating and excellent working atmosphere they have been able to build in these years. Notably, one of the best parts of my PhD course has to be the numerous and heterogeneous group of friends I have met in Durham. The list of their names would be almost impossible to complete, but to all of them, and they know who they are, goes my most profound affection and love. Thanks guys for giving me the experience of a life time. For Fiona: I do not have enough words, or I am not good enough, to fully express my feelings. Thanks for being there, thanks for all the laughs and tears. You mean the world to me.

Finally, I wish to dedicate this thesis to my family. In particular, to Raffaele Palumbo. My father. His too early departure last year has left all of us deprived of a beautiful and honest person. The one from whom I have learnt the most in all my life. I look at myself in the mirror and I see you dad. Thanks for teaching me to work hard and to always walk with my head held high. I miss you and I love you.

Abstract

This thesis provides a study of a single chip, multi-channel surface plasmon resonance (SPR) imaging system. The equipment has no moving parts and uses a single sensor "chip" onto which multiple channels can be incorporated. A light emitting diode is used as a photon source while a CCD camera forms the detector. The optical configuration has been designed to achieve a uniform illumination of the sample over a fixed area with a range of incident angles. Poly(ethylene imine), PEI, poly(ethylene-co-maleic acid), PMAE, poly(styrene sulfonate), PSS, and a cationic modified polyacrylic ester, PMADAMBQ, are used as the molecular "bricks" in layer-by-layer (LbL) self-assembled organic architectures. Reflectivity changes in real time are used to follow the adsorption steps during the deposition of the multilayer films. Sensing experiments are mainly focused on the first row transition metals such as iron (II), nickel (II), copper (II) and zinc (II). Sensing of anionic sodium dodecylbenzene sulphate, $C_{12}H_{25}C_6H_4SO_3Na$, and a reversible pH-dependent response for a PEI/PMAE/PMADAMBQ LbL film are also reported. Using a two bilayer structure, PEI/PMAE/PMADAMBQ/PMAE, a detection limit of less of one part per million for copper ions in solution is measured. Atomic force microscopy is used to elucidate the morphology of the organic films. In some cases, the visualization of isolated polymeric chains is demonstrated. It is proved that polyelectrolytes of different charge density form dissimilar structures. The outer surface of PEI/PSS bilayers appears to be more uniform than that of PEI/PMAE bilayers. This is believed to have an influence on the sensing performance of the LbL architectures. The use of the SPR sensing system for simultaneous interrogation of different polyelectrolyte thin films is demonstrated. Two different LbL self-assembled films, PEI/PSS and PEI/PMAE, are built-up on the same chip. Their response to a variety of metal ions is shown to be independent and reasonably reproducible. Moreover, consistent results are obtained when using sensing chips stored for a relatively long time.

Contents

Chapter 1

Introduction

1.1 Introduction and text organization

The demand for reliable systems for bio-chemical sensing is increasing. Opto-chemical sensors have a major role in this sector mainly because of their non-invasive methods of detection. It is believed that progress in this field will come from a combination of new sensing materials with new transduction technologies. This thesis reports work undertaken on developing a novel sensing system. The design of each of its components is presented and the investigation and the characterization of the materials used as active sensor are described in detail. Sensing tests have been performed on cationic and anionic species together with studies on the pH sensitivity. The selectivity and reliability of the system are also examined.

In Chapter 2 a general introduction to sensing systems is given. It is argued that the properties and characteristics of a sensing device are better understood if a clear definition of the term "sensor" has been provided. Special attention is given to opto-chemical sensing systems and to functional organics and polymers as the sensing materials. Thin film assembly methods are also introduced. In Chapter 3, the optical principle exploited for the sensing, surface plasmon resonance (SPR), is described. A theoretical discussion of plasmon waves, their generation and their characteristics provide a background to the practical applications and commercial products based on such technology. A detailed report on the class of materials used in this thesis, polyelectrolytes, and the assembly technique, layer-by-layer self-assembly (LbL), can be found in Chapter 4.

As described in Chapter 5, before arriving at the final SPR set-up, different phases of design, construction and evaluation were necessary. The technical solutions to the various elements of the sensing system are described. To characterize the polyelectrolyte architectures, atomic force microscopy was used. Details of the results from such investigations are provided in Chapter 6. Theoretical models concerning the adsorption of polymer chains onto solid (soft and rigid) supports are also discussed.

The majority of the sensing experiments were concerned with the detection of metal ions in solution, such as sodium, iron, nickel, copper and zinc. The impact of first-row transition metals on the environment and health is discussed in Chapter 7 and their

interactions with polyelectrolyte thin films are examined. Several polymer architectures (i.e. organic films composed of various combinations of poly(ethylene imine), PEI, poly(ethylene-co-maleic acid), PMAE, poly(styrene sulfonate), PSS, and a cation modified polyacryic ester, PMADAMBQ) have been used for metal ion, anion and pH sensing. These experiments form the basis for the next phase of the research: multichannel sensing. In Chapter 8, alternative designs of the sensing chip are proposed and discussed. Sensing experiments using such substrates involve tests with several metal ion species. Response characteristics for each of the channels are analyzed and the different mechanisms contributing to the sensing are discussed. Finally, sensing tests on chips kept under storage for a relatively long time are described. In Chapter 9, a summary of the conclusions derived from the research is outlined and some suggestions for further work are provided.

Chapter 2

Introduction to sensors

2.1 Introduction

Over the last fifty years, the development of sensing devices has grown steadily. The sensing sector maintains a considerable level of interest for both the academic and industrial worlds. Microelectronic technologies allow miniaturization of the sensing systems which have been expanding in the areas of medicine, biology, safety and environmental protection. In the future, bottom-up approaches could allow a further reduction in their dimensions (i.e. nanosensors). The cost of these systems is also important, especially for automation in industrial processes, for environmental monitoring over large areas or for personal devices (i.e. portable chemical and biological sensing systems constantly monitoring the environment). Very different materials, organic and inorganic, are used in sensors, depending on the phenomenon under investigation. Silicon, organic polymers, metals, ceramics and glasses all have applications in physical and bio-chemical sensing systems.

In this introductory chapter, a brief survey of the different technologies and their applications will be given. The concept of a sensor will first be described. Then, some of the most important parameters that define a sensor will be introduced. Sensing systems will be classified through their application fields, the means of transduction exploited and on the basis of the type of measured quantity. The field of the optical-chemical sensors will be treated in some detail. Among all the classes of materials that can be used as the active elements, close attention will be given to functional organics and polymers. A more detailed description of the principles and materials exploited for the research work presented in this thesis will be provided in subsequent chapters.

2.2 Sensors: some definitions

One of the first challenges encountered in describing a sensing system is to provide a satisfactory definition of sensor. In particular, it is important to distinguish between a measuring system, transducer and sensor, Fig. 2.1 [1]. One of the best definitions is that a *sensor* is an element able to convert a variation of any quantity, property or physical state, the input signal or *measurand*, into a "useful" (i.e. something we are able to read and interpret) output signal. A sensor, therefore, is an element sensitive to the input and able to communicate with a measuring or control system [2]. Natural sensors, like those found in living organisms, usually respond to electrochemical signals; their physical

nature is based on ion transport. In artificial sensors, information is usually transmitted through the transport of electrons or photons. Sensors which are used in artificial systems must communicate through the same language as the device to which they are interfaced.

Sensors may be one of two types: active and passive. Active sensors directly generate a signal in response to an external stimulus. The input stimulus energy is converted into output energy without the need for an additional power source (e.g. thermocouple, pyroelectric detector and piezoelectric sensor). In contrast, passive sensors require an external energy source for their operation. The signal is then modified by the sensor to produce a useful output. Passive sensors are sometimes called "parametric" because their properties change in response to an external stimulus and these changes can subsequently be converted into an output signal. For example, a thermistor is a temperature sensitive resistor. It does not directly generate any energy signal, but by passing an electric current through it (excitation signal) its resistance can be measured by detecting variations in current and/or voltage across the thermistor. These variations (measured in ohms) are directly related to the temperature change [2].

The importance of the sensor in the measurement process increases for small input variations. The smaller these variations, the more important it is to use a sensor of high sensitivity, able to respond primarily to the parameter of interest, even in the presence of disturbance factors.

The task of translating or transmitting the information from one system to another is given to the *transducer*. A single transducer can manage several sensors while communicating to condition and control the signals. The nature of the phenomenon under scrutiny defines the nature of the sensor, while a transducer is defined by the process or the environment in which operates. Therefore, the same sensor could be used by different transducers while a single transducer could use simultaneously several sensors (each with its own characteristics and specification). For example, a chemical sensor may have a part (the real sensor interfacing with the external environment under investigation) that converts chemical energy into thermal energy, while a thermopile (the transducer) converts heat into an electrical signal [2]. The combination of the two makes it possible to produce an electric signal in response to a chemical reaction, but it

is only the first element that is really able to detect the measurand, while the task of the thermopile is to translate the signal generated by the sensor into a useful output. However, the two terms (i.e. sensor and transducer) tend to be confused, mainly because of the high level of integration in modern sensing systems. More frequently, complete sensing "boxes" including sensor(s)/transducer, signal acquisition, conditioning, processing and interface are designed and introduced into the market.

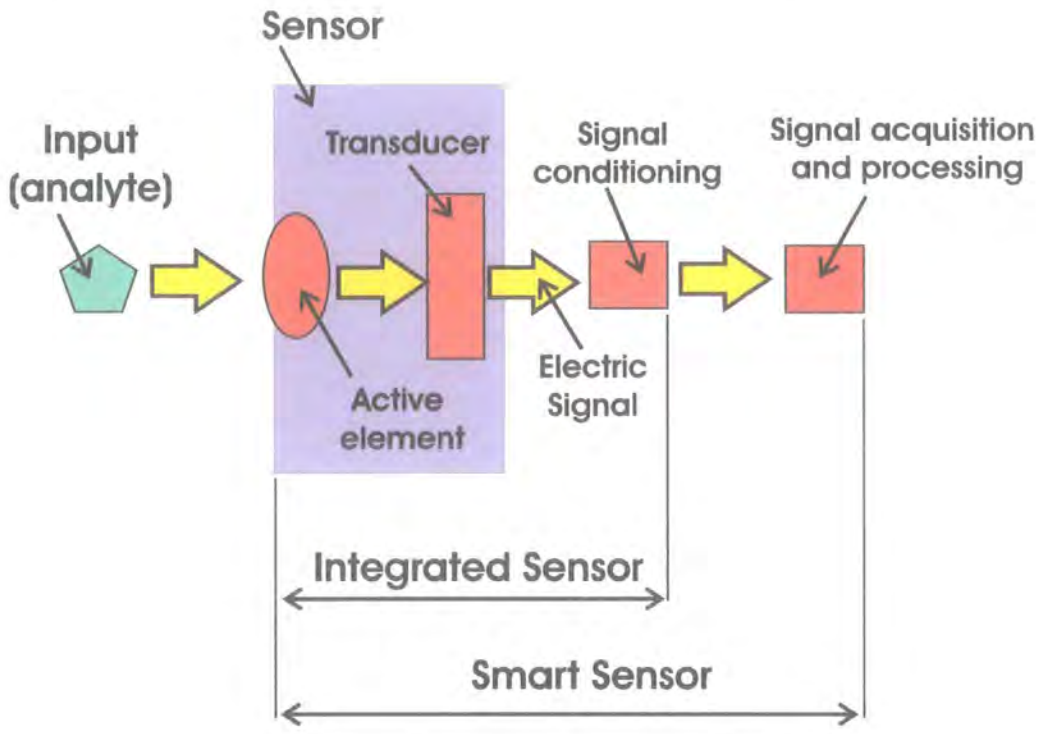

Figure 2.1 Schematic representations of a sensor, an integrated sensor and a smart sensor.

As shown in Fig. 2.1, the combination of the sensing element with the conditioning system is called an *integrated system*, while the addition of signal processing and acquisition results in a *smart sensor* [3].

A smart sensor is an important advancement towards the simplification of the measurement and the optimization of the measuring system. Issues related to the degradation of the device, to thermal drift and to non-linearity in the response can be addressed by a smart sensor in an automatic manner. Moreover, self-diagnosis of the working state and self-calibration are very attractive features in a measuring system making it able to adapt to different environments. In the future, the integration between the sensor and the information processing will be taken even further towards the *expert*

sensor, a fully autonomous system able to detect the measurand and make decisions on the best way to deal with any measured changes.

2.3 Sensor parameters

A correct definition of the parameters of a sensing system is fundamental for a better understanding of the sensor behaviour and for establishing uniform standards. It is then possible to have a consistent comparison between the performances of different sensing systems. Parameters need to be attributed to the correct part of the sensing system. For example, some parameters only characterize the active element(s), while others define the performance of the entire sensing system.

An ideal sensor should have characteristics such as a high selectivity and sensitivity, reversibility, long term reliability and stability, short response and recovery times, good signal to noise ratio, multiplexing capabilities, low cost, a minimal complexity for use and portability for in-situ applications [1, 2, 4]. Compatibility with integrated circuits and microprocessors, flexibility in the assembly of different platforms and sensors in a single system are also highly desirable features.

Reliability, sensitivity and selectivity are characteristics that depend directly on the material used as sensor. Other features such as response time and noise are more complex since several components of the sensing system play a role. In particular, it is important to note that the main source of noise in a sensing system is, very often, the system itself, with all its electronic components making a contribution. Shielding of the multiple noise sources within the system is, therefore, essential.

The response of a sensor is calculated from the value of the output before the measurement starts, R_{st} and the value measured in the presence of a measurand, R_{meas}

$$\left|\frac{\Delta R}{R_{st}}\right| = \left|\frac{R_{meas} - R_{st}}{R_{st}}\right| \tag{2.1}$$

The sensitivity of a sensor is defined as the derivative of the parameter R_{meas} with respect to the measurand, m (the input). If there is a linear variation between the input and the sensor response (Fig. 2.2), then the sensitivity can be defined

$$S = \frac{\Delta R_{meas}}{\Delta m} \tag{2.2}$$

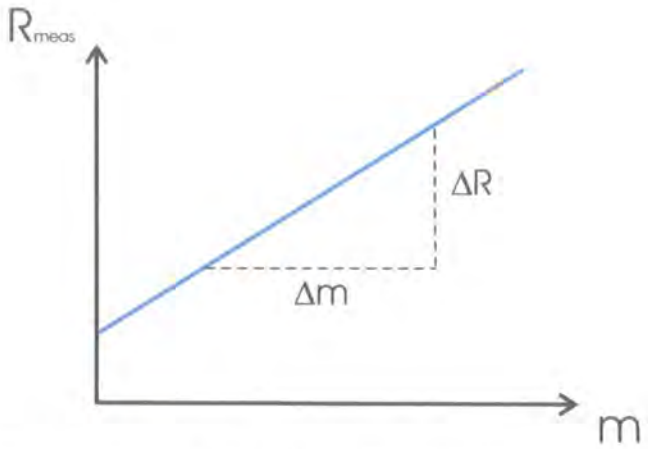

Figure 2.2 Sensitivity for a linear sensor. R_{meas} is the response of the sensing device, while m is the measurand. (Reproduced from [1]).

When the response curve of the sensing system is not linear, then the sensitivity can be expressed

$$S = S(m) = \frac{dR_{meas}}{dm} \tag{2.3}$$

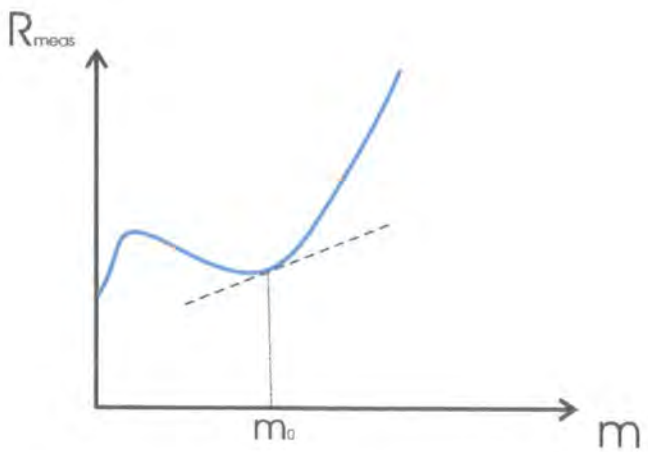

Figure 2.3 Sensitivity for a non-linear sensor. R_{meas} is the response for the sensing device, while m is the measurand. (Reproduced from [1]).

As shown in Fig. 2.3, the selectivity S_{m_0} for a practical value of the measurand m_0 is

$$S = \left.\frac{dR_{meas}}{dm}\right|_{m=m_0} = S_{m_0} \tag{2.4}$$

Other fundamental parameters are the response and recovery times, Fig. 2.4. The response time defines the time interval for the response signal R_{meas} to change from 10% to 90% of its final value R_f. If the system is reversible, then it is also possible to define a recovery time, as the time for the response signal to change from 90% to 10% of R_f.

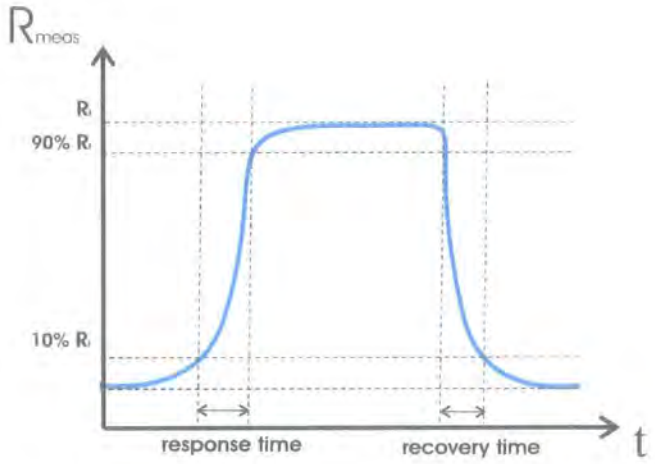

Figure 2.4 Response curve for an ideal sensing system. (Reproduced from [1]).

Furthermore, the designation of the signal to noise ratio (SNR or S/N) in a measuring system is fundamental. This is defined as the ratio of the strength of the signal plus noise carrying information to the unwanted interference (noise). It is usually measured in decibel (dB) and it is equal to 20 times the base-10 logarithm of the amplitude ratio (i.e. voltage of the signal to voltage of the noise $\frac{V_s}{V_n}$), or 10 times the logarithm of the power ratio. If $V_s = V_n$ then the S/N ratio is equal to zero. In this situation the signal is unreadable. Similarly, for a noise level superior to that of the useful signal no conclusion at all can be drawn from the acquired information. Positive S/N ratios are therefore desirable and necessary. Thus, long efforts are spent in the attempt of its maximization.

For bio-chemical sensors, selectivity is very important. This is a measurement of the ability of the sensor to respond to only one input in the presence of interferences. In most biological systems, specificity is achieved by shape recognition, which involves a comparison with a reference. As shown in Fig. 2.5, according to the Emily Fisher description, the size, shape and position of binding sites on the receptor give an almost unique "lock-key" combination [5] that makes it possible for the active site to be selective to a restricted number of bio-chemical species. High selectivity means that the contribution from the primary species dominates, and that the interference from other species is minimal. However, an absolutely selective sensor does not really exist and there is always some interference present.

Sensor resolution is the minimum change in the measurand which a sensing device can resolve. In other words, it is the size of the incremental steps in the response obtained for a linear increase of the input signal. Thus the resolution is not necessarily constant over the whole measuring range. The sensor resolution depends on the accuracy with which the monitored physical phenomenon or chemical analyte can be determined by the specific sensor device and, as such, is limited by sensor system noise. As explained previously, every component of the system is a potential source of noise [6].

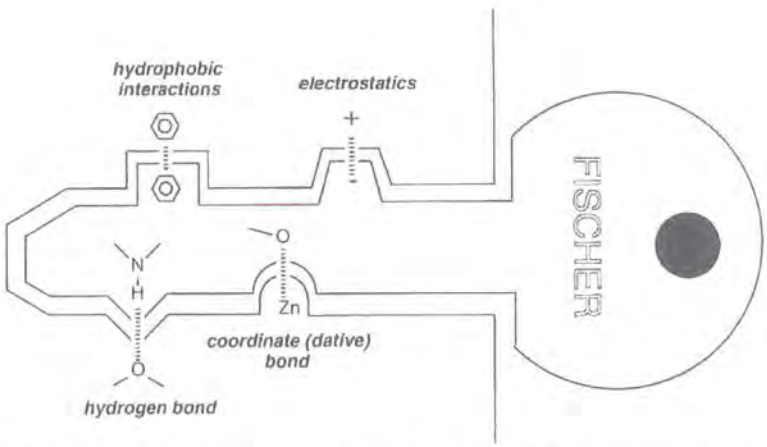

Figure 2.5 The lock and key principle: receptor sites on the active material (lock) are complementary to the analyte (key), therefore selectivity is guaranteed. (Reproduced from [5]).

The accuracy of the measurement is very dependent upon the experimental circumstances and the degree of optimization of the particular sensor. Therefore, the ultimate resolution may differ from that of a model system. Another important

parameter of a sensing system is its operative/dynamic range, i.e. the range of values of the measurand, which can be detected by the sensor.

2.4 Sensing system classification

Sensor classification schemes range from very simple to the complex. One approach is to consider all its properties, such as what it measures (stimulus), its specifications, the conversion mechanism, the material(s) it is fabricated from and its field of application [2]. Classification schemes based on the physical or chemical means of transduction have been used [7], but these can be difficult to follow. Therefore, sensors are often classified according to what they measure. It is then possible to look in detail at the different options possible and to consider the characteristics and features of each sensing system. According to this classification, there are three sensor "families" or groups: physical sensors; chemical sensors; and biological sensors.

Physical sensors are selective and sensitive to physical phenomenon, such as pressure, force, acceleration, specific heat, current, electric charge, magnetic field, resistance and light. They form a major part of the sensor industry, with an increasing number of applications [2, 8].

2.5 Chemical sensors

Chemical sensors are devices sensitive to stimuli produced by various chemical compounds or elements. The most important property of these sensors is selectivity. Changes in the chemical environment are transformed into sensor properties such as electrical conduction, thermal conductivity or optical effects [2, 4, 9, 10]. Chemical sensors can be subdivided into gas and liquid sensors.

According to the first law of thermodynamics, changes in the internal energy of a system are accompanied by the absorption or release of heat. Thermal chemical sensors detect this heat variation and are able to monitor a specific chemical reaction. A temperature probe is coated with a chemically selective layer. When this is in contact with the analyte, heat is produced or released by the chemical reaction. The thermal probe detects this change and correlates it with the reaction.

Electrochemical sensors are probably the most versatile chemical sensors. Some of these measure voltage (potentiometric), others monitor electric current (amperometric) or conductivity/resistivity (conductometric). Electrochemical detectors are used where a chemical reaction takes place or when the charge transport is modulated by the interaction of the chemical species under observation. The main requirement is to have a closed circuit (i.e. at least two electrodes). This is true not only for the cases in which a current (a.c. or d.c.) is measured, but even for potentiomentric sensors, where the loop needs be closed to measure the voltage.

In potentiometric devices, the two electrodes form a balanced configuration. One acts as a reference and the reaction taking place on it (i.e. half-cell chemical reaction) is known, reversible and non-interfering. On the other hand, the reaction of the targeted chemical species with the electrode coating creates an imbalance in the bridge circuit. Potentiometric ion sensors use ion-selective membranes with which the sensor responds to the presence of the ion of interest. ChemFETs are chemical potentiometric sensors exploiting the field effect transistor (FET) principle. They are used in biological and medical monitoring due to their small size and low power consumption. ChemFETs can be ion, gas, enzyme or immuno-selective sensors.

Conductometric detectors measure the change in conductivity of the electrolyte in a electrochemical cell. Normally, a Wheatstone bridge is used with the conductometric sensor forming one of the resistance arms of the bridge. An example of amperometric sensor is a Clark oxygen sensor that uses an electrolyte solution contained within the electrode assembly to transport oxygen from an oxygen-permeable membrane to the metal cathode [2].

The next significant chemical sensor group is that of the concentration measuring systems. The concentration of a chemical species in gas, vapour of liquid form can modify or modulate the physical property (e.g. resistance, refractive index) of the active sensing material. In this family of sensing devices, the sub-groups of resistive, gravimetric and fluid density sensors are found.

Examples of a resistive-chemical sensor are detectors of hydrocarbon fuel leaks and concentration sensors for air cleanliness. The first uses a polymeric matrix with a

conductive filler. The matrix swells in the presence of the hydrocarbons resulting in the separation of the conductive particles. Thus, the conductivity of the system falls. When the hydrocarbon source is removed, the polymer returns to its original volume and the sensor is conductive again. In air monitoring sensors, a semi-conductive material can be used. The sensor is heated above the ambient temperature. The resistance of the semi-conductive material drops when exposed to gases like methyl mercaptan (CH_3SH), ethyl alcohol (C_2H_5OH) or smoke.

Gravimetric devices are oscillating sensors for the measurement of mass. They operate at ultrasonic frequencies and register the shift in the resonant frequency of a piezoelectric crystal when an additional mass is deposited on its surface. This class of sensors is extremely sensitive; a typical sensitivity is 5 MHz $cm^2 kg^{-1}$. This means that a shift in frequency of 1 Hz corresponds to 200 ng cm^{-2} of added weight. The dynamic range is quite wide with typical maximum value of 20 $\mu g\ cm^{-2}$. To assure selectivity, a chemically active layer can be used to coat the resonant crystal. Another class of gravimetric sensors is represented by surface acoustic wave (SAW) detectors. Their working principle is based on the propagation of mechanical waves along a solid surface which is in contact with a medium of lower density (i.e. air, liquid).

2.5.1 Optical-chemical sensors

Optical-chemical sensors translate information from the chemical domain to the optical one and then finally to an electric signal. An optical probe is used to interrogate the chemically active layer. In the last thirty years, these have found wide applications. The operational principle is based on the interaction of electromagnetic waves with a material. The optical properties of the sensors (e.g. refractive index, absorption, scattering and fluorescence) are modified by the chemical reaction with the measurand. In general, the first requirement for this class of sensor is the generation of an optical excitation beam. This beam could be used either for chemically modifying the active sensors (e.g. photisomerization) and/or the analyte, or it could be used simply as a probe. For sensors exploiting phenomena such as chemi-luminescence or bio–luminescence, optical excitation is not required because it is the chemical reaction itself that generates an electromagnetic signal. For other optical sensing systems, it is

necessary to convert the chemical reaction and the molecular selectivity to a second optical signal, through, for example, indicators immobilized on a support. Alternatively, secondary reaction products like oxygen, carbon monoxide, ammonia might be detected using a bioreactive layer. Finally, waveguides or optical fibres transmit and propagate the optical response towards light sensors that convert it to a electric signal [3].

The first optical sensors used the analysis of optical absorption spectra generated by the interaction of the sensing layer with the analytes (e.g. CO_2, O_2) [11]. Several similar techniques are now available, such as spectroscopy through luminescence, fluorescence, infrared, ultraviolet or visible absorption, interferometry, ellipsometry and surface plasmonic resonance. The use of optical fibres should guarantee the development of compact, miniaturized and low cost sensors for laboratory or in-situ application. One of the main advantages of this category of chemical sensor is that they do not need to have an electric current passing through the sensing material (consequently the issue of power dissipation is absent) and can operate at ambient temperature.

Every gas, liquid or solid, with a covalent bound and strong dipolar characteristic interacts with infrared radiation at a specific frequency. On the basis of this principle, infrared absorption sensors have been developed. Whenever a target molecule interacts with the chemically active layer of the sensor, new absorption bands are generated and the original spectrum is modified. Comparison of a series of spectra allows the identification of the analyte and the determination of its concentration [12].

Fluorescence based sensors are able to detect very low concentrations of chemicals with good selectivity. A polymeric matrix may host the receptors (or the matrix itself may be a receptor for the analyte). When the sensor probe is exposed to the analyte the polarity of the sensing receptor changes and, with it, its emission spectrum. Using an optical fibre coated at one end with the sensing material, the same propagation channel (i.e. the fibre) is used first to interrogate the sensor (exciting signal or input) and then to collect the response (output). A multiwavelength spectral detector, positioned at the end of the fibre, then compares the two optical signals [3].

Optical sensors exploiting *evanescent* waves utilize a light beam passing through a waveguide that propagates as an evanescent wave in the medium surrounding the

waveguide. Evanescent ("vanishing") waves are formed when sinusoidal waves travelling in a medium of refractive index n_1 are (internally) reflected from an interface with a second medium of refractive index n_2 at an angle greater than a specific value (critical angle). Internal reflection means that no refracted wave is generated in the second medium, but the incident wave is fully reflected within the first medium. Although no net energy is transferred from one medium to the other, an optical disturbance occurs in the second medium which takes the form of an evanescent wave. The intensity of such radiation decays exponentially with the distance from the interface at which they are formed. If in the second medium (the sample) a chemical species is able to absorb electromagnetic radiation at the wavelength of the probe, then there will be a reduction in the intensity of the reflected light passing through the waveguide. Such a variation will be registered by a detector at the end of the optical support. Reduction in the intensity profile can therefore indicate the presence of the analyte and provide information about its concentration [13].

Particular types of evanescent wave sensors are surface plasmon resonance (SPR) sensing systems. A detailed introduction to such devices, their theoretical principles, application and characteristics, will be presented in the Chapter 3. In SPR sensing systems, a surface plasmon polariton (SPP) is exploited, i.e. electric charge oscillation associated with an electromagnetic wave.

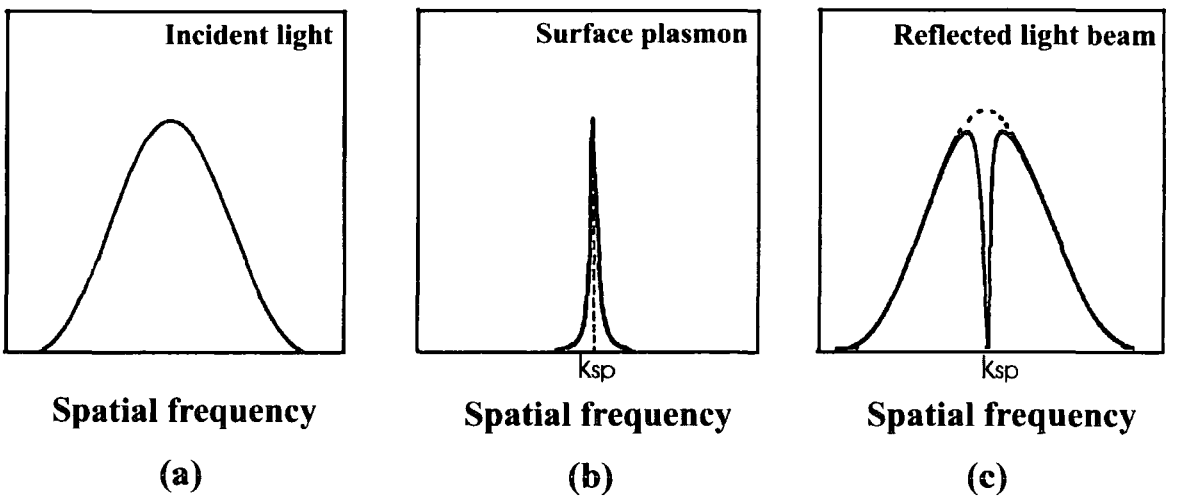

Figure 2.6 Surface plasmon resonance principle. Spatial frequency spectra of: (a) the incident beam; (b) the surface plasmon; (c) the reflected beam. k_{sp} is the wave vector associated with the surface plasmon. (Reproduced from [14]).

This plasmon wave is generated by an excitation light beam with a *p*-polarization. In other words, the incident radiation has its electric vector in the plane of incidence, i.e. the plane that contains both the incident and reflected wavector and it is perpendicular to the incident surface. The associated magnetic field will have a single component tangential to the interface. At a specific angle value, part of the energy associated with the excitation beam can be used to generate a charge oscillation. The reflected beam will possess an intensity minimum due to the generation of the plasmon wave, Fig. 2.6.

Plasmons are generated at the boundary between two media of opposite dielectric constants (for example a metal and a dielectric). The electric field associated with the evanescent wave propagates inside the two media, being much more concentrated on the dielectric side. Any changes in the dielectric in proximity of the interface are detected by the field and transduced into changes in the plasmon wave oscillation. Finally, this results in a shift in the profile of the reflected beam. Comparison with the original profile gives an indication of the changes in the dielectric. If a selective sensing layer is interposed between the two media, the arrangement can be used for a very sensitive optical sensing.

2.5.2 Biological sensors

Biosensors use biological or living materials to provide their sensing functions [15]. In many ways they can be defined as a special type of chemical sensor [2]. Evolution of species by means of natural selection has led to extremely sensitive organs which can respond to the presence of just a few molecules. Artificial sensors exploit biologically active materials in combination with different physical sensing elements. The bio-recognition element works like a bio-reactor on the top of the conventional sensor. The response of the biosensor will be determined by the diffusion of the analyte, by the reaction products, by the co-reactants or interfering species and/or by the kinetics of the recognition process. Organisms, tissues, cells, organelles, membranes, enzymes, receptor, antibodies and nucleic acid can all be detected by means of a bio-sensor. One of the key issues for biological sensing systems is the immobilization of the active element on the physical transducer. The biologically active material must be confined to the sensing element and kept from "leaking" while allowing contact with the analyte

solution. Furthermore, the reaction products must readily diffuse out of the sensing layer to not denature its biologically-active characteristics. Most of the materials are proteins or contain proteins in their chemical structure. Two of the main techniques employed to immobilize the proteins are binding (adsorption or covalent binding) and retention. Physical retention involves separating the biologically active material from the analyte solution with a layer on the surface of the sensor which is permeable to the analyte and to any products of the recognition reaction, but not to the biologically active materials [2]. Biosensors are divided in two main groups: biocatalytic sensors and bioaffinity sensors (or immunosensors). For both categories, electrochemical devices or optical sensing systems have been extensively studied and implemented [15].

2.6 Materials

Many different materials are used within modern sensing systems. Active sensing elements may comprise of inorganic or organic materials, electrical conductors, semiconductor or insulating compounds, biological substances or elements in solid, liquid gas or plasma form [2].

One of the most important sensor materials is silicon [2, 15]. The material has been used in sensing devices for over forty years. It has a relatively low production cost and the process for its fabrication and purification is well known. Devices based on silicon are found in the measurement of radiation, mechanical stress and strain, temperature, magnetic field and in analytical chemistry. Many systems based on the light-sensitive silicon p-n junction have been produced, such as photodiodes, CCD cameras, photo-transistors, pin diodes and strip detectors for nuclear radiation. Silicon sensors for pressure, strain, stress, acceleration or surface-acoustic waves are extremely versatile and successful products. The temperature sensitivity of silicon can be exploited in a "tandem" transducer, i.e. transducer in which the conversion is based on a tandem of two effects. Hence, it is possible to measure infrared radiation, vacuum, flow, pressure and acceleration. Measurement of magnetic field is possible thanks to silicon sensors exploiting the Hall effect. Silicon also has some applications in the chemical signal domain. However, despite much effort, only a few products have appeared on the market. Among the most successful is the ion-sensitive field-effect transistor (ISFET),

the Pd-gate MOSFET, the gate-controlled diode for blood analysis, silicon gas chromatographs on a single wafer and silicon based humidity sensors [8].

Metals can be used as sensing elements and can be divided in two main groups: nonferrous and ferrous. Magnetic sensors to measure motion, distance or magnetic field strength use ferrous metals such as steel. In contrast, non ferrous metals are permeable to magnetic fields and are, therefore, used whenever these fields are of no concern. Physical properties and mechanical processing are two key factors that guide the choice of the metal [2].

Ceramics are very useful in sensors. This is due to their structural strength, excellent thermal stability, to their being inert to many chemicals, to a favourable volume/weight ratio, easy bonding or coupling with other materials and excellent electrical conductance. Examples of ceramic materials used in sensing are alumina, Al_2O_3, beryllia, BeO, boron nitride, BN, aluminium nitride, AlN (for fast heat transfer) and silicon carbide, SiC (its high dielectric constant makes it suitable for capacitive sensors) [2]. Finally, glasses have had an influence on the sensing world thanks to the use of optical fibres for strain and stress detection or in conjunction with chemically active receptor (biosensors).

2.6.1 Functional organics, polymers and organized molecular assemblies

Functional organics and polymers have recently gained a widely recognized role in the science and technology of sensors [15-19]. Thin films based on these materials can be produced via several techniques such as spin coating, physical vapour deposition, chemical vapour deposition, electrochemical methods, the Langmuir-Blodgett (LB) film deposition method and self-assembly [20]. In contrast, thick film processing for polymeric materials is traditionally based on screen printing, tape transfer methods and firing/curing at elevated temperature [19].

As shown in Table 2.1, polymers can be used in many different sensors, thanks to their low cost, simple fabrication techniques and the wide choice of molecular structures. Moreover, they can be deposited onto different substrates. It is also possible to build in

situ chains of neutral or charged molecules and even place functional groups inside the bulk material, or onto its surface, enabling the production of films with various physical and chemical properties.

Sensing effect	Polymer examples	Typical additives	Sensor type
Flexibility, elasticity	PI (KAPTON®), PE, Myalar®, Epoxies	–	Mechanical
Piezoresistive	PI, PVAc, PIB, PTFE, PMMA, Polyesters, epoxies, PE, PU, PVA	Metal powder, Carbon black, V_2O_3, PPy	Mechanical
Percolation			Temperature
Percolation + swelling			Chemical
Piezoelectric	PVDF, P(VDF-trFE)	–	Mechanical, acoustic
Pyroelectric			IR
Photopyroelectric			Chemical, materials
Electret	PTFE, Teflon-FEP	–	Acoustic
Permittivity, thickness and refraction index changes	CA, PI, PEU, PS, PEG, Polysiloxanes (e.gPDMS)	Functional groups	Chemical (RH, ions, molecules in gases and liquid)
Conductimetric	SPEs, ECPs, their copolymers	Salts, ionic compounds	
Potentiometric	SPEs, ECPs, their copolymers, PVC, PV(C/A/Ac), Silopren®	Salts, ionic compounds, plasticizers and ionophores	
Gravimetric	CAB, PHMDS,PDMS,PE,PTFE, PCTFE,PIB,PEI,PCMS,PAPMS,PPMS, Fluoropolyol	Functional groups, supramolecular receptors	
Calorimetric	PDMS, PSDB	Catalysts	
Molecular separation	CA, PE, PTFE, PVC, PP, FEP, PCTFE, PDMS, PS, PHEMA, Mylar®, PU, PVA Silicon rubber, PEthI	–	
Colourimetric, fluorescence	PVP, PAA, PVC, PVI, PTFE, PS, PHEMA, PMMA, Celluslose, Epoxies,®	Dyes	
Enzyme- and immunoreactions	PVC, PAA, PVA, PE, PEI, PVPY, PU, PMMA, PHEMA, Nafion®, ECPs, (e.g. PPy)	Enzymes, antibodies	Biosensors
Piezoelectric	PVDF, PTFE, PPy	–	Actuators
Low friction			

Table 2.1 Polymeric materials as sensing active element. Sensing effects, most important polymers, additives and sensor types in which they are applied. (Reproduced from [19]).

In recent years, polyelectrolytes, a particular class of polymers carrying electrostatic chargeable groups, have received consideration as active sensor elements [21-23]. These can be assembled via the layer-by-layer, LbL deposition technique in ultra-thin structures. In Chapter 4, a more complete survey of the development of this research field will be given. This category of organic architectures ranks along with Langmuir-Blodgett films and self-assembled monolayers (SAM). Despite being less "elegant" than LB films, due to their "fuzzy" architectures, they have some advantages over LB multilayers in terms of a simple deposition method, a wider number of suitable substances to chose from and a higher stability [23].

Langmuir-Blodgett films are based on a specific category of substances called amphiphiles, i.e. molecules insoluble in water, with one end that is hydrophilic, and, likely to be soluble in water, and the other that is hydrophobic and insoluble. Extensive reviews of the LB technique, its characteristics and methodologies can be found in literature [16-18, 24]. A classic example of amphiphilic molecule is the octadecanoic acid, $(CH_2)_{16}CH_3CO_2H$ where the long hydrocarbon tail ($(CH_2)_{16}CH_3-$) is hydrophobic, and the carboxylic acid group head ($-CO_2H$) is hydrophilic, Fig. 2.7(a).

LB films have been assembled from fatty acids and related compounds, substituted aromatic compounds, fluorocarbon amphiphiles, ionophores and dyes, porphyrins and phthalocyanines, fullerenes, charge-transfer compounds, biological compounds, gold nanoparticle coated by thiol groups and polymers [16, 17, 25-28]. To obtain a monolayer film, amphiphilic molecules are dissolved in a suitable solvent such as chloroform or toluene and dispersed, drop-wise, on a clean surface of ultra-pure water. Once the solvent has evaporated, the molecules on the water surface will distribute themselves across the entire area available with their hydrophobic tails in air and their hydrophilic heads in water. Such an arrangement resembles that of a material in a gas phase. Because the molecules are far apart, they do not interact and do not form a continuous film. However, the molecular surface density can be increased by reducing the area available to the floating molecules. This is accomplished using special equipment (a Langmuir trough) with moving barriers. In Figure 2.7(b), it is possible to understand how the phase of the molecules changes from gaseous to expanded to condensed, by the reduction of the area available.

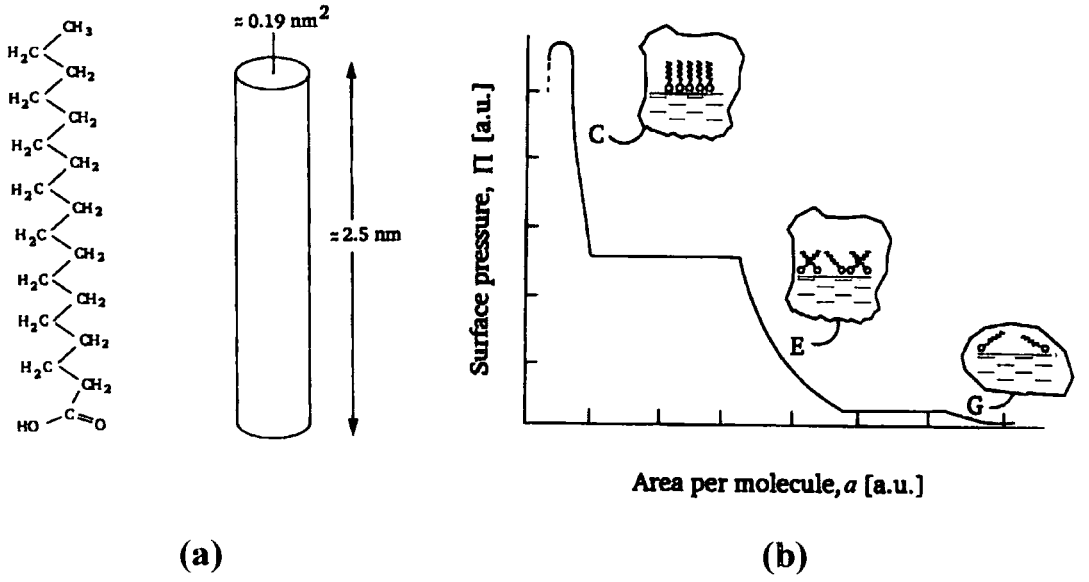

Figure 2.7 (a) Chemical structure for octadecanoic acid. The approximate geometrical shape and dimensions are shown on the right. (b) Surface pressure versus area per molecule isotherm for a long-chain organic compound. Surface pressure and area are in arbitrary units (a.u.). (Reproduced from [16]).

The LB deposition method is based on immersing a solid substrate, chemically treated to be hydrophilic, through the amphiphilic monolayer at the air/water interface, Fig. 2.8. The first monolayer is transferred onto the substrate as it is raised through the water. Then, as the substrate is immersed again, another monolayer is transferred. As shown in Fig. 2.8, monolayers can be transferred for each down and up-stroke (Y-type or head-to-head and tail-to-tail patterns), for each down-stroke only (X-type) or up-stroke only (Z-type). Moreover, mixed depositions are possible and the deposition type can change during the LB transfer process. Films incorporating more then one molecular species are realizable if, for example, the substrate is first immersed in a substance and then, after the deposition of the first monolayer(s) through the condensed phase of a second compound (alternate-layer LB film).

SAM monolayers are molecular assemblies that are formed *sua sponte* by the immersion of an appropriate substrate into a solution of an active surfactant in an organic solvent. Examples of this type of molecular organization are organosilicon on hydroxylated surfaces (e.g. SiO_2 on Si, Al_2O_3 on Al, glass), alkanethiols on gold, silver and copper; dialkyl sulfides on gold, alcohols and amines on platinum, and carboxylic acids on aluminium oxide and silver [17, 29].

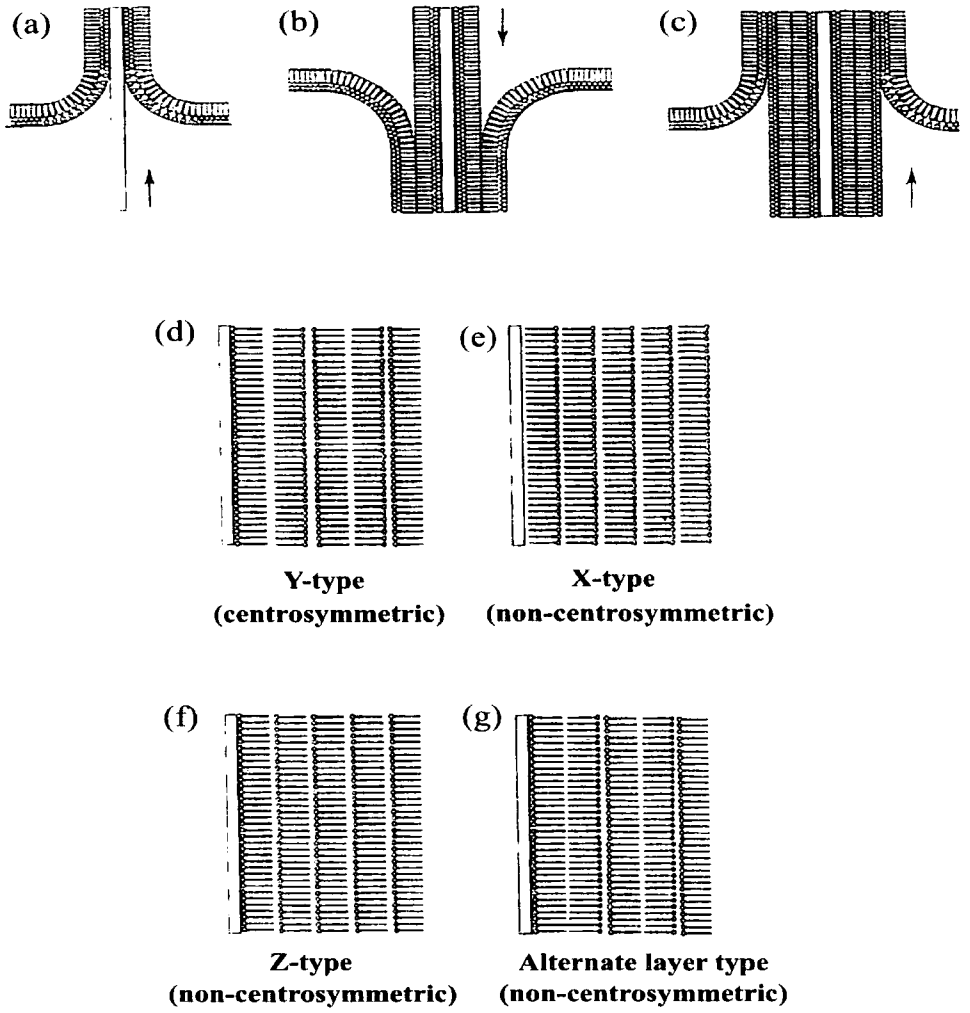

Figure 2.8 The LB transfer process showing the deposition of an amphiphilic monolayer onto a hydrophilic substrate (a, b, c). The four possible structures achievable using the LB technique: (d) Y-type, (e) X-type, (f) Z-type and (g) the alternate-layer type. (Reproduced from[24]).

As shown in Fig. 2.9(a), a self-assembling molecule consists of three parts. The first is the head group that ensures chemisorption onto the substrate. The head group attaches to a specific site on the substrate thanks to strong chemical interactions, such as the covalent Si–O bond in the case of alkyltrichlorosilanes on hydroxylated surfaces, the covalent but slightly polar Au–O bond of alkanethiols on gold or the ionic $-CO_2^- Ag^+$ bond in the case of carbolxylic acids on AgO/Ag. As a result of these strong interactions, the molecules tend to occupy every site on the surface. Therefore, they pack in the form of a compact monolayer, as illustrated in Fig. 2.9(b). The second important part of the molecule is the alkyl chain. Thanks to their dense self-packing, there are mutual attraction forces due to short-range interactions, dispersive, London-type or van der Waals forces, and for alkyl chains with polar bulky groups, long-range electrostatic interactions.

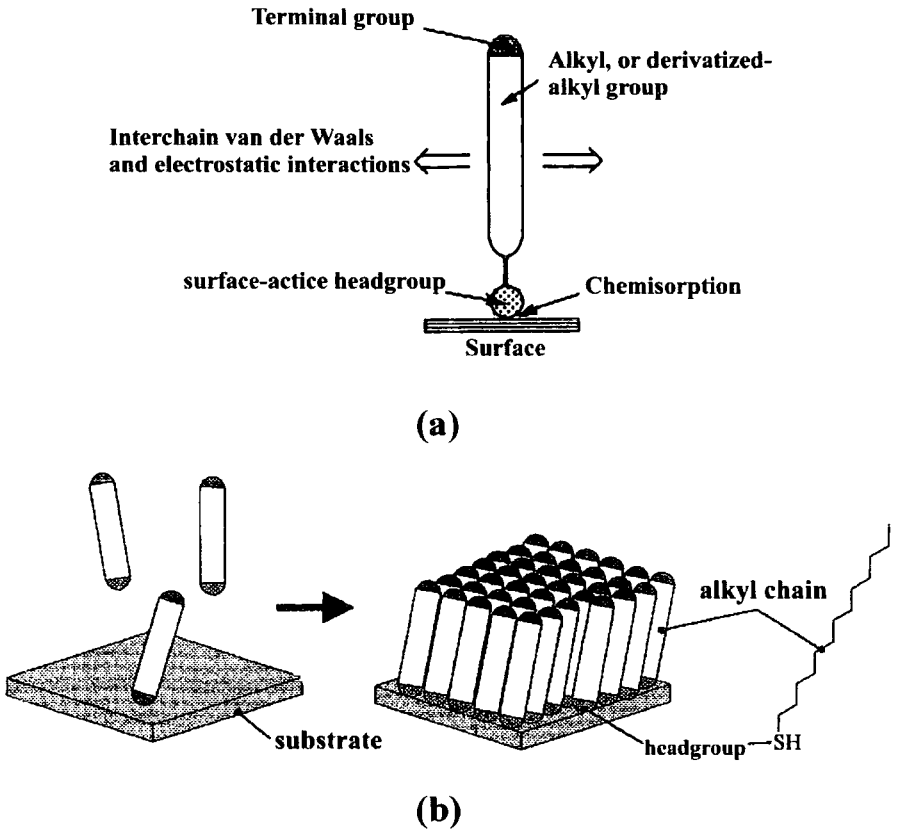

Figure 2.9 SAM monolayers. (a) Schematic view of the forces in a self assembled monolayer. (Reproduced from [17]). (b) Schematic representation of the formation of a self-assembled monolayer of an alkanethiol derivative on gold. (Reproduced from [29]).

It is important to note that self-assembly is only possible thanks to the chemisorption of the head group. The interactions between the alkyl chains start only when the monolayer is in place on the substrate. With the exception of long-range electrostatic forces, all the other interactions are too weak to allow (by themselves) the self organization of the monolayer. The third part of the molecule is the terminal functional group, as in the case of an alkyl chain, a methyl, CH_3 group [17]. A suitable terminal group can be used to obtain multilayer structures with monolayers adsorbed one on top of another, as in the case of multilayers of organosilane derivatives. Here, the formation of the monolayer is followed by the chemical activation of the same layer. The layer can then be used to provide support for another monolayer and so on [17, 29]. Other methodologies for multilayer growth exploit selective ionic interactions, bipolar amphiphiles and, as will be explained in Chapter 4, self assembly of polyelectrolytes [29].

LB and SAM thin films have been extensively studied and employed in sensing devices [16-18, 30-32]. Examples are chemioresistive devices based on the resistance changes

of an LB film made from gas-sensitive materials. Since the output currents of these sensors are very low (in the range of picoamperes), they can be integrated into a silicon FET to improve the signal/noise ratio. It is also possible to exploit the organic film as the semiconductive layer in a diode or a transistor. In this case, the gas should be allowed to interact readily with the organic film. To overcome problems related to poor selectivity, an array of different sensing elements is arranged within a single measurement system, an *electronic nose* [33]. The pattern of resistance changes in the sensor array is used to fingerprint the analyte in gas or vapour state. Otherwise, multiple measurements on one sample can be made, as in admittance spectroscopy using several frequencies [31, 34]. In this way the dynamic electric properties of the dielectric LB film are investigated. The capacitance and conductivity of the organic film are modulated by interaction with the gaseous or vapour molecules. Changes in the capacitance and conductance can result from a change in permittivity due to bulk dissolution of the analyte in the LB film, from a change in the permittivity due to specific interaction film-analyte or from swelling of the thin film. Optical SPR sensing using LB or SAM films as active elements has also been studied. This work is mainly based on the SPR investigation of thin films exposed to gases or vapours [27, 35-38].

2.7 Conclusions

In this chapter, an introduction to sensing systems has been presented. A general survey of the application of sensors has been given together with some useful definitions to distinguish the components that form a sensing system, e.g. sensor or active element, transducer, signal conditioning, signal read and control systems. Some of the most important features that characterize sensing devices have been introduced. The response output, sensitivity, selectivity, resolution and accuracy have been described in detail. Sensors can be classified on the basis of the means of transduction exploited or on the basis of the type of measured quantity. Here, the second method has been adopted. Following this, sensing devices can be divided in physical, chemical and biological sensors.

Chemical and biological sensing systems have been described in more detail, because these are directly related to the investigations presented in this thesis. Several optical principles and methods of interrogation and transduction of the bio-chemical interaction

active-element/analyte have been presented. Among these, SPR was introduced in its basic form, while a more detailed theoretical and technological description will be given in Chapter 3.

Different materials are employable as active sensors. Systems exploiting functional organics and polymers have been discussed. The LB and SAM deposition techniques for the preparation of thin films from such materials were introduced. A third deposition method for organic ultra-thin films, LbL will be discussed in Chapter 5. Finally, applications of LB and SAM architectures for electrochemical or optical sensing were outlined.

References

1. D'Amico, A., Di Natale, C., and Taroni, A., Sensors Parameters, in *Sensors for Domestic Application - Proceedings of the First European School on Sensors (ESS '94)*, A. D'Amico and G. Sberveglieri, Editors. 1995, World Scientific: London.

2. Fraden, J., *Handbook of Modern Sensors*. 2nd ed. 1996, New York: Springer-Verlag, Inc.

3. Boisde, G. and Harmer, A., *Chemical and Biochemical Sensing with Optical Fibers and Waveguides*. 1996, London: Artech House.

4. Janata, J., *Principles of Chemical Sensors*. Modern Analytical Chemistry, ed. D. Hercules. 1989, New York: Plenum Press.

5. Beer, P.D., Gale, P.A., and D.K., S., *Supramolecular Chemistry*. Oxford Chemistry Primers, ed. J. Evans. 1999, Oxford: Oxford University Press.

6. Johansen, K., Stalberg, R., Lundstrom, I., and Liedberg, B., Surface plasmon resonance: instrumental resolution using photo diode arrays. Measurement Science & Technology, 2000. 11(11): p. 1630-1638.

7. Ballentyne, D.W.G. and Lovett, D.R., *A Dictionary of Named Effects and Laws in Chemistry, Physics and Mathematics*. 1980, London: Chapman & Hall.

8. Middelhoek, S., Celebration of the tenth transducers conference: The past, present and future of transducer research and development. Sensors and Actuators A: Physical, 2000. 82(1-3): p. 2-23.

9. Hubert, R.J., Janata, J., Lundstrom, I., Svensson, C., and Zemel, J.N., *Solid State Chemical Sensors*, ed. J. Janata and P. Hubert. 1985, Orlando, Florida: Academic Press, Inc.

10. Edmonds, T.E., ed. *Chemical Sensors*. 1988, Blackie and Son Ltd.: Glasgow and London.

11. Opitz, N. and Lubbers, D.W., New Fast-Responding Optical Method to Measure PCO_2 in Gases and Solutions. Pflugers Archiv-European Journal of Physiology, 1975. 355: p. R120-R120.

12. Li, J.P., Tredgold, R.H., and Jones, R., Interactions of Nitrogen-Dioxide with Langmuir-Blodgett-Films of a Copper Porphyrin. Thin Solid Films, 1990. 186(1): p. 167-176.

13. Agranovich, V.M. and Mills, D.L., *Surface Polaritons, Electromagnetic Waves at Surfaces and Interfaces*. Modern Problems in Condensed Matter Sciences, ed. V.M. Agranovich and A.A. Maradudin. 1982, Amsterdam-New York-Oxford: North-Holland Publishing Company.

14. Matsubara, K., Kawata, S., and Minami, S., A Compact surface-plasmon resonance sensor for measurement of water in process. Applied Spectroscopy, 1988. 42(8): p. 1375-1379.

15. Aizawa, M., Biosensors, in *Introduction to Molecular Electronics*, M.C. Petty, M.R. Bryce, and D. Bloor, Editors. 1995, Edward Arnold: London.

16. Petty, M.C., *Langmuir-Blodgett Films : an Introduction.* 1996, Cambridge ; New York: Cambridge University Press.

17. Ulman, A., *An Introduction to Ultrathin Organic Films: from Langmuir-Blodgett to Self-Assembly.* 1991, San Diego: Academic Press, Inc.

18. Richardson, T.H., Langmuir-Blodgett films: from deposition to application, in *Functional Organic and Polymeric Materials*, T.H. Richardson, Editor. 2000, John Wiley & Sons Ltd: Chichester.

19. Harsanyi, G., *Polymer Films in Sensor Applications.* 1995, Lancaster, Pennsylvania, U.S.A.: Technomic Publishing Company, Inc.

20. Petty, M.C., Organic thin-film deposition techniques, in *Functional Organic and Polymeric Materials*, T.H. Richardson, Editor. 2000, John Wiley & Sons Ltd: Chichester.

21. Iler, R., Multilayers of colloid particles. J. Colloid Interface Sci., 1966. 21: p. 569-594.

22. Decher, G., Fuzzy nanoassemblies: toward layered polymeric multicomposites. Science, 1997. 277(5330): p. 1232-1237.

23. Decher, G. and Schlenoff, J.B., eds. *Multilayer Thin Films-Sequential Assembly of Nanocomposite Materials.* 2003, WILEY-VCH: Weinheim.

24. Richardson, T.H., Langmuir-Blodgett films, in *Introduction to Molecular Electronics*, M.C. Petty, M.R. Bryce, and D. Bloor, Editors. 1995, Edward Arnold: London.

25. Maggini, M., Karlsson, A., Pasimeni, L., Scorrano, G., Prato, M., and Valli, L., Synthesis of N-Acylated Fulleropyrrolidines - New Materials for the Preparation of Langmuir-Blodgett-Films Containing Fullerenes. Tetrahedron Letters, 1994. 35(18): p. 2985-2988.

26. Goldenberg, L.M., Bryce, M.R., and Petty, M.C., Chemosensor devices: voltammetric molecular recognition at solid interfaces. Journal of Materials Chemistry, 1999. 9(9): p. 1957-1974.

27. Granito, C., Wilde, J.N., Petty, M.C., Houghton, S., and Iredale, P.J., Toluene vapour sensing using copper and nickel phthalocyanine Langmuir-Blodgett films. Thin Solid Films, 1996. 285: p. 98-101.

28. Rella, R., Serra, A., Siciliano, P., Tepore, A., Valli, L., and Zocco, A., Effects of NO_2 oxidizing gas on a novel phthalocyanine Langmuir-Blodgett thin film. Thin Solid Films, 1996. 286(1-2): p. 256-258.

29. Evans, S.D. and Williams, L.M., The formation of organized molecular assemblies via spontaneous adsorption: monolayers to multilayers, in *Functional Organic and Polymeric Materials*, T.H. Richardson, Editor. 2000, John Wiley & sons, Ltd: Chichester.

30. Petty, M.C., Gas-Sensing Using Thin Organic Films. Biosensors & Bioelectronics, 1995. 10(1-2): p. 129-134.

31. Petty, M.C. and Casalini, R., Gas sensing for the 21st century: the case for organic thin films. Engineering Science and Education Journal, 2001. 10(3): p. 99-105.

32. Richardson, T.H., Dooling, C.M., Worsfold, O., Jones, L.T., Kato, K., Shinbo, K., Kaneko, F., Treggoning, R., Vysotsky, M.O., and Hunter, C.A., Taking advantage of optical and electrical properties of organic molecules for gas sensing applications. Thin Solid Films, 2001. 393(1-2): p. 259-266.

33. Snopok, B.A. and Kruglenko, I.V., Multisensor systems for chemical analysis: state-of-the-art in Electronic Nose technology and new trends in machine olfaction. Thin Solid Films, 2002. 418(1): p. 21-41.

34. Casalini, R., Kilitziraki, M., Wood, D., and Petty, M.C., Sensitivity of the electrical admittance of a polysiloxane film to organic vapours. Sensors and Actuators B-Chemical, 1999. 56(1-2): p. 37-44.

35. Simpson, T.R.E., Cook, M.J., Petty, M.C., Thorpe, S.C., and Russell, D.A., Surface plasmon resonance of self-assembled phthalocyanine monolayers: Possibilities for optical gas sensing. Analyst, 1996. 121(10): p. 1501-1505.

36. Wilde, J.N., Nagel, J., and Petty, M.C., Optical sensing of aromatic hydrocarbons using Langmuir- Blodgett films of a Schiff base co-ordination polymer. Thin Solid Films, 1998. 329: p. 726-729.

37. Kato, K., Dooling, C.A., Shinbo, K., Richardson, T.H., Kaneko, F., Tregonning, R., Vysotsky, M.O., and Hunter, C.A., Surface plasmon resonance properties and gas response in porphyrin Langmuir-Blodgett films. Colloids and Surfaces a-Physicochemical and Engineering Aspects, 2002. 198: p. 811-816.

38. Conoci, S., Palumbo, M., Pignataro, B., Rella, R., Valli, L., and Vasapollo, G., Optical recognition of organic vapours through ultrathin calix[4]pyrrole films. Colloids and Surfaces A: Physicochemical and Engineering Aspects, 2002. 198-200: p. 869-873.

Chapter 3

Surface plasmon resonance and its application to bio-chemical sensing

3.1 Introduction

Surface Plasmon Resonance, SPR, has been the subject of theoretical and experimental research for several decades [1-4]. However, only at the beginning of the 1980 was it demonstrated that SPR could be exploited in gas and biological species detection [5-7]. Since then, a growing interest in the SPR principle and technology has been shown by both the scientific community and commercial companies. Nowadays, SPR systems are widely distributed in industrial and university research laboratories. Nevertheless, there is still space for further developments that could expand the capabilities of this technology.

In this chapter, the solid state and electromagnetism concepts that underpin the SPR phenomenon will be discussed. A simple model of the conductive electrons in metals combined with the application of Maxwell's equations to a dielectric/metal/dielectric interface will demonstrate the existence of electronic waves within the thin metal layer. Such collective motion can be triggered by simply illuminating the metal surface. Several practical systems to generate plasmon waves will be introduced: (a) prism-based solutions, (b) grating based systems, (c) waveguide-based plasmon excitation and (d) SPR microscopy (or imaging).

Sophisticated sensing systems can exploit surface plasmon waves. A high sensitivity to (bio)-chemical species is achieved via organic active films deposited onto a metal surface. Specific recognition mechanisms allow selective recognition. Such active materials act as transducing media transforming the chemical interactions into changes in the optical properties of the film, which may be measured by analysis of the SPR curve.

An insight into the commercial SPR market will be given together with some indication of future fields of application, such as in-situ investigation and SPR imaging. A more detailed analysis on SPR multichannel systems will be introduced at the beginning of Chapter 5.

3.2 Surface Plasmon Resonance

Surface plasmons are collective oscillations of electrons that may exist at the interface of two media with dielectric constants of opposite signs, such as in a metal-dielectric system or, under specific conditions, a dielectric-semiconductor system. This perturbation will propagate over a distance of approximately a few microns along the boundary. The electric fields, $\vec{E}$, perpendicular to the interface and penetrating the adjacent media will decay exponentially within a distance comparable to the wavelength of the incident light. Because of these $\vec{E}$-fields, a surface plasmon is able to sense variations (e.g. refractive index) in its surroundings. If both media can be described by a continuum approximation with a dielectric tensor and a magnetic permeability tensor (in general both are frequency dependent and complex) then the basic properties of surface plasmons can be calculated as solutions to Maxwell's equations. One of the simplest theoretical models describing a collection of charged particles in a metal (i.e. the conduction electrons or conductive plasma) is that proposed by Drude [8]. According to this theory, the conduction electrons can be considered as a homogenous "gas" of mobile negative particles within a regular positive potential imposed by the immobile metal ions (positively charged) of the lattice (see Fig. 3.1).

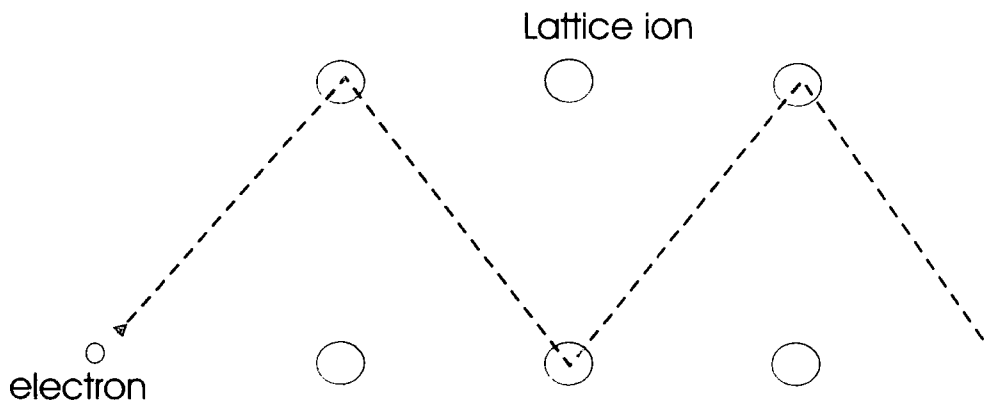

Figure 3.1 Drude's model of a conduction electron in a lattice of metal ions. (Reproduced from [8]).

Using this model together with Maxwell's equations, it is possible to obtain, to a good approximation, the electric and thermal conductivity of metals and to predict the conditions under which plasmons can be supported. Several detailed studies on this subject can be found in the literature [3, 4, 9].

3.2.1 Theoretical basis of surface plasmon resonance: solid state physics and electromagnetism

Electromagnetic radiation in isotropic media consists of oscillating orthogonal electric $\vec{E}$ and magnetic $\vec{B}$ fields transverse to the direction of propagation. On passing such a wave through a linear polarizer, the radiation transmitted will become plane-polarized, i.e. $\vec{E}$ and $\vec{B}$ oscillate in a well defined plane containing the appropriate electromagnetic field vector and the direction of propagation.

When plane polarized electromagnetic radiation falls, at an incident angle θ_i, on a smooth planar interface, two different situations can be considered. In the first, the incident radiation has its electric vector in the plane of incidence, i.e. the plane that contains both the incident and reflected wavector and is perpendicular to the incident surface. Such a situation is illustrated in Figure 3.2.

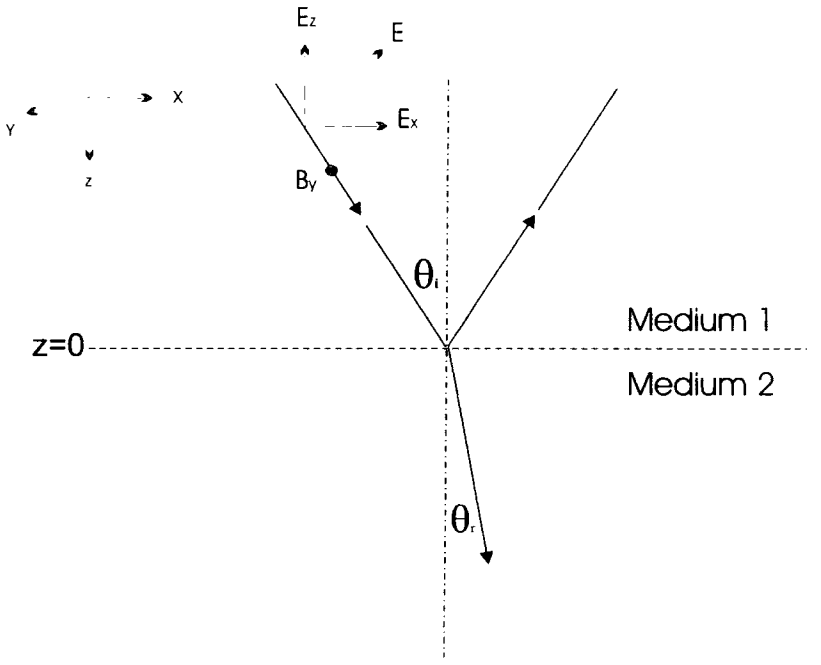

Figure 3.2 Representation of TM (transverse magnetic) radiation incident upon a planar interface between two media at an angle of incidence θ_i. (Reproduced from [10]).

$\vec{E}$ and $\vec{B}$ can be then described

$$\vec{E} = (E_x, 0, E_z)$$
$$\vec{B} = (0, B_y, 0) \tag{3.1}$$

This case is representative of p-polarized radiation, otherwise known as TM (transverse magnetic) radiation because $\vec{B}$ has one only component, B_y, tangential to the interface.

In the second case, $\vec{E}$ will be orthogonal to the plane of incidence, while $\vec{B}$ will have a component B_z normal, and B_x tangential, to the interface

$$\vec{E} = (0, E_y, 0)$$
$$\vec{B} = (B_x, 0, B_z) \tag{3.2}$$

This is the case of s-polarized or TE (transverse electric) radiation. All the other cases of linearly polarized radiation can be described as sums of these two extremes.

It is first assumed that the two media are lossless, i.e. non-absorbing; furthermore, both media are non-magnetic. There is no discontinuity at the interface between the media. The behaviour of the incident radiation will, therefore, be governed by the discontinuity in the dielectric constants. Photons, with momentum $\hbar k$ ($\hbar = \frac{h}{2\pi}$, h being Planck's constant; $k = \frac{2\pi}{\lambda}$ is the wavevector or wave number) in a medium of refractive index n_1, will have a (pseudo)-momentum $\hbar k n_1$. At a planar interface, assuming there is no change in the photon frequency, this momentum will be conserved. The reflected signal will have a component along x equal to that of the incident radiation (at least for a smooth planar surface) while the component along z will simply change sign. Otherwise, for the refracted signal, where there is a change in refractive index from n_1 to n_2, the wavelength will change from λ_1 to $\lambda_2 = \frac{\lambda}{n_2}$. The component along x of the wavevector will remain unchanged while k_z will vary. The conservation of the tangential momentum at the interface can be expressed

$$k_{x1} = k_1 \sin\theta_i = k_{x2} = k_2 \sin\theta_r$$
$$n_1 \sin\theta_i = n_2 \sin\theta_r \tag{3.3}$$

This relation is known as Snell's law and it is a direct consequence of the translational invariance of the system parallel to the interface. A straightforward explanation of the surface plasmon phenomenon comes from the application of this law.

It is assumed that $n_1 = \sqrt{\varepsilon_1}$ and $n_2 = \sqrt{\varepsilon_2}$, with ε_1 and ε_2 the relative permittivities of the first and the second media, respectively. Moreover, the condition $n_2 < n_1$ is also assumed. The greatest in-surface-plane component available in medium 2 is given for $\theta_t = 90^o$. It can be shown that a limiting angle of incidence θ_c exists, given by

$$\sin\theta_c = \frac{\sqrt{\varepsilon_2}}{\sqrt{\varepsilon_1}} \tag{3.4}$$

θ_c is called the *critical angle*. Beyond this angle no incident radiation can propagate in medium 2 simply because it will have, along the surface plane, a momentum bigger than medium 2 could support. At θ_c, the incident radiation is said to undergo total internal reflection. Under this condition there is no net energy transfer from one medium to another. However an optical disturbance occurs at the 1-2 interface, Fig. 3.3 . This disturbance takes the form of an *evanescent* ("vanishing") wave orthogonal to the plane surface, oscillating at the same frequency as the incident radiation and exponentially decaying within the range of the wavelength into the two media. An important feature is that the two opposite penetrating fields are distributed asymmetrically, with a high concentration in medium 2. It is this *evanescent* field that, under particular conditions, can excite the surface plasmons.

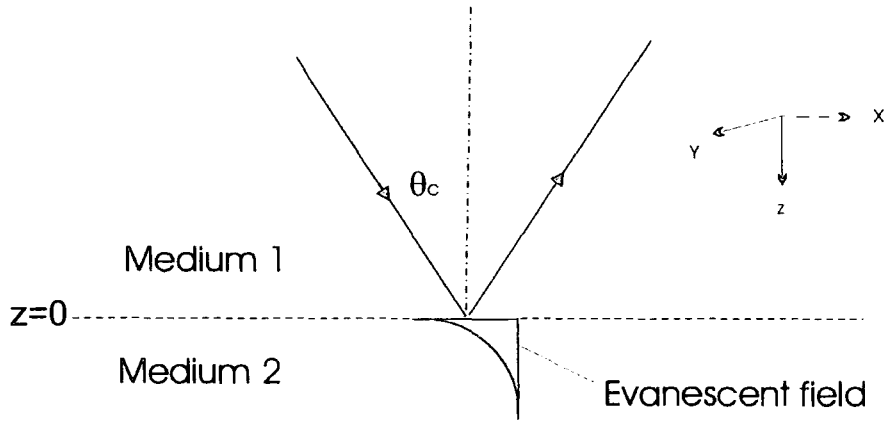

Figure 3.3 Total internal reflection: excitation of an evanescent field at the interface between two media.

To understand the nature of the plasmon wave excitation, it is useful to examine the boundary limitations of the vectors $\vec{E}$ and $\vec{B}$ at the 1-2 interface. While the component E_x will remain unchanged, E_z will undergo a discontinuity. From medium 1 to medium 2 the value of the permittivity will change from ε_1 to ε_2 but, because no free charges exist within the two media, the value of the displacement $\vec{D}$, or better its component along z, has to be constant. This can be expressed

$$\begin{aligned} D_z &= \varepsilon_1 \varepsilon_0 E_{z1} = \varepsilon_2 \varepsilon_0 E_{z2} \\ \varepsilon_1 &\neq \varepsilon_2 \Rightarrow E_{z1} \neq E_{z2} \end{aligned} \tag{3.5}$$

The first requirement for the excitation of surface plasmons is therefore: *only p-polarized radiation will create a time-dependent polarization charge at the interface* (because p-polarized radiation has a component $E_z \neq 0$ along z, while s-polarized radiation has $E_z=0$).

The second requirement comes from the choice of the materials at the interface. A surface plasmon is a surface-bound mode involving a charge density that is actively trapped at the boundary [10]. To establish such a "trap" it is necessary to focus on the material properties. Binding the charge to the surface implies that D_{z1} and D_{z2} must have opposite signs. This can be achieved only if the *dielectric permittivities of the two media are of opposite signs*. Consider a metal as medium 2. A metal is a good conductor of current and heat, and generally, but not always, it will act as a reflector for the radiation incident at its surface.

Reflection of radiation from metals occurs under certain conditions. This property is related to the metal's permittivity, which is itself a function of the frequency of the incident electromagnetic wave. The permittivity-frequency relation is described in terms of a dispersive behaviour. For an ideal metal with undamped free electrons the following relationship can be written

$$\varepsilon_{metal} = 1 - \left(\frac{\omega_p}{\omega} \right)^2 \tag{3.6}$$

where ε_{metal} is the permittivity, ω the frequency of the radiation and ω_p the plasma frequency, i.e. the highest frequency at which the free electrons in the metal can

oscillate. Above ω_p, ε_{metal} will be real and positive and the metal will be transparent to radiation (e.g. metals are partially transparent to gamma radiation but opaque when exposed to visible light or microwaves). Below ω_p, the permittivity will be negative and the electrons will quickly respond to external applied fields. An imaginary component of the permittivity is introduced to take account of absorptive effects due to defects and vibrations. Finally, if infrared light is utilized, even semiconductors can be used in place of the metals since they can have, for these frequencies, a negative permittivity [3].

3.2.2 From Maxwell's equations to SPR

Exciting a surface plasmon requires the coupling of a dielectric (dielectric permittivity $\varepsilon_{dielectric}$ - real and positive) with a metal (ε_{metal} - complex number with the real component negative if the frequency of the incident wavelength is below the plasma frequency, ω_p). As has been explained, this is not the only solution possible, but is the most straightforward. In order to describe this excitation in more detail and to explain the behaviour of the incident light at the dielectric-metal interface, it is necessary to use Maxwell's equations for an electromagnetic wave. To a first approximation, only the real and negative components of ε_{metal} will be included in the calculations. Furthermore, only p-polarized electromagnetic waves will be considered because of the requirement of normal $\vec{E}$ fields to create surface charges. As shown in Equ. (3.3), the conservation of the tangential momentum at the 1-2 interface assures that the component of the wave number k along x remain unchanged, $k_{x1} = k_{x2} = k_x$, while $k_{z1} \neq k_{z2}$. Considering the system of axis in Fig. 3.2, the propagation of the plasmon in the x-direction on the interface plane can be described by the equations

$$\begin{aligned} \vec{E}_1 &= (E_{x1}, 0, E_{z1}) e^{i(k_x x - \omega t)} e^{ik_{z1} z} \\ \vec{H}_1 &= (0, H_{y1}, 0) e^{i(k_x x - \omega t)} e^{ik_{z1} z} \end{aligned} \tag{3.7}$$

for the medium 1 (dielectric), and

$$\begin{aligned} \vec{E}_2 &= (E_{x2}, 0, E_{z2}) e^{i(k_x x - \omega t)} e^{ik_{z2} z} \\ \vec{H}_2 &= (0, H_{y2}, 0) e^{i(k_x x - \omega t)} e^{ik_{z2} z} \end{aligned} \tag{3.8}$$

for medium 2 (metal).

Applying Maxwell's equation $\nabla \cdot \vec{E} = 0$, to $\vec{E}_1$ and $\vec{E}_2$

$$E_{z1} = -E_{x1}\frac{k_x}{k_{z1}}$$
$$E_{z2} = -E_{x2}\frac{k_x}{k_{z2}} \tag{3.9}$$

To find the relationship between H_y and E_x, the third Maxwell equation (or Faraday's law of electromagnetic induction) $\nabla \times \vec{E} = -\mu\frac{d\vec{H}}{dt}$ is used. As medium 2 is non-magnetic, $\mu=\mu_0$, and

$$H_{y1} = \frac{\omega E_{x1}\varepsilon_1\varepsilon_0}{k_{z1}}$$
$$H_{y2} = \frac{\omega E_{x2}\varepsilon_2\varepsilon_0}{k_{z2}} \tag{3.10}$$

Finally, the boundary conditions at $z=0$ need to be applied. As the discontinuity is orthogonal to the interface plane, this implies a continuity equation for the tangential component of $\vec{H}$, ($H_{y1}=H_{y2}$) and $\vec{E}$, ($E_{x1}=E_{x2}$). From the combination of all these relations, the following simple expression between the relative permittivity and the normal components of the wave vectors in both media is obtained

$$\frac{\varepsilon_1}{k_{z1}} = \frac{\varepsilon_2}{k_{z2}} \tag{3.11}$$

Also, the following expressions for the z-component of the wavevectors in the two media are found

$$k_{z1} = -i\sqrt{k_x^2 - \varepsilon_1 k^2}\text{ , requiring } k_x^2 > \varepsilon_1 k^2; \tag{3.12}$$
$$k_{z2} = -i\sqrt{k_x^2 - \varepsilon_2 k^2}\text{ , requiring } k_x^2 > \varepsilon_2 k^2$$

where $k = \frac{\omega}{c}$. To localize the wave at the surface, with exponential decays into both media, it is necessary to have $ik_{z1}>0$, and $ik_{z2}<0$. Therefore, k_{z1} and k_{z2} are imaginary with opposite signs. The permittivities ε_1, ε_2 are also of opposite sign.

From $ik_{z1}>0$, it can be deduced that the surface mode wavevector k_x is greater than the maximum wavevector in the dielectric, $\sqrt{\varepsilon_1}k$. Since the pseudo-momentum of a photon is expressed by $\hbar k_x$, this implies that there is a momentum mismatch between the incident light and the surface plasmon mode. The momentum of the incident optical wave has to be enhanced to match that of the surface plasmon. This momentum change can be achieved using attenuated total reflection (ATR) in prism couplers and optical waveguides, and diffraction at the surface of diffraction gratings. The second condition, $ik_{z2}<0$, is automatically satisfied with ε_2 negative.

Combining equation (3.11) with the relationships in (3.12), gives an expression linking k_x with the relative permittivity of the two media

$$k_x = k\sqrt{\frac{\varepsilon_1\varepsilon_2}{\varepsilon_1+\varepsilon_2}} \tag{3.13}$$

Very often the surface mode wavevector k_x, is indicated with the notation k_{sp} to avoid confusion with the component of the wavevector of the incident or reflected light parallel to the interface (see further discussion). To have a propagating mode, k_x has to be a real number. As ε_2 is negative, this requires $|\varepsilon_2|>\varepsilon_1$.

In summary: satisfying Maxwell's equations for an electromagnetic wave at the interface of the two media leads to the conditions (1) $|\varepsilon_2|>\varepsilon_1$ and (2) $\varepsilon_2<0$. This fulfils the conditions for a trapped surface wave, with real k_x and appropriate k_z.

However, the relative permittivity of a metal is actually a complex number $\varepsilon_{metal}=\varepsilon_2=\varepsilon_{2r}+i\varepsilon_{2i}$. Hence equation (3.13) takes the new form

$$k_x = k\sqrt{\frac{\varepsilon_1(\varepsilon_{2r} + i\varepsilon_{2i})}{\varepsilon_1 + \varepsilon_{2r} + \varepsilon_{2i}}} \tag{3.14}$$

or $k_x = k_{xr} + ik_{xi}$. Provided $|k_{xi}| << k_{xr}$, with $|\varepsilon_{2r}| >> \varepsilon_1$ and ε_{2i}, real and imaginary parts of the plasmon wavevector are

$$\begin{aligned} k_{xr} &\approx k\sqrt{\varepsilon}\left(1 - \frac{\varepsilon_1}{2\varepsilon_{2r}}\right) \\ k_{xi} &= \frac{1}{2}k\left(\frac{\varepsilon_{2i}\varepsilon_1^{3/2}}{\varepsilon_{2r}^2}\right) \end{aligned} \tag{3.15}$$

The imaginary component determines the width of the resonance and is proportional to $\left(\frac{\varepsilon_{2i}}{\varepsilon_{2r}^2}\right)$. In the ideal case, a metal should have $|\varepsilon_{2r}| >> \varepsilon_{2i}$. However, only few metals (e.g. Au, Ag, Al) can support sharp, well-defined resonance curves in the visible region of the spectrum. What is interesting in these equations is that they show a strong dependence of k_{xr} and k_{xi} on ε_1. Any change in the refractive index of medium 1 will perturb the plasmon mode. Therefore, a surface plasmon resonance based device can be used to sense either the presence of an overlayer upon the metal or its alteration. For example, a Langmuir-Blodget film [11] or protein film [12] can be used to coat a metal surface and, as a result of its interaction with a gaseous species present in the atmosphere, detect its nature and concentration.

3.3 SPR devices: working principles and applications

The electromagnetic fields of a surface plasmon wave (SPW) are distributed in a highly asymmetric fashion and the vast majority of the field is concentrated in the dielectric (see Fig. 3.4). A SPW propagating along the surface of silver is less attenuated and exhibits higher localization of the electro-magnetic field in the dielectric than a SPW supported by gold. However, gold is more suitable for application in liquids because it is relatively stable (e.g. does not oxidize). As the excitation of a SPW by an optical wave results in resonant transfer of energy into the SPW, there will be a resonant absorption of the energy of the optical wave. Because of the strong concentration of the

electromagnetic field in the dielectric (an order of magnitude higher than that in typical evanescent field sensors using dielectric waveguides) the propagation constant of the SPW, and consequently the resonance condition, is very sensitive to variations in the optical properties of the dielectric adjacent to the metal layer supporting the wave. Therefore, changes in the optical parameters of the transducing medium can be detected by monitoring the interaction between the SPW and the optical wave.

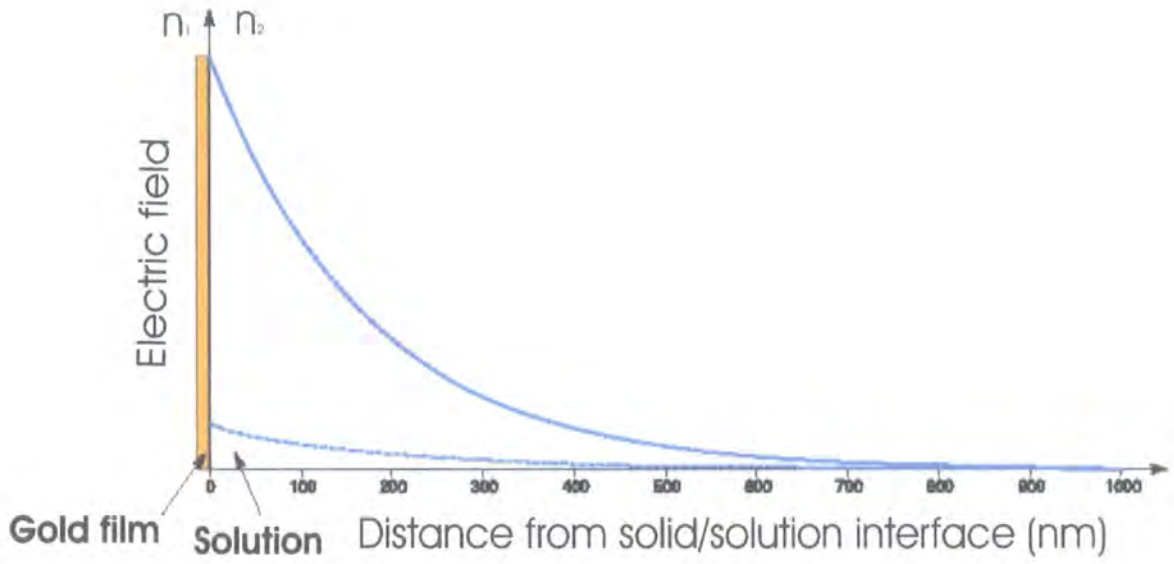

Figure 3.4 Relative evanescent electric field amplitude (E) versus distance to solid/solution interface (nm). Continuous line for SPR-evanescent wave (metal film), dashed line for non-absorbing total internal reflection, TIR (no metal film). (Reproduced from [13]).

If the momentum of the optical wave has been enhanced to match the momentum of the SPW (see further discussions), then a plot of the intensity of the reflected beam against the angle will show a typical SPR plot represented in Fig. 3.5.

As shown, any change to the metal surface (e.g. adsorption of organic molecules) or in the dielectric close to it will result in a variation of the SPR profile (see shift from plot SPR01 to plot SPR02 in Fig. 3.5). What a SPR sensor does is to correlate the detected variations in the reflected beam with the specific phenomenon (e.g. adsorption of chemical species on the metal surface, change of the dielectric surrounding the metal, degradation of the metal itself) that cause these changes to happen. In addition, a mathematical regression law, supported by theoretical calculation, which matches the experimental data, may be found.

In the late 1970s, the potential applications of SPR for the optical characterization of thin films [14] and for the control of processes on metallic surfaces [15] were discovered and first employed for sensing applications. However, it was only in 1982 that Nylander and Ljedberg made a fundamental step forward and used SPR for (bio)chemical-sensing, and studies of biomolecular interactions [5, 6].

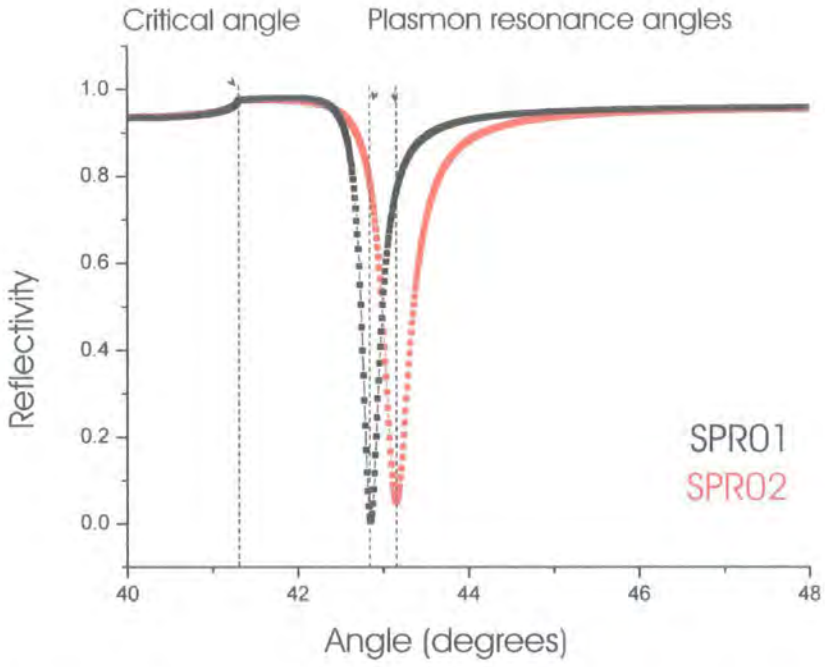

Figure 3.5 Surface plasmon resonance curves. In this case the intensity of the reflected beam is plotted versus the angle of incidence of the light probe. Any change on the metal surface or in the dielectric will modify the plasmon profiles. Variations in reflectivity and in angular position of the reflectivity minimum are used to detect these phenomena. In the example shown, the plot SPR02 is associated with a thin organic film adsorbed to the metal surface, while SPR01 is the SPR profile for the metal only.

The recent success in the integration of organic films (such as Langmuir-Blodgett films, self-assembled monolayers, hydrogels) into microelectronic and optoelectronic devices has led to the development of a number sensors based on SPR [16, 17]. Significant numbers of biomolecular analysis systems have also been produced. The technique is able to monitor rapidly any dynamic process (e.g. adsorption or degradation) on a wide range of interfaces in real time, without the need to label the adsorbate and without the need for complex sample preparation [18]. Using SPR analysis, it is possible to obtain information on the rate and extent of adsorption, enabling the determination of dielectric properties, the association/dissociation kinetics and the affinity constants of specific ligand-ligate interactions [19].

Generally, an SPR optical sensor, comprises an optical system, a transducing medium which interrelates the optical and (bio)chemical domains, and an electronic system supporting the optoelectronic components of the sensor and allowing data processing. The transducing medium transforms changes in the quantity of interest into changes in the refractive index, which may be determined by optical interrogation. The optical part of the SPR sensor contains a source of radiation and structure in which a SPW is excited and interrogated. In the process of interrogation, an electronic signal is generated and processed. Major properties, e.g. selectivity and sensitivity, of an SPR sensor are determined by the characteristics of the active film. The sensor sensitivity, stability, and resolution depend upon properties of both the optical system and the transducing medium.

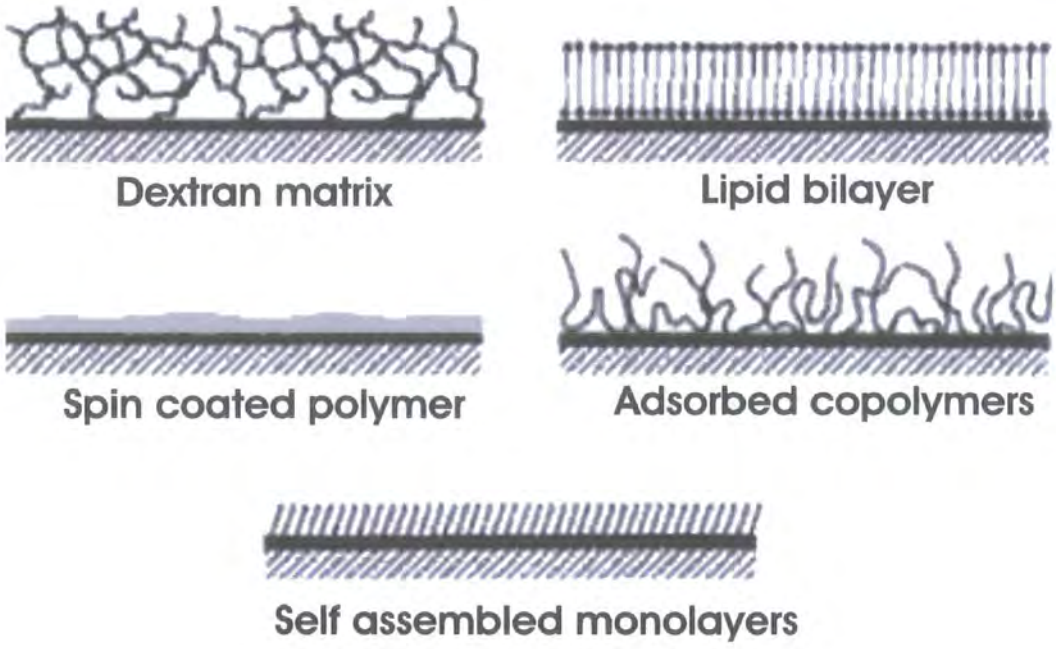

Figure 3.6 The surface of the metal film can be modified to present a variety of surfaces. (Reproduced from [19]).

The selectivity and the response time of the sensor are primarily determined by the behaviour of the transducing medium, thanks to a sensing layer added on top of the metal surface, as shown in Fig. 3.6. Because the probe length of detection inside the dielectric is limited to the wavelength λ [20], ultra-thin films are favoured. Different architectures are available such as Langmuir-Blodgett films, self assembled monolayers,

layer-by-layer self-assembled films and hydrogels. The particular application of the sensor drives the choice of the material suited for the metal coating.

3.3.1 Momentum enhancement

As discussed previously, momentum enhancement is needed to couple the incident radiation to the plasmon wave. The surface plasmon wavevector is $k_x = k\sqrt{\frac{\varepsilon_1\varepsilon_2}{\varepsilon_1+\varepsilon_2}}$; with $k = \frac{\omega}{c}$, ω frequency of the incident light and c the speed of the light. In order to reduce confusion, hereafter k_x will be referred to simply as k_{sp}. Moreover, since it as been established that, generally, a metal is used to sustain the plasmon, a consistent annotation will be used (i.e. $\varepsilon_1 = \varepsilon_d$, relative permittivity of a dielectric; $\varepsilon_2 = \varepsilon_m$, relative permittivity of a metal).

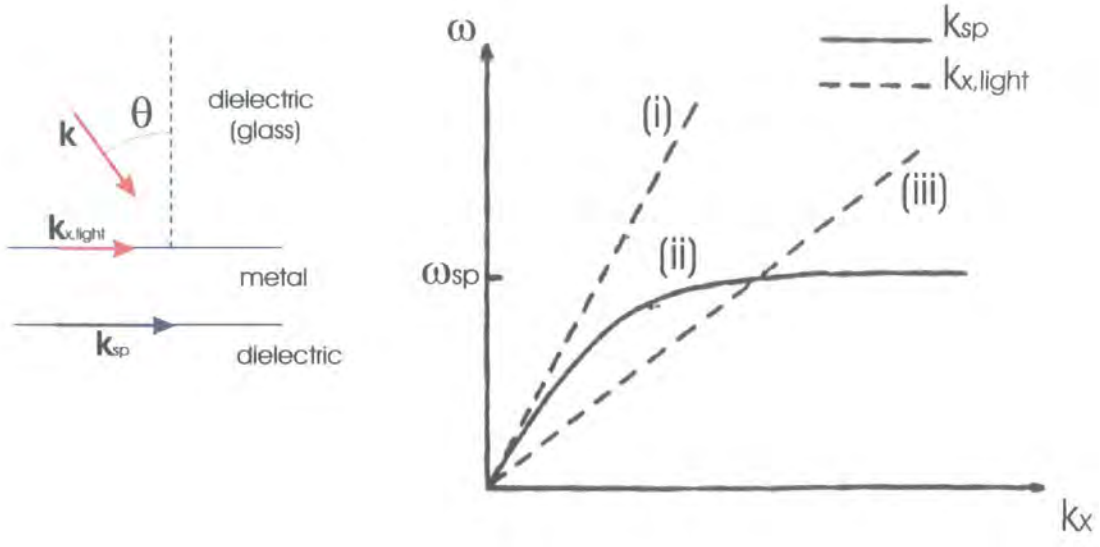

Figure 3.7 (a) The layer system used for surface plasmon resonance. k wavector of the incident light while $k_{x,light}$ is its component along the x axis; k_{sp} wavevector of the plasmon wave. (b) Dispersion curves for (i) light in air; (ii) the surface plasmon; (iii) light in glass. Surface plasmon resonance occurs at the intercept of curves (ii) and (iii). By varying the angle of incidence, the resonance can be obtained for any frequency below ω_{sp}. (Reproduced from [5]).

The light incident on a surface at an angle θ has a wavevector component parallel to the surface, $k_{x,light} = k\sqrt{\varepsilon_d}\sin\theta$. The propagation constant of a SPW is always higher than

that for an optical wave in the dielectric. Consequently, a SPW cannot be excited directly by incident photons at a planar metal–dielectric interface (see Fig. 3.7(a)). In fact, a plasmon is excited on metal surface if and only if $k_{x,light} = k_{sp}$. In Figure 3.7(b) the dispersion curve of the plasmon, k_{sp}, is plotted against ω (curve (ii)). If the light passes through air before being incident on the metal surface (curve (i)), then the two plots do not intersect. Therefore $k_{sp} \neq k_{x,light}$ and no surface plasmon is generated. One of the coupling methods is to make the light to pass through a glass prism or semicylinder. In this way $k_{x,light}$ will shift from position (i) to (iii) in Fig. 3.7(b). This time, there is an intersection between the $k_{x,light}$ plot and the dispersion curve of the plasmon k_{sp}. In other words, the coupling between the incident light and the surface wave is now achieved.

The method described above is only one of the techniques available to enhance of the momentum of the incident optical wave. In Figure 3.8, three of the most common methods are illustrated: (a) attenuated total reflection (ATR) in prism or semi-cylinder couplers and (b) diffraction at the surface of a grating, or (c) optical waveguides.

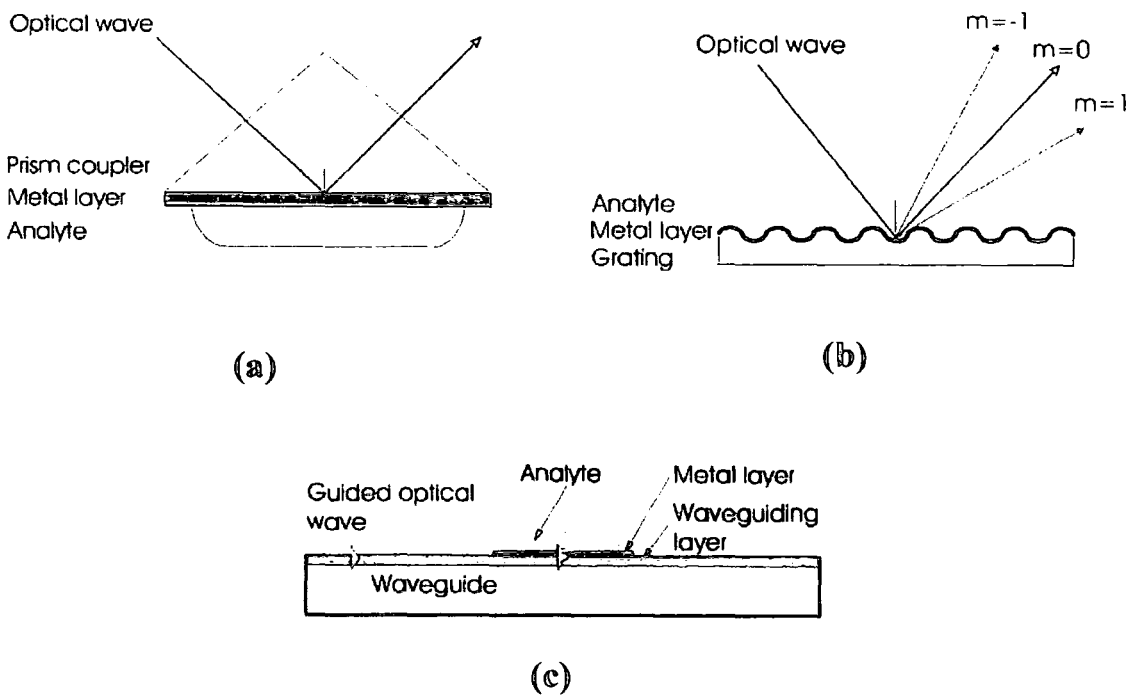

Figure 3.8 Plasmon coupling: most used configurations of SPR sensors. (a) Prism coupling: Kretschmann configuration. (b) Grating coupling. (c) Waveguide excitation. (Reproduced from [17]).

It is also possible to excite SPR by an optic fibre, thereby providing a high degree of miniaturization, Figure 3.9.

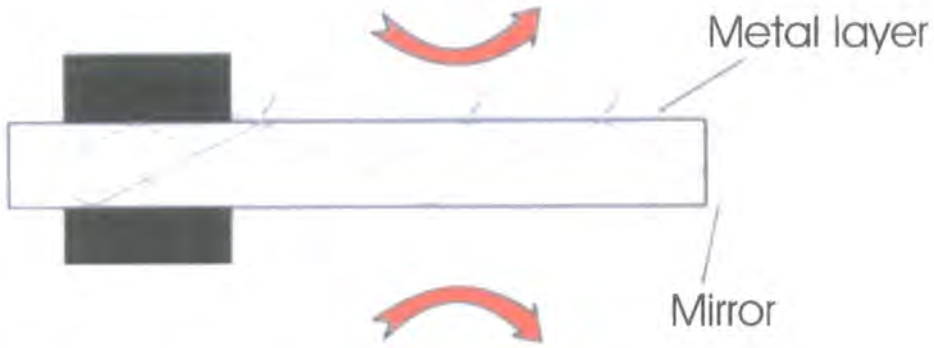

Figure 3.9 SPR excitation via an optic fibre.

Since the SPW is dependent both on the incident angle and the wavelength of the light, two different approaches are suitable for collecting SPR data: (a) scanning angle SPR (or SPR angle shift), (b) SPR wavelength shift. A third variation, SPR Microscopy was introduced in 1988 [21, 22], and because of its characteristic features will be discussed later.

In scanning angle SPR, the wavelength of the radiation is fixed while the incident angle (within the range $\theta_c<\theta<90^o$) is varied. In this way it is possible to have a qualitative picture of the resonance from plots of reflectivity versus angle. Otherwise, the angle can be fixed while the wavelength is varied (however, the limitation $\omega \leq \omega_p$ has to be respected, as shown in Figure 3.7(b)). Only one of the wavelengths will excite the evanescent field and for its value a minimum in the intensity of the reflected light will be found. Therefore a plot of reflectivity versus wavelength similar to that of reflectivity versus angle is obtained. In a recent study [23], a theoretical analysis and comparison of the sensitivity of SPR sensors using diffraction at gratings and attenuated total reflection in prism couplers was presented. According to this research, the grating-based SPR sensors using wavelength interrogation are much less sensitive than their prism coupler based counterparts. In the angular interrogation mode, the sensitivity of SPR sensors using diffraction gratings depends on the diffraction order and does not differ much from that of SPR sensors based on prism couplers.

It is also known that the sensitivity of SPR sensors is affected by the variation of temperature of the sensing environment, leading possibly to lower sensitivity at elevated temperatures. According to Leung and co-workers [24] the angular interrogation approach, at least for prism couplers, seems to have the preferred stability against temperature variations. These workers also postulate that the required sensitivity for wavelength interrogation for prism-based SPR excitation can probably be achieved by operating the optical sensor at temperatures lower than ambient.

3.3.2 Prism coupling

At the end of the 1960s, Otto [1] and Kretschmann [2] described two experimental techniques for optical excitation of surface plasmons by the method of total attenuated reflection. This method results in the appearance of reflection minima which are clearly identified with the generation of surface waves. The two methods are illustrated in Figure 3.10. The system developed by Otto (prism-air-metal: PAM) consists of a prism separated by an air gap from a thick metal or semiconductor sample. When light is incident at angles greater than θ_c, the *critical angle*, it will be normally reflected back out through the prism. However, under total internal reflection conditions, there will always be an exponentially decaying evanescent field extending into the air gap. For such a system, a difficulty arises in keeping the prism-metal distance within the decaying distance of the electromagnetic field. However, if this is achieved, then there is no limitation to the thickness of the metal. In the Kretschmann system (prism-metal-air: PMA), the prism and metal or semiconductor are placed directly in contact with each other. A very thin metal film, of the order of tens of nanometres, is needed. As described above, a value of incident angle greater than the critical angle (and, for practical purpose over a range $\theta_c<\theta<90^o$) is required to excite a plasmon wave on the surface. Kretschmann's geometry has been found to be very suitable for sensing and has become the most widely used coupling method [17].

A third configuration is also possible with a hybrid of the two previous arrangments. The coupling of the light to plasmons is accomplished by the resonant mirror (RM) principle. A small layer of silica (~ 1 mm) is deposited on a prism base. On top of the silica, there is a metal layer with a very high refractive index (e.g. titania in the

commercial IAsys device from Affinity Sensors [25]). This silica layer is thin enough to allow the evanescent field generated on the prism-silica interface to couple into the high refractive index metal. This allows the metal layer to function as an optical waveguide. Repeated total internal reflection of the guided mode within the waveguiding metal layer results in the production of an evanescent field at the metal-dielectric interface. The exact angle of the incident light at which there is a resonance between the waveguided mode and the resulting evanescently coupled light is directly dependent on the refractive index of the dielectric on the outer surface of the metal. In such a device there is virtually no loss of the reflected light intensity associated with the resonance condition. Instead, resonance is accompanied by a change in phase of the reflected light, which is recorded interferometically.

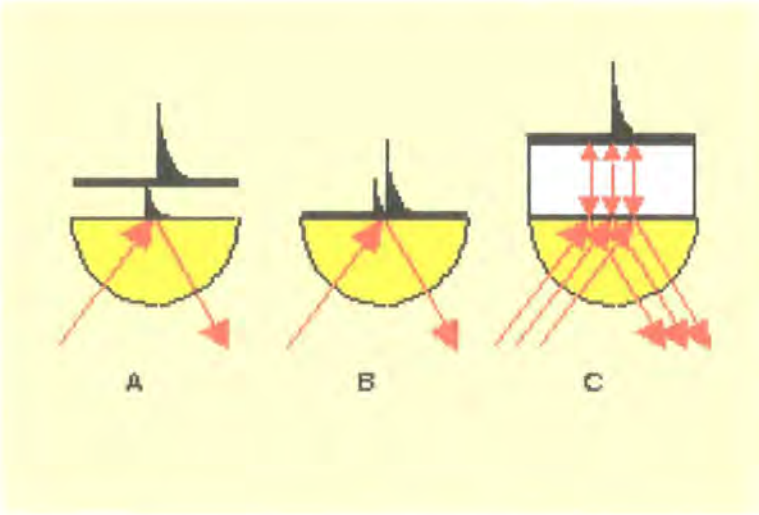

Figure 3.10 Prism coupling: Otto's (a), Kretschmann's (b) and mixed hybrid (c) geometry. (Reproduced from [26]).

Some workers have used a similar approach to excite *long-range surface plasma waves* or LRSPWs [27, 28] to enhance the device sensitivity. By inserting a thin dielectric between the prism and metal, two different interfaces are obtained and two different, but coupled, surface plasmons can be excited. A reflectivity plot will now show two minima in the intensity of the reflected beam. One of these is rather broad and of not much use for sensing. Such a plasmon mode is called a *short range surface plasmon*, SRSP and represents a case in which more energy is lost in metal film. More interesting is the second minimum. This is due to the long-range surface plasmon LRSP and it is far sharper and narrower that a normal resonance minimum. Because the sensitivity of the

device is proportional to $\frac{dR}{dk_{sp}}$ (where R is the intensity of the reflected beam), such an arrangement might be useful for sensing in liquid where, using Kretschmann's configuration, a broadening of the reflectivity plots is registered. In extreme cases such broadening could severely limit the efficiency of the sensing device.

Many other solutions and approaches are available such as the differential SPR sensor [29], or the multi-channel planar substrate SPR probe [30], based on a folded light pipe combined with a telecentric lens (Figure 3.11).

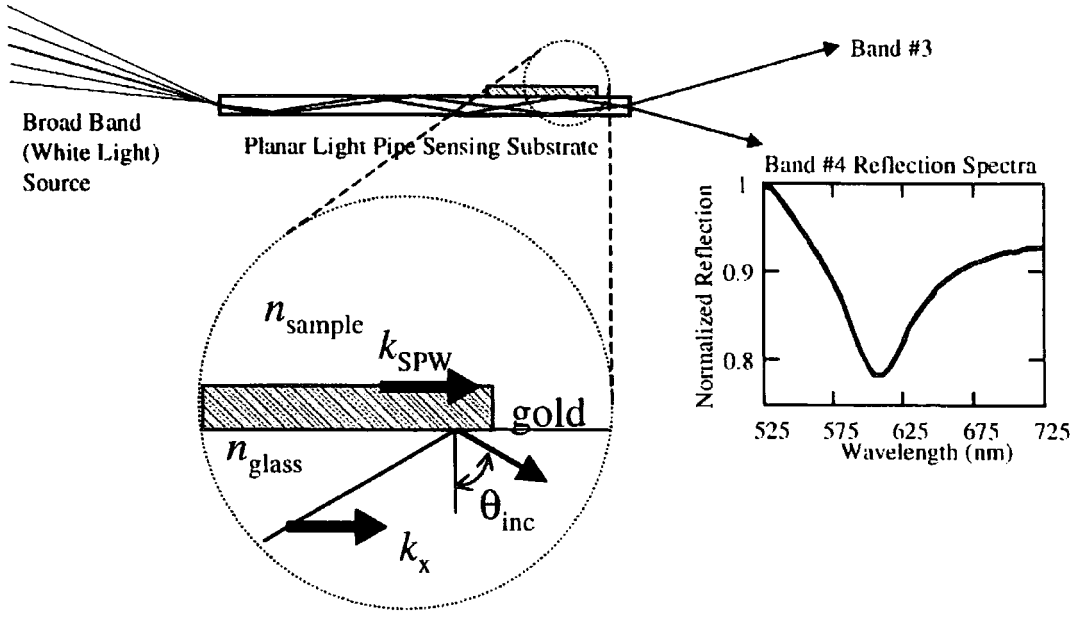

Figure 3.11 Schematic diagram of a planar light pipe SPR sensor. (Reproduced from [31]).

Because it is believed that optical sensors are particularly useful in portable and remote control instrumentation, there is much research activity focused on their development. In particular, one of the main efforts is to reduce the number of moving components. In 1996 [32-34], Texas Instruments introduced the first version (and for the moment the only one commercially available) of a portable SPR sensor (Fig. 3.12). Refined versions of this sensor are, at the moment, the object of study to verify their applicability for high-level research [35].

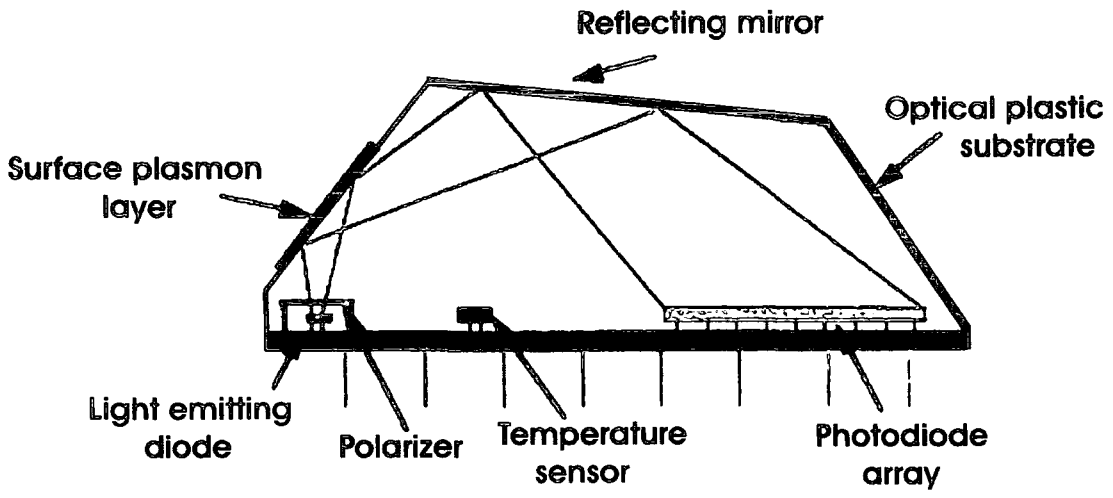

Figure 3.12 The miniature, integrated surface plasmon resonance transducer (TI-SPR-1). (Reproduced from [32]).

Micro-fibre technology has shown to be mature enough to expand the range of miniaturized SPR sensors. In the last few years, several systems have been proposed [36]. There are two main approaches: (a) multimode and (b) single mode [37]. In SPR sensors based on multimode fibres [36, 38-40], the sensing element encompasses a multimode optical fibre with an exposed core, coated with a thin metal layer supporting SPW. These sensors exhibit a rather limited resolution due mainly to the modal noise presented in multimode fibres. This causes the strength of the interaction between the fibre-guided light wave and the SPW to fluctuate. To overcome this inherent limitation, SPR sensors based on a single-mode optical fibre have been proposed [40]. These include sensors based on tapered [41] and side polished [40] single-mode optical fibres. The devices using tapered fibres rely either on spectral interrogation at rather short wavelengths (and therefore exhibit rather low sensitivity) or on amplitude interrogation (also exhibiting low sensitivity due to rather broad SPR dips caused by variations in the SPR condition along the sensing region). Amplitude SPR sensors based on side polished single-mode optical fibres offer superior sensitivity [40], although they suffer from adverse sensitivity due to fibre deformations (as any fibre deformations change the state of polarization of the fibre mode and consequently affect the strength of its interaction with an SPW). A novel approach to the development of fibre optic SPR sensing devices is based on spectral interrogation of SPR in the side-polished fibre optic sensing

element using depolarized radiation [42]. This allows the construction of highly sensitive all-fibre optic sensors less affected by fibre deformations.

3.3.3 Grating coupling

Incident light can be coupled directly to the plasmon mode by distortion of the interface surface, and consequent introduction of diffraction effects. If the distortion of the surface is periodic, it is said to act as a diffraction grating. At the beginning of the twentieth century, Wood observed strong angular dependent variations in the intensity of light that was reflected from an optical metal grating [43]. This excitation is characterized by a charge density oscillation in the metal, which is accompanied by an electromagnetic field that extends in both media. Since the energy is confined to the vicinity of the metal surface, and the conduction electrons of a metal can be treated as a plasma, this excitation leads to surface plasmon resonance.

When an electromagnetic wave is incident on a diffraction grating, the reflected beam will be split into a series of diffracted beams at various angles α [3, 4, 9]. These reflected waves are called *orders* and the non-diffracted beam is said to be the 0^{th} order. As shown in Figure 3.13, an integer value is applied for the other orders.

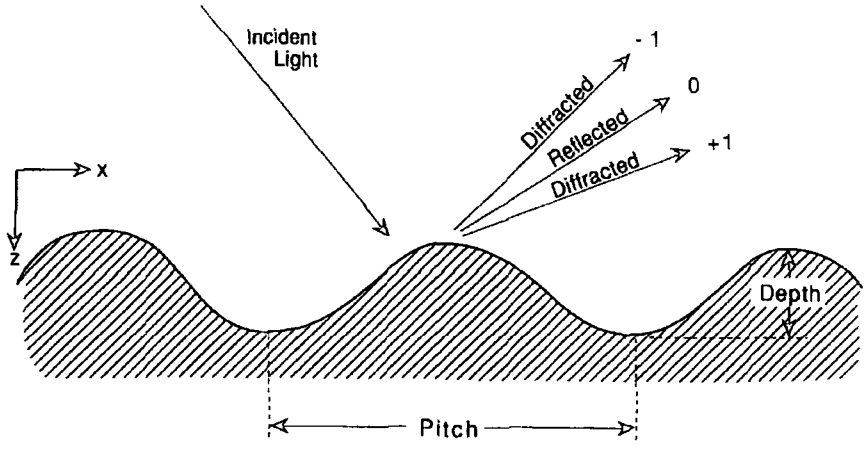

Figure 3.13 Schematic representation of the diffraction of light from a grating's surface. Numbers indicate the order of the diffracted beams. (Reproduced from [10]).

According to De Broglie's relationship, the wavevector of a photon is

$$p = \frac{h}{\lambda} = \hbar \cdot k \tag{3.16}$$

After diffraction, the wavelength of the radiation is unchanged, therefore conservation of the total momentum of the photon is expected. However, if $\alpha \neq \theta$ then the value of k_x must have changed (see Figure 3.14). Discrete steps of change are observed, according the relation

$$k \sin\alpha = k \sin\theta + N \cdot G \tag{3.17}$$

where N is a parameter indicating the order of the diffraction and G is the grating wavector. The latter is function of the *pitch* λ_g of the grating, i.e. the distance between two peaks or valleys in the surface profile, according to the expression $G = \frac{2\pi}{\lambda_g}$. If a metallic grating is used to provide a metal/dielectric interface, a plasmon can be observed if

$$k_{sp} = k \sin\theta + N \cdot G \tag{3.18}$$

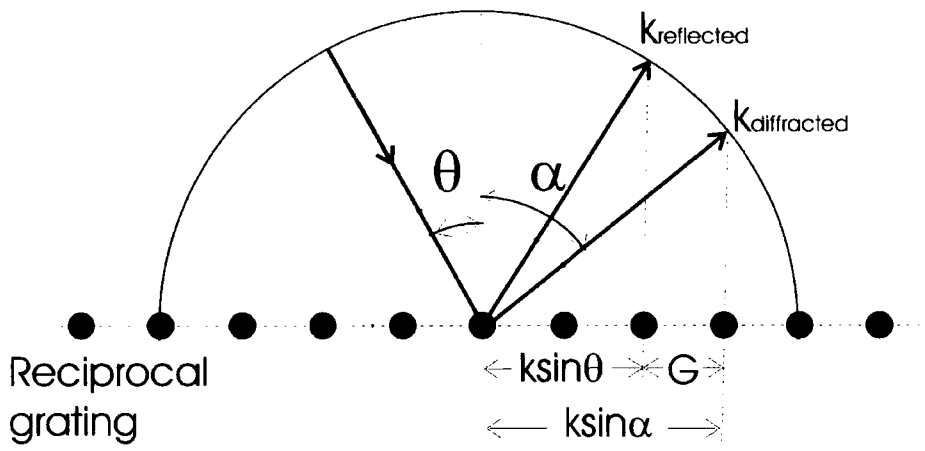

Figure 3.14 Representation in reciprocal space of the diffraction of light from grating. (Reproduced from [10]).

Generation of SPR from gratings has the advantage that there are no complications in the metal thickness or dielectric spacers. The coupling is dictated by the groove depth of the grating. However, experience has shown that it is more difficult to model reflectivity data from such a device than for prism-based coupling [10].

A typical plot of reflectivity versus incident angle is shown in Fig. 3.15. The minimum that appears at θ=32.5° is due to a second plasmon wave travelling in the opposite direction of the wave for which the minimum at θ=15° is associated. Such a wave is a function of the distortion from sinusoidality of the grating. The two critical angles, at θ=12° and θ=35°, correspond to diffracted orders that disappear below the horizon of the grating surface. The major disadvantage in using a grating is that it is not well suited for working in a liquid. If a grating is immersed in a solution, the latter must allow the light to propagate, i.e. to be optically transparent at the wavelength of the probing light, in order to excite the SP. This has been accomplished in some studies [44, 45], but the difficulty of finding a suitable liquid medium has suggested the use of metal gratings for gas and vapours.

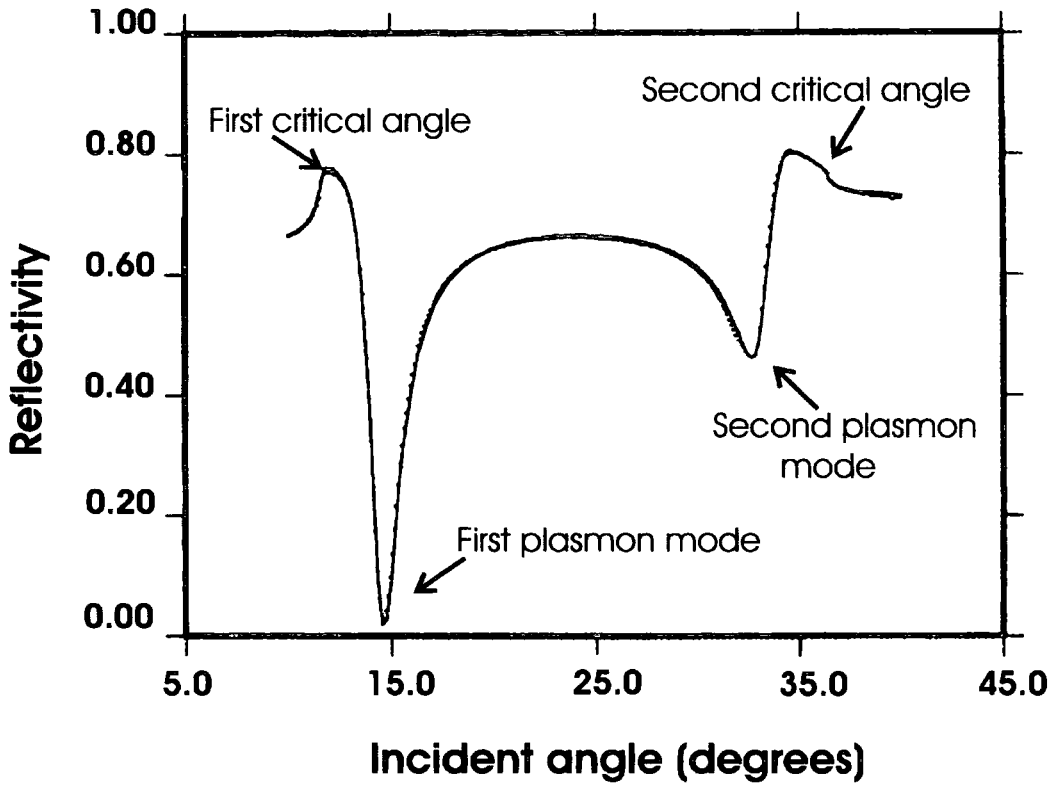

Figure 3.15 Reflectivity data obtained from a diffraction grating. (Reproduced from [10]).

3.3.4 SPR microscopy

Recently, a new approach for data collection and analysis has been introduced [21, 22, 46, 47]. This does not introduce any innovation in the coupling technique, but is a novel way to "read" the SPR resonance. The technique combines the sensitivity of scanning angle SPR measurements with the spatial capabilities of imaging [48]. One of the first applications was in imaging phospholipid monolayer films [46] (see Fig. 3.16). In this experiment, a monolayer film of dimyristoylphosphatidic acid was transferred to a gold-coated solid support at a lateral pressure where both condensed and expanded domains coexist. The light areas in Fig. 3.16 correspond to condensed lipid domains; the dark areas correspond to expanded lipid domains. Since this seminal work, various groups have employed SPR microscopy to investigate the surface morphology of several systems, such as self-assembled monolayer films, mono- and multilayer films prepared by the Langmuir-Blodgett technique, and multilayer films built by alternate polyelectrolyte deposition. Thanks to specially designed arrays of surface-bound species, SPR microscopy has been used to study antibody-antigen, DNA-DNA, and DNA-protein interactions [47].

Figure 3.16 Surface plasmon resonance image of a DMPA (dimyristoylphosphatidic acid) monolayer transferred to a gold solid support. The film is composed of condensed and expanded domains; the condensed phases appear as the light regions in the image (reproduced from [46]).

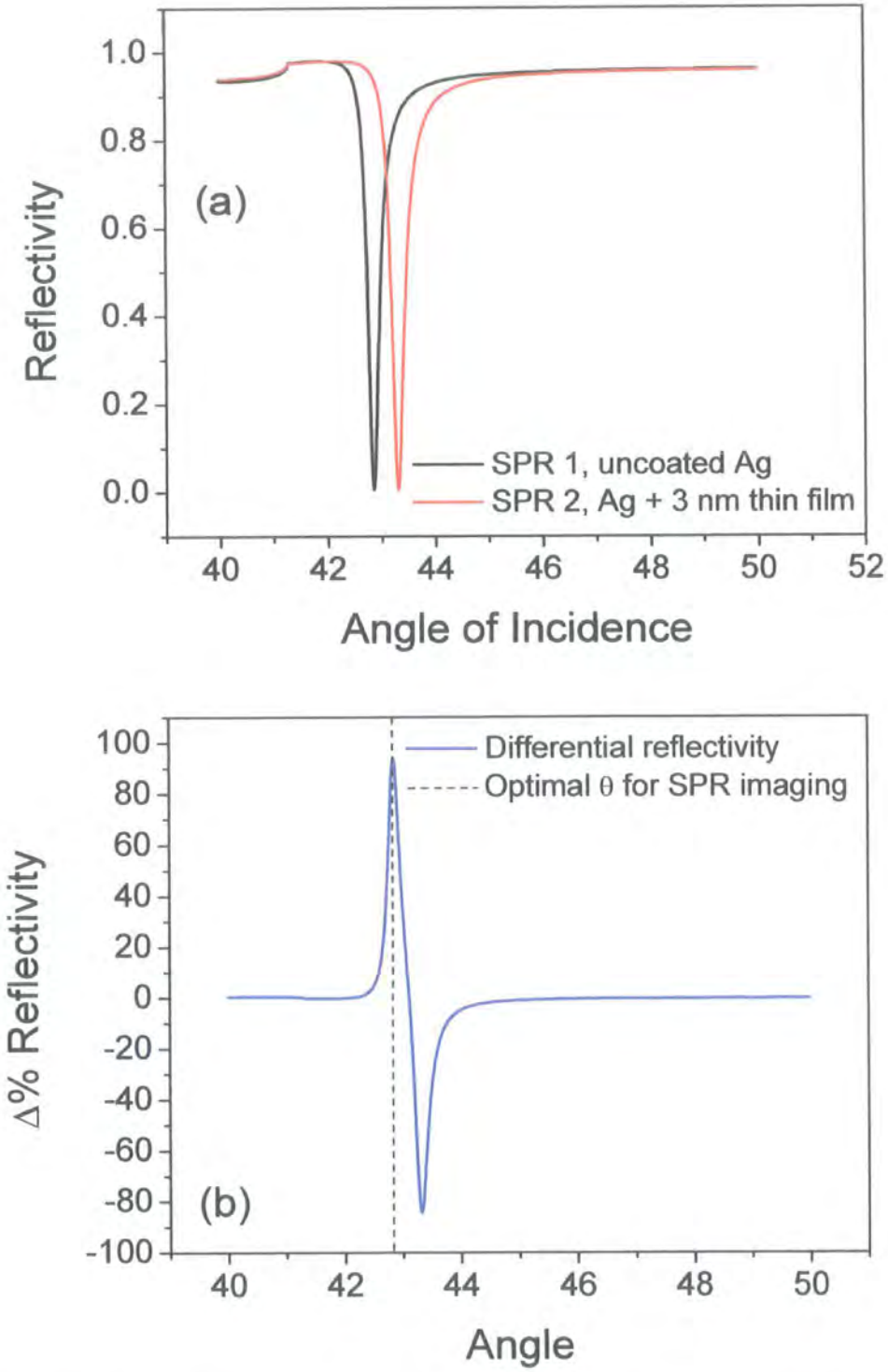

Figure 3.17 (a) Calculated SPR curves at 632.80 nm excitation probe. The black line refers to a three layer system composed of a BK7 glass prism (n=1.515), a 50 nm thick Ag film (ε_{Ag}= -17.784+0.587i) and an infinite layer of air (n_{air}=1.00); the red line refers to a similar system with a fourth 3 nm thick organic film (ε=1.5) deposited onto the Ag. (b) Differential SPR reflectivity curve obtained by subtracting the two curves in (a). The dotted line indicates the optimum angle setting for an SPR imaging measurement.

In a SPR microscopy experiment, spatial differences in the intensity of the reflected radiation (due to differences in film thickness or index of refraction across the metal surface) are measured at a fixed angle. A collimated beam of light is used to illuminate the sample assembly at a single incident angle (near the SPR angle) and the light reflected from the surface is detected by a charge coupled device (CCD) camera to produce the SPR image. In Figure 3.17(a), two different SPR plots are shown. The first curve (SPR 1) is the theoretical prediction of a plasmon excited by an incident light at λ=632.8 nm, using a prism of refractive index n=1.515 and a thin silver film ($\varepsilon_{Ag} = -17.784 + 0.597i$) exposed to air ($n_{air} = 1.000$). In the second case, a thin film with $\varepsilon = 1.396$ is assumed to be deposited on the metal. A shift in the SPR angle due to the increased film thickness and change in the refractive index of the top layer is recorded. The *differential reflectivity curve* is obtained by subtracting the two SPR curves (Fig. 3.17(b)). The maximum and minimum values represent the angles of maximum contrast assuming that not all the silver surface has been coated by the thin film. Therefore, these represent the optimum angles at which to collect data in order to perform SPR microscopy.

The working principle of this approach consists of using a heterogeneous surface where thin films of different thickness and refractive index co-exist. If two different regions are present on the surface, at the angle corresponding to the maximum difference, the areas producing a bigger SPR angle shift will appear on the screen as light spots against a dark background. At the angle corresponding to the minimum difference, the image contrast will be reversed. Both angles are suitable for imaging this two-component substrate. However, if additional adsorption events are to be monitored, it is advantageous to perform experiments at the smaller incident angle to prevent crossover of the image contrast, as the films become increasingly thick.

3.4 Commercial systems and future applications

SPR sensors have been successfully commercialized for over a decade, Table 1. With few exceptions these all use prism coupling for the momentum enhancement. The angle of the incidence of the light probe is achieved by (a) rotation of the light source or the sensing head and (b) using a focused light beam across a range of angles.

SPR manufacturer	System	Description
BIAcore AB (Uppsala, Sweden) http:/www.biacore.com	BIAcore	Prism coupling, microfluidic
Affinity Sensors (Frankiln, MA, USA) http:/www.affinity-sensors.com	IASys	Resonant mirror, cuvette
Nippon Laser Electronics (Hokkaido, Japan) http://www.nle-lab.co.jp	SPR-670	Prism coupling, microfluidic
Artificial Sensing Instruments (Zurich, Switzerland) http:/www.microvacuum.com/	OWLS	Grating coupling, cuvette
IBIS technologies BV (Ensched, The Netherlands) http:/www.ibis-spr.nl	IBIS I/II	Prism coupling, cuvette
Texas Instruments (Dallas, TX, USA) http:/www.ti.com/spreeta	TISPR	Optics integrated within the sensor module, flow cell
GWC Technologies, Inc. (Madison, WI, USA) http://www.gwcinstruments.com	SPRImager	Prism coupling, SPR Imaging, flow cell

Table 3.1 SPR commercial systems.

In the future, *in-situ* sensing and SPR imaging will probably expand the current capabilities of SPR systems.

One of the main requirements for in situ detection is a compact and remote sensor (easy to use and transport, and suitable for hostile environments) [10]. For "real-time" studies, the response time should be as short as possible and the measurement should be made in a non destructive manner. A certain (high) grade of selectivity to a particular analyte is, of course, required, with the ability to work outside a controlled environment. Since SPR is an optical phenomenon, it is ideally suited to these requirements. Optical chemical sensors are promising because the light probe essentially senses the chemicals in a non-destructive manner. Micro-optic components such as optical fibres or wave-guides are the key platforms for this type of chemical sensor.

SPR imaging is very promising because it adds a second dimension of analysis. Working on 2-dimensional images of the sensing chip, it should be possible to analyze different areas of the sample where various active materials are deposited. In this way, several different interactions with the analyte(s) can be detected at the same time.

Applications of SPR to metal ion sensing [49-52], dioxins, polychlorinated biphenylx and atrazine [53] or detergent studies [54] seem to be very interesting fields with plenty of scientifically and commercially stimulating opportunities.

3.5 Conclusions

Surface plasmons are collective oscillations of electrons at the interface of a metal with a dielectric. A theoretical introduction to surface plasmon resonance has been based on elements of solid state physics and electromagnetism. Exploiting the Drude's model of a system of conduction electrons moving in a lattice of immobile metal ions, it was shown that plasmon waves can be derived from Maxwell's equations given the right boundary conditions. Polarized (p-polarized) radiation is needed to excite an evanescent wave.

Because of the strong concentration of the evanescent electric field $\vec{E}$ in the dielectric adjacent to the metal thin film, SPR systems are able to detect variations in the optical properties of the dielectric. An active film deposited on the metal dielectric interface can be used to enhance the sensitivity of the SPR sensors to specific (bio)-chemical species present in the dielectric. The concept of momentum enhancement has been discussed and several coupling methods (prism, grating or waveguide) introduced. The novel technique of SPR imaging was also discussed. Finally, a brief overview of the available commercial products and potential fields of expansion for SPR technology has been presented.

References

1. Otto, A., Excitation of surface plasma waves in silver by the method of frustrated total reflection. Z.Physics, 1968. 216: p. 398-410.

2. Kretschmann, E., Die Bestimmung optischer kostanten von metallen durch anregungvon oberrflachenplasmaschwingungen. Z. Physics, 1970. 241: p. 313-324.

3. Agranovich, V.M. and Mills, D.L., *Surface Polaritons, Electromagnetic Waves at Surfaces and Interfaces*. Modern Problems in Condensed Matter Sciences, ed. V.M. Agranovich and A.A. Maradudin. 1982, Amsterdam-New York-Oxford: North-Holland Publishing Company.

4. Raether, H., *Surface Plasmons on Smooth and Rough Surfaces and on Gratings*. 1988, Berlin: SpringerVerlag.

5. Nylander, C., Ljedeberg, B., and Lind, T., Gas detection by means of surface plasmons resonance. Sensors and Actuators, 1982. 3: p. 79-88.

6. Nylander, C., Ljedeberg, B., and Lundstrom, I., Surface plasmons resonance for gas detection and biosensing. Sensors and Actuators, 1983. 4: p. 299-304.

7. Nylander, C., Chemical and Biological Sensors. Journal of Physics E-Scientific Instruments, 1985. 18(9): p. 736-750.

8. Tippler, P.A., *Physics for Scientists and Engineers*. Third ed. 1995, New York: Worth Publishers.

9. Sambles, J.R., Bradbery, G.W., and Yang, F.Z., Optical-Excitation of Surface-Plasmons - an Introduction. Contemporary Physics, 1991. 32(3): p. 173-183.

10. Lawrence, C.R. and Geddes, N.J., Surface Plasmon Resonance (SPR) for Biosensing, in *Handbook of Biosensors and Electronic Noses: Medicine, Food, and the Environment*, E. Kress-Rogers, Editor. 1997, CRC Press: Boca Raton.

11. Conoci, S., Palumbo, M., Pignataro, B., Rella, R., Valli, L., and Vasapollo, G., Optical recognition of organic vapours through ultrathin calix[4]pyrrole films. Colloids and Surfaces A: Physicochemical and Engineering Aspects, 2002. 198-200: p. 869-873.

12. Liedberg, B., Nylander, C., and Lundstrom, I., Biosensing with surface-plasmon resonance - How it all started. Biosensors & Bioelectronics, 1995. 10(8): p. R1-R9.

13. www.biacore.com.

14. Pockrand, I., Swalen, J.D., Gordon, J.G., and Philpott, M.R., Surface plasmon spectroscopy of organic monolayer assemblies. Surface Science, 1978. 74: p. 237-244.

15. Gordon, J.G. and Ernst, S., Surface plasmons on smooth and rough surfaces on gratings. Surface Science, 1980. 101: p. 499-506.

16. Mandelis, A. and Christofiles, C., *Physics, Chemistry and Technology of Solid State Gas Sensor Devices*. 1993: John Wiley and Sons, Inc.

17. Homola, J., Yee, S.S., and Gauglitz, G., Surface plasmon resonance sensors: review. Sensors and Actuators B: Chemical, 1999. 54(1-2): p. 3-15.

18. McDonnell, J.M., Surface plasmon resonance: towards an understanding of the mechanisms of biological molecular recognition. Current Opinion in Chemical Biology, 2001. 5(5): p. 572-577.

19. Green, R.J., Frazier, R.A., Shakesheff, K.M., Davies, M.C., Roberts, C.J., and Tendler, S.J.B., Surface plasmon resonance analysis of dynamic biological interactions with biomaterials. Biomaterials, 2000. 21(18): p. 1823-1835.

20. Johansen, K., Arwin, H., Lundstrom, I., and Liedberg, B., Imaging surface plasmon resonance sensor based on multiple wavelengths: sensitivity considerations. Review of Scientific Instruments, 2000. 71(9): p. 3530-3538.

21. Yeatman, E. and Ash, E.A., Surface-plasmon microscopy. Electronics Letters, 1987. 23(20): p. 1091-1092.

22. Rothenhausler, B. and Knoll, W., Surface-plasmon microscopy. Nature, 1988. 332(6165): p. 615-617.

23. Homola, J., Koudela, I., and Yee, S.S., Surface plasmon resonance sensors based on diffraction gratings and prism couplers: sensitivity comparison. Sensors and Actuators B-Chemical, 1999. 54(1-2): p. 16-24.

24. Chiang, H.-P., Wang, Y.-C., Leung, P.T., and Tse, W.S., A theoretical model for the temperature-dependent sensitivity of the optical sensor based on surface plasmon resonance. Optics Communications, 2001. 188(5-6): p. 283-289.

25. Hall, D., Use of optical biosensors for the study of mechanistically concerted surface adsorption processes. Analytical Biochemistry, 2001. 288(2): p. 109-125.

26. Marquart, A., http://home.hccnet.nl/ja.marquart/index.html. 2002.

27. Sarid, D., Long-range surface-plasma waves on very thin metal-films. Physical Review Letters, 1981. 47(26): p. 1927-1930.

28. Matsubara, K., Kawata, S., and Minami, S., Multilayer system for a high-precision surface-plasmon resonance sensor. Optics Letters, 1990. 15(1): p. 75-77.

29. Berger, C.E.H. and Greve, J., Differential SPR immunosensing. Sensors and Actuators B: Chemical, 2000. 63(1-2): p. 103-108.

30. Johnston, K.S., Booksh, K.S., Chinowsky, T.M., and Yee, S.S., Performance comparison between high and low resolution spectrophotometers used in a white light surface plasmon resonance sensor. Sensors and Actuators B-Chemical, 1999. 54(1-2): p. 80-88.

31. Johnston, K.S., Mar, M., and Yee, S.S., Prototype of a multi-channel planar substrate SPR probe. Sensors and Actuators B-Chemical, 1999. 54(1-2): p. 57-65.

32. Melendez, J., Carr, R., Bartholomew, D.U., Kukanskis, K., Elkind, J., Yee, S., Furlong, C., and Woodbury, R., A commercial solution for surface plasmon sensing. Sensors and Actuators B-Chemical, 1996. 35(1-3): p. 212-216.

33. Melendez, J., Carr, R., Bartholomew, D., Taneja, H., Yee, S., Jung, C., and Furlong, C., Development of a surface plasmon resonance sensor for commercial applications. Sensors and Actuators B-Chemical, 1997. 39(1-3): p. 375-379.

34. Elkind, J.L., Stimpson, D.I., Strong, A.A., Bartholomew, D.U., and Melendez, J.L., Integrated analytical sensors: the use of the TISPR-1 as a biosensor. Sensors and Actuators B: Chemical, 1999. 54(1-2): p. 182-190.

35. Spangler, B.D., Wilkinson, E.A., Murphy, J.T., and Tyler, B.J., Comparison of the Spreeta(R) surface plasmon resonance sensor and a quartz crystal microbalance for detection of Escherichia coli heat-labile enterotoxin. Analytica Chimica Acta, 2001. 444(1): p. 149-161.

36. Niggemann, M., Katerhamp, A., Pellmann, M., Bolsmann, P., Reinbold, J., and Cammann, K., Remote sensing of tetrachloroethene with a micro-fibre optical gas sensor based on surface plasmon resonance spectroscopy. Sensors and Actuators B: Chemical, 1996. 34(1-3): p. 328-333.

37. Slavik, R., Homola, J., and Ctyroky, J., Single-mode optical fiber surface plasmon resonance sensor. Sensors and Actuators B: Chemical, 1999. 54(1-2): p. 74-79.

38. Trouillet, A., Ronot-Trioli, C., Veillas, C., and Gagnaire, H., Chemical sensing by surface plasmon resonance in a multimode optical fibre. Pure and Applied Optics: Journal of the European Optical Society Part A, 1996. 5(227-237).

39. Jorgenson, R.C. and Yee, S.S., A fiberoptic chemical sensor-based on surface-plasmon resonance. Sensors and Actuators B-Chemical, 1993. 12(3): p. 213-220.

40. Homola, J. and Slavik, R., Fibre-optic sensor based on surface plasmon resonance. Electronics Letters, 1996. 32(5): p. 480-482.

41. Díez, A., Andrés, M.V., and Cruz, J.L., In-line fiber-optic sensors based on the excitation of surface plasma modes in metal-coated tapered fibers. Sensors and Actuators B: Chemical, 2001. 73(2-3): p. 95-99.

42. Slavik, R., Homola, J., Ctyroky, J., and Brynda, E., Novel spectral fiber optic sensor based on surface plasmon resonance. Sensors and Actuators B: Chemical, 2001. 74(1-3): p. 106-111.

43. Wood, R.W., On a remarkable case of uneven distribution of light in a diffraction grating spectrum. Phil.Magm., 1902: p. 396-402.

44. Cullen, D.C., Brown, R.G.W., and Lowe, C.R., Detection of immuno-complex formation via surface-plasmon resonance on gold-coated diffraction gratings. Biosensors, 1987. 3(4): p. 211-225.

45. Cullen, D.C. and Lowe, C.R., A direct surface-plasmon polariton immunosensor - preliminary investigation of the nonspecific adsorption of serum components to the sensor interface. Sensors and Actuators B-Chemical, 1990. 1(1-6): p. 576-579.

46. Hickel, W., Kamp, D., and Knoll, W., Surface-plasmon microscopy. Nature, 1989. 339(6221): p. 186-186.

47. Brockman, J.M., Nelson, B.P., and Corn, R.M., Surface plasmon resonance imaging measurements of ultrathin organic films. Annual Review of Physical Chemistry, 2000. 51: p. 41-63.

48. Yeatman, E.M., Resolution and sensitivity in surface plasmon microscopy and sensing. Biosensors & Bioelectronics, 1996. 11(6-7): p. 635-649.

49. Pearson, C., Nagel, J., and Petty, M.C., Metal ion sensing using ultrathin organic films prepared by the layer-by-layer adsorption technique. J. Phys. D: Appl. Phys, 2001. 34: p. 285-291.

50. Mirkhalaf, F. and Schiffrin, D.J., Metal-ion sensing by surface plasmon resonance on film electrodes. Journal of Electroanalytical Chemistry, 2000. 484(2): p. 182-188.

51. Lee, S.-M., Kang, S.-W., Kim, D.-U., Cui, J.-Z., and Kim, S.-H., Effect of metal ions on the absorption spectra and surface plasmon resonance of an azacrown indoaniline dye. Dyes and Pigments, 2001. 49(2): p. 109-115.

52. Kim, S.-H., Han, S.-K., Jang, G.-S., Koh, K.-N., Kang, S.-W., Keum, S.-R., and Yoon, C.-M., Surface plasmon resonance study on the interaction of a dithiosquarylium dye with metal ions. Dyes and Pigments, 2000. 44(3): p. 169-173.

53. Shimomura, M., Nomura, Y., Zhang, W., Sakino, M., Lee, K.-H., Ikebukuro, K., and Karube, I., Simple and rapid detection method using surface plasmon resonance for dioxins, polychlorinated biphenylx and atrazine. Analytica Chimica Acta, 2001. 434(2): p. 223-230.

54. IBIS-SPR, Surface Plasmon Resonance as a Tool in Detergent Research. 2000/2001, IBIS Technologies BV.

Chapter 4

Polyelectrolytes and the layer-by-layer deposition technique

4.1 Polyelectrolytes: an introduction

The term *polyelectrolyte* (PE) refers to polymer systems consisting of a *macroion*, i.e. a macromolecule carrying covalently bound anionic or cationic groups, and a low-molecular weight *counterion* for electroneutrality [1]. Such materials possess a wide range of molecular and supramolecular structures and a strong dependence of their properties, in solution or in a dispersion, on the surrounding medium. They are closely connected with the process of life (e.g. nucleic acid and proteins) playing an indispensable role in many branches of modern technology. The increased interest in PEs is mainly due to their ability to form organized structures in, or from, solution. The macroions act as the base units of a network, linked by different intermolecular forces that often show a high degree of interaction with the environment.

Polyelectrolytes, usually in water solutions, are used to promote the solubility of macromolecules and chemical compounds and in the stabilization of colloid systems, for waste water treatment, paper making (i.e. neutralization of the so-called anionic trash from the pulp) and as supersorbers. Furthermore, aqueous PEs are employed for phase separation, in surface coatings and adhesives, membranes, microcapsules and controlled release devices, as functional polymers for chemical catalysis or energy transfer and energy transformation processes, and for biomedical purposes by interaction with living matter in the blood stream, cell membranes and the immune system.

The PE family can be divided in three main sub-groups, Figure 4.1. The first group includes all the *strong* polyelectrolytes, i.e. polyions with a well defined and constant charge when in solution in the pH range between 0 and 14 (e.g. poly(styrene sulfonate), PSS or poly(diallyldimethylammoium chloride), poly-DADMAC). All weak polyelectrolytes belong to the second class. These charged polymers are able to form a polyion-counterion system in solution only over a limited range of pH (being dissociated outside this range), e.g. poly(ethylene immine), PEI or poly(acrylic acid), PAA.

Finally, polyampholytes represent a third group. Their chains carry both anionic and cationic groups that are activated in alkaline or acid media, respectively (e.g. proteins or

maleic acid-diallymine copolymer). Therefore, by varying the pH of the solution in which they are immersed, it is possible to reverse the sign of their electrostatic charge.

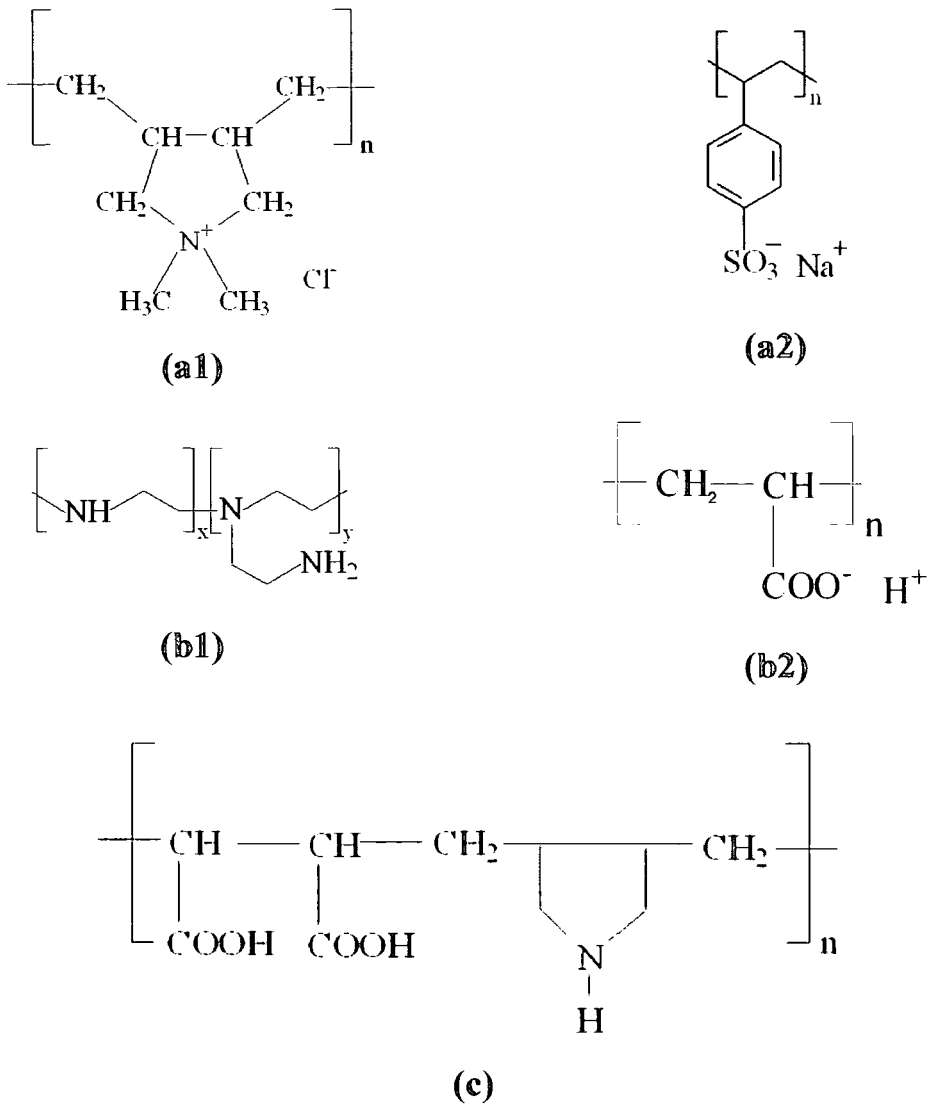

Figure 4.1 Polyelectrolyte sub-groups. Strong polyelectrolyte: (a1) poly(diallyldimethylammonium chloride), PDADMAC; (a2) poly(styrene sulfonate) sodium salt, PSS. Weak polyelectrolytes; (b1) poly(ethyleneimine), PEI; (b2) poly(acrylic acid), PAA. Polyampholytes: (c) maleic acid-diallylamine copolymer.

As shown in Table 4.1, both natural and synthetic PEs, and organic and inorganic PEs are known (e.g. water soluble inorganic polyelectrolytes, polyphosphates and water-soluble polysilicates).

Despite the huge variability in the polymer backbone structure there is a rather small number of different ionic sites responsible for the peculiar behaviour of polyions in solution (see Fig. 4.2).

Polymer class	Application
Natural PE	
Pectin	Nutrition
Aginate	Nutrition, pharmacy, microcapsules, textile industry
Gum arab	Pharmacy, adhesives
Anionic starch	Paper industry
Cationic starch	Paper industry
Chitosan	Membranes, pharmacy
Synthetic PE	
Polyacrylic acid and copolymers	Water treatment, microcapsules
Maleic acid anhydride copolymers	Adhesives, paper industry
Polyethylene imine	Paper industry
Polyamidamine	Sludge treatment
Ionones	Water treatment, membranes
Poly-DADMAC	Water treatment, membranes

Table 4.1 Classes of commercial polyelectrolytes and their application. (Reproduced from [1]).

Figure 4.2 Chemical structures of ionic sites of polyelectrolytes.

One of the most interesting properties is the ability of PEs to dissolve in water (aqueous media are generally the most common environments) even if, as for polystyrene, they possess a hydrophobic backbone.

The physical chemistry and processing characteristics of PEs are dependent on their behaviour in solution and/or dispersion. PEs combine properties derived from long chain molecules with those that result from charge interactions. However, this combination is more than a simple superposition. There are four important parameters that need to be considered.

The first is the acidic or basic strength of the ionic site. Strong ionic sites give strong PEs and vice versa, similar to the division of weak and strong acids or bases in low molecular weight chemistry. The average distance between adjacent charges along the chain (i.e. charge density) and the regularity of distribution of the ionic sites also play an important role in determining PE properties. Another important parameter is the location of the charged sites within the molecular geometry of the polymer, i.e. does the charge form part of the backbone (integral PE) or is it attached to it (pendant PE)? Finally, the solubility and structure of polyelectrolytes depends markedly on the nature of the counterions with which they are associated.

A significant parameter is the *viscosity,* η_{spec} , of strong and weak polyelectrolytes expressed as function of the polymer concentration, c. In strong PEs this is found to depend mainly on the ionic strength of the aqueous medium (due to the electrostatic shielding of the electric charges). In contrast, in weak PEs, the pH affects the degree of dissociation for a given ionic group and consequently its charge density. For comparison see Fig. 4.3, in particular note, in Fig. 4.3 (b), that in the pH range of the isoelectric point for the polymer considered, there exists a viscosity minimum.

Particular attention in these studies is given to the formation of complexes between charged macromolecules and oppositely charged macroions, surfactants or colloidal particles. Here, Coulombic forces are predominantly, but not exclusively, involved. In addition, hydrogen-bonds and hydrophobic forces are important [2].

PEs in solution show a rather high ionic conductance with migration of macroions and/or charged polymer colloids if subjected to an electric field. Ionic conductance is observed in gels and other polyelectrolytes that swell in water (with a strong influence on the water content for the latter type).

PEs represent a promising class of materials for nanotechnology applications thanks to a convenient method to assemble these compounds into thin film architectures of nanometre dimensions: the Layer-by-Layer (LbL) deposition technique. Examinations of the interactions within these systems have estabilished the diversity of structures, film morphology and surface properties achieved by altering shielding and adsorption conditions.

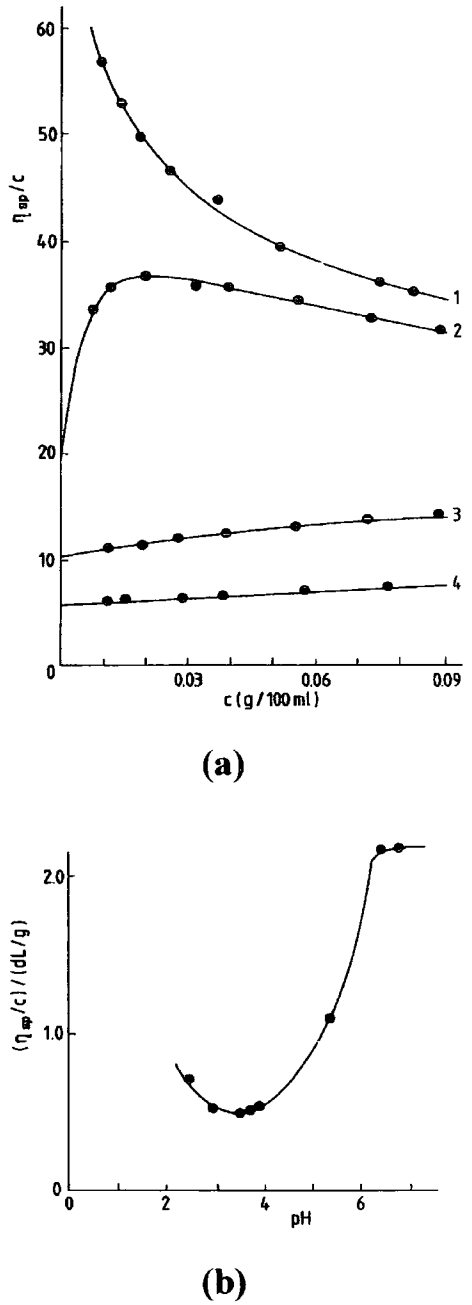

Figure 4.3 Viscosity plots. (a) Strong polyelectrolyte: dependency of η_{spec}/c for aqueous solution of Na-carboxymethylcellulose at different ionic strength: (1) no NaCl added, (2) 2.5x 10^{-4} mol NaCl/litre, (3) $5x10^{-3}$ mol NaCl/litre, and (4) $5x10^{-2}$ mol NaCl/litre. (b) Weak polylectrolyte: plot of η_{spec}/c vs pH of an aqueous solution of an alternating copolymer of maleic acid and n-methyldiallylamine. (Reproduced from [1]).

4.2 Layer-by-Layer self assembly

The Layer-by-Layer deposition technique is one of the most useful developments in the last few years in the field of monolayer assembly. This method *gives opportunities for*

creative design and application of function-specific films. Multilayers bridge the gap between monolayers and spun-on or dip-coated films, and they provide many of the aspects of control found in classical Langmuir-Blodgett (LB) films, yet multilayers are more versatile, in many respects, and easier to create.[1]

LbL assembly is based on the principle of alternate deposition of oppositely charged polyions (Fig.4.4).

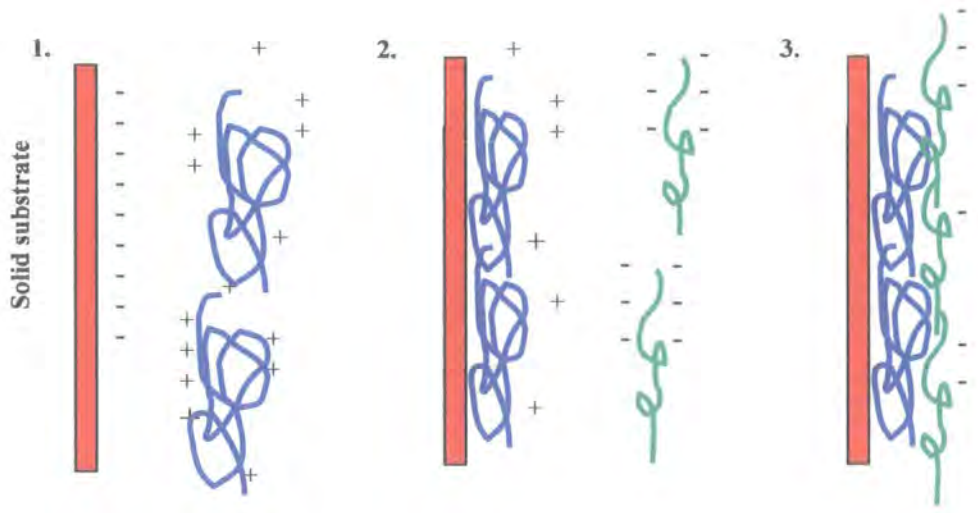

Figure 4.4 Scheme of layer-by-layer self-assembly. In this example, a negatively charged substrate is immersed in a solution of a positively charged polyelectrolyte. The electrostatic attraction between the two results in the adsorption of the polymer on the substrate surface, therefore the solid/ solution interface is now positively charged. Repeating the immersion in a polyanion solution will result in the formation of a second adsorbed layer. Such an operation can be repeated several times to obtain the desired thickness of the multilayered film.

The pioneer of this area was Iler [3], who studied charged colloid particles and proteins. Others authors (e.g. Fromherz, Mallouk et al.) have also worked on this topic. However, only with the work, in 1991, of Decher and Hong [4, 5], did the scientific community start to focus on this technique. In a very successful paper that has become a milestone in the field, Decher describes the LbL assembly as a *fuzzy nanoassembly* [6]. One of the main themes of research in the last 13 years has been to define the order in these structures and to enhance and manipulate their molecular organization.

[1] Jean-Marie Lehn, foreword of *Multilayer Thin Films-Sequenial Assembly of Nanocomposite Materials*. 2003, Decher, G., Schlenoff J.B., ed., WILEY-VCH.

A certain degree of interpenetration and overlapping of the polymer layers has been confirmed [6-8]. However, such architectures still manage to possess a defined layer order [6, 8]. Each layer has a fixed spatial location but within it there is some deviation. The considerable amount of work invested in LbL films has resulted in an increased ability to tune and control this deviation. A high degree of control and understanding is necessary for the full exploitation of the assembled nanocomposites. This is accomplished only if the location and/or orientation of every molecule is known with respect to each other and in respect to the macroscopic device [6].

LbL assembly is template-assisted and its starting point is normally a solid substrate with a negatively charged surface (see Figure 4.4) [9]. The adsorption of a cationic polyelectrolyte is carried out at a relatively high concentration and the solution pH or salt content must be controlled to provide a high degree of ionization. Following the polycation adsorption, a number of ionic groups remain exposed at the interface with the solution, resulting in a reversal of the surface charge. The substrate is then rinsed in pure water or, preferably, in a buffer solution to keep the polyions ionized. Rinsing may remove weakly attached material. The substrate is now ready for exposure to a solution containing the anionic polyelectrolyte. Again, a layer is adsorbed and the surface charge restored. By alternating these two steps, multilayer structures are obtained with a precisely repeatable layer thickness. It is possible to vary the thickness of the ultra-thin ordered film from 10 to 1000 nm. A precision of better than 1 nm in the layer thickness is achieved as well as a definite knowledge of the molecular composition. These thin organic layers can thus be tailored for particular applications [10-15]. In addition, it should be noted that alternate adsorption is not restricted to electrostatic forces. Using metal coordination or specific interactions (e.g. for biomolecules) it is possible to obtain similar multilayer architectures.

The advantages of LbL deposition over the "classical" Langmuir-Blodgett assembly (a technique of great elegance and fascination but, possibly, one that is less practical) include: (a) a high versatility (being applicable to almost every solvent accessible surface); (b) a vast range of substances may be deposited (not just polymers, but colloids, proteins, DNA, inorganic compounds etc.); and (c) tailoring of surface interactions and therefore of the interaction between the assembled object and its environment (e.g. surfaces specially designed for bio-compatibility, corrosion

protection, anti-static coatings, sensing, surfaces with specific adhesion or wetting properties, improved surface conductivity or ion transport).

Many processing parameters such as solution concentration, ionic strength, adsorption time, solvent composition, temperature, humidity, pH allow a degree of control of the assembly process and therefore of the nanocomposite functionality and characteristics. However, a change in any of these parameters could bring an unexpected variation in the multilayer properties (e.g. its thickness). Therefore, particular attention to the deposition conditions is essential.

The deposition method has the advantage of simplicity, versatility and speed. Furthermore, there is a wide range of different materials available to build complex supramolecular structures. A number of different applications for LbL layers has been suggested [2, 8, 9, 16-19]. Polyelectrolyte architectures have been exploited for surface compatibilization and surface protection, (bio)sensors, enzyme immobilization, gene transfection, separation membranes and chromatography columns, light emitting devices or photonic structures, high charge density batteries, orientation layers, optical data storage and magnetic films, controlled particle and catalyst preparation and encapsulation and drug delivery [2, 8, 16, 20]. Already a number of patents exist [21 1993 1993, 22 1996 1996, 23 2002 2002, 24 2002 2002, 25 2002 2002]. A commercial ophthalmic lens will be the first commercial product, that use an LbL polyelectrolytes coating, to be launched on the market [8].

4.2.1 Film growth

The alternate LbL assembly process may exhibit a non-linear film growth in the early stages. During the formation of the first two to three layers, only small amounts of polyion are adsorbed. In contrast, in subsequent adsorptions, film mass and thickness increase linearly with the number of adsorption cycles. Tsukruk et al. [11] have suggested an island-type adsorption model for the first polyion layer on a weakly charged solid support. On increasing the number of steps, the islands spread on the support until they achieve a full coverage. From this point, linear growth commences. By changing the ionic strength (i.e. varying the salt concentration) of a strong

polyelectrolyte solution, the thickness of the single layer, and consequently the overall film thickness can be precisely adjusted. When the solid substrate is in contact with a low ionic strength solution (e.g. water) there is a strongly charged polyion adsorption process, which results in a highly packed and well-attached layer. In a high ionic strength solution, the polyion chains are partially neutralized, which provides an adsorption process with major loops and a much greater film growth step. In general, high ionization of polyions results in a smaller step of film growth and lower ionization gives a larger growth step. In Chapter 6, a more detailed description of growth regimes will be given.

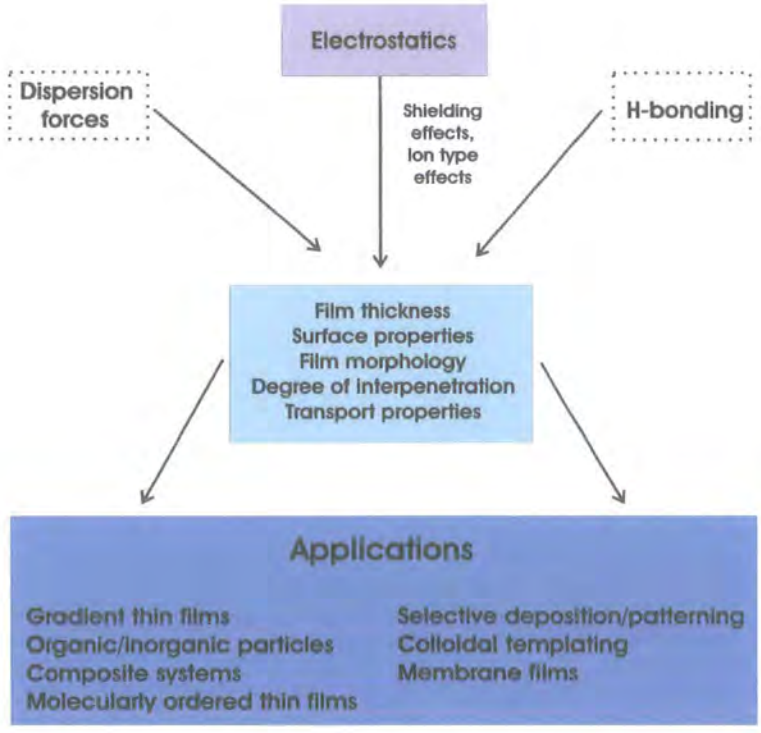

Figure 4.6 Schematic diagram of forces influencing properties of layer-by-layer films, and the applications achieved by controlling or manipulating these interactions with processing. (Reproduced from [2]).

The kinetic of the film growth for LbL self-assembly should, very likely, have some similarity with that of other classes of thin films. Defining σ, as the number of atoms adsorbed per square cm (or molecules per square cm, or, as in the case of most of the LbL self-assembly, macromolecules per square cm) and ν, as the rate of evaporation, it is possible, then, to introduce a time constant $\tau=\sigma/\nu$. The use of the term *evaporation* should not come as surprise since the original application of such theories was in gas-

solid interaction studies. What it is important to notice is that the adsorbed atom or molecule has a probability to leave the surface or to remain on it, in function of various parameters such as temperature or applied energy field. The time constant τ represents the average life of an adsorbed atom or molecule on the surface while its reciprocal $1/\tau$ is the average probability per second for the adsorbed entity to leave the surface itself [26]. In the vast majority of the cases, the observation of such adsorption process in function of the time t (via, for example, the analysis of the intensity of the reflected beam in a SPR set-up [27] or Auger electron spectroscopy [28]) leads to the following kinetic model for the quantity under observation y

$$y = a(1 - e^{-\frac{t}{\tau}}) \tag{4.1}$$

with a, the constant of saturation level (i.e. the asymptotic value to which the equation tends). More importantly, these kinds of analysis bring an estimation of the amount of material adsorbed and, ultimately, to the surface coverage achieved, i.e. the ratio of the number of sites occupied by the adsorbed species and the total number of sites available on the solid surface. For example, SPR studies can correlate the angular or wavelength shift in the plasmonic surface wave (induced by the adsorption of bodies on the surface of a thin metal film) to a variation in refractive index and thickness of the adsorbed layer. Although the evaluation of these parameters is not independent, alternative approaches such as the use of the Feijter's equation can then lead to the final determination of the amount of material adsorbed [29].

Several mechanisms of adsorption have been proposed together with various adsorption isotherms either in the form "Amount adsorbed vs. Equilibrium concentration" [30], or "Surface coverage vs. Pressure" [28]. The most common model is the Langmuir isotherm describing ideal chemisorption systems. It does assume that the adsorption cannot proceed beyond monolayer coverage, that all the sites are equivalent and that the surface is uniform and, finally, that the ability of a molecule to adsorb at a given site is independent of the occupation of neighbouring sites. To overcome the limitation of this model other, alternative, approaches have been proposed such as the Freundlich isotherm that takes in consideration the influence of the heat of adsorption on the surface coverage and can be applicable to both chemisorption and physisorption

systems. To take in account that not all sites are energetically equivalent, the Temkin isotherm can be exploited. Finally, since the overlayer may act as a substrate for further adsorption (multilayer growth), the isotherm does not level to a saturated value at high pressures like in the Langmuir model, but it is expected to rise indefinitely because there is no limit to the amount of material that may adsorb to form the multilayer structure. The most widely used isotherm for such an event was derived by Brunauer, Emmet, and Teller and is called the BET isotherm. More detailed information of this subject can be found in the specialized literature [28, 30-32].

Understanding the nature of the forces that drive the LbL assembly is one of the main concerns of the scientific community. As noted previously, electrostatic attraction between positively and negatively charged species is considered to be fundamental for the assembly of the final structure of the polyion layered thin film [2]. However, forces (see Figure 4.6) such as hydrophobic interactions, charge transfer interactions, π–π stacking forces or hydrogen-bonding strongly contribute to the success of LbL deposition for a given system [33, 34]. In particular cases, alternative interactions may be strong enough to allow for a layer-by-layer self-assembly without ion-ion interactions [35]. Therefore, the type and the amount of charged groups fixed to a polymer cannot be the only criteria to predict the success of LbL assembly. Secondary interactions can also play a role in the selective deposition of polymers on surfaces, the formation of acentric polar structures, and the nature of permeation and ion transport within the film. According to Kotov [33] and his "free energy analysis model" the contribution of hydrophobic interactions in LbL adsorption has to be considered carefully. In Kotov's model, the free energy of adsorption of a positively charged polyelectrolyte to a negatively charged polyelectrolyte surface includes several independent contributions. These include the energy associated with the release of small counterions and the partial removal of the hydration shell around both positively and negatively charged polyelectrolytes. Moreover, the energy associated with the formation of the polyelectrolyte complex, a free energy associated with the liberation of structured water molecules around hydrophobic portions of the polyelectrolytes, and the increased short-range van der Waals interactions between these hydrophobic regions also have to be considered.

The analysis suggests that without the added effects of hydrophobic interactions at the surface, typical polyion systems would not adsorb at all (e.g. protein complexes do not form stable layers on hydrophilic aluminosilicates, but form very stable layers on hydrophobic negatively charged polyelectrolyte surfaces). LbL assembly is favoured primarily by a gain in *entropy*, not in enthalpy [19]. When low molar mass counterions are liberated after the adsorption of a polyion on a charged surface there is first an increase of the system entropy. An additional entropy gain derives from the liberation of solvent molecules from the solvation shell of the polymer-bound ionic groups. The number of electrostatic bonds in the overall system is not altered on polyion adsorption, thus the change in enthalpy, at least to a first approximation, can be neglected. However, the number of ions per molecule/nano-object adsorbed may play a role in the binding, as well as the equivalence of this number for the polycation and polyanion used.

Polyelectrolyte adsorption under normally chosen conditions is nearly irreversible, so that the built-up films do not represent equilibrium structures. Therefore in LbL assembly particular attention has to be devoted to the kinetic control of the process [19]. In order to control film growth, careful adjustments of the various process parameters are needed. A great contribution in the understanding of such phenomena has come from the studies conducted by Rubner and co-workers on weakly charged polyelectrolytes [15, 36, 37]. By varying the pH of weak PEs solutions, this work has showed it is possible to affect the relative amount of charge along the backbone. The layer thickness and stability can thereby be controlled. For strong polyelectrolyte chains, this can be accomplished by altering the ionic strength by the addition of salts to the polymer solution. The ions dissociated from the salt shield the electric charge of the strong PEs, resulting in a more flexible chain.

For weak PEs, systematic control of the layer thickness, the level of layer interpenetration, and the surface "wettability" of sequentially adsorbed layers of poly(acrylic acid) (PAA) and poly(allyamine hydrochloride) (PAH) was achieved by variations in the linear charge density of both polymers [37]. The thickness contributed by an individual polyion layer was found to depend primarily on the pH of the polymer's dipping solution and, within the pH range examined, was not influenced by the thickness or level of interpenetration of the previously adsorbed layer.

It is evident that controlling the characteristics of film assembly on such a nanoscale level, via pH variations or adding salt to the polyion solution, can result in a significant improvement in the film architecture, which can be tailored for particular applications.

Other researchers have examined the adsorption process for hydrophobically-modified polyelectrolytes [38], finding that these polymers uncoil on adsorption on a highly charged surface, and can form quite stable multilayer films. When the films are exposed to air-drying or storage in other solvents, rearrangement takes place rapidly on the surface. These short-range interactions can be exploited to create thicker films based on hydrophobic and electrostatic interactions on surfaces.

Hydrogen bonding can also be a useful force in sequential adsorption-based self-assembly. Since the first demonstration of hydrogen bonding as the basis for alternating polyion assembly [39], others have explored the possibilities of H-bonding as an assembly tool in layer-by-layer films. In particular, Pontes et al. [40] have pursued this approach to build up thick multilayer films using a single adsorption step taking advantage of the lack of self-limiting adsorption behaviour.

4.2.2 Substrates and templates

The range of substrates that can be used as templates for the multilayer self-assembly is wide with little restriction on their type or shape. The only feature required by the surface of the substrate is for it to possess an electric charge. This can be achieved in different ways. For example, it is possible to use freshly cleaved mica or a glass/quartz slide, or a silicon wafer, covered by a layer of cationic polyethylenimine (PEI). Good quality surfaces are obtainable by amino silanization procedures, by plasma treatment, as well as by sonification in an appropriate solution or by the deposition of a charged amphiphile monolayer using the LB method. Freshly prepared metal substrates, usually slightly negatively charged can also be used. After a few polyelectrolyte adsorption cycles, the top surface will develop a strong electric charge. The choice is not limited to planar surfaces, microcapsules, colloids, tubules or biological cells are now common templates (see Figure 4.7).

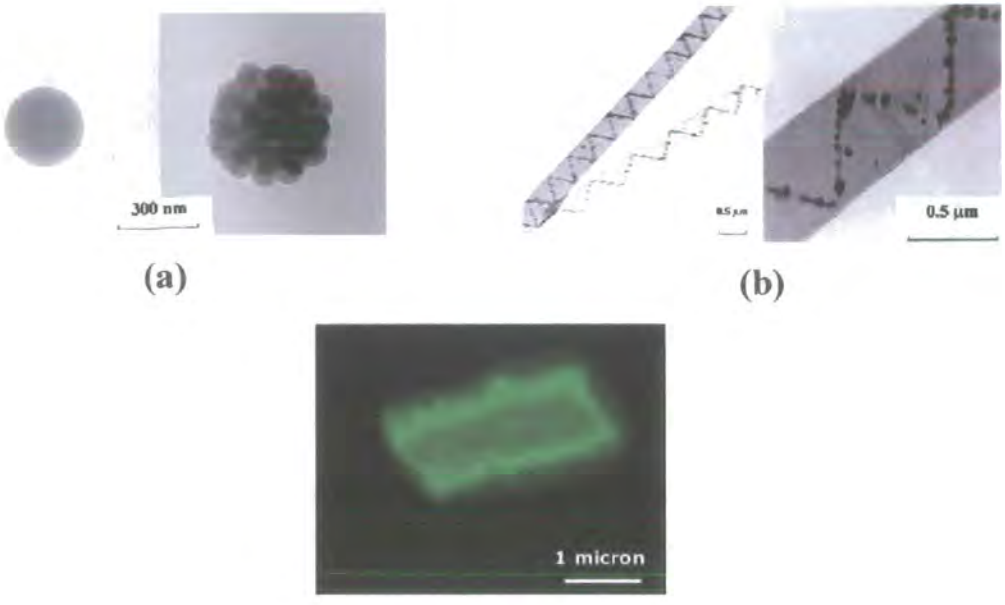

Figure 4.7 LbL self-assembly on various templates. (a) 75-nm diameter silica gel enclosing a 300-nm colloidal templates. (b) Nanoparticle helices inside lipid tubules. (c) PE fluorescent shell around a microcrystal. (Reproduced from [41]).

4.3 Materials suited for the process

Together with polyelectrolytes, other materials can be used as LbL building blocks; for example small organic molecules or inorganic compounds, macromolecules, biomacromolecules such as proteins or DNA, colloids (metallic or oxidic colloids or latex particles) [8, 18, 19].

As the LbL method exploits electrostatic attraction, the compound must bear a minimum number of charged groups, below which the deposition procedure does not work. As stated previously, additional strong interactions may reduce the minimum charge required (e.g. π–π stacking for instance seems to contribute to the multilayering when using certain organic dyes as one component [42, 43]). The association of molecules with only a small number of charged groups may lead to "secondary-valence polyelectrolytes" which, in the aggregate form, deposit well.

Some workers propose that, for successful deposition, the appropriate matching of the charge density of the PE pair is more important than a minimum charge density [19]. Therefore, if one of the partners is a standard strong polyelectrolyte, the second polyion

should also have a high charge density. However, the charge-matching criterion does not seem to be applicable to those polyelectrolytes with an intermediate charge density such as poly(styrene sulfonate) [17] or polymeric dyes [44-46].

A poor match between the two oppositely charged polyelectrolytes does not necessarily mean that no film will be formed. Instead of reproducible linear growth, asymptotically limited growth, or pseudo-exponential growth of multilayers may be observed for a small number of deposition cycles. If very thin films are desired, the molecular limitations for LbL assembly are reduced.

A wide category of materials (or nano-objects) which can be considered as hard, rigid polyelectrolytes, have been successfully employed to prepare LbL coatings. Among these are stable colloidal dispersions of charged silica [47], metal oxides [3, 48], polyoxometalates [49], semiconductor nanoparticles [50], fullerenes [51], metal colloids [52], metal-supramolecular complexes [53-55], charged latex spheres [3] and microcrystallines [56]. Charged platelets, deriving from exfoliated layered crystals, are particularly interesting for their small molecular dimensions, and for being something of an intermediate character between polyelectrolytes and nano-objects. These include delaminated clay platelets such as positively charged hydrotalcite [56], negatively charged hectorite [3], and montmorillonite [57, 58].

4.3.1 Internal architectures

The internal architecture of LbL multilayers has been the focus of much work [6, 7, 16]. What is now clear is that, at least for the most of the systems investigated, multilayer growth proceeds linearly after the deposition of the first layers. In Figure 4.8, this is confirmed by the change in absorbance versus adsorption cycles for a multilayer composed of coloured polymers of opposite charge.

It is now widely accepted that LbL architectures are stratified, but do not consist of well-separated, distinguishable alternating layers (see Fig. 4.9). Instead, adjacent layers interpenetrate and possess an interdigitated structure along the film normal [6, 19].

Neutron and X-ray reflectivity [8], electrochemical studies [59] and non-radiative energy transfer experiments [60] support such model.

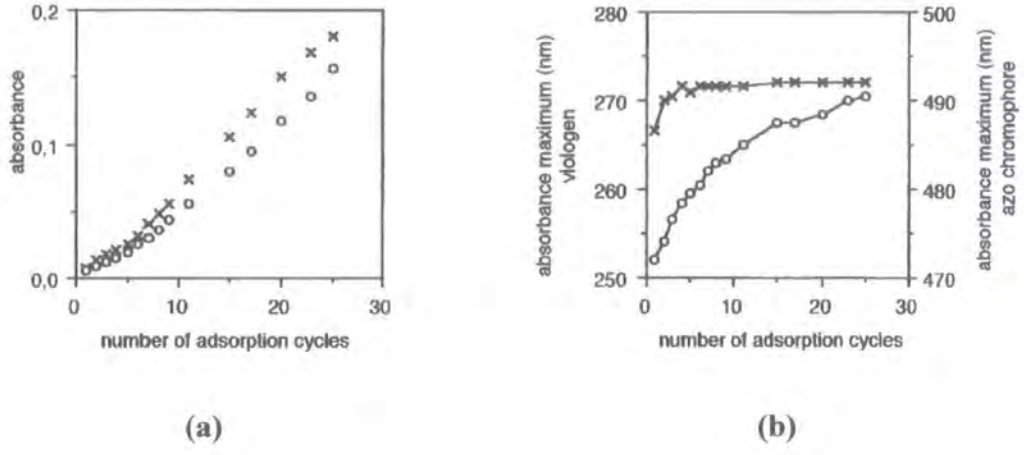

Figure 4.8 LbL multilayer from a "double dye-labelled" polycation with an azobenzene chromophore in its chain, and an inorganic polyanion hectorite incorporating a viologene chromophore. (a) the visible absorbance of the azo dye at about 480 nm (o), and by the UV-absorbance maximum of the violegene group at about 270 nm (x) is plotted against the number of adsorption cycles. (b) the shift of the absorbance maximum with ongoing film growth for the azobenzene chromophore (o) and for the viologene chromophore (x) is shown. (Reproduced from [19]).

Bottom and top layers, i.e. the layers that are in contact with the external environment (substrate, air, liquid) show different characteristics to the inner ones. The roughness of the first deposited layer can range from molecularly flat to several nanometers and seems to depend mainly on the roughness of the substrate.

The LbL assembly can possess a certain tolerance against defects in the underlying layers or on the surface of the support, much more than that shown by other self-organization methods, such as the LB technique and chemical self-assembly. Researchers attribute this to the flexible nature of the polyions, which do not need to bind to a precise site on the substrate, and thus allow defect sites to be covered [9, 19]. The molecules of the top layer have trains anchoring them to the coating, while loops or tails from their long chains dangle in the solution (see Chapter 6, Fig. 6.8). The resulting surface charge reversal determines the amount of adsorbed polyion in the next step. Thus the nature of the underlying layer will affect the amount of the newly adsorbed species [61, 62].

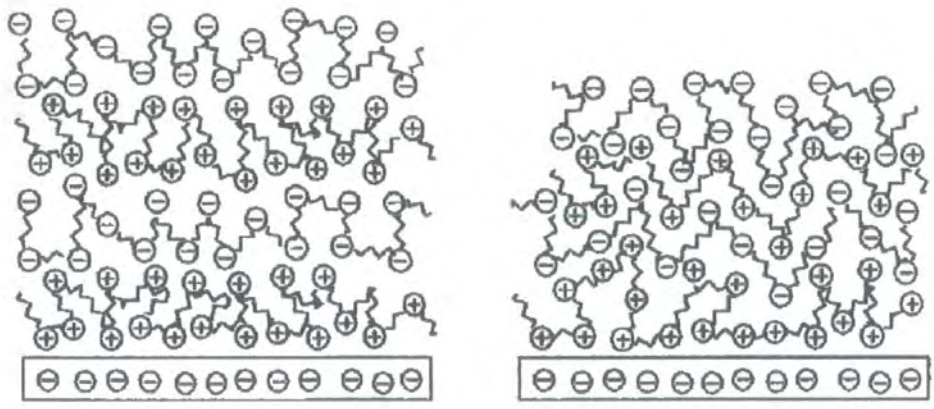

(a)

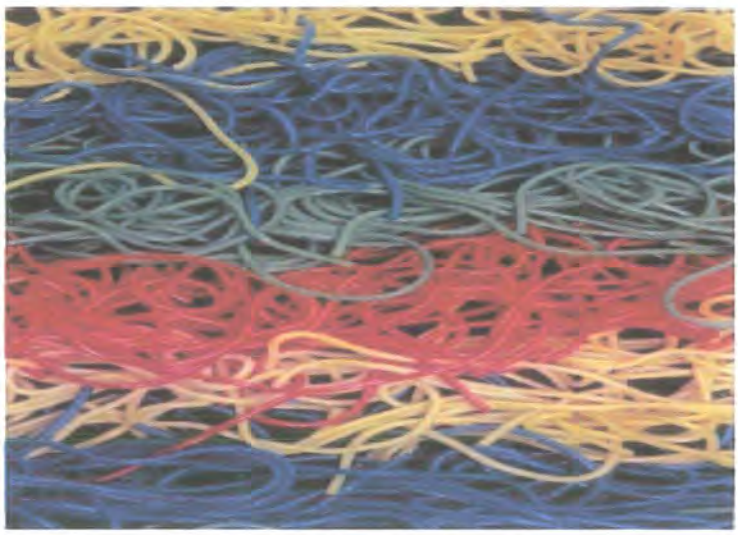

(b)

Figure 4.9 (a) Comparison between a true multilayer structure and a fuzzy polyion assembly. (Reproduced from [19]). (b) Schematic picture of polycation / polyanion multilayer. Neighbouring layers interpenetrate by about 30%, so that only first and third layers are well separated. (Reproduced from [9]).

Interestingly, some workers [19] have found that the thickness of complex multilayers C1-A-C2-A-C1-A-C2 (where A denotes a polyanion, and C1 and C2 denote different polycations) differs significantly from the case of multilayers C2-A-C1-A-C2-A-C1, i.e. from a film with an inverted polycation sequence, although both films contain the same number of layers of A, C1 and C2. The thickness and structure of the LbL multilayer are therefore characteristic of the chosen pair of charged species, and strongly depend on the adsorption conditions [8, 9, 36, 37].

From the above, a rearrangement of the uppermost layer is expected when a new layer is adsorbed. This provides the LbL-multilayer with a "soft" structure: polyion self-

assembled films should be regarded as dense hydrogels rather than as rigid, compact well defined lattices. Normally, the technique is not expected to provide a high control over the arrangement of molecules within the layers. However, with time and effort spent in research, control of the self-assembly process is improving [63-67]. LbL assembly is a kinetically controlled deposition technique and it takes place at an interface, i.e. under inherently non-centrosymmetric conditions. Therefore non-centrosymmetric structures with well-defined surfaces are obtainable when the molecules are oriented during the adsorption step, and if subsequently their reorientation is prevented [2].

4.3.2 Characterization

Several techniques have been used to characterize LbL films [8]. These fall into two main groups: (i) methods for *ex-situ* characterization (i.e. the polyelectrolyte film is examined after the process of self-assembly has been completed); and (ii) methods for *in-situ* characterization (i.e. methods that allow a real time study of the film growth). In the first group we have UV/VIS spectroscopy [68], ellipsometry [69], X-ray reflectometry [6], Atomic Force Microscopy [70] and Nuclear Magnetic Resonance [71]. The other group includes zeta potential measurements [72], the quartz crystal microbalance technique (QCM) [73], surface plasmon resonance [29, 74, 75], in-situ Atomic Force Microscopy [76] and optical waveguide lightmode spectroscopy [70].

Using reflectivity techniques, especially neutron and X-ray reflectometry, Decher and co-workers have elucidated the internal structures of LbL films [5, 6, 16, 77, 78]. These techniques are well suited to the characterization of multilayer films as they allow the determination of concentration gradients along the layer perpendicular direction. Early studies with X-ray reflectometry on multilayer films composed of flexible, strong polyelectrolytes of approximately equal charge-to-charge distances (polyanions and polycations with one charged group per monomer unit) could only identify *Kiessig fringes* arising from the interference of X-ray reflected at the substrate/film and film/air interfaces (see Fig. 4.10(a), traces XR-1 to XR-3). In these X-ray scans, different numbers of fringes were evident from the different film thickness, obtained either by changing the total number of layers or by deposition from polyelectrolyte solutions of

different ionic strength. Even neutron reflectograms of films in which all the polyanion layers were labelled with deuterium [$(A/B_d)_n$ film architecture, where A is a polycation, B is a polyanion, B_d is a perdeuterated polyanion, and n is the number of deposition cycles] showed Kiessig fringes as the only characteristic feature (see Fig. 4.10(b), traces NR-1 and NR-2). Only when specific layer positions in a multilayer film were deuterated, was it possible to observe *Bragg peaks*, which clearly demonstrated an internal layer structure, by neutron reflectometry (i.e. the architecture of the film being described by the expression $((A/B)_mA/B_d)_n$ with $m = 1, 2, \ldots$). Such peaks are evident in Figure 4.10(b), traces NR-3 to NR-6. A single Bragg peak was also observed by X-ray reflectivity of films in which every fourth layer was a polyanion containing side groups of azo dyes. It is thus possible to conclude that the absence of Bragg peaks in $(A/B)_n$-type films does not arise from small density differences between different layers, but rather from large overlaps between adjacent layers.

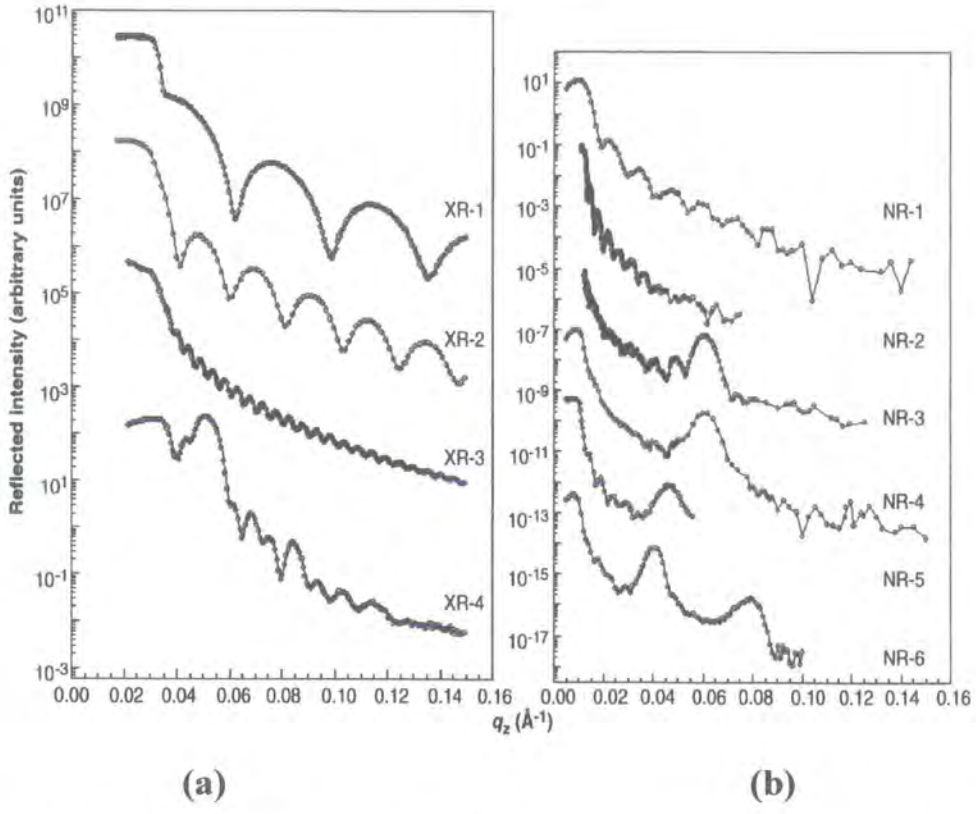

Figure 4.10 (a) X-ray reflectivity scans of multilayer films composed of poly(styrene sulfonate) and poly(allylamine hydrochloride). XR-4 is a reflectivity scan of a multilayer with the architecture $((A/B)_3A/G)_4$, where G consists of negatively charged gold colloids of 13.5 nm diameter. The high intensity of the (001) Bragg peak arises from the large electron density difference between the polymers and the gold. (b) Neutron reflectivity scans of multilayer film; all except NR-5 were obtained from films composed of sodium poly(styrene sulfonate) and poly(allylamine). NR-5 is obtained from a film composed of poly(styrene sulfonate) and PPV precursor. NR-1 and NR-2 are from films uniformly deuterated, while NR-3 to NR-6 are from films periodically deuterated. (Reproduced from [8]).

4.3.3 Film properties and chemical modification

LbL films are generally stable and are able to withstand moderate mechanical, or thermal or chemical stress. When AFM tips are placed in the contact mode on the multilayer surface, a reasonable stability to mechanical stress is evident [79]. Generally mechanical scratching is observed with levers of high stiffness (16 N m^{-1}), and some defects are induced for certain systems with levers of low stiffness (0.2 N m^{-1}). The substrate also plays a key role in the film's mechanical resistance. It is easier to produce cracks in the coating by applying a high pressure if the underlying substrate is porous [19]. Although polyelectrolyte multilayers are not in a state of thermodynamic equilibrium, they usually show good ageing behaviour [6, 19], probably because of the high number of ion pairs present, which reduce the mobility of the polyelectrolyte chains and effectively "freeze" the structure of the adsorption layers. Drying the film leads to some reduction of the film thickness. However the recovery of water in the dried films is almost complete under ambient conditions [80, 81]. Annealing has been shown to increase the density of the films and, in certain cases, to improve the internal order [8], [20]. Heating enhances the local mobility, providing the polymeric chains with a certain degree of freedom to rearrange. Cross-linking may also enhance the thermal stability of LbL-films [19].

LbL films can undergo certain chemical reactions without any disruption to their multilayer structure. Because of the strong ionic bonding, strong polyelectrolytes show a high degree of solvent resistance [35, 82] even at high ionic strength [19, 83] and under strongly acidic or basic conditions [53, 84, 85]. In general, in can be assumed that most of the polyelectrolyte films are inert towards dissolution by the more common organic solvents. However, some polyelectrolyte multilayers dissolve in ternary solvent mixtures [86] or upon prolonged exposure to dimethylformamide (DMF) or water/alcohol mixtures [87, 88]. Moreover, LbL architectures deposited from weak polyelectrolytes dissolve at pH values that substantially reduce their charge. This feature, together with a sensitivity to high salt concentration [89], allows some multilayer architectures to be exploited as hollow capsules (see Fig. 4.11) for drug delivery [90, 91].

Thanks to this remarkable stability of polyelectrolyte coatings, workers have been trying to perform chemical reactions with the films, to fine-tune the structure. This approach provides specific coatings that would otherwise be difficult, if not impossible, to obtain from direct LbL assembly. Chemical modification can be achieved via two routes: (a) reactions induced by physical parameters and (b) by the addition of chemical reagents.

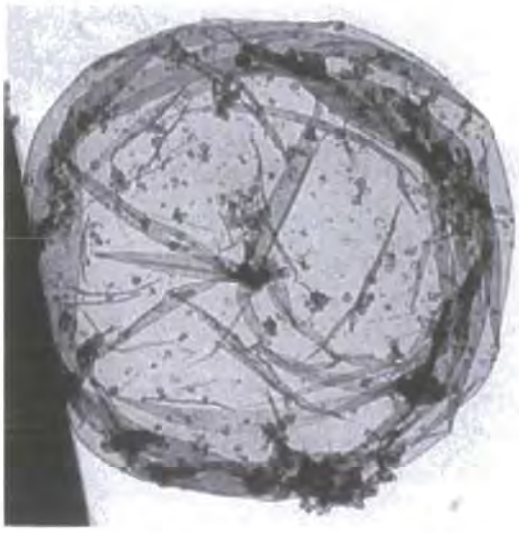

Figure 4.11 TEM image of an air-dried hollow polymer capsule comprising eight [(PSS/PAH)$_4$] polyelectrolyte layers, obtained after decomposition of an encapsulated enzyme. The polymer capsule spreads out on the carbon surface on which it is dried, and folds and creases can be seen. Some un-decomposed enzyme can still be seen in the interior of the capsule. (Reproduced from [92]).

The first category is widely exploited. Photochemical reactions are quite common because of their ability to proceed homogeneously throughout thin films when the absorbance of the film at the wavelength of irradiation is not too high. The use of irradiation to create orientation within the layers can be applied, for example, to liquid crystals and can be useful for optical storage [93, 94]. Photo-bleaching or photo-ablation can be successfully used to create patterns in the films [8, 44]. However, photoreactions using LbL films are mainly focused on photo-polymerizations or on cross-linking reactions in order to improve stability [86, 87].

Not surprisingly, given the nature of the self-assembly, electrochemistry is a widely exploited tool to obtain fundamental information about LbL multilayers [49, 50, 59, 95-98]. Potential applications of electrochemistry on polyelectrolyte thin films are in electrocatalysis, chemical sensing or electrochromism. Moreover, electrochemical methods can be employed to control the ionic content of the films [8, 59].

Thermal elimination can also be used. For example, elimination of sulfides from charged precursor polymers of poly(phenyl vinylene) is now a quite common procedure [17, 59, 99]. Recently, thermal amidation of poly(carboxylate) with poly(amine) has been reported, in order to stabilize the ESA coatings by cross-linking [100, 101]. Some workers have explored calcinations [8] to obtain ultrathin inorganic films or hollow spheres [102, 103].

The hydrogel nature of LbL assembled thin films becomes extremely important in the second category of reactions, which use chemical reagents to modify the chemical structure or the polymeric architecture. A key point is whether the chemical reaction will modify the coating homogeneously, will be confined to the surface only, or will result in a compositional gradients. Diffusion of protons, water and salts has been identified [8, 19, 59] as has the influence of the pH of contact solution on the internal structure of the films [104, 105]. Protonation/de-protonation reactions can control the charge density in the films.

The following chemio-modifications should also be noted: wet chemical cross-linking by protein amino groups [106], reduction of graphite oxide by hydrazine and hydrogen [50], chemical ring closure of polyimides [49], azo coupling, the intercalation of acridin orange and related dyes into DNA [38], enzymatic activity in LbL self assembled structures [12] and molecular recognition reactions [107, 108]. There are also CoMPAS reactions (coatings by multiple polyelectrolyte adsorption/surface activation): following the adsorption of a reactive polyelectrolyte, a chemical reaction to reverse its surface potential subsequently takes place allowing docking of the next polymer layer [19].

4.4 Patterning of polyelectrolyte multilayers

The intrinsic flexibility of the LbL technique and the increasing ability to modify chemically the adsorbed multilayers, has resulted in a wide interest in the patterning of such architectures. There are a number of different approaches. These include last layer dip coating [74, 109, 110], standard photolithography [111, 112], ink-jet printing in an additive or subtractive mode [39, 113] and micro-contact printing [114, 115].

The first technique is a direct way of studying the variations in surface properties that result from different outer surface layers. The method consists of allowing the polymeric solutions access only to specific areas of the substrate surface. A more detailed insight of this method will be given in Chapter 8.

Traditional microlithography can be combined with electrostatic layer-by-layer nanoassembly to produce three types of structure. As shown in Fig. 4.12, a photoresist layer is first applied to a substrate and a pattern produced through a mask by UV-irradiation.

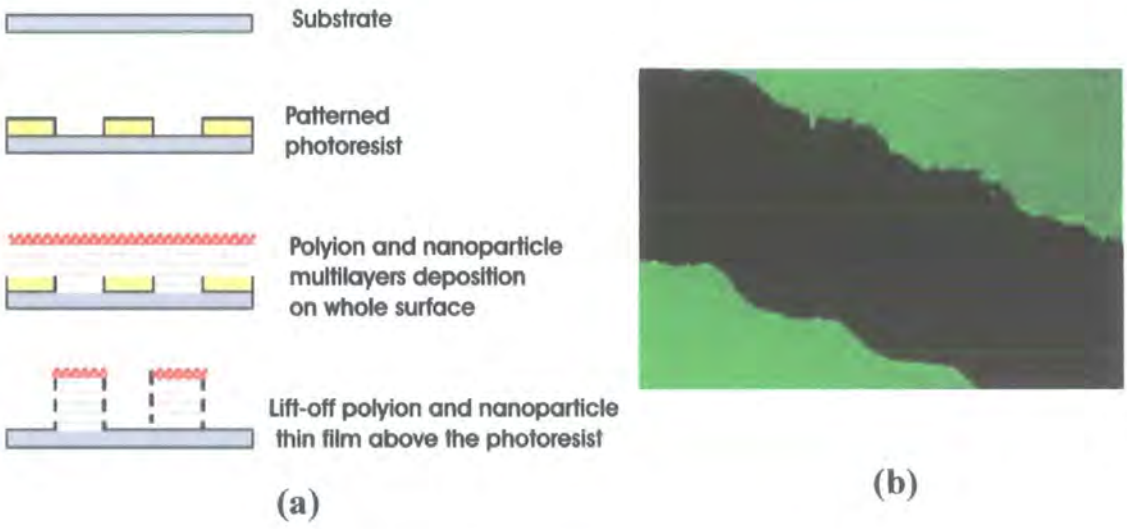

Figure 4.12 (a) Scheme of patterning nanoparticle thin films with ultrasonic treatment. (b) Images of patterns of 25 μm width with a fluorescent multilayer of poly(ethyleneimine) + (poly(styrene sulfonate)/poly(dimethyldiallyalmmonium chloride))x3 + (fluoresbright/poly(dimethyldiallyalmmonium chloride))x3 on silicon. (Reproduced from [112]).

Following this step, LbL multilayers are assembled using the traditional dip coating method. Once this phase is completed, the photoresist with the polyions on top is washed with acetone accompanied with sonication, leaving the patterned LbL on the substrate. The polyion layers are sufficiently permeable to let acetone molecules penetrate, dissolving the photoresist and stripping off the multilayers from these regions. One of the main advantages of the lithographic approach is that it is compatible with existing silicon micromanufacturing technology. However, in the lithographic approach it is difficult to assemble biological (proteins, DNA) multilayers onto charged patterns because of the need to dissolve the underlying photoresist in the final stage of

the process. This method provides a technology for nano-devices such as nano-electronic chips or nano-electromechanic systems, NEMS, which have numerous potential applications. It might also allow the patterning of sensors for use in biomedical applications (bioMEMS production) [111, 112, 116].

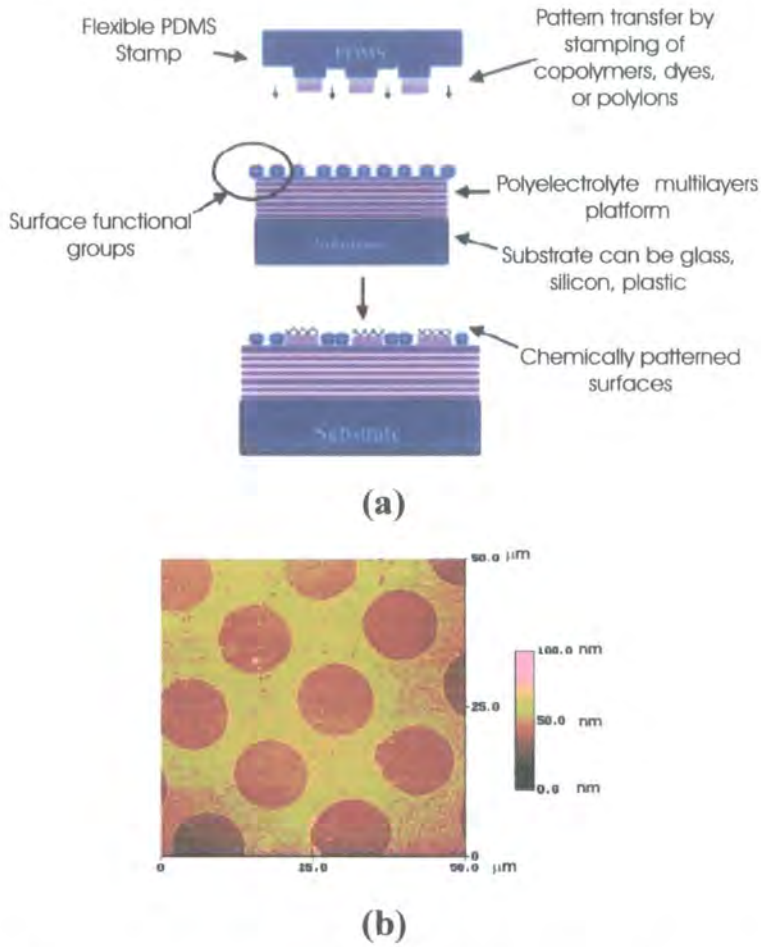

Figure 4.13 (a) Schematic diagram showing the transfer of a functional polymer to a surface with complementary functionality using polymer-on-polymer stamping. (b) Atomic force microscope image of a transferred poly(diallyldimethylammonium chloride) layer on a poly(diallyldimethylammomium chloride)/poly(styrene sulfonate) multilayer surface. (Reproduced from [115]).

The general procedure of micro-contact printing (or polymer-on-polymer stamping, POPS) is shown in Figure 4.13. A functional polymer solution is used to ink a poly(dimethylsiloxane) (PDMS) stamp molded from a lithographically prepared master. After evaporation of the solvent, the PDMS stamp is briefly dried under a N_2 stream and is brought into contact with the substrate for few minutes at room temperature. All the stamped surfaces are then rinsed with ethanol to remove unbound or loosely bound excess polymer. This technique can be used to create a surface where negative regions

are next to positive ones. These different areas can then selectively adsorb other molecules or promote electroless plating to make circuit patterns. The application to electronic and photonic devices, platforms for cell culture, and biosensors could all benefit from such a patterning method [2, 117, 118].

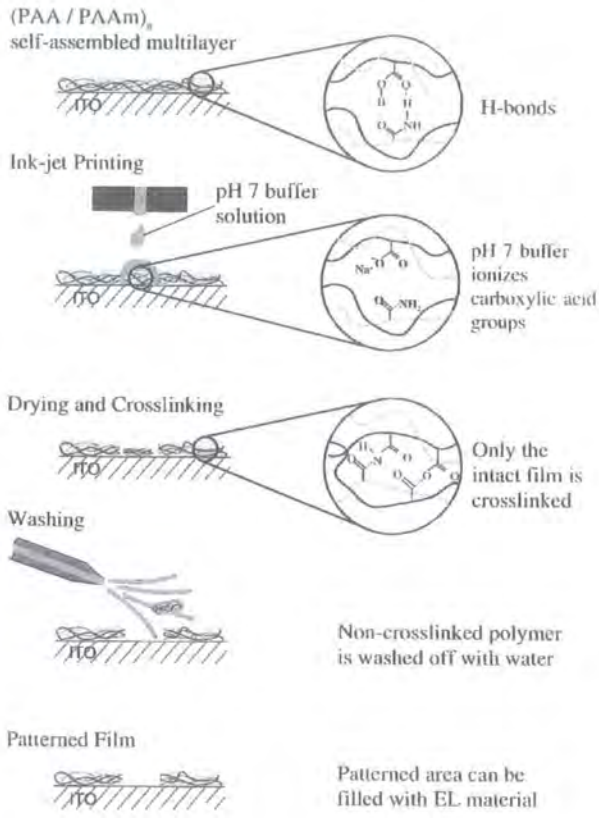

Figure 4.14 Patterning of a poly(acrylic acid), PAA/poly(acrylamide) PAAm hydrogen-bonded multilayers by the subtractive ink-jet printing process. (Reproduced from [113]).

Ink-jet printing can be exploited using either additive or subtractive approaches. In the additive method, a commercial ink-jet printer can be used to print an aqueous polymer solution onto substrates as thick as typical glass slide [119]. The subtractive method exploits a chemical or thermal treatment to remove polyelectrolyte multilayers from specific areas of the substrate. In this case, hydrogen-bond interactions are used to assemble multilayer films [39, 113, 120]. Using weak polyacids as components of the mulilayers it is possible to dissolve the organic film by simply increasing the degree of ionization (by increasing the pH) [121]. In the example shown in Fig. 4.14, poly(acrylic acid), PAA, and poly(acrylamide), PAAm, were assembled onto an ITO substrate. For both polymer solutions, the pH was 3. Notably, at a pH higher than 4.5 the multilayer dissolves. However, if the multilayer is thermally treated at 90 °C for 8 h (or for a

shorter time at higher temperature) it becomes insoluble in these higher pH solutions. This seems to be due to crosslinking reactions that produce both anhydride and imide linkages. To create a pattern on the substrate surface, a phosphate buffer solution at pH 7 is printed on the multilayer; the carboxylic groups are thereby ionized and the film is dissolved. Then, the substrate is dried and thermally treated. As result of the thermal treatment, the intact film is cross-linked. The non crosslinked polymer is removed from the substrate by washing with water. The patterned area can subsequently be filled with, for example, electroluminescent material to create a light emitting device [122].

4.5 Conclusions

LbL self-assembly has proved itself to be a powerful method for self-organization. The seminal work of Iler in 1966 [3] reported on the sequential adsorption of oppositely charged colloids. However, only in the last ten years has a new impetus been provided by Decher and co-workers [4, 5, 68]. The number of research groups engaging in this area has now increased considerably and with it the number of papers published in scientific journals.

In this chapter, an introduction to the characteristics of the materials used for the LbL deposition has been given. A classification based on their charge density, functional groups and behaviour in solution was proposed. The different procedures involved in the LbL self-assembly have been explained in detail. A description of the different substrates and templates employed and of the thin film growth regimes has been illustrated. Insight into the most suitable materials for the self-assembly process and the internal architecture of the multilayers have also been given. The main methods of characterization for the organic films (in-situ and ex-situ) were described. Thanks to these, an extensive knowledge of the LbL architectures properties has been achieved. This is allowing an increasing degree of control of the thin film functionalities via chemical modification and/or modulation of the polymer solution characteristics, such as pH and ionic strength. Finally, some of the most successful patterning techniques for LbL multilayers have been described. These included polymer-on-polymer stamping, photolithography and ink-jet printing in subtractive or additive modes.

References

1. Dautzenberg, H., Jaeger, W., Kötz, J., Seidel, C., and Stscherbina, D., Polyelectrolytes. Formation, Characterization and Application. 1994, Hanser/Gardner: Munich.

2. Hammond, P.T., Recent explorations in electrostatic multilayer thin film assembly. Current Opinion in Colloid & Interface Science, 2000. 4(6): p. 430-442.

3. Iler, R., Multilayers of colloid particles. J. Colloid Interface Sci., 1966. 21: p. 569-594.

4. Decher, G. and Hong, J.D., Buildup of ultrathin multilayer films by a self-assembly process .1. Consecutive adsorption of anionic and cationic bipolar amphiphiles on charged surfaces. Makromolekulare Chemie-Macromolecular Symposia, 1991. 46: p. 321-327.

5. Decher, G. and Hong, J.D., Buildup of ultrathin multilayer films by a self-assembly process .2. Consecutive adsorption of anionic and cationic bipolar amphiphiles and polyelectrolytes on charged surfaces. Berichte Der Bunsen-Gesellschaft-Physical Chemistry Chemical Physics, 1991. 95(11): p. 1430-1434.

6. Decher, G., Fuzzy nanoassemblies: toward layered polymeric multicomposites. Science, 1997. 277(5330): p. 1232-1237.

7. Decher, G., Molecular multilayer films: The quest for order, orientation, and optical properties, in *Photonic and Optoelectronic Polymers*. 1997, ACS: Washington. p. 445-459.

8. Decher, G. and Schlenoff, J.B., eds. *Multilayer Thin Films-Sequential Assembly of Nanocomposite Materials*. 2003, WILEY-VCH: Weinheim.

9. Lvov, Y., Chapter 4: Thin film nanofabrication by alternate adsorption of polyions, nanoparticles, and proteins, in *Handbook of Surfaces and Interfaces of Materials*, H.S. Nalwa, Editor. 2001, Academic Press.

10. Lvov, Y.M., Lu, Z.Q., Schenkman, J.B., Zu, X.L., and Rusling, J.F., Direct electrochemistry of myoglobin and cytochrome p450(cam) in alternate layer-by-layer films with DNA and other polyions. Journal of the American Chemical Society, 1998. 120(17): p. 4073-4080.

11. Tsukruk, V.V., Bliznyuk, V.N., Visser, D., Campbell, A.L., Bunning, T.J., and Adams, W.W., Electrostatic deposition of polyionic monolayers on charged surfaces. Macromolecules, 1997. 30(21): p. 6615-6625.

12. Onda, M., Lvov, Y., Ariga, K., and Kunitake, T., Molecularly flat films of linear polyions and proteins obtained by the alternate adsorption method. Japanese Journal of Applied Physics Part 2-Letters, 1997. 36(12A): p. L1608-L1611.

13. McAloney, R.A., Sinyor, M., Dudnik, V., and Goh, M.C., Atomic force microscopy studies of salt effects on polyelectrolyte multilayer film morphology. Langmuir, 2001. 17(21): p. 6655-6663.

14. Lvov, Y., Ariga, K., Onda, M., Ichinose, I., and Kunitake, T., A careful examination of the adsorption step in the alternate layer-by-layer assembly of linear polyanion and polycation. Colloids and Surfaces a-Physicochemical and Engineering Aspects, 1999. 146(1-3): p. 337-346.

15. Yoo, D., Shiratori, S.S., and Rubner, M.F., Controlling bilayer composition and surface wettability of sequentially adsorbed multilayers of weak polyelectrolytes. Macromolecules, 1998. 31(13): p. 4309-4318.

16. Decher, G., Layered nanoarchitectures via directed assembly of anionic and cationic molecules, in *Comprehensive Supramolecular Chemistry, "Templating, Self-Assembly and Self-Organizzation"*, J.P. Sauvage and M.W. Hosseini, Editors. 1996, Pergamon Press: Oxford. p. 507-528.

17. Knoll, W., Self-assembled microstructures at interfaces. Current Opinion in Colloid & Interface Science, 1996. 1(1): p. 137-143.

18. Lvov, Y. and Mohwald, H., *Protein Architecture : Interfacing Molecular Assemblies and Immobilization Biotechnology*, ed. Llov and Mohwald. 1999, NY: M.Dekker Inc.

19. Bertrand, P., Jonas, A., Laschewsky, A., and Legras, R., Ultrathin polymer coatings by complexation of polyelectrolytes at interfaces: suitable materials, structure and properties. Macromolecular Rapid Communications, 2000. 21(7): p. 319-348.

20. Arys, X., Jonas, A., Laguitton, B., Legras, R., Laschewsky, A., and Wischerhoff, E., Structural studies on thin organic coatings built by repeated adsorption of polyelectrolytes. Progress in Organic Coatings, 1998. 34(1-4): p. 108-118.

21. Decher, G., One- or multi-layered layer elements applied to supports and their production. May 4, 1993, Bayer Aktiengesellschaft (Leverkusen, DE): United States Patent 5,208,111.

22. Rubner , M.F., Molecular self-assembly of electrically conductive polymers. July 16, 1996, Massachusetts Institute of Technology (Cambridge, MA): US 5,518,767.

23. Schlenoff , J.B., Apparatus for capillary electrophoresis and associated method. June 11, 2002: US 6,402,918.

24. Caruso , F., Fabrication of multilayer-coated particles and hollow shells via electrostatic self-assembly of nanocomposite multilayers on decomposable colloidal templates. November 12, 2002, Max-Planck-Gesellschaft zur Forderung der Wissenschaften, E.V. (Munich, DE): US 6,479,146.

25. Aguado, Polymeric materials for making contact lenses. December 5, 2002, Novartis Ag (CH), Novartis Erfind Verwalt Gmbh (AT): WO02097481.

26. Langmuir, I., Surface Chemistry, in *Nobel Lectures Collection*. December 14, 1932: Stockholm.

27. Palumbo, A., Pearson, C., Nagel, J., and Petty, M.C., Surface plasmon resonance sensing of liquids using polyelectrolyte thin films. Sensors and Actuators B-Chemical, 2003. 91(1-3): p. 291-297.

28. McCash, E.M., *Surface Chemistry*. 2001, Oxford: Oxford University Press.
29. Pearson, C., Nagel, J., and Petty, M.C., Metal ion sensing using ultrathin organic films prepared by the layer-by-layer adsorption technique. J. Phys. D: Appl. Phys, 2001. 34: p. 285-291.

30. Parfitt, G.D. and Rochester, C.H., Adsorption of Small Molecules, in *Adsorption from Solution at the Solid/Liquid Interface*, G.D. Parfitt and C.H. Rochester, Editors. 1983, Academic Press Inc. (London) Ltd: London.

31. Atkins, P.W., *Physical Chemistry*. 1994, Oxford: Oxford University Press.
32. Hiemenz, P.C. and Rajagopalan, R., *Principles of Colloid and Surface Chemistry*. 1997, New York: Marcel Dekker, Inc.

33. Kotov, N.A., Layer-by-layer self-assembly: The contribution of hydrophobic interactions. Nanostructured Materials, 1999. 12(5-8): p. 789-796.

34. Dubas, S.T. and Schlenoff, J.B., Factors controlling the growth of polyelectrolyte multilayers. Macromolecules, 1999. 32(24): p. 8153-8160.

35. Arys, X., Jonas, A.M., Laschewsky, A., and Legras, R., Supramolecular polyelectrolytes assemblies, in *Supramolecular polymers*, A. Ciferri, Editor. 2000, Marcel Dekker: New York. p. 505-563.

36. Shiratori, S. and Rubner, M.F., Layer-by-layer adsorption of weak polyelectrolytes: A means to control layer thickness, composition and surface wettability. Abstracts of Papers of the American Chemical Society, 1998. 216: p. 259-PHYS.

37. Shiratori, S.S. and Rubner, M.F., pH-dependent thickness behaviour of sequentially adsorbed layers of weak polyelectrolytes. Macromolecules, 2000. 33(11): p. 4213-4219.

38. Cochin, D. and Laschewsky, A., Layer-by-layer self-assembly of hydrophobically modified polyelectrolytes. Macromolecular Chemistry and Physics, 1999. 200(3): p. 609-615.

39. Stockton, W.B. and Rubner, M.F., Molecular-level processing of conjugated polymers .4. Layer-by- layer manipulation of polyaniline via hydrogen-bonding interactions. Macromolecules, 1997. 30(9): p. 2717-2725.

40. Pontes, R.S., Raposo, M., Camilo, C.S., Dhanabalan, A., Ferreira, M., and Oliveira, O.N., Non-equilibrium adsorbed polymer layers via hydrogen bonding. Physica Status Solidi A-Applied Research, 1999. 173(1): p. 41-50.

41. Ai, H., Jones, S.A., de Villiers, M.M., and Lvov, Y.M., Nano-encapsulation of furosemide microcrystals for controlled drug release. Journal of Controlled Release, 2003. 86(1): p. 59-68.

42. Ariga, K., Lvov, Y., and Kunitake, T., Assembling alternate dye-polyion molecular films by electrostatic layer-by-layer adsorption. Journal of the American Chemical Society, 1997. 119(9): p. 2224-2231.

43. Yoo, D., Wu, A.P., Lee, J., and Rubner, M.F., New electro-active self-assembled multilayer thin films based on alternately adsorbed layers of polyelectrolytes and functional dye molecules. Synthetic Metals, 1997. 85(1-3): p. 1425-1426.

44. Decher, G., Lehr, B., Lowack, K., Lvov, Y., and Schmitt, J., New nanocomposite films For biosensors - Layer-by-Layer adsorbed films of polyelectrolytes, proteins or DNA. Biosensors & Bioelectronics, 1994. 9(9-10): p. 677-684.

45. Advincula, R., Aust, E., Meyer, W., and Knoll, W., In situ investigations of polymer self-assembly solution adsorption by surface plasmon spectroscopy. Langmuir, 1996. 12(15): p. 3536-3540.

46. Lvov, Y., Yamada, S., and Kunitake, T., Non-linear optical effects in layer-by-layer alternate films of polycations and an azobenzene-containing polyanion. Thin Solid Films, 1997. 300(1-2): p. 107-112.

47. Lvov, Y., Ariga, K., Onda, M., Ichinose, I., and Kunitake, T., Alternate assembly of ordered multilayers of SiO2 and other nanoparticles and polyions. Langmuir, 1997. 13(23): p. 6195-6203.

48. Fendler, J.H., Self-assembled nanostructured materials. Chemistry of Materials, 1996. 8(8): p. 1616-1624.

49. Moriguchi, I. and Fendler, J.H., Characterization and electrochromic properties of ultrathin films self-assembled from poly(diallyldimethylammonium) chloride and sodium decatungstate. Chemistry of Materials, 1998. 10(8): p. 2205-2211.

50. Kotov, N.A., Dekany, I., and Fendler, J.H., Ultrathin graphite oxide-polyelectrolyte composites prepared by self-assembly: Transition between conductive and non-conductive states. Advanced Materials, 1996. 8(8): p. 637-641.

51. Luo, C.P., Guldi, D.M., Maggini, M., Menna, E., Mondini, S., Kotov, N.A., and Prato, M., Stepwise assembled photoactive films containing donor-linked fullerenes. Angewandte Chemie-International Edition, 2000. 39(21): p. 3905-+.

52. Schmitt, J., Decher, G., Dressick, W.J., Brandow, S.L., Geer, R.E., Shashidhar, R., and Calvert, J.M., Metal nanoparticle/polymer superlattice films: Fabrication and control of layer structure. Advanced Materials, 1997. 9(1): p. 61-&.

53. Caruso, F., Schuler, C., and Kurth, D.G., Core-shell particles and hollow shells containing metallo- supramolecular components. Chemistry of Materials, 1999. 11(11): p. 3394-3399.

54. Kurth, D.G. and Osterhout, R., In situ analysis of metallosupramolecular coordination polyelectrolyte films by surface plasmon resonance spectroscopy. Langmuir, 1999. 15(14): p. 4842-4846.

55. Clark, S.L., Handy, E.S., Rubner, M.F., and Hammond, P.T., Creating microstructures of luminescent organic thin films using layer-by-layer assembly. Advanced Materials, 1999. 11(12): p. 1031-1035.

56. Kotov, N.A., Haraszti, T., Turi, L., Zavala, G., Geer, R.E., Dekany, I., and Fendler, J.H., Mechanism of and defect formation in the self-assembly of polymeric polycation-montmorillonite ultrathin films. Journal of the American Chemical Society, 1997. 119(29): p. 6821-6832.

57. Kotov, N.A., Fendler, J.H., and Dekany, I., Chemical and electrochemical reductions of self-assembled ultrathin films composed of graphite oxide - Platelets and polyelectrolytes. Abstracts of Papers of the American Chemical Society, 1996. 211: p. 11-COLL.

58. Lvov, Y., Ariga, K., Ichinose, I., and Kunitake, T., Molecular film assembly via layer-by-layer adsorption of oppositely charged macromolecules (linear polymer, protein and clay) and concanavalin A and glycogen. Thin Solid Films, 1996. 285: p. 797-801.

59. Schlenoff, J.B., Ly, H., and Li, M., Charge and mass balance in polyelectrolyte multilayers. Journal of the American Chemical Society, 1998. 120(30): p. 7626-7634.

60. Baur, J.W., Rubner, M.F., Reynolds, J.R., and Kim, S., Forster energy transfer studies of polyelectrolyte heterostructures containing conjugated polymers: A means to estimate layer interpenetration. Langmuir, 1999. 15(19): p. 6460-6469.

61. Lvov, Y.M. and Decher, G., Assembly of multilayer ordered films by alternating adsorption of oppositely charged macromolecules. Kristallografiya, 1994. 39(4): p. 696-716.

62. Lvov, Y., Ariga, K., Ichinose, I., and Kunitake, T., Assembly of multicomponent protein films by means of electrostatic Layer-by-Layer adsorption. Journal of the American Chemical Society, 1995. 117(22): p. 6117-6123.

63. Clark, S.L., Montague, M., and Hammond, P.T., Selective deposition in multilayer assembly: SAMs as molecular templates. Supramolecular Science, 1997. 4(1-2): p. 141-146.

64. Clark, S.L. and Hammond, P.T., Engineering the microfabrication of layer-by-layer thin films. Advanced Materials, 1998. 10(18): p. 1515-+.

65. Zheng, H.P., Lee, I., Rubner, M.F., and Hammond, P.T., Two component particle arrays on patterned polyelectrolyte multilayer templates. Advanced Materials, 2002. 14(8): p. 569-572.

66. Lee, I., Zheng, H.P., Rubner, M.F., and Hammond, P.T., Controlled cluster size in patterned particle arrays via directed adsorption on confined surfaces. Advanced Materials, 2002. 14(8): p. 572-577.

67. Jiang, X.P., Ortiz, C., and Hammond, P.T., Exploring the rules for selective deposition: Interactions of model polyamines on acid and oligoethylene oxide surfaces. Langmuir, 2002. 18(4): p. 1131-1143.

68. Decher, G., Hong, J.D., and Schmitt, J., Buildup of ultrathin multilayer films by a self-assembly process .3. Consecutively alternating adsorption of anionic and cationic polyelectrolytes on charged surfaces. Thin Solid Films, 1992. 210(1-2): p. 831-835.

69. Biesalski, M., Johannsmann, D., and Ruhe, J., Synthesis and swelling behavior of a weak polyacid brush. Journal of Chemical Physics, 2002. 117(10): p. 4988-4994.

70. Lavalle, P., Gergely, C., Cuisinier, F.J.G., Decher, G., Schaaf, P., Voegel, J.C., and Picart, C., Comparison of the structure of polyelectrolyte multilayer films exhibiting a linear and an exponential growth regime: An in situ atomic force microscopy study. Macromolecules, 2002. 35(11): p. 4458-4465.

71. Kim, S., Jackiw, J., Robinson, E., Schanze, K.S., Reynolds, J.R., Baur, J., Rubner, M.F., and Boils, D., Water soluble photo- and electroluminescent alkoxy-sulfonated poly(p-phenylenes) synthesized via palladium catalysis. Macromolecules, 1998. 31(4): p. 964-974.

72. Ladam, G., Schaad, P., Voegel, J.C., Schaaf, P., Decher, G., and Cuisinier, F., In situ determination of the structural properties of initially deposited polyelectrolyte multilayers. Langmuir, 2000. 16(3): p. 1249-1255.

73. Baba, A., Kaneko, F., and Advincula, R.C., Polyelectrolyte adsorption processes characterized in situ using the quartz crystal microbalance technique: alternate adsorption properties in ultrathin polymer films. Colloids and Surfaces A: Physicochemical and Engineering Aspects, 2000. 173(1-3): p. 39-49.

74. Palumbo, M., Pearson, C., Nagel, J., and Petty, M.C., A single chip multi-channel surface plasmon resonance imaging system. Sensors and Actuators B: Chemical, 2003. 90(1-3): p. 264-270.

75. Palumbo, M., Pearson, C., Nagel, J., and Petty, M.C., Surface plasmon resonance sensing of liquids using polyelectrolyte thin films. Sensors and Actuators B: Chemical, 2003. 91(1-3): p. 291-297.

76. Yamada, T. and Shiratori, S., In situ observation of the initial adsorption process of layer-by-layer sequential adsorbed polyelectrolyte film using an AFM. Electrical Engineering in Japan, 2002. 141(2): p. 1-7.

77. Schmitt, J., Grunewald, T., Decher, G., Pershan, P.S., Kjaer, K., and Losche, M., Internal structure of layer-by-layer adsorbed polyelectrolyte films - a Neutron and X-Ray reflectivity study. Macromolecules, 1993. 26(25): p. 7058-7063.

78. Losche, M., Schmitt, J., Decher, G., Bouwman, W.G., and Kjaer, K., Detailed structure of molecularly thin polyelectrolyte multilayer films on solid substrates as revealed by neutron reflectometry. Macromolecules, 1998. 31(25): p. 8893-8906.

79. Tsukruk, V.V. and Reneker, D.H., Scanning Probe Microscopy of Organic and Polymeric Films - from Self-Assembled Monolayers to Composite Multilayers. Polymer, 1995. 36(9): p. 1791-1808.

80. Lvov, Y., Decher, G., and Mohwald, H., Assembly, structural characterization, and thermal-behavior of layer-by-layer deposited ultrathin films of Poly(Vinyl Sulfate) and Poly(Allylamine). Langmuir, 1993. 9(2): p. 481-486.

81. Decher, G., Lvov, Y., and Schmitt, J., Proof of multilayer structural organization in self-assembled polycation/polyanion molecular films. Thin Solid Films, 1994. 244(1-2): p. 772-777.

82. Caruso, F., Caruso, R.A., and Mohwald, H., Production of hollow microspheres from nanostructured composite particles. Chemistry of Materials, 1999. 11(11): p. 3309-3314.

83. Sukhorukov, G.B., Schmitt, J., and Decher, G., Reversible swelling of polyanion/polycation multilayer films in solutions of different ionic strength. Berichte Der Bunsen-Gesellschaft-Physical Chemistry Chemical Physics, 1996. 100(6): p. 948-953.

84. Sukhorukov, G.B., Donath, E., Davis, S., Lichtenfeld, H., Caruso, F., Popov, V.I., and Mohwald, H., Stepwise polyelectrolyte assembly on particle surfaces: a novel approach to colloid design. Polymers for Advanced Technologies, 1998. 9(10-11): p. 759-767.

85. Donath, E., Sukhorukov, G.B., Caruso, F., Davis, S.A., and Mohwald, H., Novel hollow polymer shells by colloid-templated assembly of polyelectrolytes. Angewandte Chemie-International Edition, 1998. 37(16): p. 2202-2205.

86. Sun, J., Wu, T., Sun, Y., Wang, X., Shen, J., and Cao, W., Fabrication of a covalently attached multilayer via photolysis of layer-by-layer self-assembled films containing diazo-resins. Chem. Commun., 1998. 17: p. 1853-1854.

87. van Ackern, F., Krasemann, L., and Tieke, B., Ultrathin membranes for gas separation and pervaporation prepared upon electrostatic self-assembly of polyelectrolytes. Thin Solid Films, 1998. 329: p. 762-766.

88. Krasemann, L. and Tieke, B., Composite membranes with ultrathin separation layer prepared by self-assembly of polyelectrolytes. Materials Science & Engineering C-Biomimetic and Supramolecular Systems, 1999. 8-9: p. 513-518.

89. Schuler, C. and Caruso, F., Decomposable hollow biopolymer-based capsules. Biomacromolecules, 2001. 2(3): p. 921-926.

90. Caruso, F., Yang, W.J., Trau, D., and Renneberg, R., Microencapsulation of uncharged low molecular weight organic materials by polyelectrolyte multilayer self-assembly. Langmuir, 2000. 16(23): p. 8932-8936.

91. Caruso, F., Nanoengineering of particle surfaces. Advanced Materials, 2001. 13(1): p. 11-+.

92. Caruso, F., Trau, D., Mohwald, H., and Renneberg, R., Enzyme encapsulation in layer-by-layer engineered polymer multilayer capsules. Langmuir, 2000. 16(4): p. 1485-1488.

93. Ishikawa, J., Baba, A., Kaneko, F., Shinbo, K., Kato, K., and Advincula, R.C., Photo-induced in-plane alignment of LC molecules on layer-by-layer self-assembled films containing azo dyes evaluated by attenuated total reflection measurements. Colloids and Surfaces A: Physicochemical and Engineering Aspects, 2002. 198-200: p. 917-922.

94. Advincula, R., Park, M.K., Baba, A., and Kaneko, F., Photoalignment in ultrathin films of a layer-by-layer deposited water-soluble azobenzene dye. Langmuir, 2003. 19(3): p. 654-665.

95. Lvov, Y.M., Kamau, G.N., Zhou, D.L., and Rusling, J.F., Assembly of electroactive ordered multilayer films of cobalt phthalocyanine tetrasulfonate and polycations. Journal of Colloid and Interface Science, 1999. 212(2): p. 570-575.

96. Cassagneau, T. and Fendler, J.H., High density rechargeable lithium-ion batteries self-assembled from graphite oxide nanoplatelets and polyelectrolytes. Advanced Materials, 1998. 10(11): p. 877-+.

97. Badia, A., Arnold, S., Scheumann, V., Zizlsperger, M., Mack, J., Jung, G., and Knoll, W., Probing the electrochemical deposition and/or desorption of self-assembled and electropolymerizable organic thin films by surface plasmon spectroscopy and atomic force microscopy. Sensors and Actuators B: Chemical, 1999. 54(1-2): p. 145-165.

98. Wu, A., Yoo, D., Lee, J.K., and Rubner, M.F., Solid-state light-emitting devices based on the tris-chelated ruthenium(II) complex: 3. High efficiency devices via a layer- by-layer molecular-level blending approach. Journal of the American Chemical Society, 1999. 121(20): p. 4883-4891.

99. Ferreira, M., Onitsuka, O., Stockton, W.B., and Rubner, M.F., Self-assembled heterostructures of electroactive polymers: New opportunities for thin-film

devices, in *Photonic and Optoelectronic Polymers*. 1997, American Chemical Society: Washington. p. 437-444.

100. Harris, J.J., DeRose, P.M., and Bruening, M.L., Synthesis of passivating, nylon-like coatings through cross- linking of ultrathin polyelectrolyte films. Journal of the American Chemical Society, 1999. 121(9): p. 1978-1979.

101. Ichinose, I., Muzuki, S., Ohno, S., Shiraishi, H., and Kunitake, T., Preparation of cross-linked ultrathin films based on layer-by- layer assembly of polymers. Polymer Journal, 1999. 31(11): p. 1065-1070.

102. Caruso, F., Caruso, R.A., and Mohwald, H., Nanoengineering of inorganic and hybrid hollow spheres by colloidal templating. Science, 1998. 282(5391): p. 1111-1114.

103. Caruso, F., Spasova, M., Susha, A., Giersig, M., and Caruso, R.A., Magnetic nanocomposite particles and hollow spheres constructed by a sequential layering approach. Chemistry of Materials, 2001. 13(1): p. 109-116.

104. Hiller, J.A., Mendelsohn, D., and Rubner, M.F., Reversibly erasable nanoporous anti-reflection coating from polyeletrolytes multilayers. Nature Materials, 2002. 1(1): p. 59-63.

105. Hiller, J.A. and Rubner, M.F., Reversible molecular memory and pH-switchable swelling transitions in polyelectrolytes multilayers. Macromolecules, 2003. 33(11): p. 4078-4083.

106. Brynda, E., Houska, M., Wikerstal, A., Pientka, Z., Dyr, J.E., and Brandenburg, A., Characterization of flexibility of ultrathin protein films by optical sensing. Langmuir, 2000. 16(9): p. 4352-4357.

107. Brynda, E., Houska, M., Brandenburg, A., Wikerstal, A., and Skvor, J., The detection of human beta(2)-microglobulin by grating coupler immunosensor with three dimensional antibody networks. Biosensors & Bioelectronics, 1999. 14(4): p. 363-368.

108. Brynda, E., Homola, J., Houska, M., Pfeifer, P., and Skvor, J., Antibody networks for surface plasmon resonance immunosensors. Sensors and Actuators B-Chemical, 1999. 54(1-2): p. 132-136.

109. Palumbo, M. and Petty, M.C. Ultrathin polymer films:application to metal ion sensing. in *A.C.S. National Meeting*. 2003. New York: American Chemical Society.

110. Palumbo, M., Nagel, J., and Petty, M.C., Surface plasmon resonance detection of metal ions: layer-by-layer assembly of polyelectrolytes sensing layers on a multichannel chip. IEEE Sensors Journal, 2003. submitted 3rd October 2003.

111. Hua, F., Lvov, Y., and Cui, T.H., Spatial patterning of colloidal nanoparticle-based thin film by a combinative technique of layer-by-layer self-assembly and

lithography. Journal of Nanoscience and Nanotechnology, 2002. 2(3-4): p. 357-361.

112. Hua, F., Cui, T.H., and Lvov, Y., Lithographic approach to pattern self-assembled nanoparticle multilayers. Langmuir, 2002. 18(17): p. 6712-6715.

113. Yang, S.Y. and Rubner, M.F., Micropatterning of polymer thin films with pH-sensitive and cross-linkable hydrogen-bonded polyelectrolyte multilayers. Journal of the American Chemical Society, 2002. 124(10): p. 2100-2101.

114. Hammond, P.T. and Whitesides, G.M., Formation of Polymer Microstructures by Selective Deposition of Polyion Multilayers Using Patterned Self-Assembled Monolayers as a Template. Macromolecules, 1995. 28(22): p. 7569-7571.

115. Jiang, X.P., Zheng, H.P., Gourdin, S., and Hammond, P.T., Polymer-on-polymer stamping: Universal approaches to chemically patterned surfaces. Langmuir, 2002. 18(7): p. 2607-2615.

116. Hua, F., Shi, J., Lvov, Y., and Cui, T., Patterning of layer-by-layer self-assembled multiple types of nanoparticle thin films by lithographic technique. Nano Letters, 2002. 2(11): p. 1219-1222.

117. Jiang, X.P., Chen, K., Zheng, H.P., Lee, I., Rubner, M., Kimerling, L., and Hammond, P.T., Selective self-organization of colloids on patterned polyelectrolyte templates. Abstracts of Papers of the American Chemical Society, 2001. 221: p. 94-PHYS.

118. Berg, M.C., Choi, J., Hammond, P.T., and Rubner, M.F., Tailored micropatterns through weal: Polyelectrolyte stamping. Langmuir, 2003. 19(6): p. 2231-2237.

119. Wang, T.C., Chen, B., Rubner, M.F., and Cohen, R.E., Selective electroless nickel plating on polyelectrolyte multilayer platforms. Langmuir, 2001. 17(21): p. 6610-6615.

120. Wang, L.Y., Wang, Z.Q., Zhang, X., Shen, J.C., Chi, L.F., and Fuchs, H., A new approach for the fabrication of an alternating multilayer film of poly(4-vinylpyridine) and poly(acrylic acid) based on hydrogen bonding. Macromolecular Rapid Communications, 1997. 18(6): p. 509-514.

121. Sukhishvili, S.A. and Granick, S., Layered, erasable, ultrathin polymer films. Journal of the American Chemical Society, 2000. 122(39): p. 9550-9551.

122. Rudmann, H. and Rubner, M.F., Single layer light-emitting devices with high efficiency and long lifetime based on tris(2,2 ' bipyridyl) ruthenium(II) hexafluorophosphate. Journal of Applied Physics, 2001. 90(9): p. 4338-4345.

Chapter 5

Design, construction and evaluation of a novel SPR system

5.1 Introduction

The following chapter is focused on the design and realization of a custom-built single chip, multi-channel surface plasmon resonance system. This is based on angular interrogation using a monochromatic light source. The entire SPR device was developed especially for the research presented in this thesis. The original schematic design drawn in collaboration with Dr. J. Nagel from the Institute of Polymer Research in Dresden is the results of several modifications. While some of the general ideas behind this design have been around for some time [1-6], there are still some issues that need to be addressed [7]. One of the main points is that of multisensing, i.e. with more than one sensing film interacting with the medium under investigation. Multi-analyte detection capability is a highly desirable feature in a SPR sensor [7].

The approach used in this work shifts the concept of multi-channels from that of a multi-cell flow system, used in some commercial devices [4, 8], to that of a specially designed sensing chip with several active materials on its surface [9, 10]. A group at Washington University has recently been involved with similar studies [6, 7, 11, 12]. In this research, a white light source was used and the sensing channels defined via spectral discrimination by means of altered angles of incidence [11] or by means of a high refractive index overlayer [5] (see Fig. 5.1). With the latter, up to four channels were investigated using two parallel white light beams with a diameter of approximately 2 mm each.

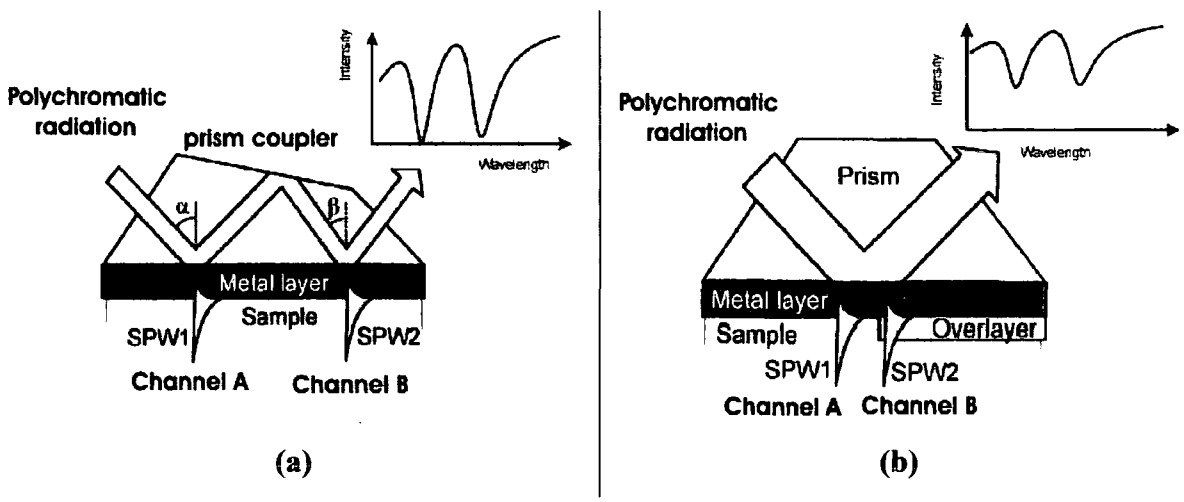

Figure 5.1 SPR dual-channel sensors based on spectral discrimination of sensing channels. (a) by means of altered angles of incidence. (b) by means of a high refractive index overlayer. (Reproduced from [13]).

The research presented in this thesis uses angular interrogation. A full array of parallel sensing films is addressed with monochromatic light. The investigation channels are distributed along a line 15 mm wide [9, 10, 14, 15].

With angular interrogation based devices, it is appropriate to note that, with a multi-cell flow system, as found in some commercial devices (see Figure 5.4), it is possible to analyze different media (solutions) using the same active film. Therefore, a relatively high measurement throughput is achieved. When several active architectures are deposited on the same chip and a single flow cell is used, the same solution can interact with different materials. For example, if an array of materials with different selectivities is arranged on the chip surface [9, 10, 15], then comparative sensing [10, 15] can be performed.

The above might lead to multi-analyte SPR detection not dissimilar to that of an electronic nose: an *electronic tongue*. Sensors based on SPR imaging [16-18] might form the base of such a device, but instrumentation able to read SPR responses independently and simultaneously from a two dimensional array needs to be developed [7].

5.2 Sensing system design

A compact size for the SPR system was thought to be one of the main design criteria. However, a certain flexibility of the optical and mechanical equipment was needed to allow for modifications during the research. The equipment should also be low cost and suitable for remote use, even in a hazardous environment.

Traditionally, the most common experimental SPR set-up uses the Kretschmann configuration [19] in association with a $\theta/2\theta$ stage, performing angular scans (see Fig. 5.2). The *sensing cell* (prism, glass slide coated with metal and eventual sensing layer, cuvette) is mounted on a revolving table and illuminated with *p*-polarized, monochromatic light. A detector positioned on the outer section of the table monitors the reflected beam. The detector rotates by 2θ, the sample by θ, thus keeping the beam spot on the detector. To account for any fluctuations in the intensity of the source, a reference beam is taken and phase-sensitive detection is employed to remove

interference from background sources. Some configurations use a stationary large area detector, covering a range of the sample's angular movement of up to 10^{o} [20]. The entire system is usually fixed on a large optical table. The use of moving parts ensures angular movement of fractions of degrees. However, using a laser as a light source provides a relatively cumbersome and expensive solution.

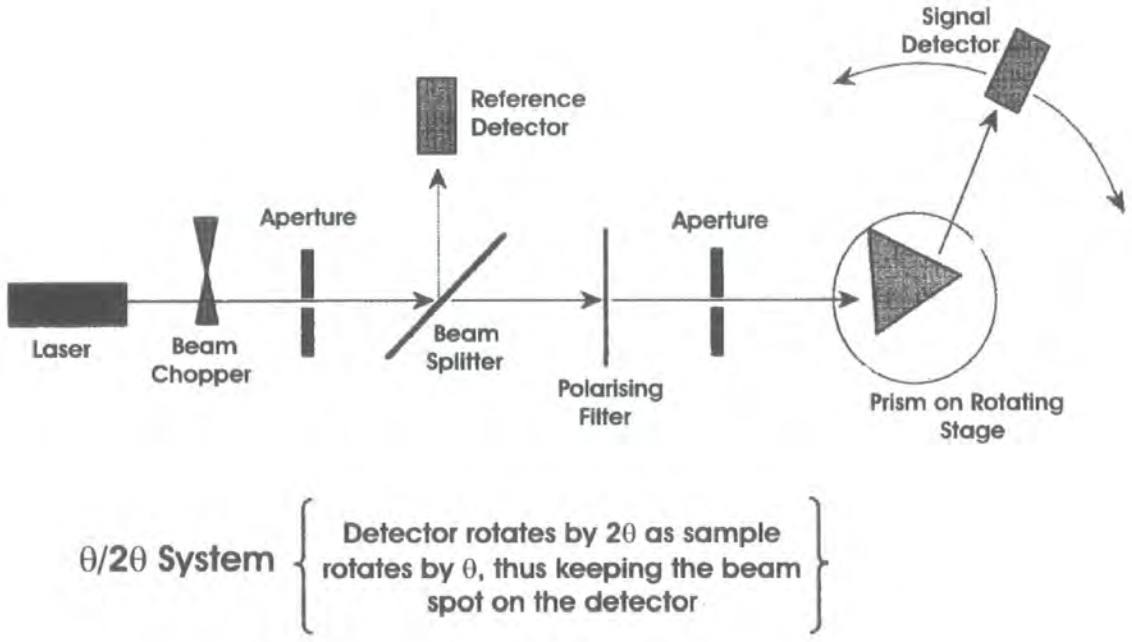

Figure 5.2 Diagram of a typical θ/2θ stage. (Reproduced from [21]).

An alternative design to the θ/2θ stage eliminates the rotating stage, i.e. a set-up with no moving parts. This provides simultaneous illumination of the sample across a fixed area with a range of incident angles (see Fig. 5.3). Thus, the entire SPR angular spectrum can be monitored in real-time and changes can be detected without performing angular scans. The absence of rotating components gives higher mechanical stability and makes the equipment ideal for in-situ measurements. Matsubara et al. [2, 3] have previously used Köhler illumination, employed for incoherent illumination of microscopes, to focus the light onto the sample [22].

The angular resolution (i.e. the smallest division that can be read) of a θ/2θ stage is typically 0.001°, which for gold in water at a wavelength of 760 nm corresponds to approximately 10^{-5} refractive index units [19]. In the case of a fixed photodiode array,

the resolution is limited by the number of pixels in the detector, the analogue-to-digital converter and the 'dip-finding' algorithm [19]. Assuming that the resolution of the system described here is limited by the number of pixels in the CCD camera and by the angular range investigated, we estimate an angular resolution of about 0.01° for a detector 752 x 582 pixels, each 8.6 μm in size, and an angular range of 6°. This is less than that of the θ/2θ arrangement. However, a significant advantage of the set-up with a CCD camera is that it is not necessary to know with absolute precision the exact position of the different sensing films, because they can imaged directly from the camera once the sensing chip has been put in place. With a photo-diode array, fine control of the spatial position is necessary, together with a precise docking sensing chip-cuvette.

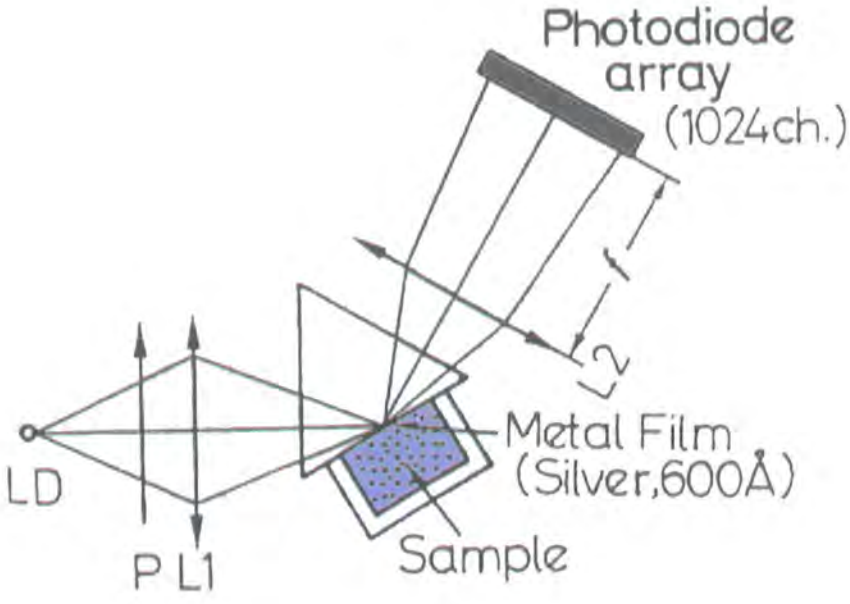

Figure 5.3 Schematic diagram of the SPR sensor developed by Matsubara. LD; laser diode; P: polarizer; L_1: focusing lens; L_2: focusing lens (Reproduced from [2]).

Biacore commercial devices exploit simultaneous illumination of the sample across a fixed area with a range of incident angles and use a photo-diode array as the detector. Furthermore, these are equipped with a multi flow cell system; on some of them, a four flow cell system is placed over the same sensor surface (see Fig. 5.4).

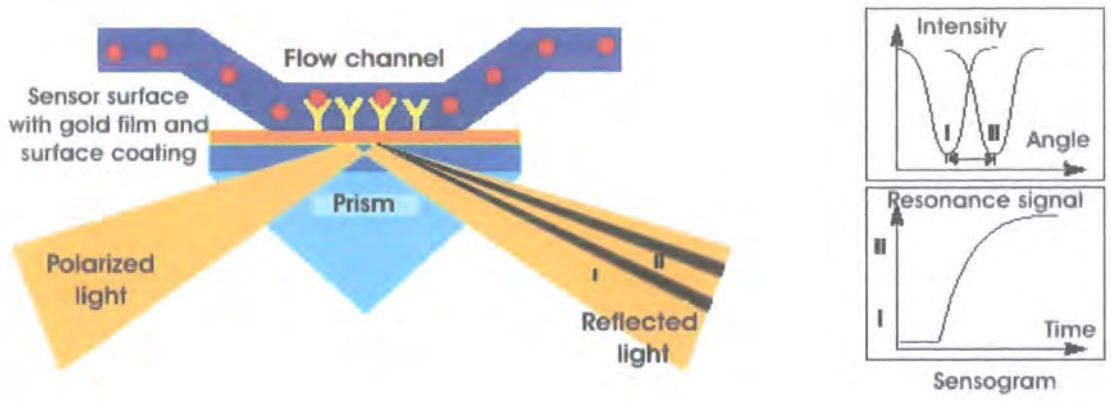

(a)

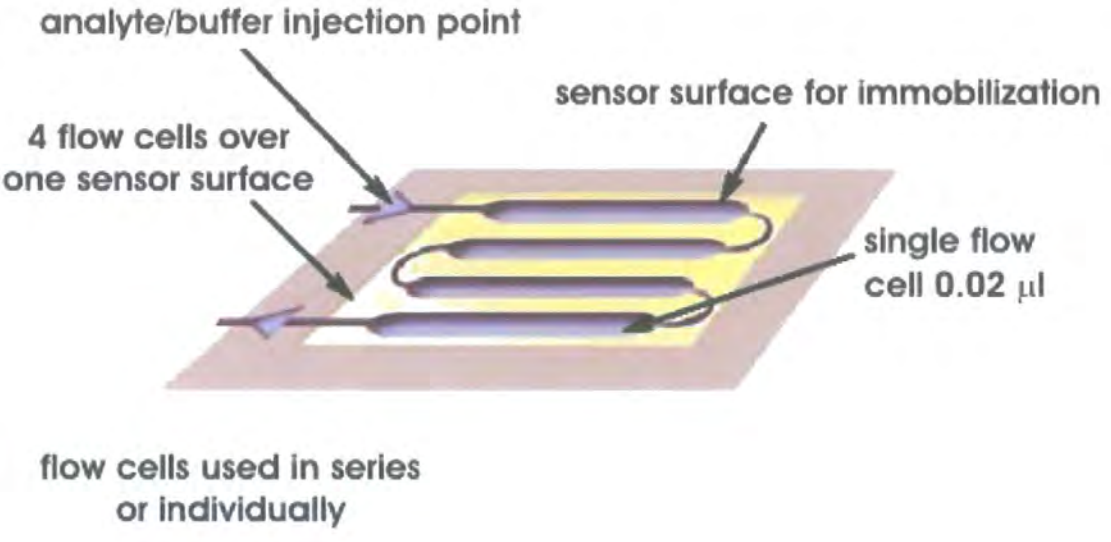

(b)

Figure 5.4 Biacore device. (a) In Biacore systems, the incident p-polarized light is focused into a wedge-shaped beam. An increased sample concentration in the surface coating of the sensor chip causes a corresponding increase in refractive index which alters the angle of incidence, the SPR angle. This SPR angle is monitored as a change in the detector position for the reflected intensity dip (from I to II). By monitoring the SPR angle as a function of time, the kinetic events on the surface are displayed in a sensorgram. (b) Biacore S51: details of the flow-cell system. 4 flow cells are placed over one sensor surface. Each of them can be used in series or separately. (Reproduced from [8]).

In the Biacore approach, the concept of "multi-channels" is interpreted as the independent addressing of different samples on the same active surface and not the addressing of different sensing films by the same analyte. Of course, it can be argued that with a Biacore system it should be possible to use a plain gold surface for the creation of unique surfaces. The flow cell system could be used, for example, to deposit

a layer-by-layer polyelectrolyte architecture on the gold surface. Considering the very high price of such a device (basic set-up, plus the cost of the sensor chips) such a solution is not ideal, especially for in-situ applications. It is not by accident that the market covered by these devices is the characterization of biopharmaceutical products.

Recent investigations [5, 6, 9, 14] have shown the advantages of multi-channel SPR sensing (hereafter multi-channel refers to a multi-(sensing films) system implemented on the same chip). The use of one channel as a reference enables more accurate quantification of molecular interaction events, discriminating between target and non-target molecular adsorption processes on the sensor surface. A CCD camera can be used to produce a set of data resembling that obtained from an array of sensor elements, each with a different selectivity [9, 23]. Using a monochrome CCD camera (COSTAR SI-M350 ½" CCD camera with C-mount) as detector (752 x 582 pixels, 8.6 μm size) and a suitable optical system to focus the reflected beam onto the camera chip, a relatively large area can be addressed. In particular, in the most advanced version of the Durham SPR system, a line of 15 mm could be interrogated at the same time [10, 15]. This feature distinguishes the system developed in this work from analogue multi-channel SPR sensors that are based on spectral discrimination and work with smaller lengths of interrogation [5, 6].

5.3 Light source

An accurate choice of the light source is fundamental to the design of a successful SPR system. To reduce the size and cost of the equipment, it was decided not to use a He-Ne laser. Working on angular-interrogation (or, in other words, with monochromatic light), the remaining alternatives were: (a) a diode laser (semiconductor laser); or (b) a light emitting diode (LED). Previous work at Durham [24] has shown clearly that, using a solid-state semiconductor laser diode, diffraction-type effects can seriously degrade the clarity of the SPR profile, see Fig. 5.5. A CCD camera, in conjunction with software for image acquisition and magnification (Photofinish) captured a series of images of the SPR profile and the beam spot for different monochromatic light sources: a gas laser He-Ne with λ=632.5 nm; a laser diode with λ=670 nm; a laser diode with λ=635 nm. Diffraction-type effects were characteristic of the laser diodes, but absent with the He-

Ne gas laser. The conclusion was that the diffraction effects have to be considered as a fundamental limitation of laser light. Such effects could be related to the oscillations within the laser cavity. Furthermore, it was suggested that important roles are played by the number of dislocations in the semiconductor material and/or from device aging.

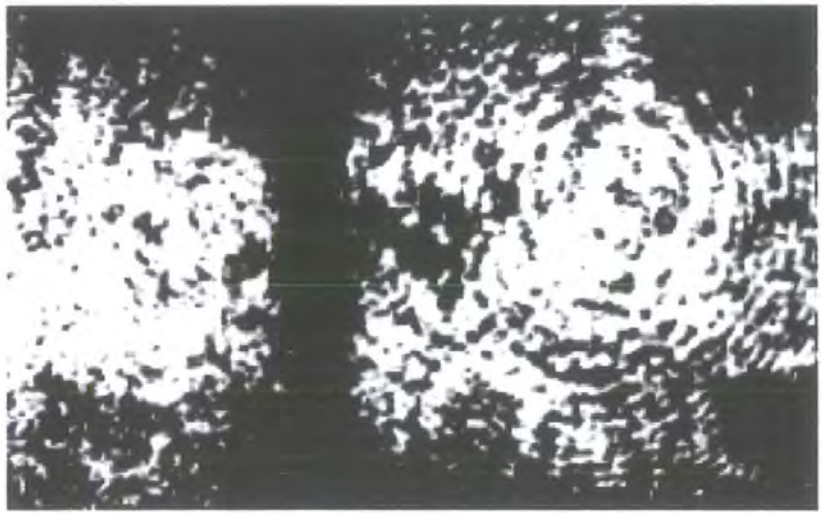

(a)

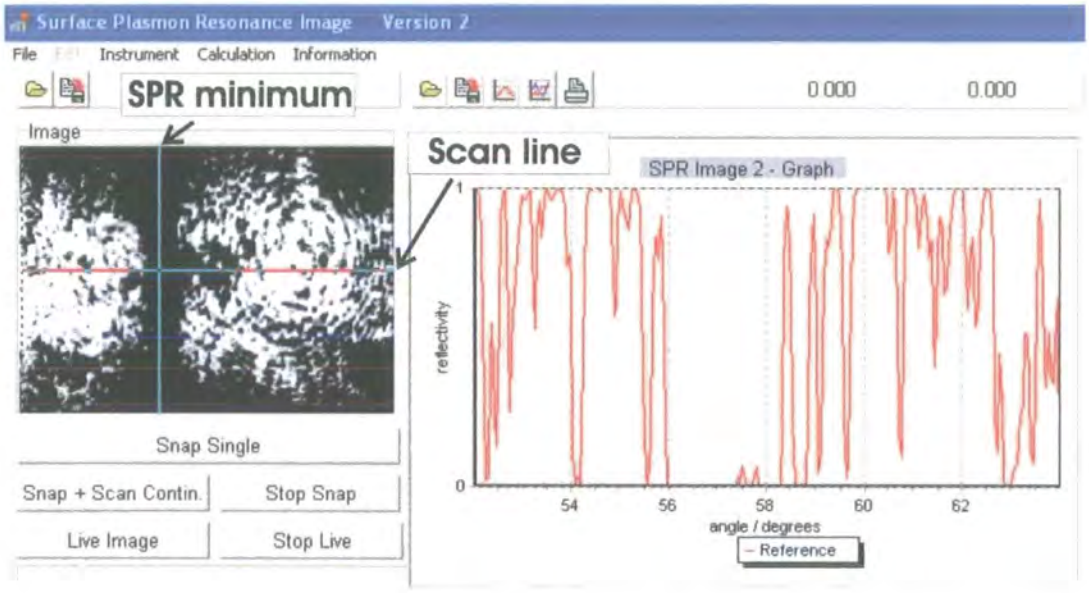

(b)

Figure 5.5 (a) SPR two dimensional diffraction effect. The black band identifies the SPR minimum. However, diffraction effects make the image difficult to read. (b) Analysis of the image through the in-house software program. Note the irregularities of the graph on the left. Despite the presence of a large resonance minimum between 56 and 58 degrees, the diffraction effects produce other minima that give the graph a very high level of noise.

It was decided to repeat the experimentation with the diode laser to confirm previous results. Once again, two different semiconductor laser diodes were investigated: (a) a RS 194-026: 670 nm, 3 mW; and (b) a RS 213-3584: 635 nm, 3 mW. The latter device produced a reduced diffraction-type effect. Therefore, it was used in some experiments to understand not only how much the diffraction-type effects could influence the SPR profile, but also to reveal the minimum response level of the CCD camera.

The following components were arranged on a single slide rail:

- the 635nm Radio Spares laser diode;
- a neutral density filter (1% transmission, 0.1% transmission or a combination of both); and
- a CCD camera (chip size: 8.6 x 8.3 μm; element array size: 752 pixels x 582 pixels) connected to a monitor to give a *real time* image and then to a PC via a video card.

Different distances, of the order of tens of cm, between the laser diode and the CCD camera were used (Fig. 5.6).

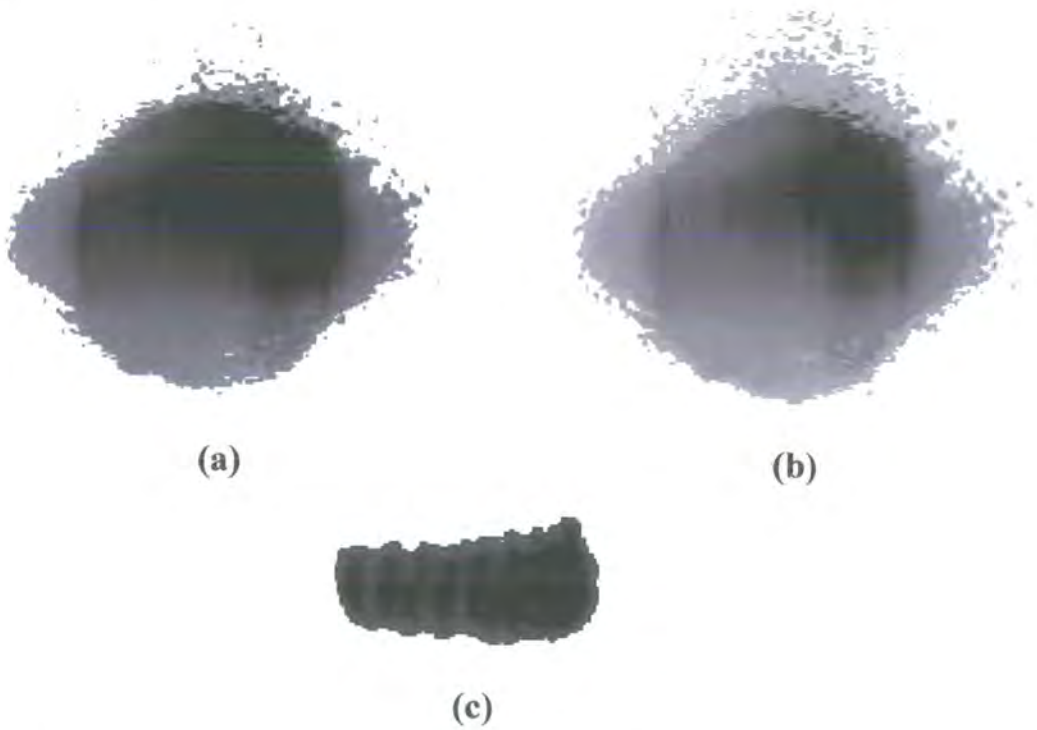

Figure 5.6 Diode device spots: (a) 1% transmission; (b) 0.1% transmission; (c) 0.01% transmission.

As it shown in Fig. 5.6, very low level of luminosity can be detected from an off-the-shelf CCD camera.

The LED was a InGaAlP device from Toshiba (TLRH190P), with a nominal peak emission wavelength of 644 nm, a high luminous intensity (typ. 15000 mcad @ 20 mA) and a limited view angle (typ. 4 deg). Spectroscopic measurements were made to verify these characteristics, Fig. 5.7 and were consistent with the technical specification given.

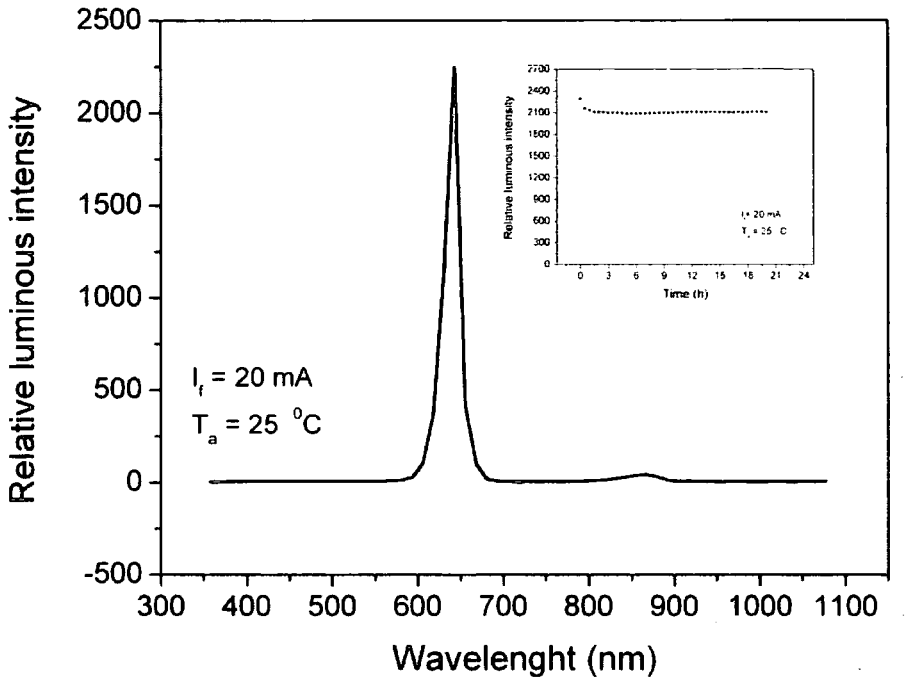

Figure 5.7 Output spectrum spectroscopy of the Toshiba TLRH190P red LED. The relative luminous intensity is measured for each LED's emission wavelength. In the insert in the right top corner the relative luminous intensity is plotted as function of time.

To test the optical stability of the LED, the output of the TLRH190P was monitored over 20 hours using an integrating sphere and a fibre optic cable connected to a RS spectrometer. Every 30 minutes, a new relative luminous intensity versus wavelength profile was automatically taken. In the first two hours of the test a reduction of approximately the 6% in the luminosity intensity was detected. Thereafter, no other significant variation occurred. The position of the peak of maximum intensity was found at λ=642.24 ± 0.37 nm. Within these limitations, and considering the average time taken by the SPR experiments (from few minutes to few hours), the LED output

may be assumed to be adequately stable. However, this assumption is only true if no variation in the input value of current occurs. Otherwise, due to its steep I-V characteristic, the brightness will be very sensitive to small current fluctuations (see Fig. 5.8).

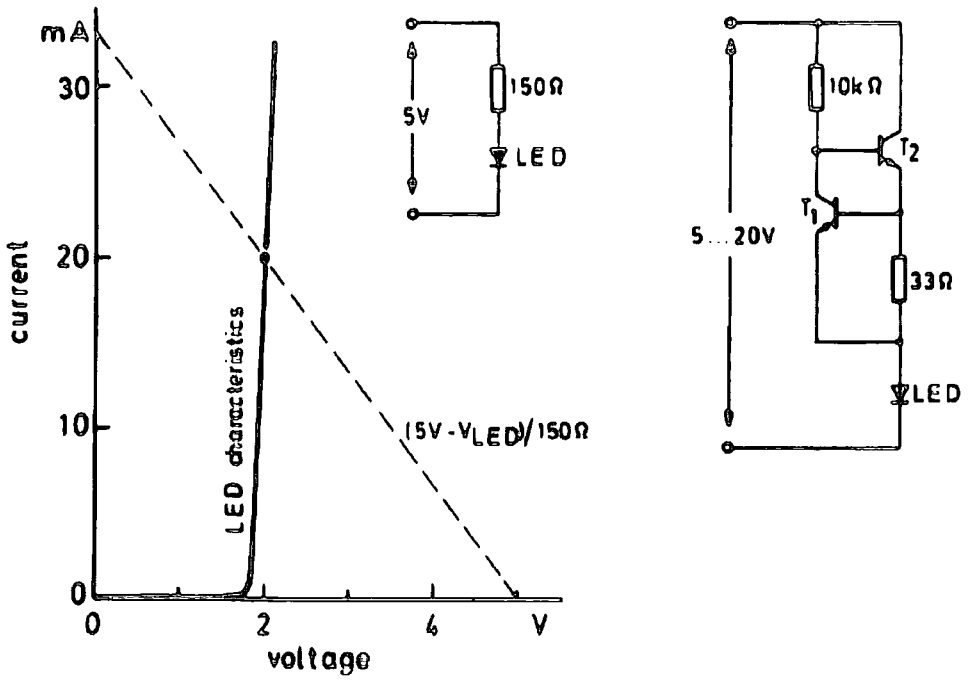

Figure 5.8 Methods of control of LED current, left: LED with series resistor, determination of working point, right: LED with constant current source for approximately 20 mA. (Reproduced from [25]).

Using an LED, two different methods can be used to ensure a constant current [25]. The very simple solution of a resistor in series with the LED (Fig. 5.8 left) is applicable when the latter is driven by a voltage source. The current though the LED (I_{LED}) is defined by the intersection of the LED characteristic with the straight line given by

$$\frac{\text{operating voltage - LED voltage}}{\text{resistance}} \tag{5.1}$$

which is $\frac{5 \text{ volts} - V_{LED}}{150\,\Omega}$ in the example shown in Fig. 5.8. If larger voltage variations are expected, LEDs are driven best using a constant current source. Integrated circuits are usually employed for such purpose. A simple constant current source can be provided by two transistors and two resistors, as shown on the right hand of Fig. 5.8. This circuit

controls the LED current via the voltage drop along the 33 Ω resistor. If the current increases, the transistor T_1 becomes more conducting, thus diminishing the current flowing into the base of the transistor T_2. As a consequence, the output current is further decreased. The value of the second resistor is determined by the minimum voltage to be expected and the base current necessary to drive T_2.

Both solutions were used in the design of the SPR device and both proved to be reliable. However, the constant current source device was used for the majority of the experiments presented in this thesis.

5.4 Mechanical and optical configuration

Two different optical configurations were designed to achieve the uniform illumination required for the excitation of the surface plasmon and to limit misleading information in the SPR profile.

The principal difference between these two solutions was the number and type of lenses used in the *beam expander* (Fig. 5.9). A uniform illumination of the sensing chip and a control of the diameter of the incident beam enhance the overall flexibility of the system. For both designs, at the exit of the beam expander, the simultaneous illumination of the sample within a range of incident angles is achieved using a semi cylindrical lens (see Fig. 5.9(a) and 5.9(b) and Fig. 5.11). The lens focuses the light in the vertical position, i.e. normal to the schematic plan shown in Fig. 5.9(a) and Fig. 5.9(b) and Fig. 5.11.

Optical system A

- The red emitting LED
- An iris diaphragm with a min aperture ϕ_{min}=1 mm and a ϕ_{max}=18 mm
- A concave lens. Three different focal lengths were tested: f_1=-40 mm; f_2=-50 mm; f_3=-100 mm
- A convex lens. Two different focal lengths were tested: f_1=60 mm; f_2= 100 mm
- A coloured glass filter RG 630
- A polarization filter type 4K in mount CL
- An iris diaphragm with a min aperture ϕ_{min}=1 mm and a ϕ_{max}=18 mm

- A convex cylindrical lens. Two different focal lengths were tested: f_1=80 mm; f_2=30 mm

Optical system **B**

- The red emitting LED
- An iris diaphragm with a min aperture ϕ_{min}=1 mm and a ϕ_{max}=18 mm
- A biconvex lens. Three different focal lengths were tested: f_1=16 mm; f_2=20 mm; f_3=25 mm
- An iris diaphragm with a min aperture ϕ_{min}=0.1 mm and a ϕ_{max}=18 mm
- A plano-convex lens. Two different focal lengths were tested: f_1=80 mm; f_2=100 mm
- A coloured glass filter RG 630
- A polarization filter type 4K in mount CL
- An iris diaphragm with a min aperture ϕ_{min}=1 mm and a ϕ_{max}=18 mm
- A convex cylindrical lens. Two different focal lengths were tested: f_1=80 mm; f_2=30 mm

All the optical components, together with the mechanical supports were purchased from LINOS Photonics. Once the beam had been expanded, the convex cylindrical lens focused it along the vertical direction (Fig. 5.10). To prove the efficiency of such a configuration, a CCD camera was placed in line with the two optical systems with and without the semicylindrical lens. Images of the unfocused and focused beam are shown in Fig. 5.10. The result is that a simultaneous illumination within a range of angles is achieved. This is true not only at a *single point*, but all along the vertical direction within the light beam original diameter i.e. along a *line*. An important factor is that this line has a two dimensional nature and, therefore, it has an associated *area*. As will be discussed further on, this has some important consequences for the SPR profiles detected by the CCD camera. It was important to place the sample as close as possible to the focusing point of the lens, so as not to compromise the quality of the data obtained, i.e. to have a SPR profile as sharp as possible.

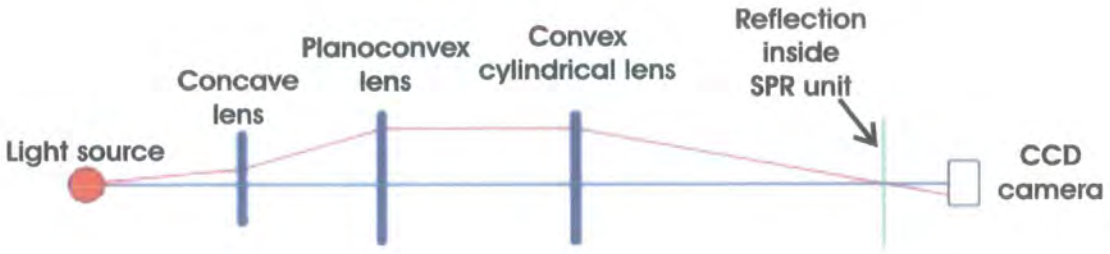

System A

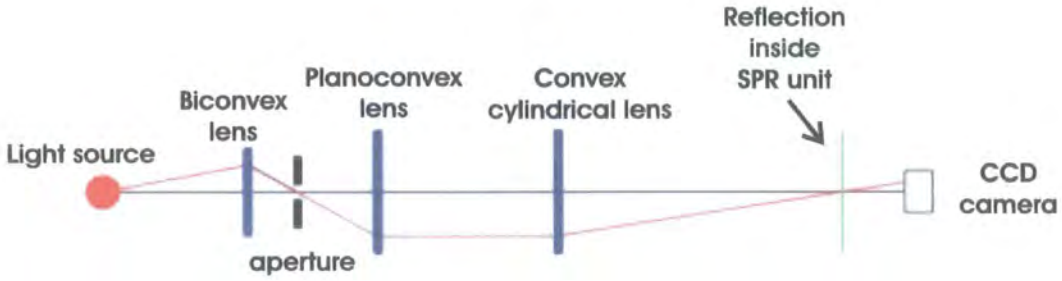

System B

Figure 5.9 Optical systems A and B: basic schemes. Only the main optical components are represented. Coloured filters and polarization filters are omitted for clarity.

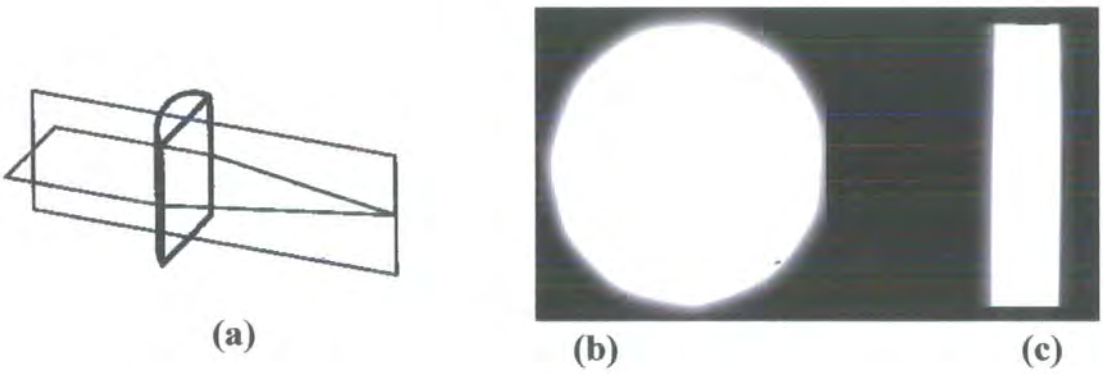

Figure 5.10 (a) Cylindrical lens. Schematic illustration of the cylindrical lens optical properties. Two images captured by the CCD camera positioned (b) before and (c) after the lens.

The optical configurations tested were satisfactory in achieving (i) good uniformity of the light beam incident the sensing chip, (ii) simultaneous illumination across a range of angles and (iii) simultaneous illumination of an entire area (i.e. along the vertical

direction) of the sample. The surface plasmon resonance was then extended to a larger area of the sample. Several configurations of the two systems were tested with lenses of different focal length. Although, as shown in Fig. 5.9, both accomplish the tasks they were designed for, the final choice was the set-up shown in Fig. 5.9(b). It is believed that this provided a higher degree of control of the beam mainly thanks to the iris placed between the biconvex lens and the planoconvex lens. This iris ensures the circularity of the beam. The SPR system was usually placed in a black box to avoid interference from external sources of radiation. The final design of the SPR system is shown in Fig. 5.11.

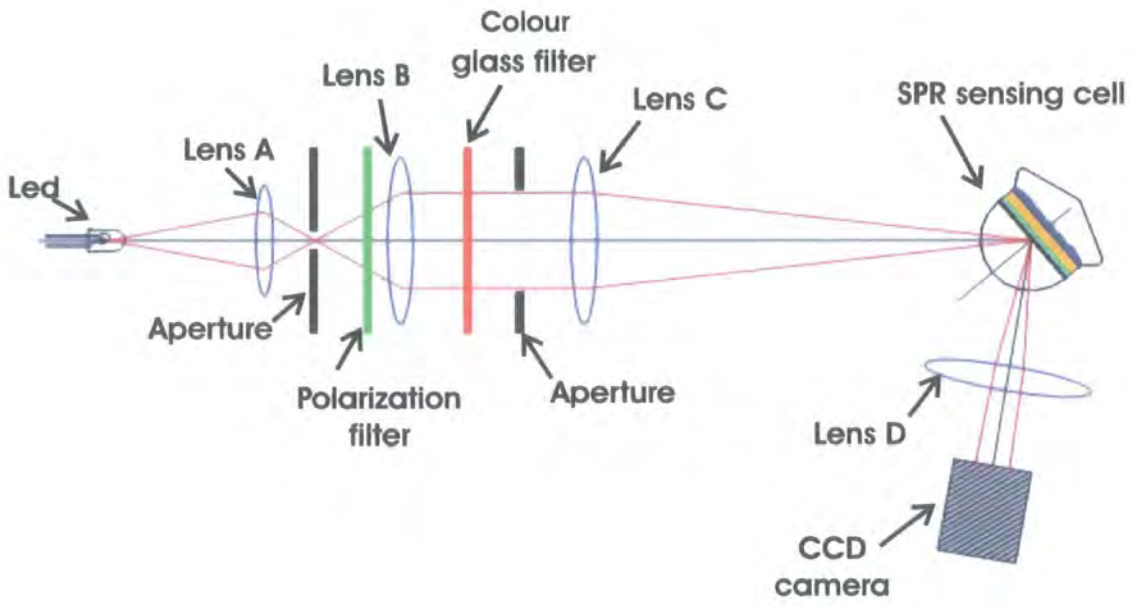

Figure 5.11 Schematic representation of the SPR system (plan view).

A semicylindrical prism of SF10 glass (R=15 mm planoconvex; 30 mm x 30 mm; centre thickness= 14 mm; flatness; L/2; polish= 3/1) was made to order from Hellma MA Ltd. Its function was to couple the light to the surface plasmons. The curved surface of the glass ensures that the incident light is always normal to its surface. The choice of a SF10 glass instead of the more conventional BK7 was deliberate. Thanks to an in-house program developed in collaboration with Dr. J. Nagel from the Institute of Polymer Research in Dresden [26], it was possible to calculate the theoretical SPR profile for a gold coating exposed to air or water and coupled to a BK7 prism or an SF10 prism. As shown in Fig. 5.12, the position of the resonance minimum is not only a function of the medium to which the metal surface is exposed, but also a function of the refractive index type of the prism. Working within a range of incident angles between

50° and 60° was thought to be optimum. Therefore SF10 was chosen as material for the semicylindrical prism and consequently for the glass slides to be coated by the metal.

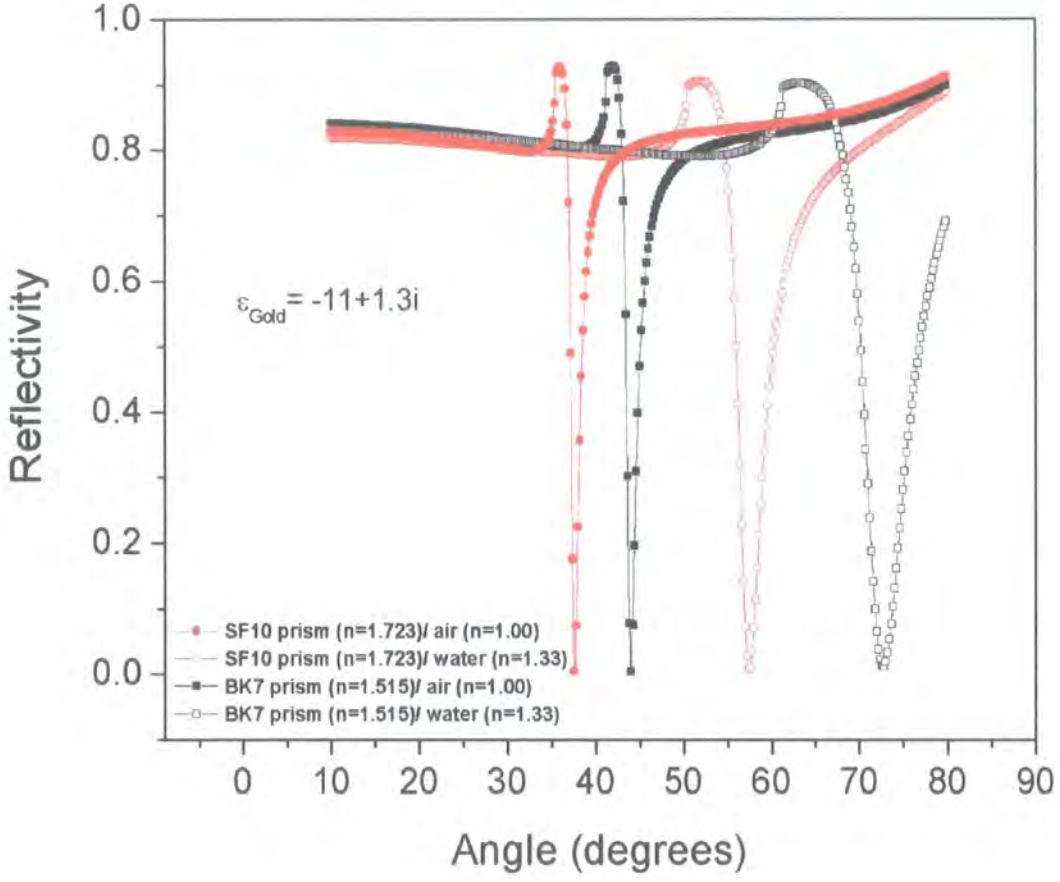

Figure 5.12 Theoretical SPR profiles. Note the shift in the resonance minimum when the medium is changed and/or the BK7 prism is substituted by an SF10 glass prism.

A matching fluid was necessary to ensure continuity in the refractive index value, filling the gap between the prism and the glass slide. An appropriate solution was Cargille Meltmount from Cargille Labs. This came in a variety of refractive indices with good adhesive properties. However, the material was a solid at room temperature and needed to be melted on a hot plate before being applied between the prism and glass slide. A specially made solution was also used. This consisted of 67% (by volume) methylene iodide, CH_2I_2 (M_w=267.8) and 33% 1-bromonaphtalene, $C_{10}H_7Br$ (M_w=207.08). As this mixture was liquid at room temperature, it was easier to apply. The disadvantage was that, within 24-36 hours, the fluid tended to flow away, as the prism and the glass slide were positioned vertically. Ideally, the metal should be coated directly on the prism; this would allow experiments over a long period (assuming a comparable long working life

for the sensing film). Already commercial examples of such approaches are available, like the SPReeta® system from Texas Instruments or the sensor chip used in the Plasmonic® device from Jandratek Ltd. The high cost of the SF10 prism, however, meant delaying the approach to a more advanced state of the research.

A specially made *cuvette* in polymethylmetacrylate (PMMA) or as it is more commonly known, Perspex, was made to hold the prism and glass slide together and to create a suitable chamber to expose the sensing chip to the solution to be studied. An early design is shown in Fig. 5.13.

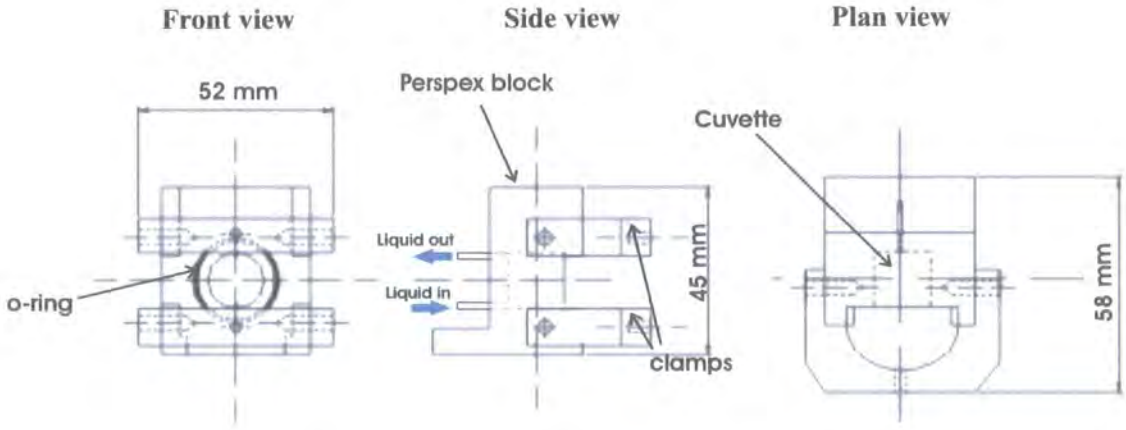

Figure 5.13 Front, side and plan view of the cell. The main dimensions (in mm) are indicated.

The cell shown in Fig. 5.13 was clamped on a specially made swivel arm. A series of screw holes allowed the position of the cell to be moved along the swivel arm according to the angular range investigated. In this way, the light beam was always focused on the middle of the sensing chip. However, this solution proved to be over-engineered and not easy to work with because of the necessity to fix the position of the cell on the swivel arm from the bottom. Therefore, a better arrangement was found with a new cell, this time suspended from above, Fig. 5.14. As shown in Fig. 5.12, changing the media in contact with the sensing chip from air to liquid changes the position of the resonance minimum. Therefore, it was essential to be able to rotate the cell to enhance the flexibility of the SPR system. From the first cell to the final one, the dimensions of the internal chamber were reduced from 15 mm x 15 mm for a total volume of 2.65 ml, to 15 mm x 6 mm for a internal volume of approximately 1 ml.

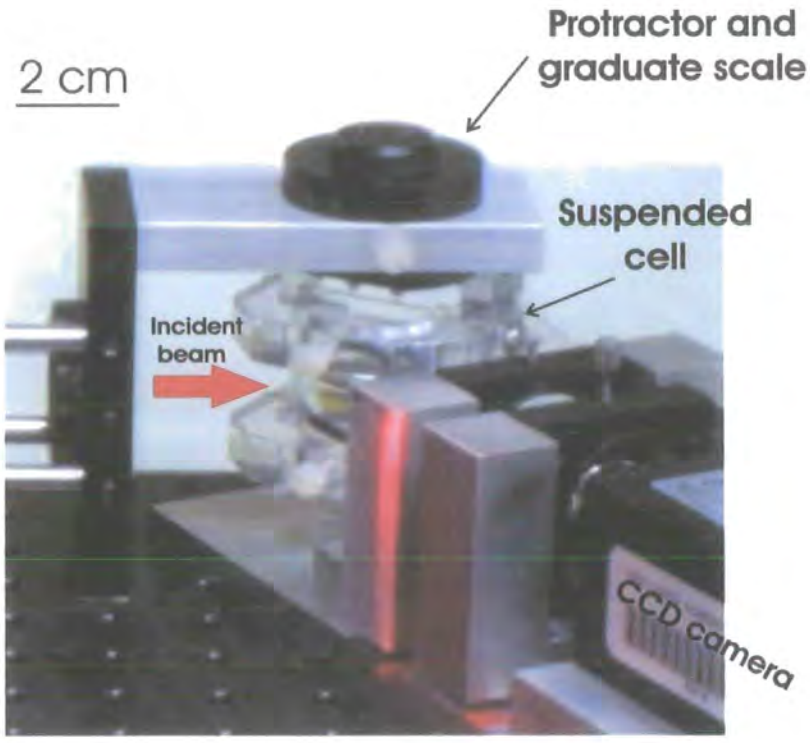

Figure 5.14 Details of the suspended cell. The incident beam is focused on the same area and changes in the angular range of investigation are obtained by simply rotating the cell.

A peristaltic pump with a variable pumping speed (in a range of few ml/min) was used to fill the cuvette with the different solutions. The two connecting tubes (inner diameter of 1 mm) were made of Teflon for easy cleaning and avoiding sample contamination.

To complete the optical design, a second system of lenses was built to focus the reflected beam onto the CCD camera. A key feature that allows different sensing channels to be interrogated simultaneously is the focusing of the beam along the vertical axis. In Figure 5.15 it is possible to appreciate how, by varying the lens configuration, it is possible to image a smaller or larger portion of the sensor chip. In particular, a special gold pattern was used to provide a dimensional reference. Using a shadow mask a pattern of several parallel gold lines of 1 mm at a distance of 2 mm each other was deposited via e-beam evaporation. Then, it was seen how much of this pattern could be observed by varying the focusing optics.

Without an optical system and with a distance of approx 5 cm between the metal surface and the CCD camera, a range of 6^{o} could be detected. In contrast, with a focusing system up to 13^{o} could be measured.

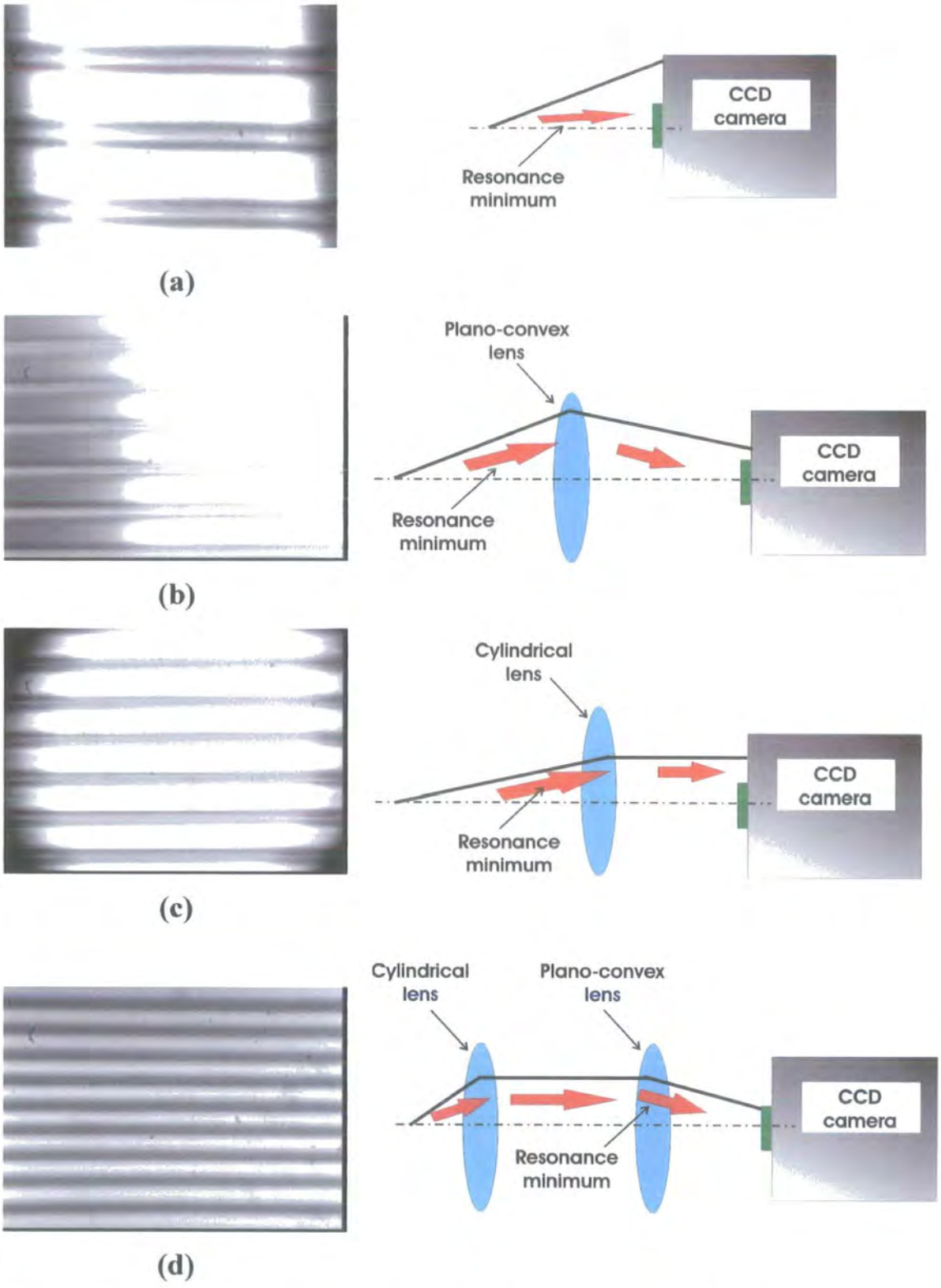

Figure 5.15 Focusing of the reflected beam. (a) no focusing; (b) plano-convex lens; (c) cylindrical lens; (d) cylindrical lens plus planoconvex lens.

As the resolution of the CCD camera decreased with an increase of the angular range investigated, it was decided to limit the latter to a range of 6-8°. A custom built swivel

arm allowed the CCD camera to be rotated according to the angular range under observation. The cuvette and swivel arm rotate around the same axes, thus the two are constantly angle coordinated.

The final version of the SPR system is shown in Fig. 5.16.

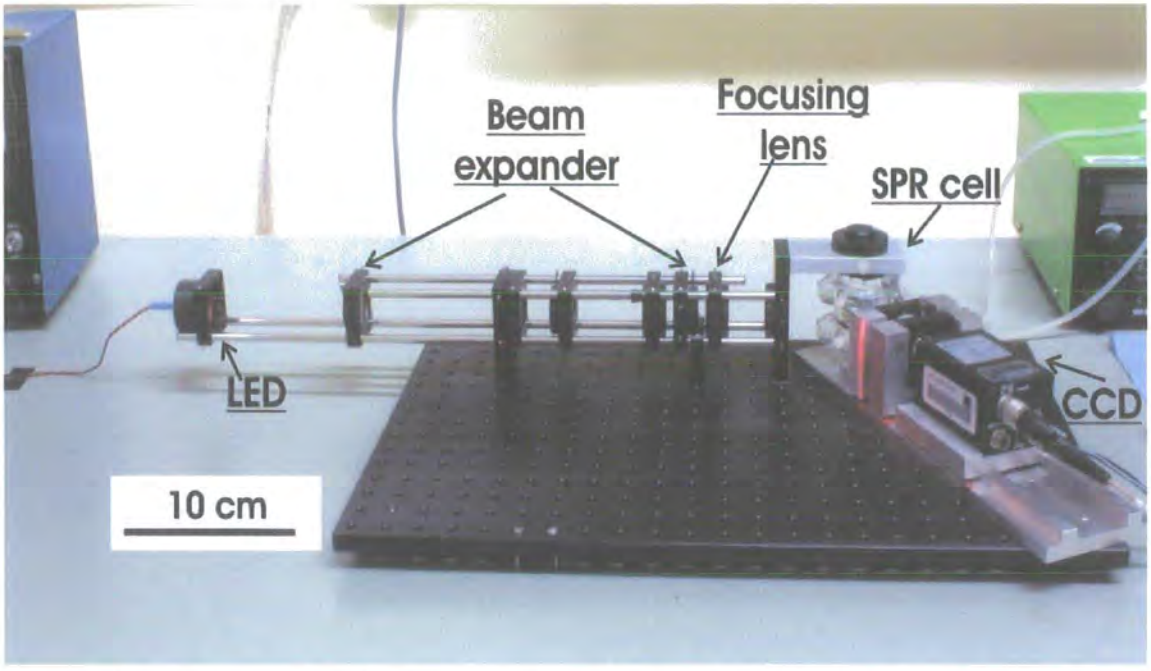

Figure 5.16 Final SPR system. The main components are indicated. On the far right the peristaltic pump is shown, which allows a continuous flow of solution within the cuvette.

5.4.1 CCD camera characteristics and acquisition/processing programme

A monochrome charge-coupled device camera (COSTAR SI-M350 ½" CCD camera with C-mount) formed the detector (752x582 pixels, 8.6 μm size), while a 10 bit analogue board (MV-Sigma SLG, Matrix Vision) provided an interface to a PC.

A charge-coupled device consists of a two-dimensional self-scanning imaging area composed of photosensitive pixels that accumulate and store electric charge. When light falls on a CCD camera, the matrix of small potential wells collect the charge. The information from these photo-sites is then re-collected, organized, and transferred. The resolution and contrast are two of the most important characteristics of the camera. The first is a measure of the imaging system's ability to reproduce details. In a CCD camera,

a single spot is resolved from the next if the distance between the two is equal or bigger than the length of a line-pair. i.e. a couple of neighbouring pixels. The analogue camera has a resolution of 570 TV lines in the horizontal direction and 480 TV lines in the vertical. The contrast is the ability to differentiate between the object and its background. For an analogue camera, this is normally given as a signal to noise (S/N) ratio in decibels (dBs). The COSTAR SI-M350 ½", has a S/N ratio of 56 dB minimum. Resolution and contrast are interconnected, since the former depends on blurring caused by diffraction and optical errors from the lens system, the dot spacing and finally on the contrast itself.

An in-house program was developed [26] to acquire and process the information from the CCD camera (Fig. 5.17).

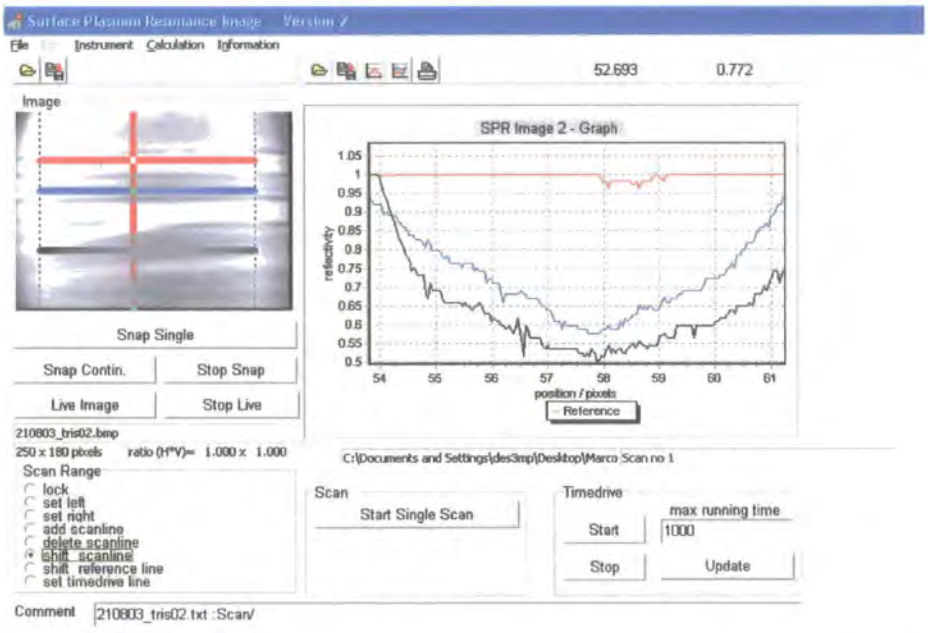

Figure 5.17 Software user interface. On the left an image of the sensor chip is evident; while on the right two SPR curves and the intensity of the reflected beam from the reference channel are shown.

Different options were available with this software. For example, a 'live' image could be viewed or single frame images recorded (single or continuous operation). The program allowed the position of the reference line and several scanning lines to be set independently. Furthermore, it was possible to fix the position of a time-drive line and to start a time-drive scan. This registered the variation of reflectivity at a fixed position for every scan line. From such a scan it was then possible to obtain information about

interfacial processes occurring inside the cuvette (e.g. to monitor the self-assembly of a thin overlayer on the gold surface or to study the interaction between a sensing layer and an analyte introduced into the cell).

A simulation programme (see Fig. 5.18) allowed a comparison to be made between the experimental data and theory, which could be used to determine the optical constants and thicknesses of metal substrate and the multi-layer structures [27]. However, there were limitations in the curve fitting of the experimental data. For example, the light emitted by an LED is not exactly monochromatic, but as shown in Fig. 5.7, it is distributed over a range of wavelengths. Therefore, there was an element of ambiguity in the results obtained.

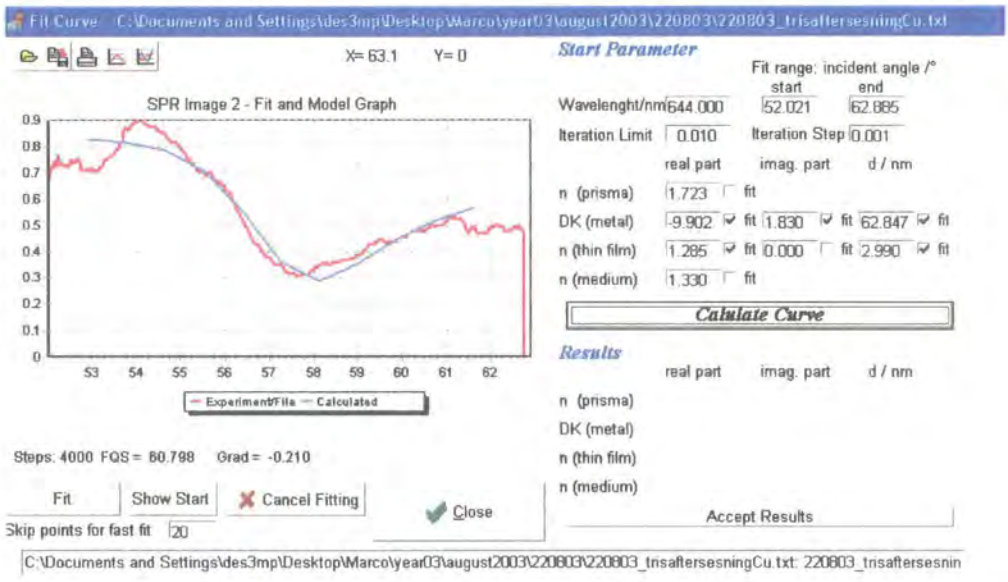

Figure 5.18 Fitting of an experimental curve.

5.4.2 Sensitivity and pixel/angle ratio

A simple two-channel chip was used to determine the absolute sensitivity and for the angular calibration of the SPR system. A glass slide (SF10) was half coated with a metal layer (nominally 50 nm of gold) while the other half was used as a reference channel. From the imaging system, it was then possible to monitor the SPR profile(s) from the metal layer(s) and the LED intensity from the uncoated glass surface. The latter was

used as a reference for all the experimental data, which were automatically corrected by the data processing routine.

To obtain the absolute sensitivity of the new SPR system, a series of scans using solutions of sucrose in pure water (concentration 0-10% by weight) were recorded. For each resonance curve, a second-order polynomial fit was used to obtain the position (pixel number) of the minimum. In Figure 5.19, the position of the SPR minimum, in terms of pixel position, is plotted against the refractive index of the solution [28].

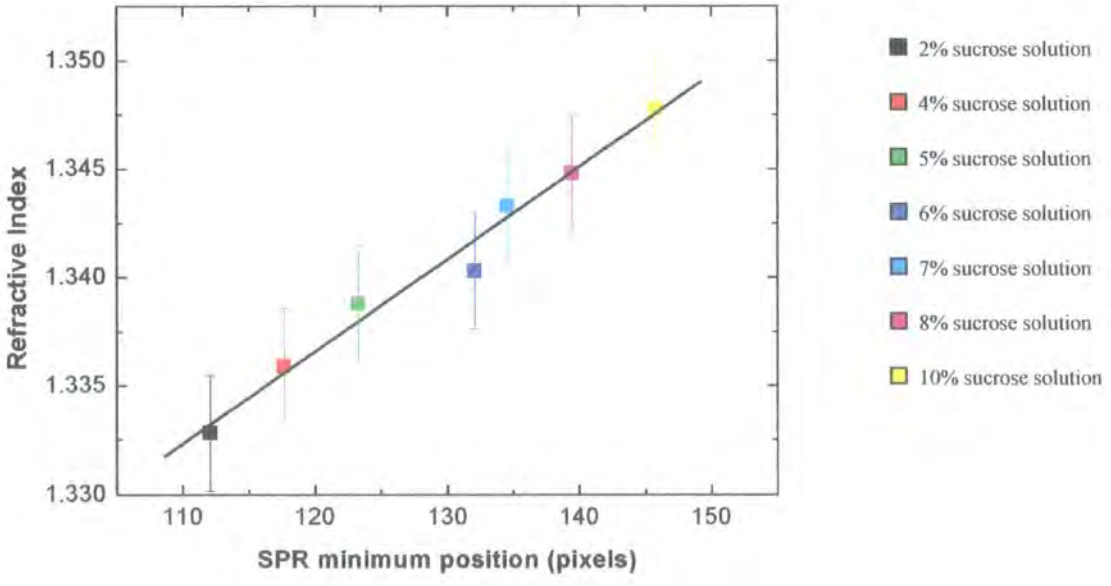

Figure 5.19 Sensitivity calibration curve using different concentration sucrose solutions (0-10% by weight). The slope of the linear fit corresponds to the SPR system sensitivity.

The straight line drawn through the data points represents the calibration. The slope of this curve gives a value of 4.3×10^{-4} refractive index units per pixel line-pair. To monitor any drift in the SPR system, the sensor was placed in ultra-pure water and the resonance curve was monitored over time. Over a period of one hour, no change in the position of the SPR minimum could be detected. During this time, a variation in the ambient temperature of ±0.2 °C was recorded. However, if the temperature of the SPR cell was deliberately varied (e.g. by focusing a lamp onto the cell) then a change in the resonance minimum could be detected. This variation was approximately 1 pixel per K.

To obtain the exact ratio pixel/angle and therefore to correlate the SPR reflectivity with the angular position, two different approaches were examined. In the first, a thick (in the range of few μm) polystyrene film would be deposited on the gold substrate by spin coating and the reflectivity profile of such an architecture examined. As shown in the theoretical profiles in Fig. 5.20, when exposing a thick polymeric film to different media (air and pure water in the examples shown) different reflectivity profiles are obtained near the critical angle.

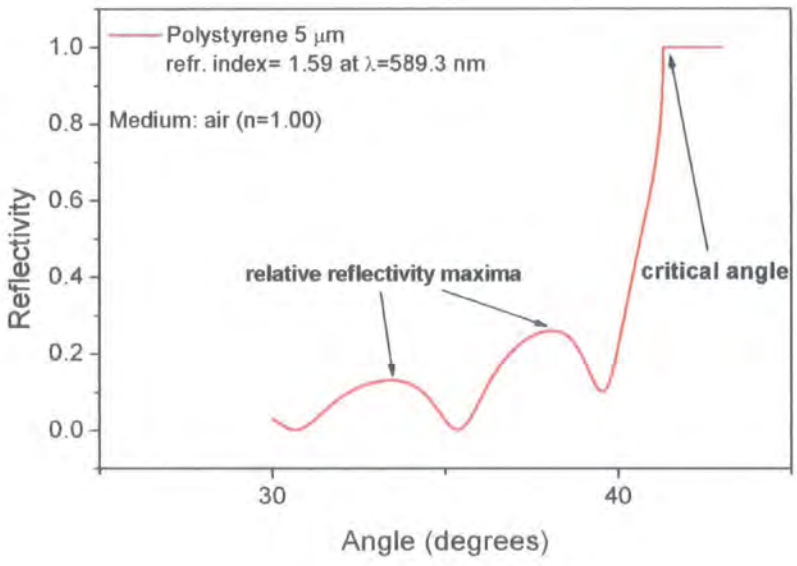

(a)

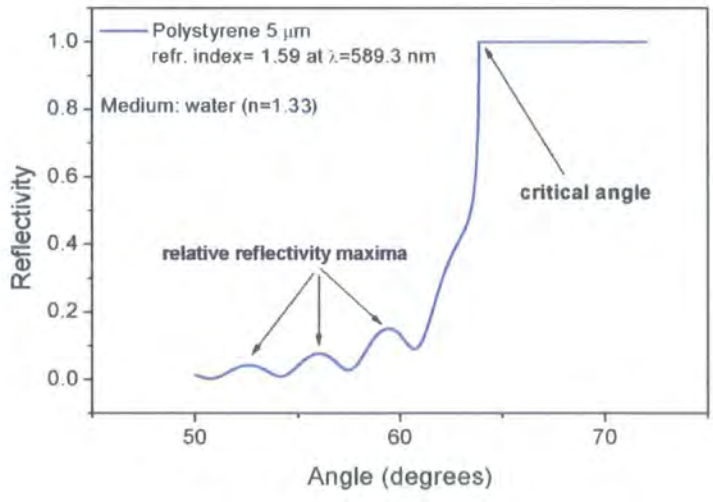

(b)

Figure 5.20 Theoretical reflectivity profiles for a 5 μm spin-casted polystyrene film exposed to different dielectrics. (a) Air, n= 1.00. (b) Water, n= 1.36.

The position of the relative maxima in reflectivity, on the left of the absolute reflectivity maximum for the critical angle (R=1), is function of the thickness of the polymeric film and of the media in contact at its surface. Therefore, this method could be used to determine the position of the reflectivity maxima (relative and absolute) in terms of pixels position and then to compare them with the angular values from the theoretical profiles. However, this requires a detailed study of the deposition of polystyrene to optimize it and obtain an exact film thickness.

Alternatively, the variation in the position of the critical angle with different media in the cell might be used to correlate pixel with angle. As discussed in Chapter 3, the position of the critical angle depends only on the refractive index of the dielectric (the medium) if the materials constituting the prism and the glass are not varied.

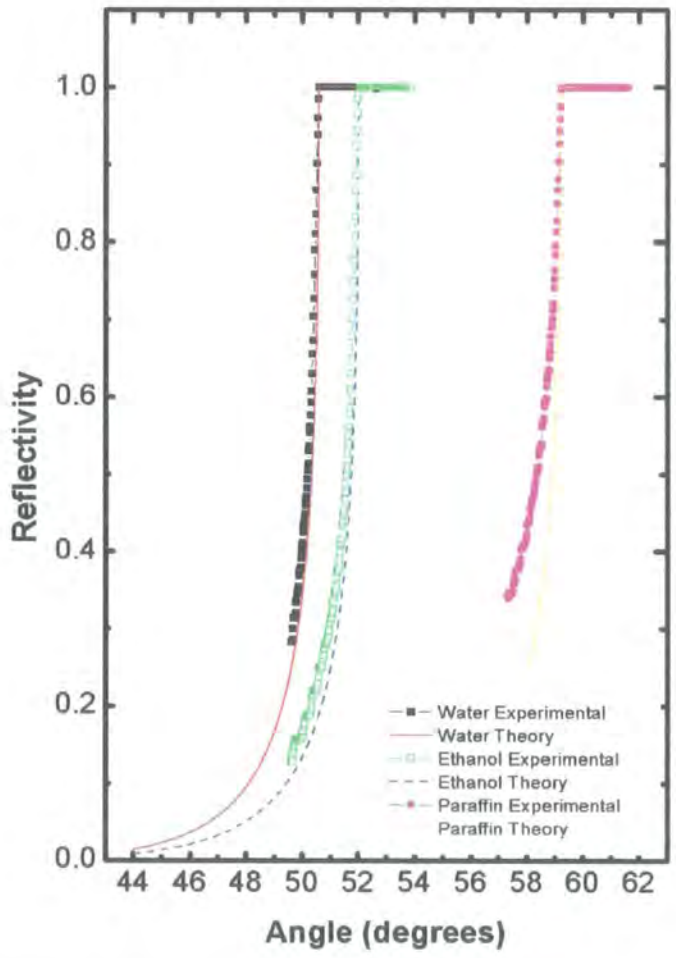

Figure 5.21 Experimental and theoretical reflectivity data for different refractive index fluids (ultra-pure water, ethanol, paraffin) in the region of the critical angles.

Experiments with different refractive index fluids (ultra-pure water, ethanol and paraffin [24]) were undertaken to determine the relationship between the pixel position and the internal angle of reflection. Comparison with theoretical data allowed determination of the pixel/angle ratio. The results are given in Fig. 5.21, which shows the theoretical and experimental reflectivity data in the region of the critical angles for the various glass/fluid interfaces. Finally, a typical SPR curve for a 50 nm thick gold film is shown in Fig. 5.22.

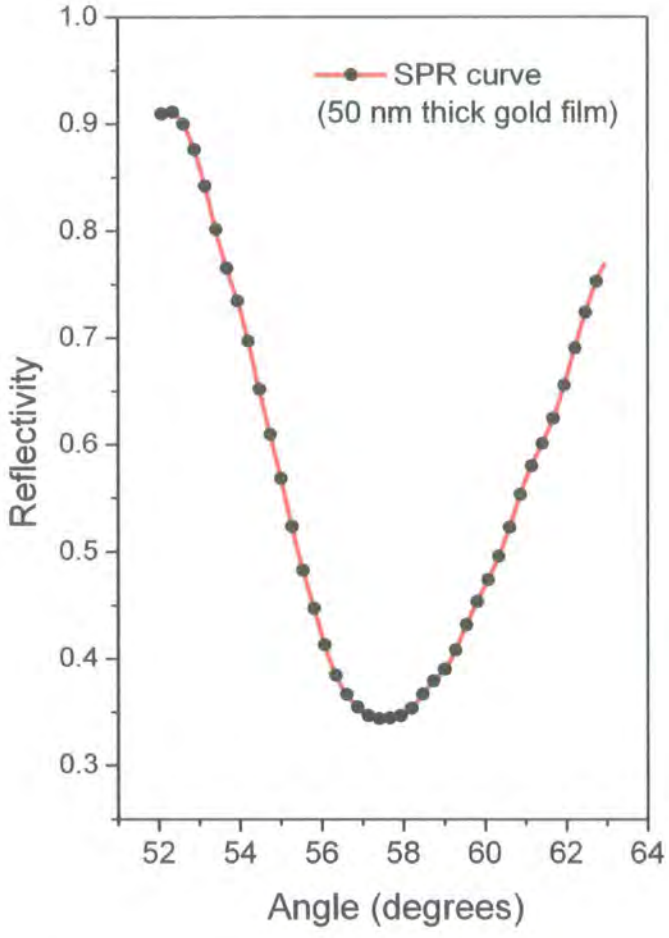

Figure 5.22 SPR profile for a gold layer of 50 nm of thickness.

5.5 Conclusions

The different phases of design and realization of a novel SPR system have been described. The main challenge of this project was the need to build a system able to interrogate and analyze data from a multi-channel single chip, i.e. a platform with several active materials. Alternative optical set-ups were tested and the final choice

provided a SPR platform with no moving part exploiting a focused beam across a range of angles. A CCD camera was used as the detector. Investigations of different light sources resulted in the adoption of a commercial light emitting diode, a Toshiba TLRH190P. A lens system allowed the CCD camera to read simultaneously all the plasmon waves generated on the sensor surface. Therefore, this system is suited to multichannel sensing. A calibration test using sucrose solutions showed a sensitivity of $4.3x10^{-4}$ refractive index units per pixel line-pair. Studies on the angular position of the critical angle as a function of the different dielectrics in contact with the metal surface allowed the exact ratio pixel/angle to be obtained and therefore the SPR reflectivity to be correlated with the angular position.

References

1. Nylander, C., Ljedeberg, B., and Lind, T., Gas detection by means of surface plasmon resonance. Sensors and Actuators, 1982. 3: p. 79-88.

2. Matsubara, K., Kawata, S., and Minami, S., A Compact surface-plasmon resonance sensor for measurement of water in process. Applied Spectroscopy, 1988. 42(8): p. 1375-1379.

3. Matsubara, K., Kawata, S., and Minami, S., Optical chemical sensor based on surface plasmon measurement. Appl. Opt., 1988. 27(6): p. 1160.

4. Lofas, S., Malmqvist, M., Ronnberg, I., Stenberg, E., Liedberg, B., and Lundstrom, I., Bioanalysis with surface-plasmon resonance. Sensors and Actuators B-Chemical, 1991. 5(1-4): p. 79-84.

5. Homola, J., Lu, H.B., and Yee, S.S., Dual-channel surface plasmon resonance sensor with spectral discrimination of sensing channels using dielectric overlayer. Electronics Letters, 1999. 35(13): p. 1105-1106.

6. Homola, J., Lu, H.B., Nenninger, G.G., Dostalek, J., and Yee, S.S., A novel multichannel surface plasmon resonance biosensor. Sensors and Actuators B: Chemical, 2001. 76(1-3): p. 403-410.

7. Homola, J., Yee, S.S., and Myszka, D., Surface plasmon resonance biosensors, in *Optical biosensors*, F.S. Ligler and C.A.R. Taitt, Editors. 2002, Elsevier.

8. www.biacore.com.

9. Palumbo, M., Pearson, C., Nagel, J., and Petty, M.C., A single chip multi-channel surface plasmon resonance imaging system. Sensors and Actuators B: Chemical, 2003. 90(1-3): p. 264-270.

10. Palumbo, M., Nagel, J., and Petty, M.C., Surface plasmon resonance detection of metal ions: layer-by-layer assembly of polyelectrolytes sensing layers on a multichannel chip. IEEE Sensors Journal, 2003. submitted 3rd October 2003.

11. Homola, J., Dostalek, J., and Ctyroky, J., A novel approach to surface plasmon resonance multichannel sensing, in *Optical Engineering for Sensing and Nanotechnology (Icosn 2001)*. 2001, SPIE-INT Society Optical Engineering: Bellingham. p. 86-89.

12. Boozer, C., Yu, Q.M., Chen, S.F., Lee, C.Y., Homola, J., Yee, S.S., and Jiang, S.Y., Surface functionalization for self-referencing surface plasmon resonance (SPR) biosensors by multi-step self-assembly. Sensors and Actuators B-Chemical, 2003. 90(1-3): p. 22-30.

13. Homola, J., Present and future of surface plasmon resonance biosensors. Analytical and Bioanalytical Chemistry, 2003. 377(3): p. 528-539.

14. Palumbo, M., Pearson, C., Nagel, J., and Petty, M.C., Surface plasmon resonance sensing of liquids using polyelectrolyte thin films. Sensors and Actuators B: Chemical, 2003. 91(1-3): p. 291-297.

15. Palumbo, M. and Petty, M.C. Ultrathin polymer films:application to metal ion sensing. in *A.C.S. National Meeting*. 2003. New York: American Chemical Society.

16. Yeatman, E. and Ash, E.A., Surface-plasmon microscopy. Electronics Letters, 1987. 23(20): p. 1091-1092.

17. Rothenhausler, B. and Knoll, W., Surface-plasmon microscopy. Nature, 1988. 332(6165): p. 615-617.

18. Brockman, J.M., Nelson, B.P., and Corn, R.M., Surface plasmon resonance imaging measurements of ultrathin organic films. Annual Review of Physical Chemistry, 2000. 51: p. 41-63.

19. Kretschmann, E., Die Bestimmung optischer kostanten von metallen durch anregungvon oberrflachenplasmaschwingungen. Z. Physics, 1970. 241: p. 313-324.

20. Palumbo, M., *Discriminazione di alcoli alifatici tramite indagini di risonanza plasmonica superficiale su film LB di un porfirinogeno*, Dipartimento dell'Ingegneria dell'innovazione. 2000, Universita' degli Studi di Lecce: Lecce.

21. Lawrence, C.R. and Geddes, N.J., Surface plasmon resonance (SPR) for biosensing, in *Handbook of Biosensors and Electronic Noses: Medicine, Food, and the Environment*, E. Kress-Rogers, Editor. 1997, CRC Press: Boca Raton.

22. Batchelder, D.N. and Willson, J.P. 1988, Patent number GB 2,197,065: U.K.

23. Wilde, J.N., Petty, M.C., Saffell, J., Tempore, A., and Valli, L., Surface plasmon resonance imaging for gas sensing. Measurement & Control, 1997. 30(9): p. 269-272.

24. Potter, L., *A portable vapour sensor using surface plasmon resonance*, Centre for Molecular and Nanoscale Electronics. 2000, Undergraduate project report, School of Engineering, University of Durham: Durham, U.K.

25. Gillessen, K. and Schairer, W., *Light Emitting Diodes: an Introduction.* International series in optoelectronics. 1987, London: Prentice/Hall.

26. Nagel, J., SPR Images. 2001: Institute of Polymer Research Dresden e.V. , Dresden, Germany.

27. Pearson, C., Nagel, J., and Petty, M.C., Metal ion sensing using ultrathin organic films prepared by the layer-by-layer adsorption technique. J. Phys. D: Appl. Phys, 2001. 34: p. 285-291.

28. *CRC Handbook of Chemistry and Physics a Ready-Reference Book of Chemical and Physical Data editor-in-chief, David R. Lide*. 82nd ed. ed. 2001, Boca Raton London: CRC Press.

Chapter 6

Atomic force microscope characterization of poly(ethyleneimine)/poly(ethylene-co-maleic acid) and poly(ethyleneimine)/poly(styrene sulfonate) multilayers

6.1 Introduction

Electrostatic interactions are the driving force behind the LbL process. Multilayer growth is influenced by the charge density of the polyion pair used to assemble the organic film. In the first stages of the film formation, the surface charge density of the solid substrate also plays an important role. The electrostatic interactions between charges on the same polymer chain and charges on the oppositely charged polymer influence the structure of the adsorbed layer, the degree of charge reversal of the outer surface after each adsorption and, finally, the structure of the multilayer film itself. However, a number of reports suggest that secondary non-electrostatic interactions, such as hydrogen-bonding or hydrophobic interactions play a significant role in the formation of LbL multilayers [1-5].

The understanding of the structure of the LbL multilayers has been increasing over the years thanks to atomic force microscopy (AFM) studies of the outer surface of such self-assembled organic films [6-11]. Investigations of the adsorption of single polyelectrolyte molecules is also helping to elucidate the different phases of organization of the polyions and the changes in conformation (coil - to - extended globule) in a controlled environment [12-14].

In this chapter, a study of the differences in topography of the outer surfaces of two polyelectrolyte LbL films is presented. Three different polyions, poly(ethyleneimine), PEI, poly(ethylene-*co*-maleic acid), PMAE, and poly(styrene sulfonic acid) sodium salt, PSS, were used to build two thin film architectures (three bilayer films in each case). The organic films were prepared using either a static self-assembly in-beaker or a dynamic self-assembly in a sealed cell with a continuous flow of the different solutions. The surfaces were scanned at different points over a large area in an attempt to find a model for the multilayer growth. In some experiments, a tip coated with a single layer of PEI/PMAE was used to scan the surface of LbL multilayers.

6.2 Atomic Force Microscopy

Atomic Force Microscopy, also called Scanning Force Microcopy (SFM), was developed in 1986 as a variation of the Scanning Tunneling Microscope (STM), thanks

to collaboration between IBM and Stanford University. In the same year Binning and Rohrer received the Physics Nobel Prize for their work on the STM together with Gerber and Weibel at IBM in Zurich, Switzerland in 1982.

There are three primary modes of use of an AFM: (a) Contact Mode, (b) Non-contact Mode and (c) Tapping Mode. Each has its advantages and disadvantages and a particular mode is normally chosen by consideration of the nature of the sample investigated. Scans can be performed either in air or, thanks to a special cell, in a liquid. In this study, an Explorer^{TM} SPM (Topometrix) was used to obtain images in air of the outer surface of the different sensing films. The SPM was set to operate in contact mode using a Contact AFM MLCT-EXMT-A, triangular-shaped cantilever, with a silicon nitride tip coated in gold.

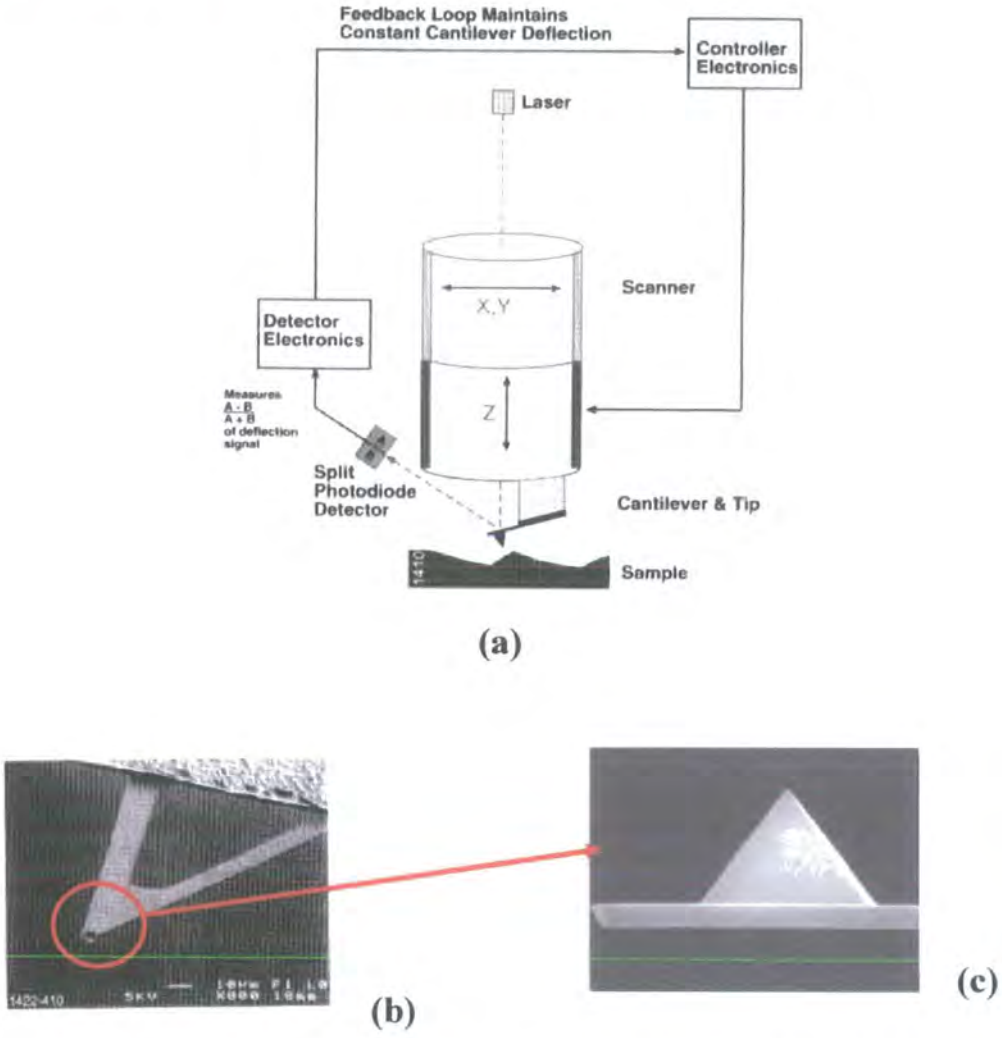

Figure 6.1 (a) Contact mode AFM. A tip attached to the end of a cantilever is used to scan the sample surface while the change in cantilever deflection is monitored with a split photodiode detector. (b) Silicon nitride cantilever. (c) Silicon nitride tip. (Reproduced from [15]).

A schematic diagram of the AFM in a contact configuration is shown in Fig. 6.1. Contact Mode AFM operates by scanning a tip attached to the end of a cantilever across the sample surface. The cantilever deflection is measured with an optical detection scheme that magnifies the cantilever motion using a laser beam reflected from the cantilever backside. In this mode, engagement of the tip with the sample surface is achieved as soon as the cantilever deflection reaches a set-point level. The tip is then rastered over the surface under feedback control that adjusts the probe-sample vertical distance to keep the tip force at the set-point level. The voltage applied to the scanner, which controls these vertical displacements, is reproduced as an AFM height image. A grey-scale or colour-coded contrast reflects surface corrugations. In addition to the height image, there are deflection and lateral force images, which reflect instantaneous deflection (error signal) and variations in lateral forces, respectively. Deflection (error) images are highly sensitive to fine surface features such as edges and steps. Lateral force images can correlate to local friction variations. The force F, between the cantilever and the sample surface, is calculated using Hooke's law, $F = -kx$, where k is the spring constant of the cantilever and x is its deflection. Normally, the spring constant varies from 0.01 to 1.0 N m^{-1}, resulting in forces ranging from nN to μN in an ambient atmosphere.

In Figure 6.1(b) and 6.1(c), pictures of a cantilever and a tip are shown. The cantilever MLCT-EXMT-A, had a length of 180 μm, a width of 18 μm, a thickness of 0.6 μm, a force constant of 0.05 N m^{-1} and a resonant frequency of 22 kHz. A gold coating was applied to the cantilever for high reflectivity. The tip was unsharpened with a typical radius of curvature < 50 nm. The fact that the stiffness of the cantilever is comparable with that of the polymer materials under study allows discrimination of sample locations with different mechanical properties. In this way, various components of heterogeneous polymer materials can be identified in the images.

6.3 LbL deposition methods

Poly(ethyleneimine) (M_w = 25,000), poly(ethylene-*co*-maleic anhydride) (M_w = 144,000) and poly(styrenesulfonate) (sodium form, M_w = 40,000), were used as building blocks for two different LbL architectures. Solutions of concentration $2x10^{-2}$ M for PEI

and 10^{-2} M for PSS and PMAE were prepared in ultra-pure water. The measured pH of the solution was equal to 8.1 for the PEI, 3.2 for the PMAE and 8.4 for the PSS. In some experiments, tris(hydroxymethyl)aminomethane, $C_4H_{11}NO_3$ (tris), buffer solutions were also prepared. The pH of the buffer solution was set at 6.6 by the addition of HCl. A test of complex formation by mixing PEI, PMAE and PSS in solution under the conditions described above was undertaken. While the cationic (PEI) and anionic (PMAE and PSS) solutions are colourless, the mixture is rather cloudy due to the formation of polymer complexes. This, in general, can be seen as a sufficient, but not always good, indication that the interaction between the polyion couple will result in the formation of a LbL multilayer. Multilayer formation may be possible even if the mixing test is not apparently successful [16].

Approximately 50 nm of gold was deposited using physical vapour deposition (PVD) on SF10 glass substrates (Hellma MA Ltd). Before the self-assembly procedure the substrates were kept under vacuum. The polymer coating was prepared as reported in the literature [17, 18] by alternately dipping the gold coated glass slides, first in PEI and then in PMAE, or PSS, for several minutes each. Two different organic film deposition methods were used: (a) manual dipping in beakers containing the polymer solutions in ultra-pure water or buffer solution and (b) direct self-assembly in the sealed cell connected to a peristaltic pump (Fig. 6.2).

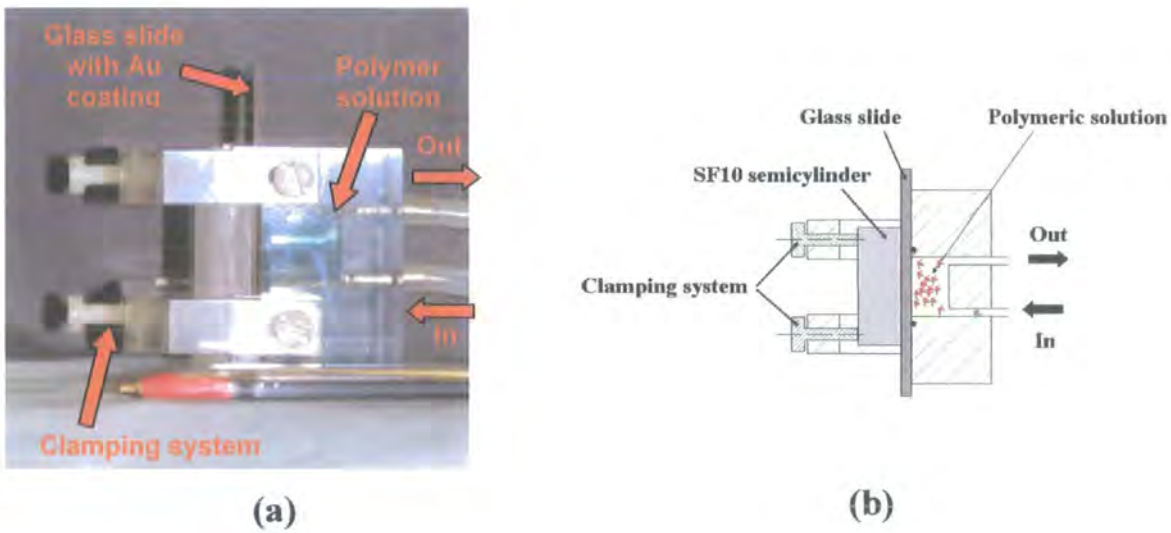

Figure 6.2 (a) A picture of the sealed cell system. (b) Section of the sealed cell. A glass slide coated with a gold thin film is clamped and pressed against a cuvette (inner volume equal to 2.6 ml). Two Teflon tubes are connected to a peristaltic pump (not shown) and ensure a continuous flow of solution inside the cuvette.

Using the sealed cell system, the polyion solutions were let to flow uninterrupted. A flow of ultra-pure water or buffer solution was used after each adsorption to remove weakly attached material. The flow rate of the polymer solution was set at quite a high value (2.5–5 ml min^{-1}) because it was intended to study the effect of the flow speed on the formation of the thin film architectures. For the in-beaker method, after each adsorption the thin films were rinsed in ultra-pure water or buffer solution. Films assembled in-beaker were dried in a nitrogen stream every two layers, while in the case of in-cell assembly, the films were dried only at the end of the process. Before being examined by AFM, the organic films were kept in sealed container under vacuum on in a clean room environment.

6.4 Zone and island models

The first type of multilayer investigated was composed of three bilayers PEI/PMAE. Poly(ethyleneimine), a weak polybase, is widely used as adhesion promoter and was the first layer adsorbed on the gold surface to achieve a positively charged substrate. The second category of organic film investigated was obtained by combining PEI and PSS to form the architecture (PEI/PSS)x3. PMAE has two carboxylic acid groups along the chain which form part of a pendant group and may be considered a weak polyacid. In aqueous solution, its charge density is limited and, consequently is very likely to have a globule conformation. In contrast, PSS is well known as a strong polyelectrolyte. Interestingly it has hydrophobic benzene groups in its backbone. It dissociates in solution because the gain in entropy, due to the release of counterions, compensates for its hydrophobic nature. This behaviour is known in other hydrophobic polyelectrolytes [13]. As a strong polyelectrolyte, it is expected that, in solution, electrostatic long-range Coulomb repulsions among the charged sites on the PSS backbone will tend to elongate its chain. However short-range intramolecular attractions among the hydrophobic groups might compete with this tendency, giving a more curved and twisted coil formation [19].

All the scans were undertaken in air in the contact mode. An initial examination of the gold surface before the LbL self-assembly was undertaken. In Figure 6.3, the surface of the uncoated glass is on the right, while the gold layer is visible on the left. The gold

coating imaged has a roughness (RMS) of approximately 4 nm with a maximum height of about 40 nm. Its structure, with peaks and valleys, is a consequence of the PVD deposition technique.

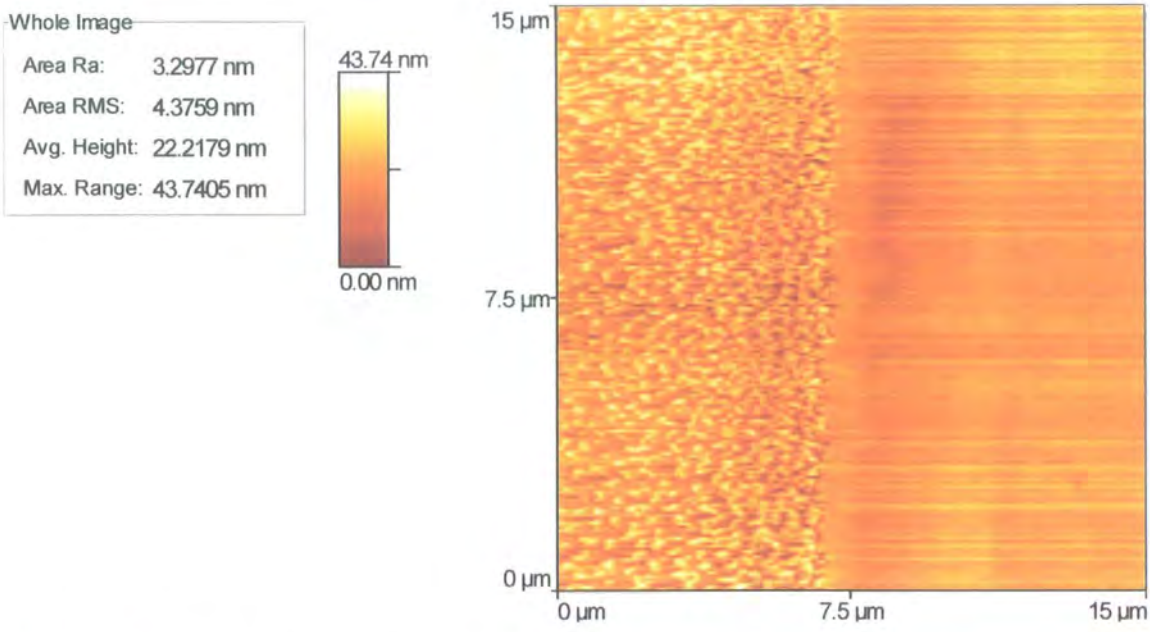

Figure 6.3 AFM scan (15 µm x 15 µm) in contact mode of the metal coated glass slide. The gold coated surface is on the left while on the right the surface of the uncoated glass is shown.

According to a view now commonly accepted and known as the *zone model* [20, 21], the basic structure of a multilayer has three distinct parts, Fig. 6.4.

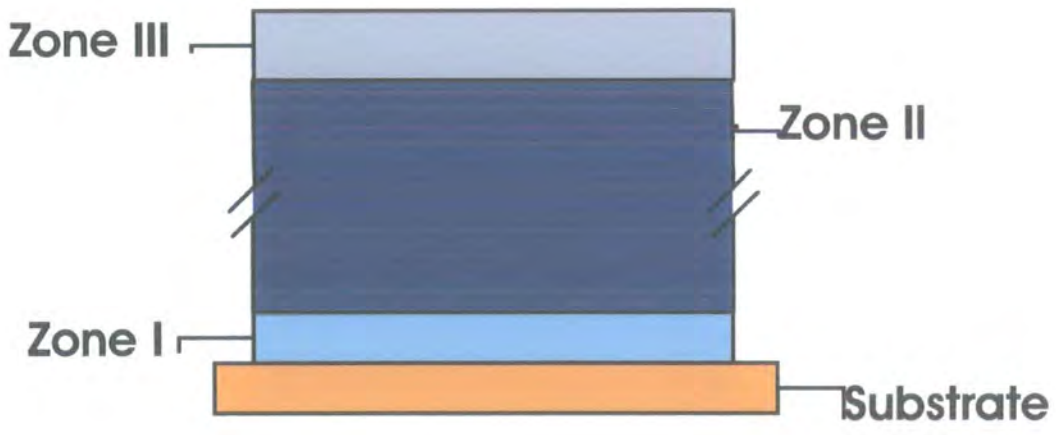

Figure 6.4 Zone model for polylectrolyte multilayers [20, 21]. Because Zone I is adjacent to the substrate its characteristics are influenced by those of the substrate itself. Zone II forms the bulk of the LbL film, while Zone III is at the interface with the external environment and constitutes a separate part of the overall architecture. The division between the different areas is flexible and diffuse and not as sharp as indicated in the diagram.

In zone I, the properties of the polymer layers are influenced by the substrate. Its thickness is generally a few layers, depending on the nature of the polyions used [9, 22]. The bulk film, zone II, has constant properties. For example, all bilayers seem to have equal thickness. The polyanion/polycation stochiometry is observed to be equal, or close to 1:1. Zone III is the region close to the outer surface of the film. It comprises of very few layers and its properties are influenced by the external environment. Transitions between one zone and another are gradual. According to the model, as more layers are added, the thickness of zone I and III will remain constant while zone II will grow [22]. In this work, the thin film architectures examined are only three bilayers in thickness. The reported AFM images therefore refer to the organization of the molecules in zone I.

In the literature, a two step process is usually reported for the adsorption of polymers onto solid surfaces. During the first step, molecules adsorb in a number increasing with the square root of time, according a diffusion-limited model. Then, there is a slow re-arrangement of the adsorbed chains and the polymer film becomes flatter. However such changes appear over a variable period of time and chains can remain kinetically trapped by the substrate for long time before any reorganization occurs [13].

Many studies report that the alternate LbL assembly process exhibits a non-linear film growth in its early stages. During the formation of the first layers, a relatively small amount of polyion is adsorbed. In contrast, in subsequent adsorptions, film mass and thickness tend to increase linearly with the number of adsorption cycles. Some recent work reports an exponential growth regime for specific polyion systems. In this case, a model based on polyelectrolyte diffusion in and out of the film coupled to the formation of polyanion/polycation complexes at the surface was given as an explanation [10].

Some workers have investigated the early stage of the film formation of LbL multilayers composed of PSS and poly(allylamine), PAA, and tried to explain the non-linear behaviour [6]. It has been suggested that the first polyion layer self-assembles on the charged substrate according to an *island-type adsorption model*. As result of AFM investigations, it was discovered that during the first several minutes of deposition, charged macromolecules tended to adsorb preferentially on selected defect sites of the oppositely charged support (scratches, microparticles and edges) and form islands

composed of polymer coils. However, for longer deposition times there was an equilibration of polymer layers and formation of a homogeneous thin layer composed of highly flattened macromolecular chains. On increasing the number of steps, the islands tended to coalesce on the support until they achieved a full coverage. From then on, a new stage of the film formation began and a linear increase of the film mass was measured. A similar behaviour has been found for LbL multilayers formed by poly(L-lysine), PLL, and hyaluronic acid, HA [9], although this time the film structure did not evolve in the same way as the previous case [6]. However, even for PLL/HA films it was found that, in the early stages of the film formation, the polymers tend to form "breath figures", as in the case of condensation of liquid on a surface from a supersaturated vapour. Areas where the polyelectrolyte layers form micrometre sized "islands" were intercalated with areas of small aggregation ("islets") scattered on the surface. When a continuous film formed on the surface, i.e. the formation of zone I was established, the second stage of the film formation began. For the PLL/HA system under study, the mass of the polymer film during the second stage grew exponentially with the number of layer pairs [9].

There are reports of changes to the film structure due to pH and ionic strength variations, and there are indications that drying could also modify the multilayer molecular organization [7, 23-25]. Ex-situ AFM analysis might give only a partial picture of what the LbL multilayers look like in solution.

6.5 Surface morphology

Films deposited on an area of approximately 75 mm^2 were scanned at several points on the surface in an attempt to identify a typical film morphology. The first series of experiments was undertaken on (PEI/PMAE)x3 films, deposited in a beaker. Figure 6.5 shows that the three bilayers do not form a uniform film on gold. Areas with a reasonable coverage were found adjacent to areas where the adsorption was only partial, Fig. 6.5(a). In the latter case, the cantilever tip was usually affected by strong repulsive forces due to isolated polymer complexes on the surface. For instance, a globular form of a cluster is visible on the right top corner of the image in Fig. 6.5(a). A maximum height of 465 nm is noted. The roughness (RMS) of the surface is now 33 nm. The bare

gold substrate in Fig. 6.3 (representative of the gold thin film used for all these series of experiments) had a RMS value equal to 4 nm. Therefore, this seems to indicate that a polymer film has been deposited on the metal coating.

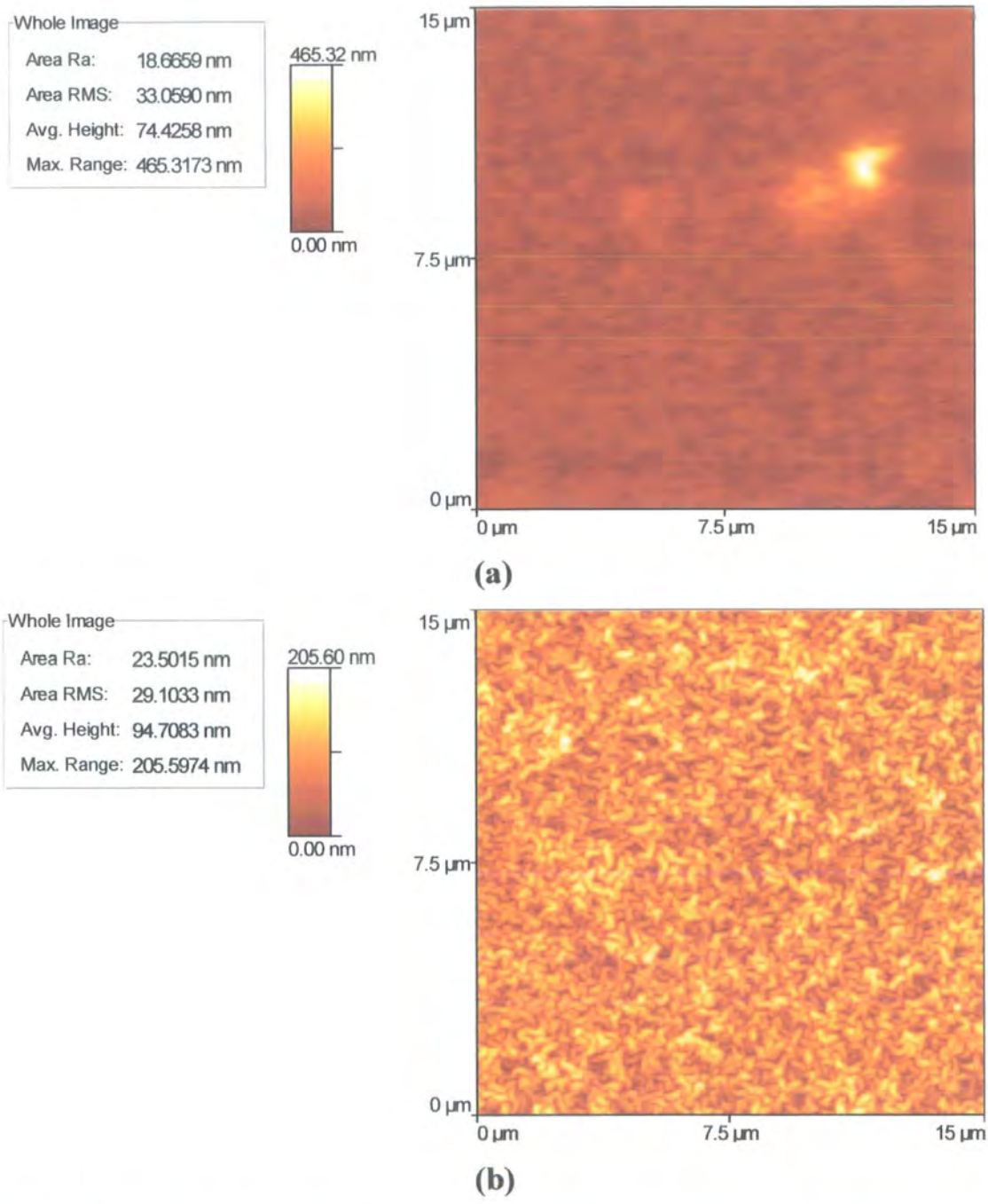

Figure 6.5 AFM scans in contact mode in air of a (PEI/PMAE)x3 film; self-assembly in beaker on a gold thin film. (a) 15 µm x 15 µm scan of the film surface in an area where the film is rougher and non-uniformly distributed. Note the presence of a globule on the top-right corner of the image; (b) 15 µm x 15 µm scan of the same film in an area with a smooth surface and uniform coverage.

An explanation of the presence of the isolated globule might be that the area imaged corresponds to a single/double bilayer PEI/PMAE, with an isolated polymer cluster on top. These globules have adsorbed without being able to complete the self-assembly of a whole layer/bilayer. The images in Fig. 6.5(a) and 6.5(b) might therefore provide an insight of how the process of self-assembly proceeds. The self assembly starts with the adsorption of single polymer chains. These chains adsorb on the surface to form clusters or islands. Then the islands increase in size with time and coalesce. Finally, there is a re-arrangement of the adsorbed chains into flatter films. In Fig. 6.5(b), one of these flatter regions is shown. A vermiculate pattern, found in other polyelectrolyte systems [7, 8], is evident. The LbL film appears to be uniformly distributed to form a relatively smooth film. A roughness (RMS) of 29 nm confirms the visual impression of a more even surface compared to that in Fig. 6.5(a). The area imaged in Fig. 6.5(b) has an average height of 95 nm and a maximum height range of 206 nm. A close analysis of the vermiculate pattern on several images gave the conclusion that the end-to-end distance of the curved polymer coils varies between 100 nm and 1000 nm. However, it should be noted that the overlapping of the chains makes difficult to distinguish clearly the coils. Studies on very diluted solutions of polyelectrolytes (far below the critical overlap concentration) or with an imposed poor interaction between the polymers and the surface (e.g. by addition of NaCl to screen the electrostatic forces) are more suited to study the conformation of the adsorbed chains (i.e. contour length or end-to-end length) [12, 13]. Such procedures are useful to understand the relation that exists between the characteristic length of the chains in solution and the shape assumed by them following the adsorption on the solid-liquid interface. Moreover, the tuning of the transition stretched chain – globule has been proved to be directly dependent by the solution pH or its ionic strength.

In a second phase of the investigation of the (PEI/PMAE)x3 architecture, it was decided to perform the self-assembly of the multilayer using a sealed cell with a continuous flow of the polymer solution. The volume of the cell was 2.65 ml. The range of speeds varied between 2.5 and 5 ml min^{-1}. One of the images obtained is shown in Fig. 6.6. In this case, a much rougher film surface was observed. The RMS value of the image is 52 nm, the average height is 114 nm and the maximum height is 394 nm. The high speed of the flow seems to have prevented the formation of distinct flatter areas. Globules of polymer clusters are widely distributed and do not form separate regions. Some of these

have been measured to have a height of a few μm. It is believed that the reason for this behaviour is influenced by the flow speed. Probably, differences in pressure and velocity along the liquid/solid interface, disturb the adsorption process. It is likely that molecules already adsorbed tend to compete with those in solution. This results in a far more complex architecture for the multilayer. Several scans of the film surface of different samples prepared under identical conditions were taken and the results were all consistent with the image in Fig. 6.6.

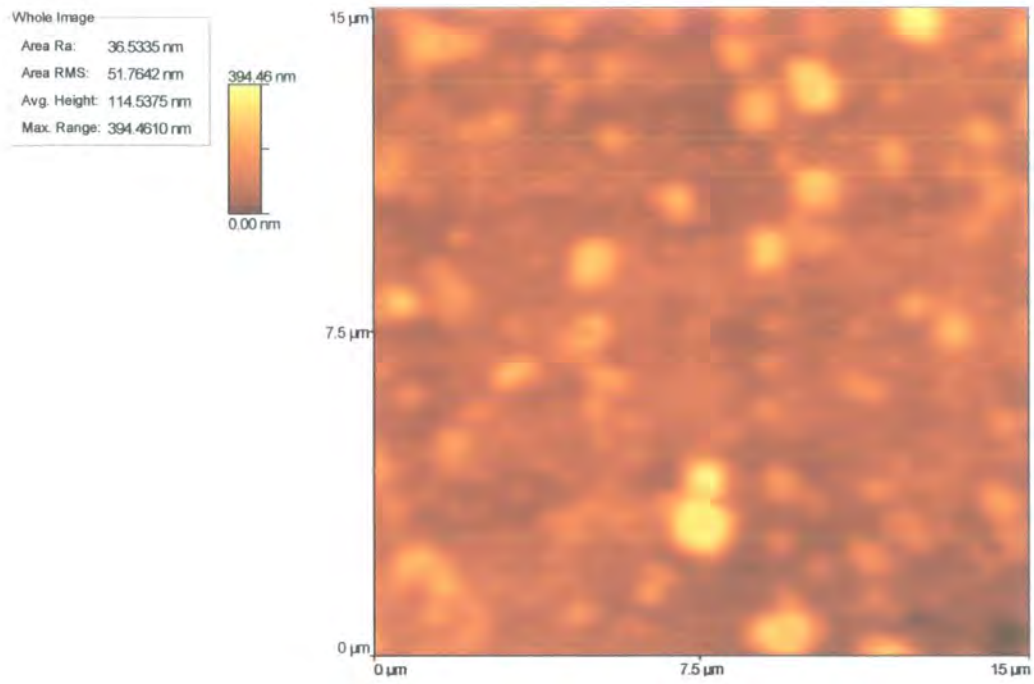

Figure 6.6 AFM scans in contact mode in air of a (PEI/PMAE)x3 film; self-assembly in cell on a gold thin film. 15 μm x 15 μm scan of film surface. Note the rougher and irregular topography in comparison with the images in Fig. 4.

The second architecture investigated was (PEI/PSS)x3. Aqueous solutions were prepared for both polyions and LbL self-assembly was performed in a beaker. Some of the AFM images are presented in Fig. 6.7. Even for this multilayer film two different regions with different adsorption degrees are visible. However, in contrast to (PEI/PMAE)x3 a much smoother surface is evident for those areas were the adsorption is fully complete (Fig. 6.7(a)). The RMS value for the surface in Fig. 6.7(a) is 3.5 nm, lower than the value found for the (PEI/PMAE)x3 surface in Fig. 6.5(b) (29 nm). The average height of the film is 20 nm while the maximum height value is 68 nm. The reason of a smother surface for the islands of (PEI/PSS)x3 compared to those of the (PEI/PMAE)x3 film has probably to be found in the different electrostatic nature of the

two polyanions. PSS is a strong polyelectrolyte with a constant charge density which is virtually independent of the pH and ionic strength of the solution, while PMAE is relatively weak polyacid with a charge density that will change with the pH and the ionic strength of the solution. However, this is only a simplified model because of the screening of the charged sites of strong polyelectrolytes by counterions in solution [8], and the role that secondary interactions have on the formation of LbL architectures [1, 2, 4]. In this simplified model, PSS chains in solution behave as rigid chains. In contrast, PMAE is affected by lower repulsion forces along its chain and, therefore, it is more flexible and tends to possess a globular conformation in solution at acidic pH. At the moment of the adsorption on the surface, and at least until the final re-arrangement of the film occurs, polymers tend to preserve the shape they have in solution, and their two-dimensional size correlates with the dimensions of the chains in solvent [13].

In one of the AFM scans of the regions with only a partial adsorption of the polyelectrolytes, it was possible to image the polymer coils, Fig. 6.7(b). Examination of the surrounding surface around suggests that the coils were adsorbed on a relatively free part of the film. It is difficult to say if the coils are PEI or PSS or a mixture of both. Because of the stretched conformation of the chain, it is possible that they correspond to PSS coils on a PEI substrate. As well as the clearly imaged polymer chains, some charged sites along the chains are also evident (i.e. corresponding to bright regions in the image).

Many factors influence the adsorption of polyelectrolytes at solid interfaces. Surface charge density, polymer charge, ionic strength, pH and chemical affinity with the underlying substrate are all factors that play an important role in the process [26]. Weak and strong polyelectrolytes respond differently to variations in the deposition conditions. One of the main features of weak polyelectrolytes is that their charge density is a function of the solution pH. Recent studies have shown that this characteristic can be exploited to tune the thickness, composition and surface properties of the LbL multilayers by variation of the experimental conditions, e.g. pH [27]. Some authors indicate that local pH, in the proximity of the surface, is different from that in bulk solution, and this is the real factor that affects the electric charge density in weak polyelectrolytes. For oppositely charged surfaces, the polymer chain charge density increases in the proximity of the surface, while it decreases for neutral surfaces [26].

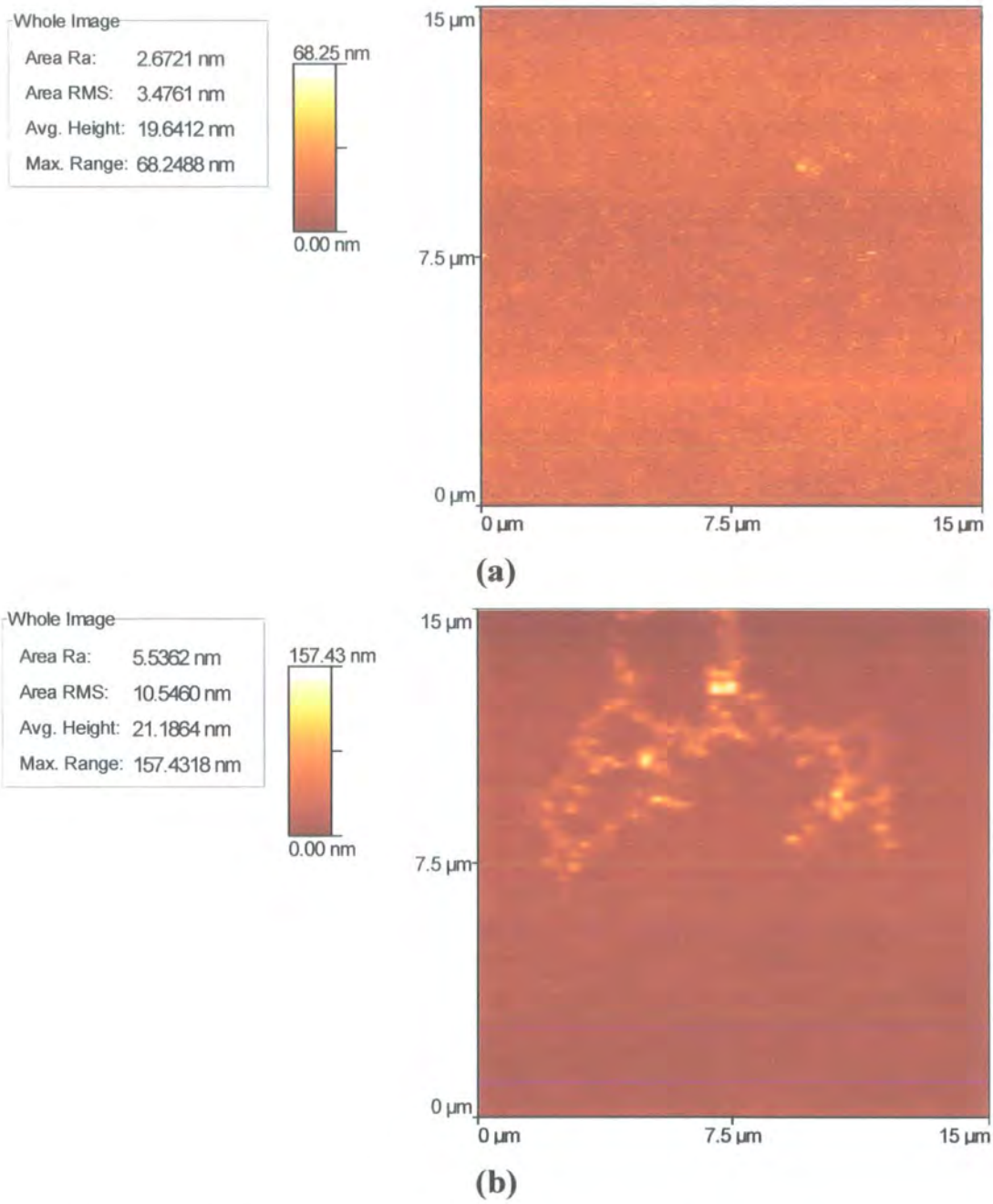

Figure 6.7 AFM scans on a (PEI/PSS)x3 film assembled on a gold thin film following the traditional in-beaker LbL deposition technique. (a) 15 µm x 15 µm scan on a portion of the surface where the self assembly of the three bilayer seems to be completed; (b) 15 µm x 15 µm scan of an area of the film where the self-assembly has been only partial. A group of polymer coils are visible on the upper half of the scan. Note the strong deflection of the tip in regions of what are believed to be charged sites along the polymer chains.

Figure 6.8 shows a schematic diagram of a strong (Fig. 6.8(a)) and weak (Fig. 6.8(b)) polyelectrolyte adsorbed on a solid substrate. The concentration of salt in solution is assumed to be negligible, i.e. no screening of the charges on the polymer chains by salt ions is considered. The surface charge density is assumed to be homogenously

distributed. Moreover, for simplicity, only electro-sorption is considered as the driving force for the adsorption process. As shown, the high charge density of the polymer in Fig. 6.8(a) allows it to adsorb almost flat on the surface. The chains are divided into three types of sub-chains. The tails represent the non-adsorbed ends, free to "dangle" in the solution. The fraction of the chain that is in direct contact with the surface is called *bound* or *train*, while the segments connecting one bound region to another and that do not have any contact with the surface are called *loops* [26]. The full red spots along the bound regions represent charged sites that anchor the polymer to the surface. The open circles represent charged sites not used in the adsorption process. These sites reverse the original charge at the interface and promote the adsorption of the next polymeric species. For weak polyelectrolytes the charge density will be generally lower. Therefore the bound fraction will be limited to fewer adsorbed sites, while the rest of the polymer chains hang loosely at the solid-liquid interface.

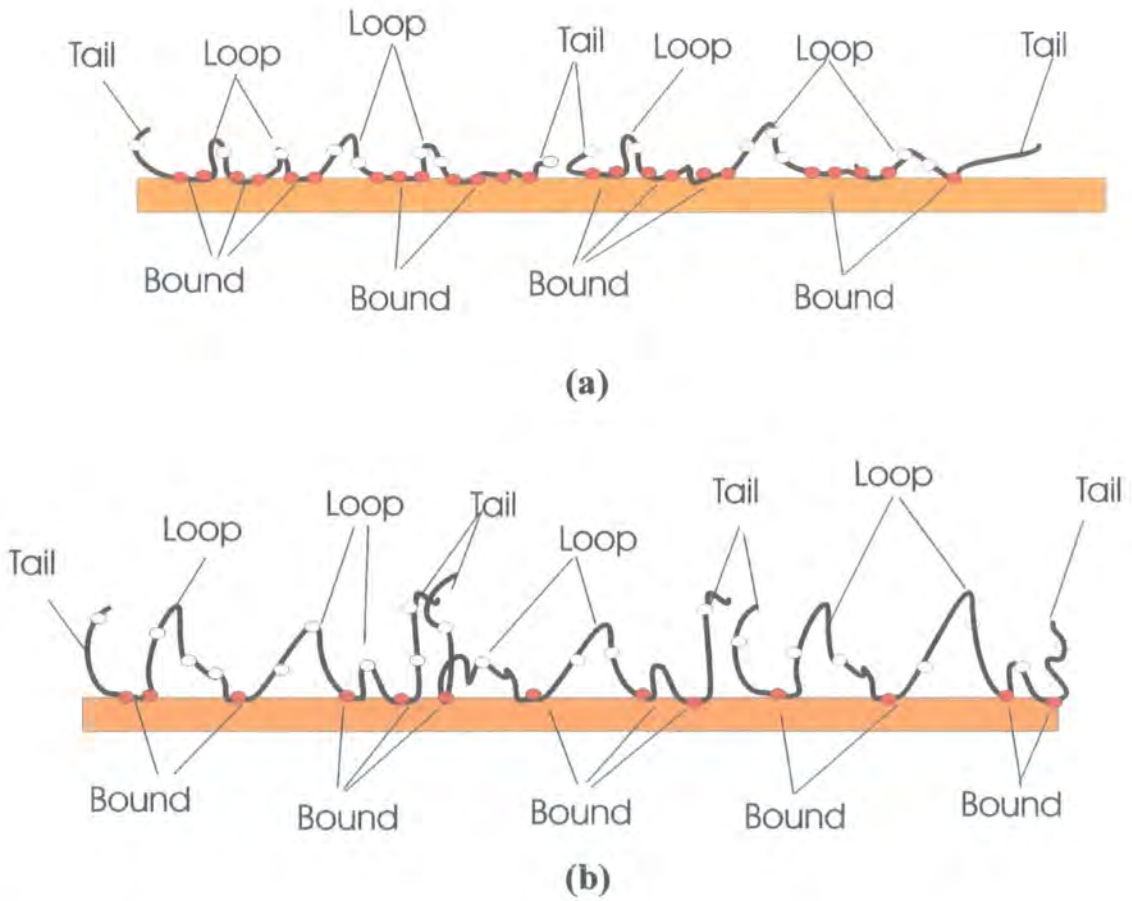

Figure 6.8 Schematic representation of strong (a) and weak (b) polyelectrolytes adsorbed on a solid substrate. The surface charge density is assumed to be constant along the entire interface. The ionic strength of the solution is considered to be very low, and only electrostatic interactions are involved in the adsorption process.

This model, although crude, agrees with the experimental results presented here. (PEI/PSS)x3 multilayers deposited in beaker are smoother while (PEI/PMAE)x3 films are rougher (compare RMS in Fig. 6.5(b) and 6.7(a)). Comparisons of the average height and maximum range height for the two films, suggest a flatter film when PSS is used as the polyanion component in the LbL multilayer formation. Friction or indentation experiments by mean of the AFM tip used in contact mode could be used to enlighten the different features between the two architectures (e.g. elastic module or surface hardness).

In a further experiment, tris buffer solutions at pH 6.6 were prepared for the self assembly of (PEI/PSS)x3 directly in cell. The AFM scan revealed a similar background structure to the sample prepared from aqueous solutions, Fig. 6.9. Comparison of Fig. 6.7(a) and Fig. 6.9, confirms that a continuous flow of the solutions in the sealed disturbs the film topography. The RMS roughness value has increased to about 9 nm compared to 3.5 nm for the film prepared in-beaker. The average height is now 29 nm while the maximum height value is 108 nm, consistent with some charged sites on the island surface.

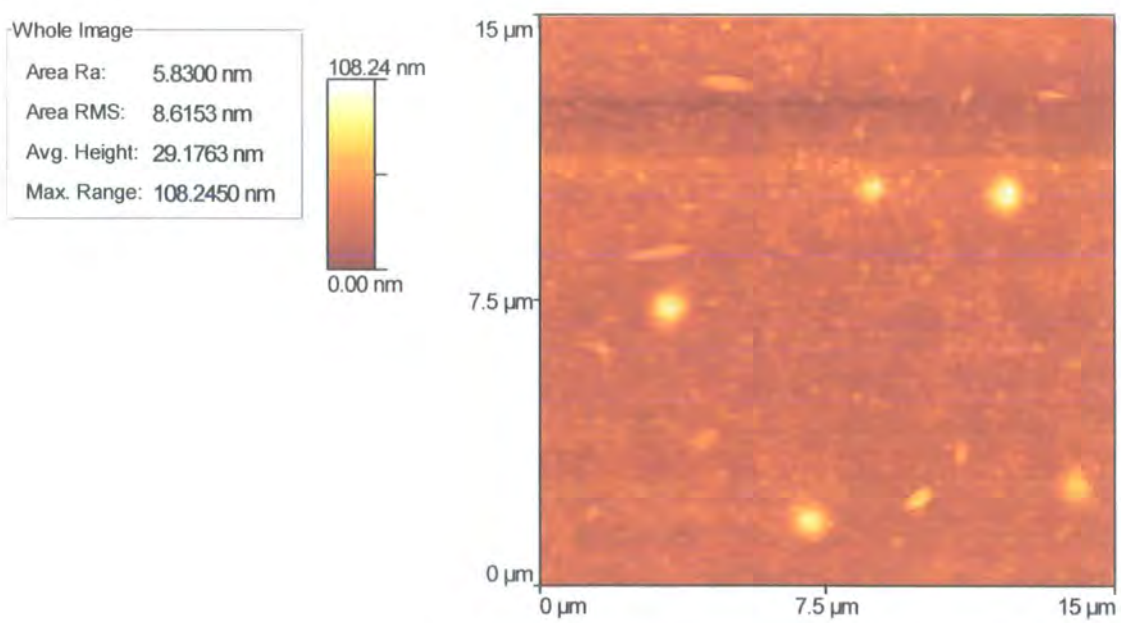

Figure 6.9 AFM scans on a (PEI/PSS)x3 film assembled on gold thin film. The polymer solutions were prepared in tris buffer solution at pH 6.6.

6.5.1 AFM studies using a LbL coated tip

In some AFM scans on (PEI/PMAE)x3 films prepared in a beaker, a tip coated with a single bilayer PEI/PMAE was used. All the scans were undertaken in air in contact mode. Figure 6.10 shows a schematic diagram of the coated tip rastering the LbL multilayers surface. Considering the negative charges on the outer surface of the LbL film, the tip should be affected by stronger repulsive electrostatic forces. Therefore, the cantilever should have a wider deflection and higher peaks on the AFM scan should clearly identify the charged sites. This technique might be useful to avoid the scratching of the surface by the tip when analyzing very soft materials or to prevent the accumulation of dirt and debris on the tip itself.

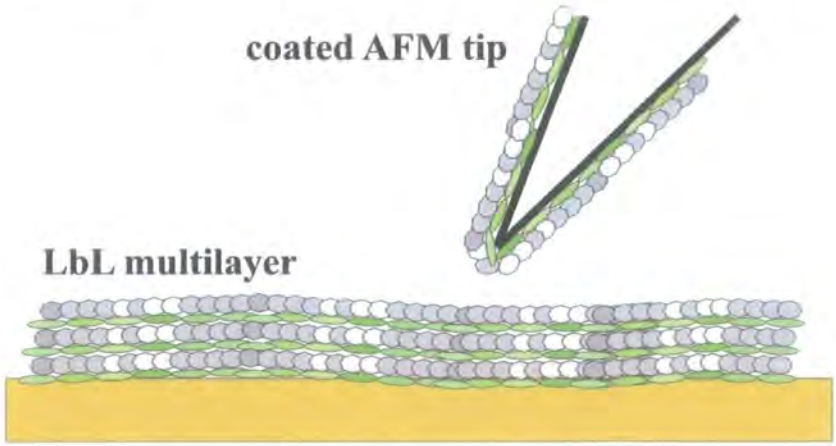

Figure 6.10 Schematic representation of an AFM tip coated with an LbL layer rastering a polyelectrolyte multilayer. Note that, in this example, the AFM tip and multilayer have the same electrostatic charge sign, therefore, repulsive Coulombic forces will affect the tip.

Results from these series of experiments are shown in Fig. 6.11. The AFM images were obtained scanning the same (PEI/PMAE)x3 multilayers, first with a normal tip (Fig. 6.11(a)) and then with a tip coated by a single bilayer PEI/PMAE (Fig. 6.11(b)). This procedure was also repeated on other samples, deposited either in-cell or in-beaker. A close analysis of Fig. 6.11 suggests that, as expected, repulsive electrostatic forces affect the imaging. As a result, there is an increase in the measured thickness of the LbL film. However, the two scans refer to two different areas of the film and local differences in morphology could be the main cause of the variation in the measured quantities, i.e. height and roughness. More experimental work is therefore necessary. Perhaps, a possible future use of coated tips is in analyzing LbL organic films possessing an electrostatic charge of opposite sign to that of the coated tip. In this way, it would be

possible to study adhesion and friction forces between complementary polymeric chains giving a further insight in the LbL multilayer formation. This approach is similar to the technique of chemical force microscopy (CFM) that has recently been introduced. Cantilever tips have been chemically modified through the chemiosorption of thiol or silane monolayers onto gold coated or onto bare silicon nitride tips. This modification enhances the interaction forces between the sample surface and the tip allowing, through the mapping of adhesion and friction forces, the identification of different chemical species on the film surface [28-30].

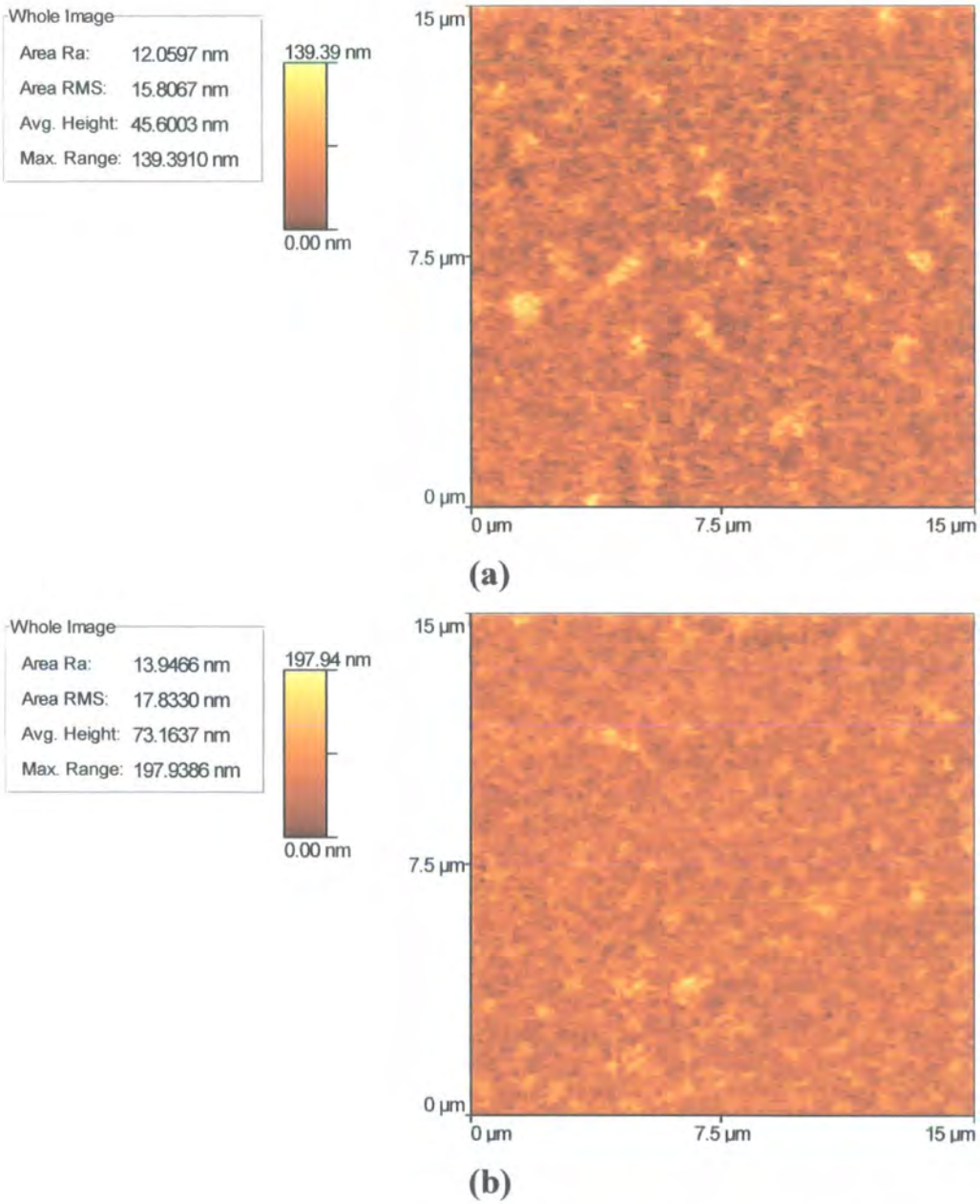

Figure 6.11 AFM scans in contact mode in air of a (PEI/PMAE)x3 film; self-assembly in beaker on a gold thin film. (a) 15 µm x 15 µm scan of the film surface using an uncoated tip; (b) 15 µm x 15 µm scan of the same film using a tip coated with a single PEI/PMAE bilayer.

6.5 Conclusions

In this chapter, a basic description of atomic force microscopy, and in particular of the operational contact mode, was introduced. Thanks to AFM investigations of the outer surface of LbL self-assembled organic films, the understanding of their structure and characteristics has been increasing over the years.

Two adsorption models describing the interaction of polymeric chains at a solid surface were presented. The first (the *zone* model) analyzes the multilayer formation and divides the LbL film into three different zones according to their distance from the solid surface. To each are attributed specific characteristics and features. The second model (the *island* model) is concerned with the initial adsorption of the polymeric chains onto the solid template. Charged macromolecules tend to adsorb on selected defect sites of the solid support and form islands composed of polymer coils. On increasing the number of deposition steps, these islands tend to coalesce until they achieve a full coverage of the surface. Such process is analogous to that of the growth of several metal thin films (eg. Ag or Au) during metal vapour condensation.

For the LbL architectures, the adsorption of the first polymer multilayers has been found to be only partial. Areas where the process is complete coexist with those where very few of the polyions have been successfully adsorbed. This behaviour of limited adsorption is, for the polymer architectures under study, independent of the electrostatic nature of the polyelectrolytes used. On the portions of the surface where the adsorption was limited, it was possible to image isolated polyelectrolyte complexes. These polyions appear to be kinetically trapped on the surface according to what is believed to be their conformation in solution. Three bilayer PEI/PMAE films possessed a globular shape, while more elongated coils were visible for PEI/PSS films. When ultra-pure water solutions were used for self-assembly in beaker, it was possible to image a cluster of such polymer chains adsorbed on the surface on the underlying PEI substrate.

Samples assembled in-beaker and in a sealed cell at high flow rate (2.5–5 ml min^{-1}) were compared. For the multilayer incorporating PMAE the effect of the continuous flow was dramatic while the differences were less for those films containing PSS. For the latter architectures, an island-type adsorption was still recognisable by AFM investigation while (PEI/PMAE)x3 self-assemblies were rougher and very irregular.

Some preliminary experiments using a chemically modified AFM tip were also presented. A single PEI/PMAE bilayer was self assembled on the tip surface. AFM images of a three bilayer thick (PEI/PMAE)x3 film, obtained by using either a chemically modified tip or a traditional one, were compared. The results obtained suggest that electrostatic repulsive forces between the chemically modified tip and the film outer surface had an affect on the sample imaging. However, more experimental work is necessary to clarify the role of interaction forces between functional groups present on the two surfaces (i.e. tip and organic film).

References

1. Hammond, P.T., Recent explorations in electrostatic multilayer thin film assembly. Current Opinion in Colloid & Interface Science, 1999. 4(6): p. 430-442.

2. Kotov, N.A., Layer-by-layer self-assembly: The contribution of hydrophobic interactions. Nanostructured Materials, 1999. 12(5-8): p. 789-796.

3. Stockton, W.B. and Rubner, M.F., Molecular-level processing of conjugated polymers .4. Layer-by- layer manipulation of polyaniline via hydrogen-bonding interactions. Macromolecules, 1997. 30(9): p. 2717-2725.

4. Schoeler, B., Poptoschev, E., and Caruso, F., Growth of multilayer films of fixed and variable charge density polyelectrolytes: Effect of mutual charge and secondary interactions. Macromolecules, 2003. 36(14): p. 5258-5264.

5. Pontes, R.S., Raposo, M., Camilo, C.S., Dhanabalan, A., Ferreira, M., and Oliveira, O.N., Non-equilibrium adsorbed polymer layers via hydrogen bonding. Physica Status Solidi A-Applied Research, 1999. 173(1): p. 41-50.

6. Tsukruk, V.V., Bliznyuk, V.N., Visser, D., Campbell, A.L., Bunning, T.J., and Adams, W.W., Electrostatic deposition of polyionic monolayers on charged surfaces. Macromolecules, 1997. 30(21): p. 6615-6625.

7. Mendelsohn, J.D., Barrett, C.J., Chan, V.V., Pal, A.J., Mayes, A.M., and Rubner, M.F., Fabrication of microporous thin films from polyelectrolyte multilayers. Langmuir, 2000. 16(11): p. 5017-5023.

8. McAloney, R.A., Sinyor, M., Dudnik, V., and Goh, M.C., Atomic force microscopy studies of salt effects on polyelectrolyte multilayer film morphology. Langmuir, 2001. 17(21): p. 6655-6663.

9. Picart, C., Lavalle, P., Hubert, P., Cuisinier, F.J.G., Decher, G., Schaaf, P., and Voegel, J.C., Buildup mechanism for poly(L-lysine)/hyaluronic acid films onto a solid surface. Langmuir, 2001. 17(23): p. 7414-7424.

10. Lavalle, P., Gergely, C., Cuisinier, F.J.G., Decher, G., Schaaf, P., Voegel, J.C., and Picart, C., Comparison of the structure of polyelectrolyte multilayer films exhibiting a linear and an exponential growth regime: An in situ atomic force microscopy study. Macromolecules, 2002. 35(11): p. 4458-4465.

11. Yamada, T. and Shiratori, S., In situ observation of the initial adsorption process of layer-by-layer sequential adsorbed polyelectrolyte film using an AFM. Electrical Engineering in Japan, 2002. 141(2): p. 1-7.

12. Minko, S., Kiriy, A., Gorodyska, G., and Stamm, M., Single flexible hydrophobic polyelectrolyte molecules adsorbed on solid substrate: Transition between a stretched chain, necklace-like conformation and a globule. Journal of the American Chemical Society, 2002. 124(13): p. 3218-3219.

13. Kiriy, A., Gorodyska, G., Minko, S., Jaeger, W., Stepanek, P., and Stamm, M., Cascade of coil-globule conformational transitions of single flexible polyelectrolyte molecules in poor solvent. Journal of the American Chemical Society, 2002. 124(45): p. 13454-13462.

14. Kiriy, A., Gorodyska, G., Minko, S., Tsitsilianis, C., Jaeger, W., and Stamm, M., Chemical contrasting in a single polymer molecule AFM experiment. Journal of the American Chemical Society, 2003. 125(37): p. 11202-11203.

15. *Scanning Probe Microscopy Training Notebook*. 2001: Digital Instruments, Veeco Metrology Group.

16. Decher, G. and Schlenoff, J.B., eds. *Multilayer Thin Films-Sequential Assembly of Nanocomposite Materials*. 2003, WILEY-VCH: Weinheim.

17. Decher, G., Fuzzy nanoassemblies: toward layered polymeric multicomposites. Science, 1997. 277(5330): p. 1232-1237.

18. Lvov, Y., Chapter 4: Thin film nanofabrication by alternate adsorption of polyions, nanoparticles, and proteins, in *Handbook of Surfaces and Interfaces of Materials*, H.S. Nalwa, Editor. 2001, Academic Press.

19. Minko, S., Kiriy, A., Gorodyska, G., and Stamm, M., Mineralization of single flexible polyelectrolyte molecules. Journal of the American Chemical Society, 2002. 124(34): p. 10192-10197.

20. Lvov, Y.M. and Decher, G., Assembly of multilayer ordered films by alternating adsorption of oppositely charged macromolecules. Kristallografiya, 1994. 39(4): p. 696-716.

21. Losche, M., Schmitt, J., Decher, G., Bouwman, W.G., and Kjaer, K., Detailed structure of molecularly thin polyelectrolyte multilayer films on solid substrates as revealed by neutron reflectometry. Macromolecules, 1998. 31(25): p. 8893-8906.

22. Ladam, G., Schaad, P., Voegel, J.C., Schaaf, P., Decher, G., and Cuisinier, F., In situ determination of the structural properties of initially deposited polyelectrolyte multilayers. Langmuir, 2000. 16(3): p. 1249-1255.

23. Sukhorukov, G.B., Schmitt, J., and Decher, G., Reversible swelling of polyanion/polycation multilayer films in solutions of different ionic strength. Berichte Der Bunsen-Gesellschaft-Physical Chemistry Chemical Physics, 1996. 100(6): p. 948-953.

24. Fery, A., Scholer, B., Cassagneau, T., and Caruso, F., Nanoporous thin films formed by salt-induced structural changes in multilayers of poly(acrylic acid) and poly(allylamine). Langmuir, 2001. 17(13): p. 3779-3783.

25. Lvov, Y., Ariga, K., Onda, M., Ichinose, I., and Kunitake, T., A careful examination of the adsorption step in the alternate layer-by-layer assembly of linear polyanion and polycation. Colloids and Surfaces a-Physicochemical and Engineering Aspects, 1999. 146(1-3): p. 337-346.

26. Fleer, G.J., Cohen Stuart, M.A., Scheutjens, J.M.H.M., Cosgrove, T., and Vincent, B., *Polymers at Interfaces*. First ed. 1993, London, UK: Chapman & Hall.

27. Shiratori, S.S. and Rubner, M.F., pH-dependent thickness behaviour of sequentially adsorbed layers of weak polyelectrolytes. Macromolecules, 2000. 33(11): p. 4213-4219.

28. Vezenov, D.V., Noy, A., and Lieber, C.M., Chemical force microscopy: probing and imaging interactions between functional groups, in *Scanning Probe Microscopy of Polymers*, B.D. Ratner and V.V. Tsukruk, Editors. 1998, American Chemical Society: Washington, DC.

29. Tsukruk, V.V., Bliznyuk, V.N., and Wu, J., pH variations of surface forces as probed by chemically modified tips, in *Scanning Probe Microscopy of Polymers*, B.D. Ratner and V.V. Tsukruk, Editors. 1998, American Chemical Society: Washington, DC.

30. Tsukruk, V.V. and Bliznyuk, V.N., Adhesive and friction forces between chemically modified silicon and silicon nitride surfaces. Langmuir, 1998. 14(2): p. 446-455.

Chapter 7

Surface plasmon resonance sensing of ions in liquids using polyelectrolyte thin films

7.1 Introduction: transition metals and their impact on health and the environment

Because of the devastating effects that certain toxic metals can have on human health, metal pollution is potentially one of the most serious forms of aquatic pollution. Through contaminated water, metals are transmitted to humans, either directly or via the food chain. Metals are introduced into the aquatic system by many processes, including the weathering of soils and rocks, volcanic eruption and a variety of human activities involving the mining, processing, or use of metals and/or substances that contain metal contaminants [1].

Metals are recognized to have a double–edged nature in their interaction with biological systems [2]. On one hand, thanks to their catalytic versatility, they are essential for many life processes. However, because of their high reactivity, metals can become toxic at low concentrations. For example, transition metals, e.g. iron, zinc, copper, are vital for many cellular processes thanks to their multiple oxidation states. Without them, life on earth as we know it would be impossible.

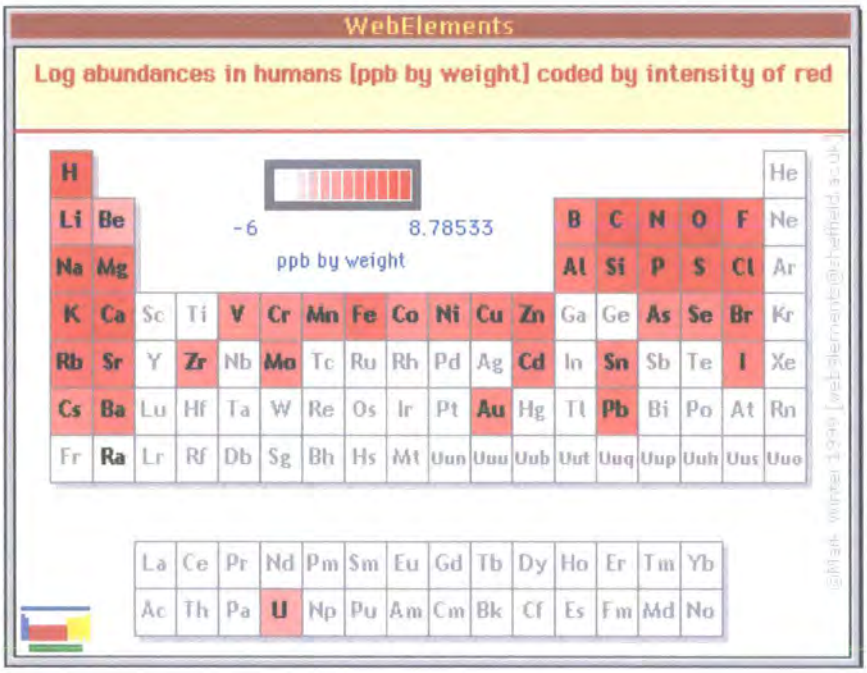

Figure 7.1 Representation of the level of chemical elements in the human body: concentrations (ppb by weight) coded by intensity of red; logarithmic scale. (Reproduction from http://www.webelements.com).

A balance in the concentration of metals in the human body is essential, since diseases can result both from their deficiency as well for their excess. For example, it is known that a deficiency of iron is associated with some forms of anaemia while its excess in the body causes liver and kidney damage. Copper in excess causes Wilson's disease with accumulation of the metal in the liver, brain and kidneys. Figure 7.1 shows the typical levels of different chemical elements in the human body.

The maximum permissible levels for metals in drinking water, according the United States federal regulations and the World Health Organisation (WHO), is shown in Table 7.1 [3, 4].

		Maximum Permissible Concentration Goal		
		U.S. EPA (1999)		**WHO (1993)**
Metal	**Chemical Symbol**	μM	μg L^{-1}	μg L^{-1}
Lead	Pb	0	0	10
Mercury	Hg	0.010	2	1
Cadmium	Cd	0.044	5	3
Antimony	Sb	0.049	6	18
Beryllium	Be	0.444	4	
Selenium	Se	0.633	50	10
Chromium	Cr	1.923	100	50
Barium	Ba	14.563	2000	700
Copper	Cu	20.458	1300	2000

Table 7.1 Maximum permissible contaminant level goals for various metals in drinking water according the U.S, Fed. Gov. Environmental Protection Agency (1999) [3] and the WHO (1993) [4] .

Metals in drinking water occur via different modes of contamination. For example, metals are dissolved in the water from natural reserves. Arsenic, barium, chromium, manganese, molybdenum, selenium and uranium find their way into drinking water by percolation of water through metal enriched geological layers. However, the main causes of contamination are linked to human activity through industrial processes and the distribution of the water via pipes and fittings. Aluminium, iron, cadmium and mercury usually are the result of industrial procedures, while copper, lead, nickel, tin and zinc originate from the second pollution source [4]. As shown in Table 7.1, the

regulations are particularly strict with the metallic content of drinking water. These limitations not only concern the water suppliers (private companies or city councils) and the general public, but all those industrial activities that involve metals and that could have them in their liquid wastes. To avoid any environmental harm (and heavy monetary fines), strict control of the metal content of industrial waste is needed.

To date, the lowest detection limits for metal in water are obtained using sophisticated spectrometry. Either mass spectrometry or atomic spectrometry can be used [5, 6]. The principle of mass spectrometry is to obtain a positively charged ion characteristic of the substance under investigation. This is accomplished, for example, by heating the sample. The molecules in the vapour state are then bombarded with high-energy electrons. The collision between an electron and the molecule (or atom) causes an electron to be ejected, leaving a positively charged ion. The ionized molecules are attracted by an applied electrostatic potential and are accelerated towards a negatively charged plate. A slit in the plate introduces the ions into a chamber where a magnetic field is present. This magnetic field deflects the positive ions by an amount which depends upon their mass and charge. Less than a nanogram of material is sufficient for a mass spectrum and only a few seconds are necessary for the operation to be completed.

Atomic spectrometry is based on the emission or absorption of electromagnetic radiation, which accompanies energy changes within a molecular or atomic system. For example, as a result of absorption, the transmitted power (intensity) of the reflected beam will be diminished, which can be related to the chemical species under investigation. Absorption is not the only atomic spectrometry method: fluorescence or emission can also be used.

Several mass and atomic spectrometry systems have been developed and a more detailed description of such devices can be found in literature [5, 6]. Quantities of copper as small as 0.02-0.01 $\mu g\ l^{-1}$ can be detected by inductively coupled plasma/mass spectrometry; a limit of 0.3 $\mu g\ l^{-1}$ is obtained by inductively coupled plasma/optical emission spectroscopy and 0.5 $\mu g\ l^{-1}$ by flame atomic absorption spectrometry. Nickel can be detected in quantities of 0.1 $\mu g\ l^{-1}$ by inductively coupled plasma/mass spectrometry; 1 $\mu g\ l^{-1}$ by electrothermal atomic absorption spectrometry or inductively

coupled plasma/optical emission spectrometry; 15 μg l^{-1} by inductively coupled plasma spectrometry and 20 μg l^{-1} by flame atomic absorption spectrometry [4].

Other analytical methods can also be used, although with a lower sensitivity. Their main advantages are in their relative simplicity of use, in the possibility of compact systems for in-situ application and in a lower cost. For example, a commercial solution proposed by Merck (Reflectoquant®) uses the principle of reflectance photometry for analysis of metals in water. Characteristic measuring ranges are 5-200 mg l^{-1} for copper, 10-200 mg l^{-1} for nickel and 0.5-200 mg l^{-1} for iron.[1] The principle exploited is based on the quantification of the intensity of a coloured reaction product from an active film immobilized on a support and the analyte. Alternatively, ion selective electrodes can be used as in the ThermoOrion Ionplus™ system. Here, a sensing electrode is used in combination with a reference electrode, or by itself, if equipped with a built-in reference. The electrode is provided with a sensing membrane selective to specific ions. When the electrode is in contact with the sample an electrical potential develops across the membrane surface. The magnitude of the potential relates to the concentration of the ion being measured: the higher the concentration the higher the potential. The presence of copper ions in a concentration range of 0.1 to 10^{-8} M (i.e. detection limit of 6.4 mg l^{-1})[2] can be detected using such device.

7.2 LbL polyelectrolyte films and their interactions with metal ions in solution

Polyelectrolyte multilayers offer numerous opportunities for use as molecularly tunable thin film coatings. By manipulating the manner in which the polymer layers are assembled, it is possible to create molecular architectures with a wide range of chemical, physical and biological properties.

In this work, polyelectrolytes are used to create ultrathin LbL films for use as active layers within a SPR sensor system. The principle of detection of metal cations in water originates from a number of different mechanisms. One is the electrostatic attraction between the positively charged ions and the negatively charged outer surface of the thin

[1] Manufacturer's claim.
[2] Manufacturer's claim.

film. Specific chemical interactions, such as chelation of the metal by the polyelectrolyte (polyanions or polycations can both be exploited for this purpose) can also be important.

Chelation is dependent on the environmental conditions in which it takes place (see Appendix A for a more detailed description of the phenomenon). The stability constant of the chelation reduction (single or multistage chelation), K_d, is a function of the pH of the solution and the main driving forces of such a process are diffusion, collision and a substitution mechanism [2]. Among all the possible sensing mechanisms, chelation is the most interesting and attractive. The selectivity of many materials to metals relies on this process.

The chemical structures of some metal acetates used to prepare the metal cations in solution are shown in Fig. 7.2.

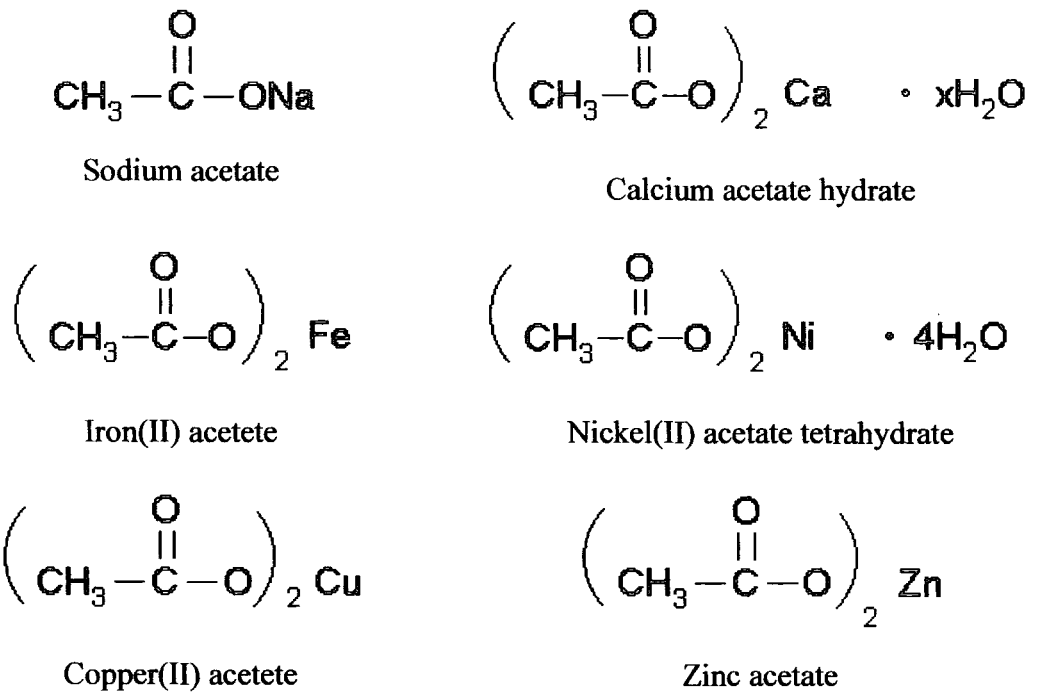

Figure 7.2 Chemical formulae of metal acetates used for the preparation of metal cation solutions.

At first sight, the mechanism for the release of the metal cations M^{n+} and the acetate anion $C_2H_3O_2$, $n(ac)^-$ in water seems to be straightforward

$$M(ac)_n \rightleftharpoons M^{n+} + n(ac)^-$$

However, such a simplistic view is complicated by the solvent itself, water, one of the most abundant compounds on the surface of the earth and the ultimate, environmental-friendly, solvent [7].

Ions in water are surrounded by water molecules and the system formed is generally indicated as an aqua-ion $[M(OH_2)_n]^{m+}$, the simplest and most fundamental species present in aqueous solution for a chemical element [7, 8]. Understanding the equilibria and dynamic processes involved in the formation and evolution of the aqua-ions is complex. All ions in water are hydrated to some extent. A primary hydration shell is formed mainly through electrostatic forces. In addition, hydrogen bonding helps to create a secondary hydration shell wrapped around the first shell and therefore around the ion itself. A tertiary shell is occasionally found for some ions. Properties of water molecules associated with the shells are different from those of "bulk" water. The degree of hydratation depends on a number of factors such as ionic size and charge density. In general, cations, because of their high positive charge density and strong interaction with the negatively polarized oxygen atom in the water molecule, are more hydrated than anions. According to the particular ion in question, the ion-water interaction depends to a differing degree on ionic and covalent interactions. Ions and water molecules are highly mobile and a dynamic exchange mechanism of the water molecules from the shells to the "bulk" occurs at any time, although within a very wide range (from nanoseconds to hundred of years) of mean residence time of bound water i.e. the average time that one water molecule spends in one of the hydratation shells before being replaced by another [7].

For metal aqua-ions, one of the more stable coordination arrangements is that of a single ion surrounded by six water molecules. Such a coordination has high symmetry and an arrangement balancing the size of the available cavity (radius of M^{n+}) with that of the adjacent water ligands. All this provides an appropriate $M\text{-}OH_2$ distance to facilitate significant bonding interactions [7]. For the metal ions investigated in this research, i.e. iron, nickel, copper and zinc, two different arrangements are recognizable for six-fold coordination: octahedral for iron, nickel and zinc and tetragonally distorted for copper (see Fig. 7.3).

(a) Octahedral field **(b) Tetragonally distorted octahedral field**

Figure 7.3 Geometry of six coordinated metal-aqua ions for some d-transition metals. Case (a) is typical for iron, nickel and zinc while conformation (b) occurs for copper (reproduced from [7]).

Such differences in coordination have a marked effect on the stability constant of the complexes that these metals form with specific ligands. Figure 7.4 shows that hexadentate ethylenediaminetetraacetic acid, *EDTA*, bidentate ethylenediamine $NH_2CH_2CH_2NH_2$, *en* and ammonia, NH_3 have a stronger interaction with the divalent copper(II) with respect to other divalent metal ions. This is a consequence of the Jahn-Teller effect, which is also responsible for the tetragonal distortion of the octahedral field for the copper aqua-ion. The precise nature of this distortion has been extensively discussed and usually results in two distinct situations. The first is the fluxional elongated rhombic octahedral distortion that is temperature variable. There is also a static elongated rhombic octahedral distortion, which is temperature independent.

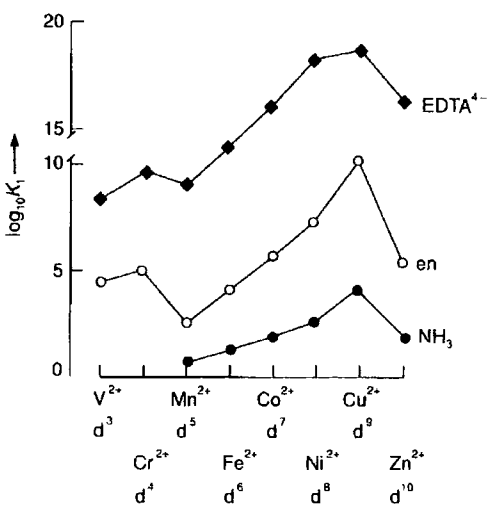

Figure 7.4 Stability constant for metal-ligand complex formation along the first row transition metals: the Irvine-Williams effect. (Reproduced from [7]).

The overall result is shown in Fig. 7.3 (b) - two of the six bonds are more elongated than the other four. Such distortion allows a strong binding of the four ligands in the plane, while the remaining axial positions are more weakly bound [8-10]. This weak axial bond is fundamental in determining the mean residence time of the water molecules in the hydration shell (continuous replacement with "bulk" water molecules). For copper, this time corresponds to fractions of a nanosecond, while for iron, zinc and nickel the time varies from fractions of a microsecond to a few microseconds.

One further important aspect is the tendency of aqua-ions to hydrolyze, mainly as a function of the pH of the solutions in which they are dispersed. Under specific conditions, the "acidity" of the proton on the water molecule reaches a level when a free water molecule itself can effectively remove it. Thus, a hydroxyl metal species and H_3O^+ are formed. For the first-row transition metals, an alkaline pH is generally necessary for the hydrolysis to occur. For iron, at pH 10, precipitation of hydrous $Fe(OH)_2$ is observed [7].

7.3 Sensing experiments

In previous work at Durham, it was shown that a PEI/PMAE bilayer could successfully be used for metal ion detection using SPR [11]. In particular, this organic thin film proved to have a strong selectivity towards Cu^{2+}. Figure 7.5(a) shows the change in reflectivity versus time of exposure for a PEI/PMAE film interacting with different metal acetates. It was possible to verify that the PEI macromolecules were fully covered by the PMAE layer. Therefore, the detection of the cations was mainly attributed to a chelating reaction of the PMAE with the metals. In Figure 7.5(b), the proton exchange mechanism trigging the chelating reaction is illustrated. These sensing experiments were performed using a traditional $\theta/2\theta$ SPR device. A detection limit of 10^{-6} M was measured for copper ions and the sensing response was found to be non linear with the metal acetate concentration [11].

The research presented in this chapter and the next is based on this experiment. However, a different approach was used in the design of the SPR system (see Chapter 4). The implementation of a multichannel sensing chip, where different sensing

materials are addressed simultaneously, is also investigated for the first time. Other issues of interest were the use of a polycation for anionic species detection, the use of an alternative polyanion to PMAE and studies on the influence of the LbL film structure and organization on the sensing performance.

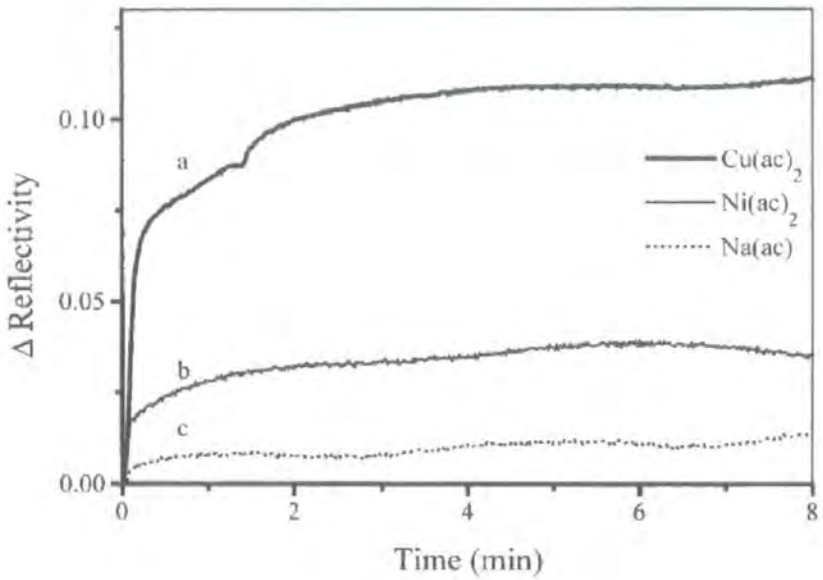

(a)

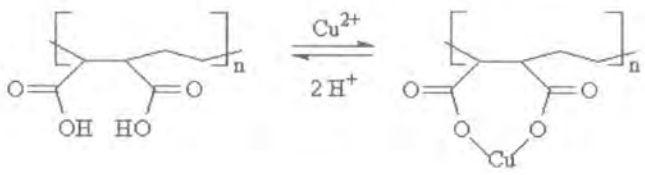

(b)

Figure 7.5 (a) Change in reflectivity versus time for a bilayer exposed to different metal acetates. Concentrations: copper acetate 10^{-3}M (curve a); nickel acetate 10^{-3} M (curve b); and sodium acetate $2x10^{-3}$ M (curve c); (b) Reaction of copper ion and maleic acid to form a chelate. Reproduced from [11].

7.3.1 Polycation PMADAMBQ for anionic and pH sensing

One of the first experiments was directed at extending the capabilities of the SPR device to the detection of anions. A possible candidate for such purpose might have been thought to be PEI, the positively charged polymer used previously in combination with the polyanion PMAE. However, PEI is known to have a high affinity to metal cations via the formation of a multi-dentate chelate, and therefore it was not ideal for anion

detection (the main risk being that of ambiguity in the response of such a polymer). At the most, PEI could be used for comparative sensing of metal cations. The stability constant $\log_{10}K$ of its chelate with copper has a value of approximately 20 [12], while the copper complex with PMAE has a $\log_{10}K$ equal to 5.5 [13]. It is reasonable to expect then that the reversal of the metal/polymer interaction is, in the case of PEI, slower than for the PMAE.

A new class of polycations, i.e. a cationic modified polyacrylic acid, PMADAMBQ, was used in this work. This particular polymer was synthesised by Dr W Jaeger of the Fraundhofer-Institut für Angewandte Polymerforschung, Tetlow, Germany [14]. The molecular structure of PEI and PMADAMBQ are contrasted in Figure 7.6.

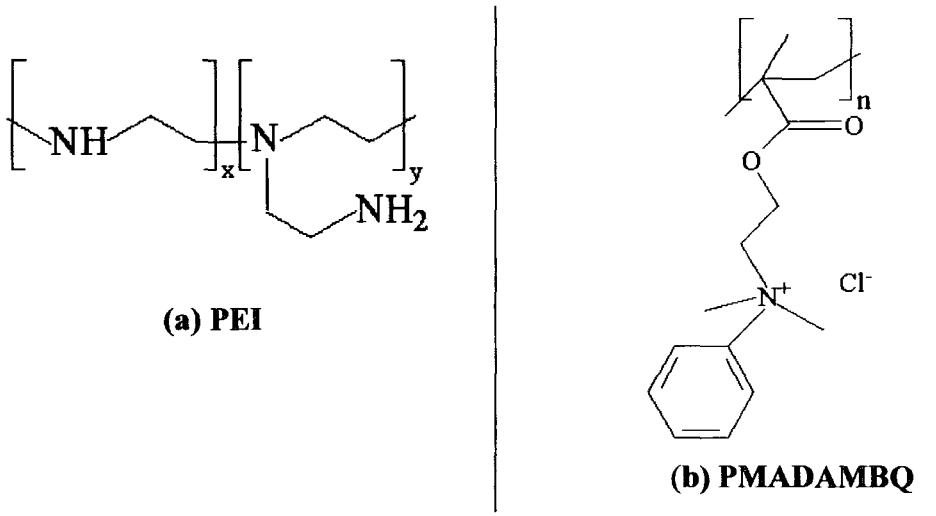

(a) PEI

(b) PMADAMBQ

Figure 7.6 (a) Poly(ethyleneimine), PEI monomer structure; (b) Cationic modified polyacrylic acid, PMADAMBQ, monomer structure.

The presence of a pendant benzene group gives the latter a hydrophobic feature. Theoretically, anions will interact with the polymer via Coulombic attraction to the positively charged nitrogen.

To establish the typical noise/drift of the SPR equipment a base line was first recorded in real time leaving the uncoated gold substrate in tris buffer at pH 6.2 for sixty minutes, Fig. 7.7. Note that with time, the signal oscillations become greater. This is thought to be related to the warming up of the CCD camera.

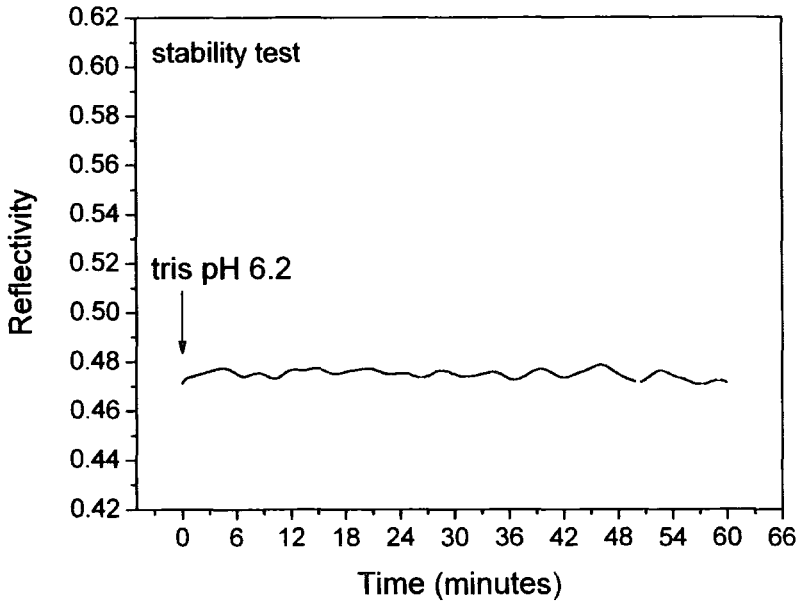

Figure 7.7 Reflectivity base line. An uncoated gold layer was left in tris buffer at pH 6.2 for sixty minutes and the reflectivity variation recorded in real time.

In an initial experiment, it was attempted to self assemble the PMADAMBQ directly on a gold surface. Solutions $2x10^{-2}$ M of PMADAMBQ and 10^{-2} M for PMAE were prepared in tri(hydroxymethyl)aminomethane, $C_4H_{11}NO_3$ (tris) buffer solution. Their pH was fixed at a value of 6.2 by the addition of HCl. Following the procedures described in literature [15], the glass slides coated with gold were immersed in the polyelectrolyte solutions for an average of 12 min. Between one immersion and the next, the substrates were rinsed in the buffer solution for 1 min; no drying step was performed until the end of the deposition process. The process of self-assembly was monitored in real time and changes in reflectivity during the adsorption of the polyelectrolytes were recorded, Fig. 7.8(a). From Figure 7.8(a) it is evident that the LbL self-assembly of a single bilayer PMADAMBQ/PMAE was unsuccessful, particularly if compared with similar data for a PEI/PMAE bilayer [11] (see Fig. 7.8(b)).

Such behaviour might be due to poor adsorption of the PMADAMBQ on the gold surface. It was therefore attempted to create an appropriate negatively charged interface to improve the adsorption of PMADAMBQ. Poly(ethyleneimine) is often use to *charge* various substrate surfaces and make these suitable for LbL self-assembly [15]. However, because PEI and PMADAMBQ are both polycations the latter cannot adsorb

directly on the former. It is necessary, then, to adsorb PMAE on top PEI in order to produce a suitable negatively charged surface.

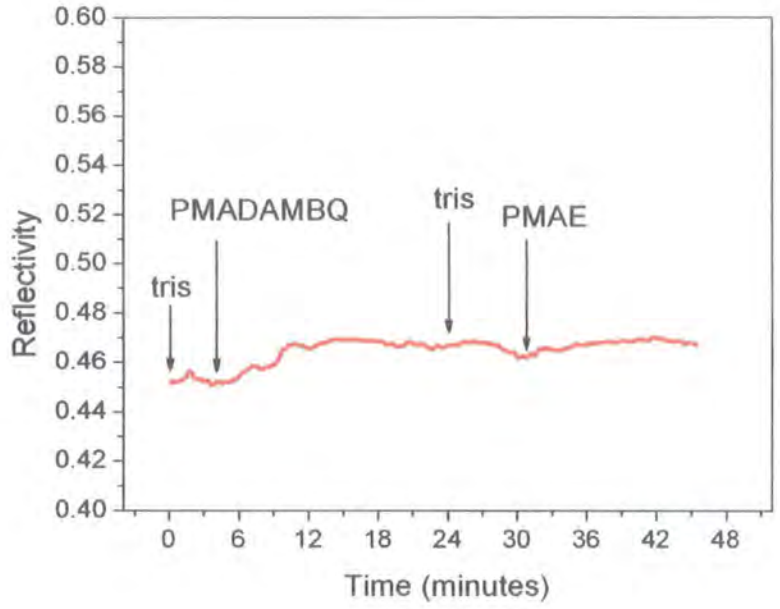

(a)

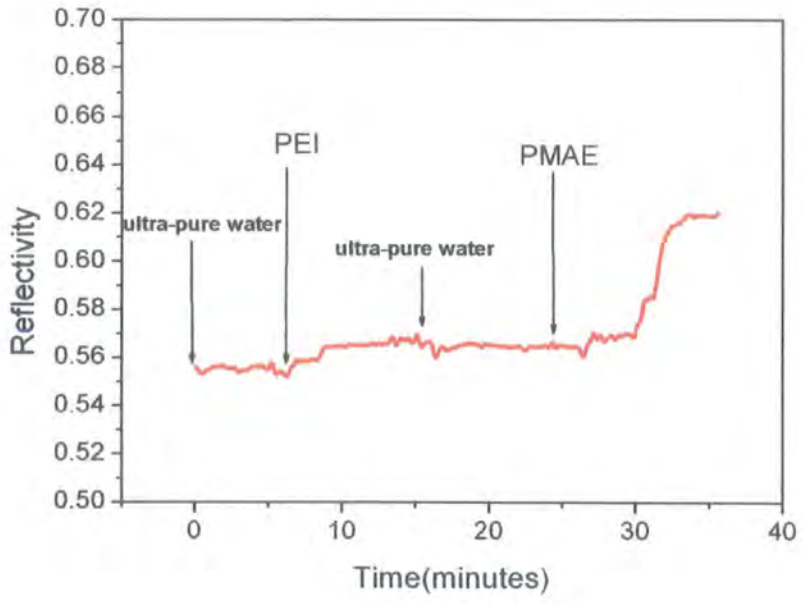

(b)

Figure 7.8 Real time changes in the reflectivity during the adsorption of PMADAMBQ plus PMAE (a) and PEI plus PMAE (b). The arrows indicate when the various solutions were admitted to the measurement cell. A flow rate of approximately 2 ml min^{-1} was used.

A PEI/PMAE bilayer was successfully assembled in previous work, giving a satisfactory coverage of metal surfaces [11]. Figure 7.9 shows clearly that when a gold

surface functionalized with a single PEI layer was used, the adsorption process of PMAE and, subsequently, of PMADAMBQ was more successful.

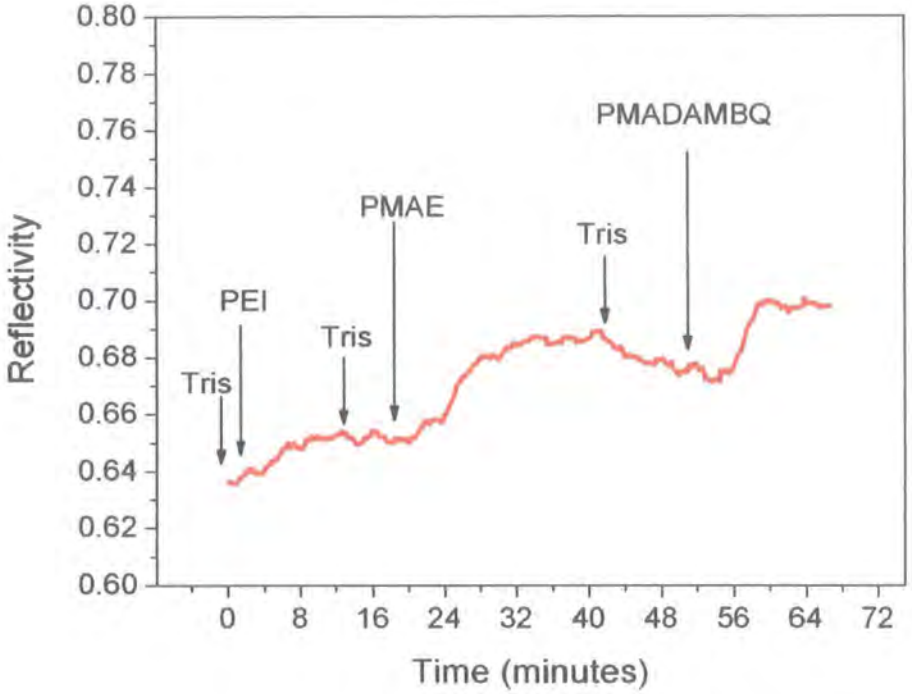

Figure 7.9 Real time changes in the reflectivity during the adsorption of PMAE and PMADAMBQ on a gold surface functionalized with a PEI layer. The arrows indicate when the various solutions were admitted to the measurement cell. The solutions were circulated at a flow rate of approximately 1.1 ml min^{-1}.

The ability of this specific multilayer film, with PMADAMBQ as outer surface, to sense appropriate negative charged species was then tested. Solutions of 10^{-5} M and 10^{-4} M of sodium dodecylbenzene, $C_{12}H_{25}C_6H_4SO_3Na$, DBSA in pH 6.2 buffers were used for this experiment. Figure 7.10 shows a clear response of a film with PMADAMBQ as the outer surface to both concentrations of DBSA. No effect was observed with HCl, used successfully to reverse the reaction of Cu and PMAE (Figure 7.15) [11], as the acid of DBSA is not water-soluble. The adsorption of DBSA may be due to hydrophobic interactions in addition to the electrostatic interactions. Therefore, the regeneration of the active film for further sensing is not straightforward and further studies are needed to explore this particular aspect. Nevertheless, this work demonstrates that anionic sensing was successful. For completeness, the adsorption of DBSA onto a polyelectrolyte film with an outer layer of PMAE was also tested. In this case, no change in the reflectivity for DBSA concentrations up to 10^{-4} M could be seen. This

points to an electrostatic repulsion of DBSA and suggests that electrostatic interactions are dominant in the case of the adsorption of DBSA.

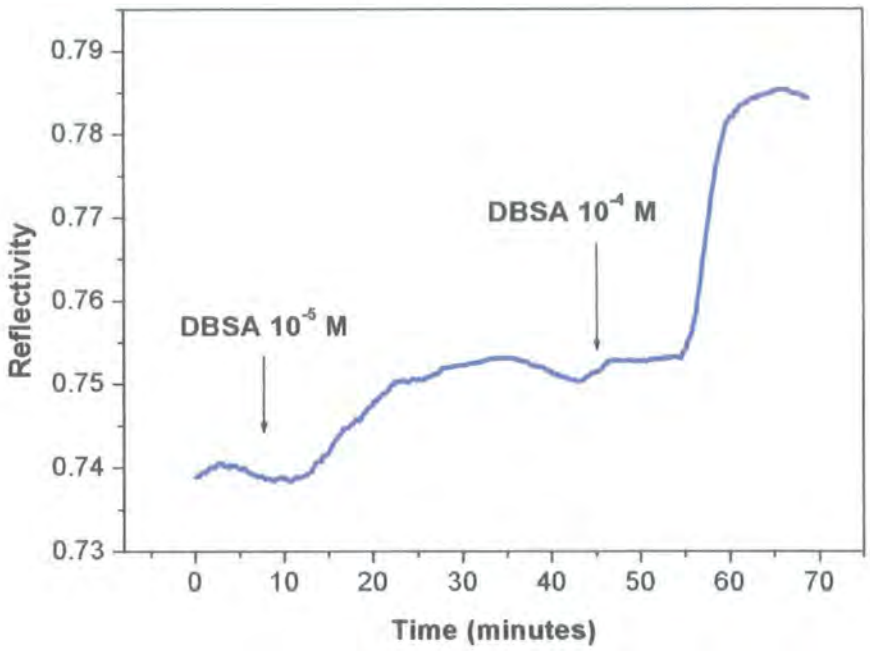

Figure 7.10 Reflectivity response of a PEI/PMAE/PMADAMBQ film to DBSA. The arrows indicate when the solutions were admitted to the measurement cell. Flow rate 1.7 ml min^{-1}.

During this series of experiments it was noted that the active film responded differently to solutions with similar ion concentrations but different pH values. This behaviour was thought to be due to an internal reorganization of the film architecture driven by the pH variation.

Shiratori and Rubner [16] have described a detailed study of the role that solution pH plays in the layer-by-layer processing of weak polyelectrolytes. Four different film growth regimes were identified in a plot of layer thickness versus pH (Fig. 7.11(b)). These were dependent on the degree of ionization of the polyelectrolytes. By controlling the pH during film deposition, it was possible to vary the thickness of an adsorbed poly(allylamine hydrochloride), PAH or poly(acrylic acid), PAA layer from 0.5 nm to 8.0 nm (Fig. 7.11(a)). The role of the salt concentration in solution had already been investigated, but this study now proved that changes in pH could have an equally dramatic effect on the film properties. Such a discovery has turned out to be a powerful tool for the molecular tuning of LbL multilayer architectures. This technique is now

widely exploited, e.g. for the engineering of cytophilic or cytophobic surfaces using similar polyelectrolytes assembled at different pH [17-19].

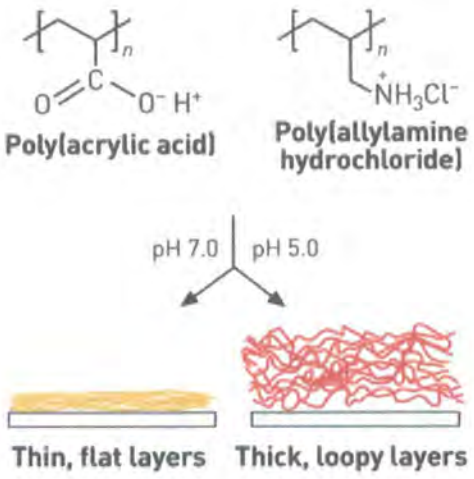

(a)

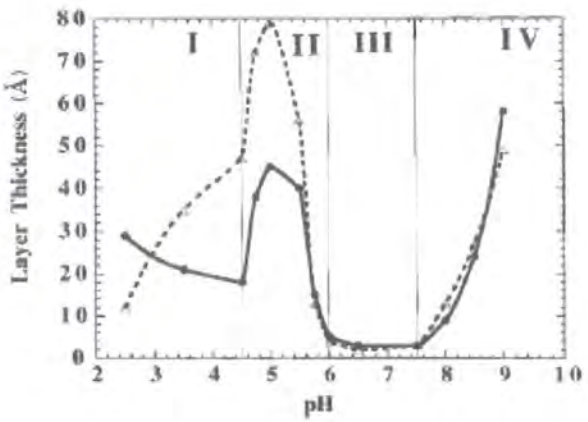

(b)

Figure 7.11 (a) Multilayers of poly(allylamine hydrochloride), (PAH)/poly(acrylic acid), (PAA) are prepared by alternate dipping in anionic and cationic polyelectrolytes. The structure and properties of the films are controlled by pH. (Reproduced from [20]). (b) Average incremental thickness contributed by a PAA and PAH adsorbed layer as function of solution pH. Both the PAH and PAA dipping solutions were at the same pH. Solid line represents the PAA layer thickness, and the dashed line is the PAH layer thickness. (Reproduced from [21]).

Investigations of the pH sensitivity were undertaken on polyelectrolyte films comprising a bilayer of PEI/PMAE coated with a single layer PMADAMBQ. Different pH solutions were made by the addition of HCl to 0.01 M tris buffer. Figure 7.12 shows the results for one of the pH-sensing experiments. The PEI/PMAE/PMADAMBQ assembly was exposed to three different buffer solutions at various pH values, in the order: pH 9.0, pH 6.2 and pH 3.5. Changes in reflectivity were monitored as a function of time.

The figure shows that the maximum reflectivity was observed when the organic film was exposed to a buffer of pH 6.2. Following exposure to pH 3.5, the reversibility was checked by exposing the film to increasing pH values (i.e. in the order pH 3.5, pH 6.2 and pH 9.0). The final reflectivity values obtained on increasing the pH values were within ±2 % of those obtained by decreasing the pHs.

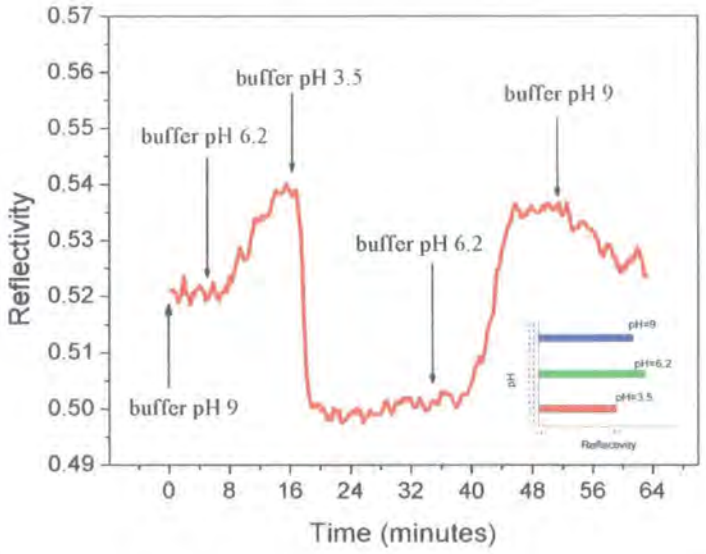

Figure 7.12 Reflectivity versus time for PEI/PMAE/PMADAMBQ film at various pH values. In the insert in the bottom right corner the variation of reflectivity associated to the solution pH value is shown.

The data shown in Figure 7.12 reveal that our SPR equipment can be used effectively to monitor pH-induced film thickness variations and that the polyelectrolyte films can be used in principle as the basis for a pH sensor. However, further work is needed to clarify whether it is the outer PMADAMBQ layer or the inner PEI/PMAE bilayer that is responsible for the thickness changes. A crucial question is if, and by how much, the architecture of the molecular assembly influences the sensing behaviour of the organic film?

It is important to note that, in the above experiment, the thickness variation was achieved not by changing the pH of the polymeric solution during the self-assembly procedure, but by a post depostion process. Recent studies [22, 23] confirm such behaviour for similar weak polyelectrolyte systems. In particular, this pH-switchable swelling transition is thought to be useful for reversibly erasable nanoporous anti-reflection coatings [22] and also the basis of "artificial muscles".

This ability of weak polylectrolytes to sense pH variations could be exploited for measuring the acidic content of solutions. At the same time, this pH sensitivity is a factor to consider in those experiments concerning the detection of chemical species in solution. The main problem is that a false reading may result from a pH variation invalidating the detection of targeted analyte. Strong polyelectrolytes have a stable high charge density and, in theory, they are the less influenced by pH. As will be discussed in Chapter 8, this is not necessarily true for films that are undergoing sensing experiments, because modification of the inner architecture and porosity could affect the pH sensitivity of old films even in presence of a strong polyelectrolyte as a component of an LbL pair. Multichannel detection could offer a solution to this. If on each channel a different combination of polymers has been deposited, they will have different sensing responses to the same solution. A cross-reference of all the data collected might allow precise screening between variations due to pH changes and variations due to different chemical species.

7.3.2 Two bilayer PEI/PMAE/PMADAMBQ/PMAE structures for copper (II) ion sensing

Following the previous series of studies, a single layer of PMAE was adsorbed on top of a PEI/PMAE/PMADAMBQ film. As discussed in Chapter 3, SPR devices have a higher sensitivity if ultra-thin films are used. Therefore, it is necessary to limit the thickness so as not to compromise the quality of the SPR profile. Some experiments with PEI/PMAE multilayers, prepared from aqueous solutions, have already shown that, at the third bilayer, the system sensitivity is reduced [24].

In Figure 7.13, the change in reflectivity in real time due to the adsorption of the precursor bilayer PEI/PMAE and, subsequently to the PMADAMBQ/PMAE bilayer is shown. The initial part of the curve (adsorption of PEI+PMAE) is consistent with our previous results [11]. However, when the PMADAMBQ solution was admitted into the measurement cell, a decrease in the reflectivity value was first registered. This may be due to partial desorption of PMAE, driven by a strong electrostatic interaction with PMADAMBQ, resulting in the formation of polyelectrolyte complexes in the solution. After rinsing with pure buffer followed by exposure to PMAE, a sharp increase in

reflectivity was observed, indicating adsorption of the anionic polyelectrolyte. This suggests that, following treatment with PMADAMBQ, the surface charge must have reversed (i.e. become positive).

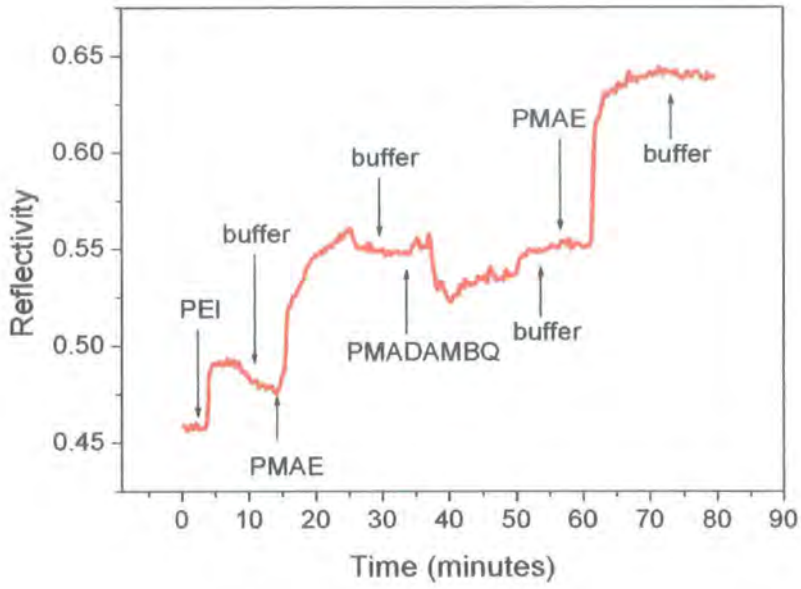

Figure 7.13 Real time changes in the reflectivity during adsorption of polyelectrolytes layers. The arrows indicate when the various solutions were admitted to the measurement cell. The solutions were circulated at a flow rate of 1.7 ml min^{-1}.

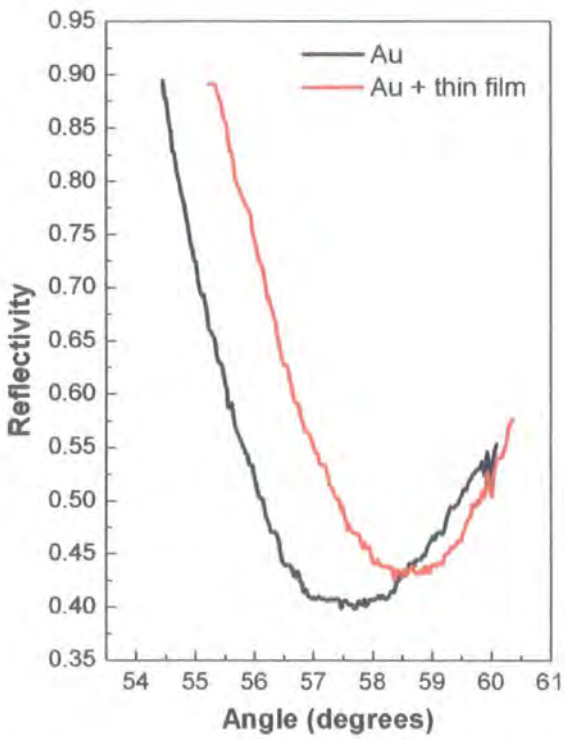

Figure 7.14 SPR curves for uncoated gold (black line) and for gold coated with two polyelectrolyte bilayers (red line) PEI/PMAE/PMADAMB/PMAE.

SPR data (reflectivity versus incident angle) for the uncoated gold and for the gold coated with two bilayers (PEI/PMAE + PMADAMBQ/PMAE), in both cases exposed to the pH 6.2 buffer solution, are shown in Fig. 7.14. The non-zero SPR minima were attributed to a lateral distribution of the light on the sample and to the finite bandwidth of the light source, resulting in the superposition of a number of SPR curves [25]. This is in agreement with work on similar devices [26]. The SPR minimum for the polyelectrolye film is shifted to higher angles by approximately 1 degree.

Using this new molecular architecture, with PMAE as the uppermost layer, a series of sensing experiments with copper acetate solution (from 10^{-5} M to 10^{-3} M) were performed. These results were consistent with those reported previously using a $\theta/2\theta$ SPR system with a He-Ne laser source [11]. Figure 7.15 shows the response to 10^{-5} M of copper acetate. The sensing effect can be completely reversed by exposing the film to HCl [11]. The reflectivity drop below 0.5 (i.e. below the value at the beginning of the experiment) following addition of the HCl is a result of the pH change. Addition of the tris buffer restores the reflectivity value approximately to that observed before the addition of the copper. The 10^{-5} M concentration of copper acetate corresponds to a limiting detection of copper ions of about 0.6 parts per million.

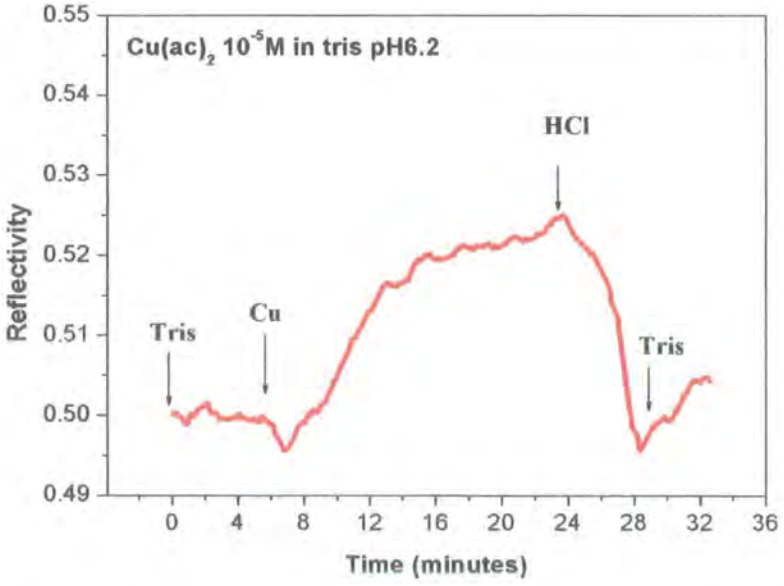

Figure 7.15 Response of the two bilayer structure assembled in figure 2 (PEI/PMAE + PMADAMBQ/PMAE) to 10^{-5} M copper acetate solution at pH 6.2 and subsequent recovery on exposure to HCl. The arrows indicate when the solutions were admitted to the measurement cell. Flow rate 1.2 ml min^{-1}.

To prove that the reflectivity change is due to a reaction between the PMAE and the copper ions and not simply to a change in the refractive index of the solution in the measurement cell, the shift in the position of the critical angle with the solution was investigated. The critical angle in the SPR curve is a function only of the refractive index of the glass slide and of the dielectric present in the cell, in contrast to the angle of the SPR minimum, which is affected by other parameters. Figure 7.16 shows reflectivity data, measured in the region of the critical angle, for the buffer solution and copper acetate (coloured lines) and for ethanol (black line). No substantial change in the position of the critical angle is evident when the buffer solution is substituted with copper acetate solution of increasing concentration (from 10^{-6} M to 10^{-3} M). This indicates that the tris buffer and copper acetate solutions possess approximately the same refractive index n=1.33 as ultra pure water at λ=633 nm [27]. However, when ethanol (n=1.36 at λ=633 nm [27]) was used, a shift in the critical angle is noted. The change in the reflectivity in Figure 7.15 can therefore be attributed mainly to the adsorption of copper onto the outer PMAE layer [11].

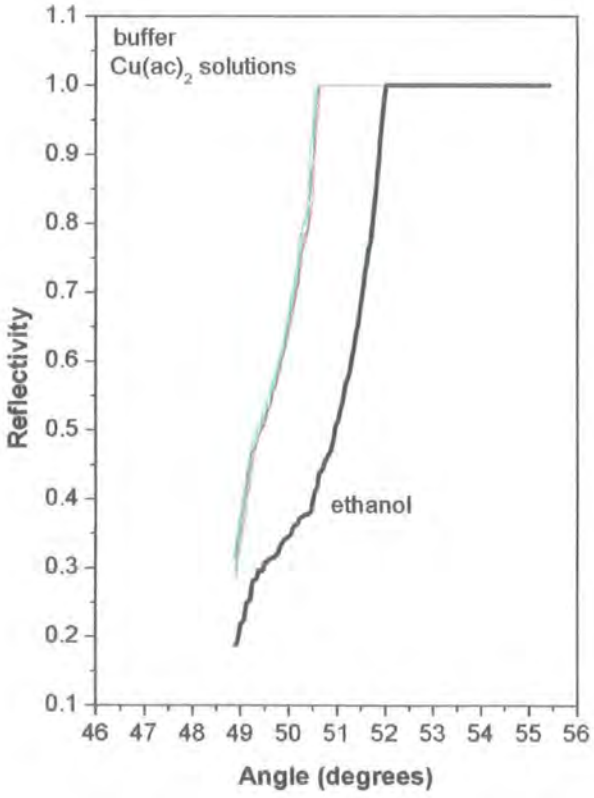

Figure 7.16 Reflectivity in region of the critical angle for different solutions in the measurement cell. Coloured lines correspond to the buffer solution and to copper acetate concentrations ranging from 10^{-6} M to 10^{-3} M. The black line is obtained using ethanol in the measurement cell.

To study the relationship between film architecture and sensing, tests were made using the multilayer structures PEI/PMAE/PMADAMBQ and PEI/PMAE/PMADAMBQ/PMAE shown in Fig. 7.17. If electrostatic forces are considered as one of the dominant factors in the sensing process, then, the detection of positive species such as copper ions is only possible with a polyanion (e.g. PMAE) as the outer layer. In contrast, a negatively charged species can be detected if a polycation is the outermost layer of the film architecture. However, interpenetration of the layers [28] might lead to conflicting results.

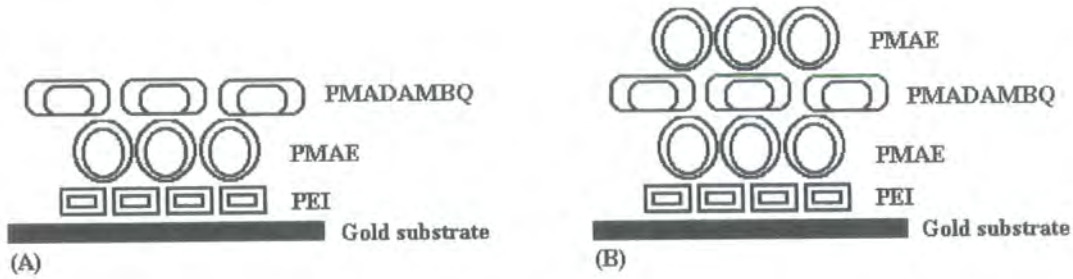

Figure 7.17 Molecular architectures of two sensing films. (A) Polycation PMADAMBQ as uppermost layer; (B) Polyanion PMAE as outer surface.

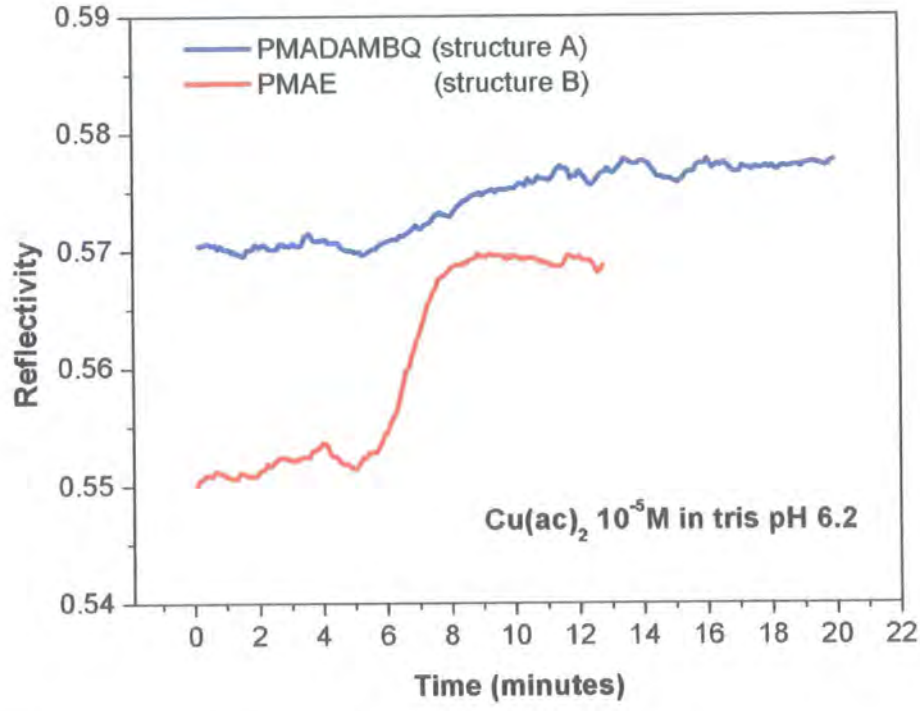

Figure 7.18 Comparison of reflectivity change for the two molecular architectures shown in Figure 7.77 on exposure to 10^{-5} M copper acetate at pH 6.2. Flow rate 1.2 ml min^{-1}.

In Figure 7.18, the different sensing performances of the two film structures to a solution of 10^{-5} M copper (II) acetate are presented. In the case of the PMADAMBQ outer layer (sample (A)), a small variation in reflectivity is registered upon exposure to the copper acetate solution. However, a much greater increase in reflectivity is noted when structure (B) is exposed to the same solution. This suggests that the outer surface is almost entirely covered with one of the polyelectrolyte layers (PMAE or PMADAMBQ), i.e. the film structure is as-deposited with little or no interpenetration of the different films.

7.4 Weak and strong polyanions

In order to prepare a multichannel platform, where different materials have different affinity or selectivity to specific analytes, it was useful to study a combination of strong and weak polyelectrolytes. In Chapter 5, it was shown how weak and strong polycations can generate different surface morphologies and structures. Such behaviour was attributed to their different charge density in solution. For example, polymeric chains can assume the form of a coil (strong polyelectrolytes) or a globule (weak polyelectrolytes at low charge density). Consequently, during the process of adsorption, the former would produce a more uniform surface while the latter would generate a rougher and more porous surface. The globular morphology might prove beneficial to chemical sensing, because of an increased opportunity of film-analyte interactions.

PMAE, as shown in Figure 7.19(a), has two carboxylic acid groups along the chain that form part of a pendant group and, therefore, may be considered a weak polyelectrolyte. The monomer structure of PSS is given in Figure 7.19(b). The use of both polyelectrolytes in a multichannel chip could elucidate the different mechanisms used by the sensing layers to detect the metal cations. In particular, this might give an indication of the relative importance that the different sensing processes (e.g. physio or chemio-sorption) have on the overall system performance. A full discussion on this issue will be presented in Chapter 8.

The plot of the reflectivity change as function of the time for the adsorption of a PEI/PSS bilayer is shown in Figure 7.20. Both solutions were prepared in ultra-pure

water. After recording the reflectivity variation with the gold surface of the sensing chip exposed to water only, the PEI solution was introduced inside the cell. An increase in the reflectivity was recorded followed by a saturation plateau.

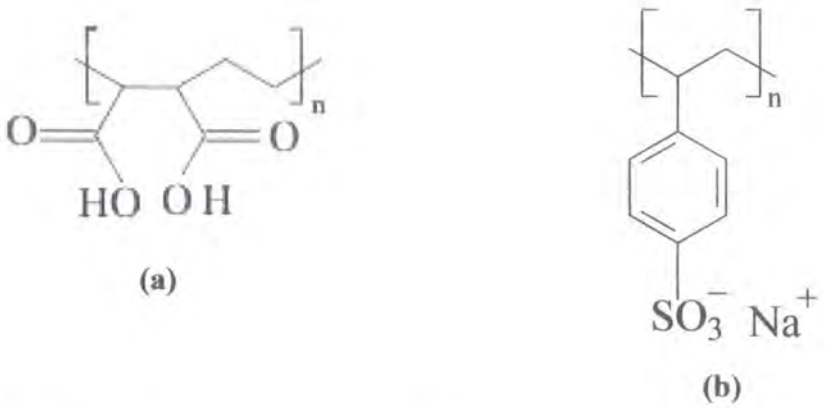

Figure 7.19 (a) Poly(ethylene-co-maleic acid), PMAE monomer structure; (b) Polystyrene sulfonate, PSS monomer structure.

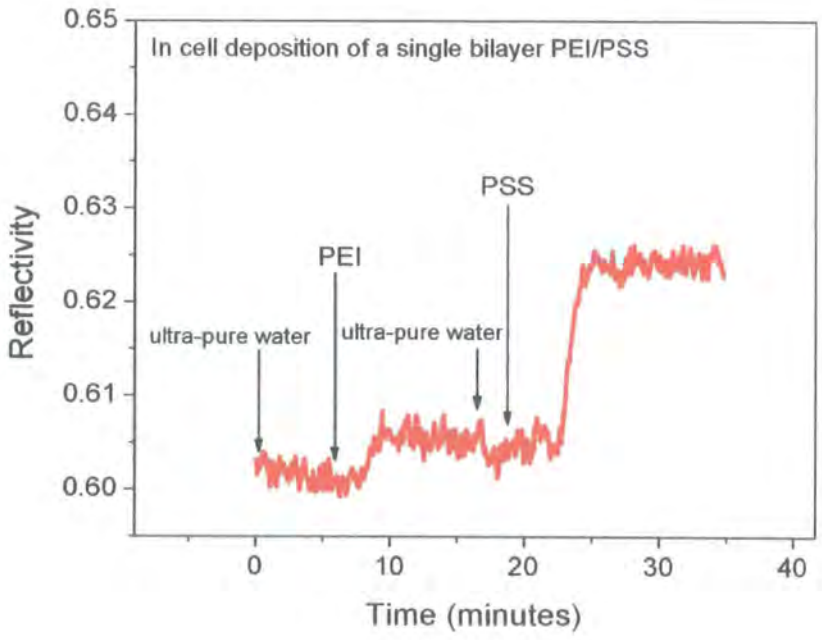

Figure 7.20 Real time changes in reflectivity during adsorption of PEI and PSS. The arrows indicate when the various solutions were admitted to the measuring cuvette. The solutions were circulated at a flow rate of approximately 2 ml min^{-1}.

The cell was washed again in pure water. As consequence, a small reduction in intensity was registered, due to the removal of weakly bounded polymeric chains from the

interface. After a few minutes, ultra-pure water was replaced by the PSS solution. The PEI chains on the gold surface provide a positively charged interface, suitable for the electrostatic driven adsorption of PSS. Again, after a quite rapid increase in reflectivity a saturation level is reached. Such saturation is indicative of complete bilayer formation. All the charged sites have been occupied and, as result, a reverse of the interface charge has been achieved.

A further experiment was undertaken, using PMAE instead of PSS as polyanion, see Fig. 7.21. A similar deposition procedure to the PEI/PSS case was followed. While the changes in reflectivity due to adsorption of PEI can be considered similar for both experiments, for the PMAE adsorption, the variation in the signal recorded is higher than for the PSS case. Even the saturation time appears to be different for the two polyanions. These differences are thought to be related to differences in electric charge density between the two polymeric chains. PSS, being strongly charged, has a very fast electrostatic interaction with the PEI substrate, while PMAE tends to have a slower reaction. Moreover, the smaller reflectivity change in Fig. 7.20 suggests a thinner PEI/PSS bilayer in comparison to the PEI/PMAE.

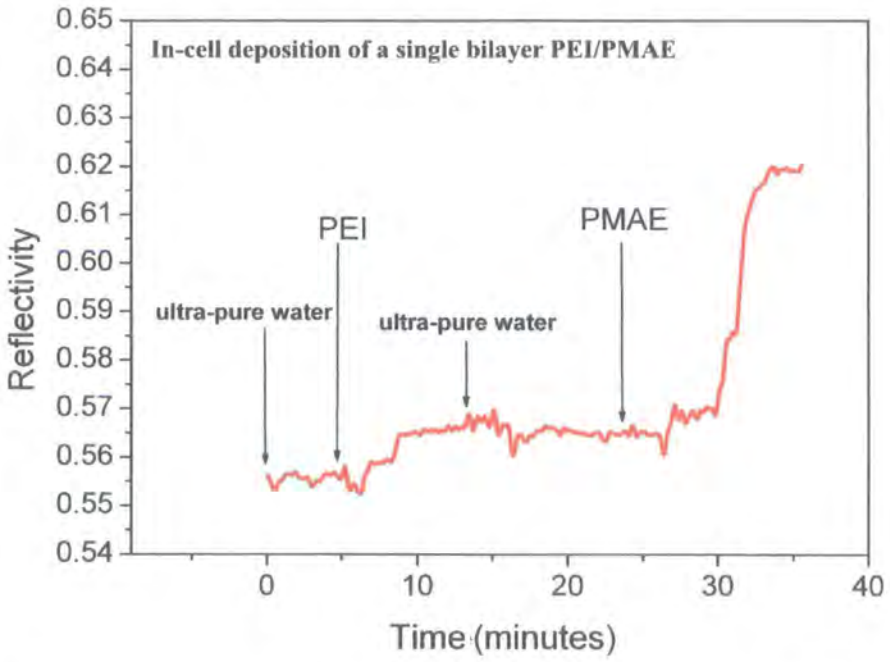

Figure 7.21 Real time changes in reflectivity during adsorption of PEI and PMAE. The arrows indicate when the various solutions were admitted inside the measuring cuvette. The solutions were circulated at a flow rate of approximately 2 ml min^{-1}.

The above explanation, of course, assumes that the polymer solutions have similar refractive index values. AFM images of the outer surface of these two architectures have demonstrated a more compact and uniform structure for films having PSS as a constituent, while PMAE gave more irregular and rougher surfaces (Chapter 6). Figs. 7.20 and 7.21 suggest than not only are the PEI/PSS films more even, as discussed in Chapter 6, but that they are also thinner compared to PEI/PMAE films. This feature might originate from the higher charge density of the strong polyanion. It should also be noted that PSS, with a benzene ring along its chain, its hydrophobic. As will be discussed in Chapter 8, it does dissolve in water because of a favourable entropy gain. However, once adsorbed at the solid-solution interface, its hydrophobic nature, together with a strong electrostatic interaction with the underlying polymeric film, might help to "squeeze" tightly the LbL architecture against the solid substrate. PMAE, in contrast, is hydrophilic and, in solution, in a globular conformation. As a consequence, the resulting adsorbed layer is thicker and porous. Specific pH conditions or variations in the ionic strength of the polymer solution might be exploited of use in tuning the properties (e.g. thickness) of these films.

7.5 Conclusions

Metals exhibit a double-edged nature in living organisms. Many (for example, the first-row transition metals) are essential for life, but they can also be extremely toxic and lethal. Drinking water is one of the main channels of ingestion of such metals. Therefore, measurement and control of its content are essential. In this chapter, a study of the use of LbL polyelectrolyte multilayers as sensors for metals cations in solution has been described. Such architectures were integrated in a novel, compact surface plasmon resonance system (see Chapter 5).

The polyelectrolyte-metal interaction and the behaviour of the metals in solution have been discussed. Metals in water tend to form aqua ions, with the central metal cation surrounded by one of more shells of water molecules. The nature and geometry of the conformation of such complexes is believed to have an influence on the sensitivity of the polymeric films. A detection limit down one part per million (copper acetate concentration of 10^{-5} M) for Cu^{2+} ions was found using a two bilayer LbL film with

PMAE as outer surface. These data are quite promising if compared with the concentration levels shown in Table 7.1 (maximum concentration level of copper in water of 20.5 x 10^{-6} M according the U.S. federal regulations or 31.5 x 10^{-6} M according the World Health Organization). Furthermore, the system performance for copper detection is comparable with that of some commercial devices exploiting ion selective electrodes or reflectance photometry.

Generally, in this series of experiments, it was found that the outer surface of the thin organic film is mainly responsible for the ion detection, while the underlying layers provide the support. However, a systematic study using different thickness of the same architecture might provide further details on the influence of the overall organic film architecture of the system sensing performance. The detection of anionic species and pH was also demonstrated. Exact knowledge of the acidity level in liquids and the real-time monitoring of the dynamics of changes in pH can be recorded using a suitable combination of several LbL multilayers.

The adsorption characteristics of two alternative polyanions, PMAE and PSS, were compared together with those of the polycation PEI. Reflectivity changes in real-time were used to follow the adsorption steps during the deposition of the multilayer film. For the two negatively charged polymers, PMAE and PSS, it was found that differences in electric charge density might have a direct influence not only on the outer surface morphology, as discussed in Chapter 6, but also on the film thickness and on the time needed by the polymer to complete the adsorption.

It the next Chapter, the information obtained from these studies will be used in an attempt to exploit the multi-channel capacity of the SPR equipment by investigating the simultaneous use of several polyelectrolyte architectures assembled on the same substrate.

References

1. Laws, E.A., *Aquatic Pollution: an Introductory Text*. Third ed. 2000: John Wiley & Sons, Inc.

2. Metals: impacts on health and enviroment. Science-Special Section, 2003. 300: p. 925-947.

3. EPA, *Code of Federal Regulations*. Vol. 40, 141.51. 1999, Washington, DC: Environmental Protection Agency.

4. WHO, *Guidelines for Drinking-Water Quality*. 2nd ed. 1993, Geneva: World Health Organisation.

5. Vandecasteele, C. and Block, C.B., *Moderm Methods for Trace Element Determination*. 1993, Chichester: John Wiley & Sons.

6. Duckett, S. and Gilbert, B., *Foundation of Spectroscopy*. Oxford chemistry primers. 1999, New York: Oxford University Press.

7. Richens, D.T., *The Chemistry of Aqua Ions : Synthesis, Structure and Reactivity*. 1997, Chichester: John Wiley & Sons Ltd.

8. Burgess, J., *Ions in solution : basic principles of chemical interactions*. 1988, Chichester: Ellis Horwood.

9. Shriver, D.F., Atkins, P.W., and Langford, C.H., *Inorganic chemistry*. 1990, Oxford: OUP.

10. McCleverty, J.A., *Chemistry of the first-row transition metals*. Oxford chemistry primers ; 71. 1999, Oxford: Oxford University Press.

11. Pearson, C., Nagel, J., and Petty, M.C., Metal ion sensing using ultrathin organic films prepared by the layer-by-layer adsorption technique. J. Phys. D: Appl. Phys, 2001. 34: p. 285-291.

12. Martel, A.E. and Calvin, M., *The Chemistry of the metal chelate compounds*. 1952, New York: Prentice-Hall.

13. Kramer, C. and Dunsch, L., Voltammetric and spectroscopic investigation of binding in complexes of divalent metal ions with styrene–maleic acid-copolymer and monomeric analogues. Electrochimica Acta, 1998. 44(5): p. 819-829.

14. Jaeger, W., Wendler, U., Lieske, A., Bohrisch, J., and Wandrey, C., Novel polyelectrolytes with regular structure - Synthesis, properties and applications. Macromolecular Symposia, 2000. 161: p. 87-96.

15. Lvov, Y., Chapter 4: Thin film nanofabrication by alternate adsorption of polyions, nanoparticles, and proteins, in *Handbook of Surfaces and Interfaces of Materials*, H.S. Nalwa, Editor. 2001, Academic Press.

16. Shiratori, S.S. and Rubner, M.F., pH-dependent thickness behaviour of sequentially adsorbed layers of weak polyelectrolytes. Macromolecules, 2000. 33(11): p. 4213-4219.

17. Decher, G. and Schlenoff, J.B., eds. *Multilayer Thin Films-Sequential Assembly of Nanocomposite Materials*. 2003, Wiley-VCH: Weinheim.

18. Mendelsohn, J.D., Yang, S.Y., Hiller, J., Hochbaum, A.I., and Rubner, M.F., Rational design of cytophilic and cytophobic polyelectrolyte multilayer thin films. Biomacromolecules, 2003. 4(1): p. 96-106.

19. Yang, S.Y., Mendelsohn, J.D., and Rubner, M.F., New class of ultrathin, highly cell-adhesion-resistant polyelectrolyte multilayers with micropatterning capabilities. Biomacromolecules, 2003. 4(4): p. 987-994.

20. Freemantle, M., Polyelectrolyte Multilayers. C&EN: Science and Technology, 2002. 80(18): p. 44-48.

21. Rubner, M., pH-controlled assembly and properties of polyelectrolyte multilayers. Abstracts of Papers of the American Chemical Society, 2002. 223: p. 021.

22. Hiller, J.A., Mendelsohn, D., and Rubner, M.F., Reversibly erasable nanoporous anti-reflection coating from polyeletrolytes multilayers. Nature Materials, 2002. 1(1): p. 59-63.

23. Hiller, J.A. and Rubner, M.F., Reversible molecular memory and pH-switchable swelling transitions in polyelectrolytes multilayers. Macromolecules, 2003. 33(11): p. 4078-4083.

24. Dhagat, P., Optical characterisation of organic thin films: application to metal ion sensing. 2002, Undergraduate project report, School of Engineering, University of Durham: Durham, U.K.

25. Palumbo, M., Pearson, C., Nagel, J., and Petty, M.C., A single chip multi-channel surface plasmon resonance imaging system. Sensors and Actuators B: Chemical, 2003. 90(1-3): p. 264-270.

26. Johansen, K., Stalberg, R., Lundstrom, I., and Liedberg, B., Surface plasmon resonance: instrumental resolution using photo diode arrays. Measurement Science & Technology, 2000. 11(11): p. 1630-1638.

27. *Handbook of Physical Quantities edited by Igor S. Grigoriev and Evgenii Z. Meilikhov editor of the English edition, A. A. Radzig*. 1997, Boca Raton, Fla. London: CRC Press. 1548p ill 29cm.

28. Yoo, D., Shiratori, S.S., and Rubner, M.F., Controlling bilayer composition and surface wettability of sequentially adsorbed multilayers of weak polyelectrolytes. Macromolecules, 1998. 31(13): p. 4309-4318.

Chapter 8

Multichannel sensing chip: alternative designs and sensing tests

8.1 Introduction

In this chapter, the development of a multichannel SPR sensor [1, 2] is presented. Three polyelectrolytes, poly(ethyleneimine) (PEI), poly(ethylene-alt-maleic acid) (PMAE) and poly(styrene sulfonate) (PSS), were used to build up two different thin film architectures. The films were assembled on the same sensing chip and tested for their ability to detect different metal ions in solution (Na, Fe, Ni, Cu, Zn).

As discussed in Chapter 5, several research groups and commercial companies are currently involved in developing approaches to multi-channel SPR sensing. This is mainly to enhance the throughput of SPR sensors, i.e. to increase the amount of samples examined per time, and to provide these with multi-analyte detection capability [3, 4].

In Fig. 8.1, a diagram of the SPR cell and the working principle of the sensing system described in Chapter 5 is shown. A convergent beam is directed onto the gold-coated sensing chip. The reflected beam will possess a characteristic intensity minimum due to the excitation of surface plasmon at the interface metal/dielectric. The variation in angular position of this minimum is recorded by a CCD camera connected to a computer for real time analysis.

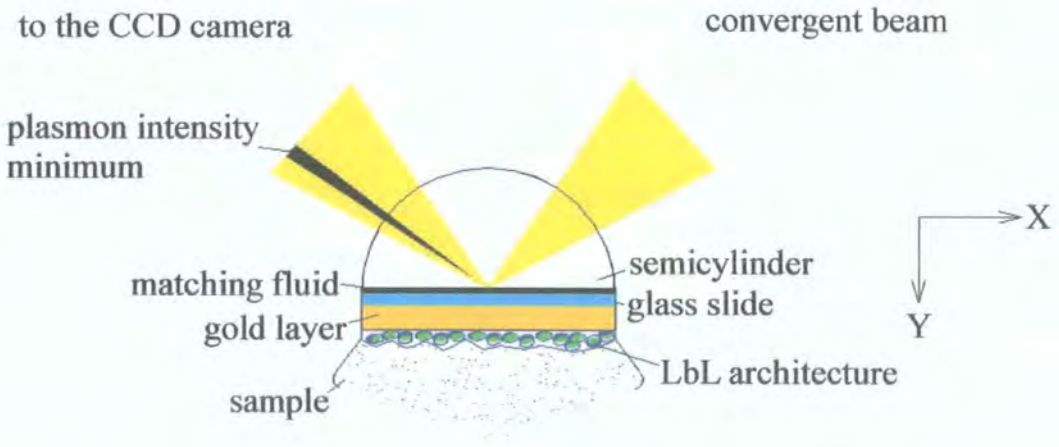

Figure 8.1 Kretschmann configuration with a convergent light beam. At a specific angle of incidence, the p-polarized, monochromatic light excites surface plasmons. As consequence, the reflected beam possesses a characteristic intensity minimum. The position of the resonance angle is function of the refractive index of the sensing medium.

The SPR system exploits the characteristics of the focused beam which is distributed along a line (see Fig. 5.10 (a), (b) and (c)). In Fig. 8.2, a proposed design for the multi-channel chip is shown. The different organic thin films are assembled in the Z direction on the gold coating. All the active materials can then be interrogated simultaneously using the same beam, like a scanner on a bar-code. Such an arrangement poses several challenges, such as the deposition of the separate active materials on the same gold coating, the development of the instrumentation to address this complex structure and a suitable data analysis method for reading the SPR response for each film independently and simultaneously.

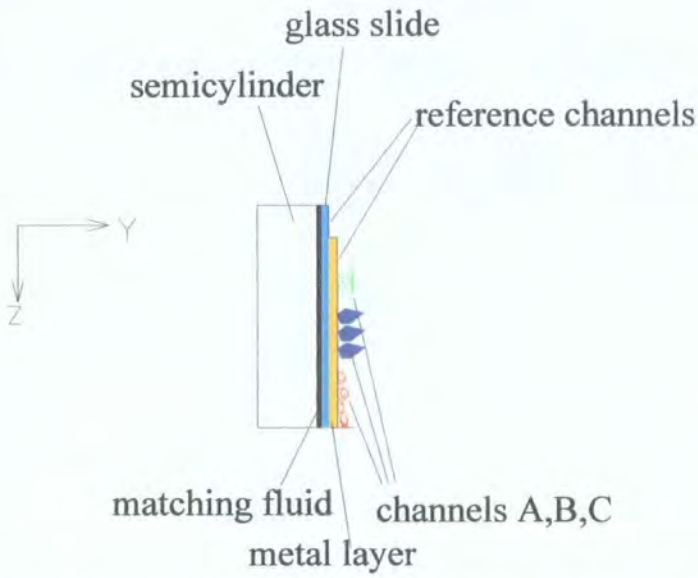

Figure 8.2 A possible multi-channel sensor chip design with different LbL multilayers deposited one next to each other.

The arrangement shown in Fig. 8.2 has a major drawback. It does not offer points of reference on the position of the various films. One possible solution is to have several gold patterns on the same chip. In this way, the individual sensing elements will be easily recognizable and independently accessible to the polymeric solutions. For example, by dipping the bottom half of the gold-coated glass slide in a specific series of polyelectrolytes, and then the other half in a different polymeric solution sequence, it is possible to have two different films on the same chip.

8.2 Sensor chip: Design 1

In a first attempt, structures similar to those used to characterize the lens system were used as a multi-channel platform (see Chapter 5). An arrangement of gold stripes, formed by thermal evaporation through a shadow mask onto SF10 glass, was prepared. On average the gold stripes had a width of 0.5 mm, and were approximately 0.8 mm apart.

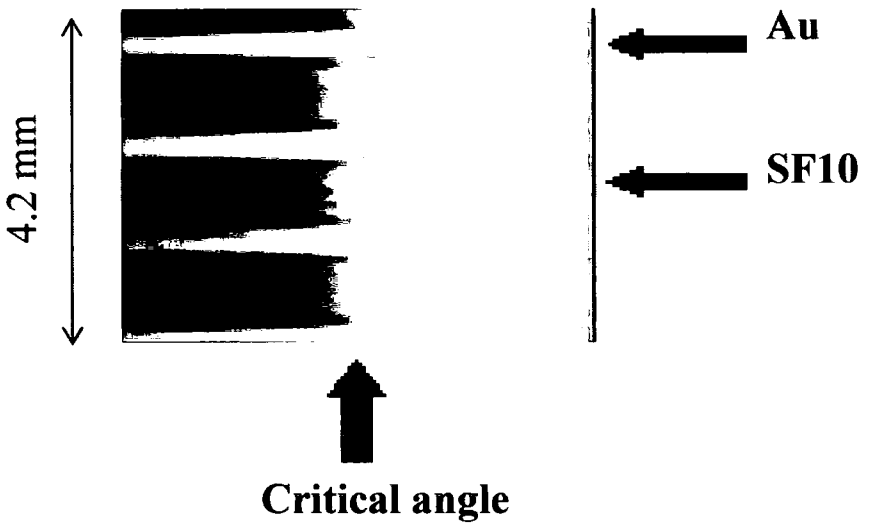

Figure 8.3 Reflected image for the multi-channel sensor chip in which Au strips are alternated with SF10 glass. From top to bottom the area investigated extends over an area approximately 4.2 mm wide. Gold stripes have an average width of 0.5 mm, and are approximately 0.8 mm apart. According to the theory a sharp variation in reflectivity is registered in the proximity of the critical angle for the uncoated region of the SF10 glass slide, while these variations are shallower and more gradual for the areas coated by the thin gold layer.

Figure 8.3 shows the reflected image for this structure captured by the CCD camera. In this case, no lens system was placed in front of the CCD camera. Therefore, the area imaged extends for only 4.2 mm. By illuminating the cell over a range of incident angles, 48° to 52.6°, it was possible to evaluate the position of the critical angle for the uncoated surface and for the Au overlayer. This is a function of the refractive index of the glass and of the dielectric present in the cell only, which is confirmed by the resonance curves for one SF10 channel and two gold-coated channels in Fig. 8.4.

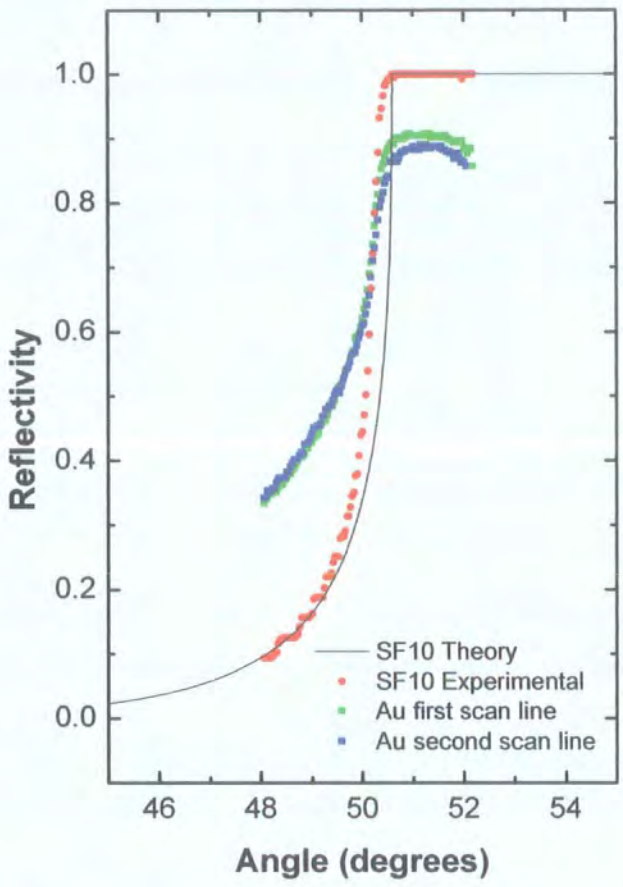

Figure 8.4 Reflectivity curves in the critical angle region for one SF10 channel and two Au-coated channels on the sensing chip imaged in Fig. 8.3.

Figure 8.5 shows the response of two channels, one with PSS as the outer layer and the other with PMAE on the outside surface. The sensing chip was prepared using the traditional LbL procedure (PEI+PMAE+PEI), except for the very last layer. In fact, as a first step, only half of the channels coated with PEI/PMAE/PEI were immersed in the PMAE solution; the other half was dipped in a PSS solution. The SPR minimum for all three samples is shifted by about 0.5° from the curve for the uncoated Au. Using the theoretical model and taking a refractive index of 1.5 for the polymer films, gives a total organic film thickness of 6 nm (2 bilayers) - consistent with previous results [8]. While the SPR curve profile for the two "(PEI/PMAE + PEI/PMAE) channels" can be considered coincident, a significant difference in response is evident from the "(PEI/PMAE + PEI/PSS) channel". This is possibly the result of poorer deposition of the PSS-containing bilayer rather than a difference in the optical constants of the various polyelectrolyte materials.

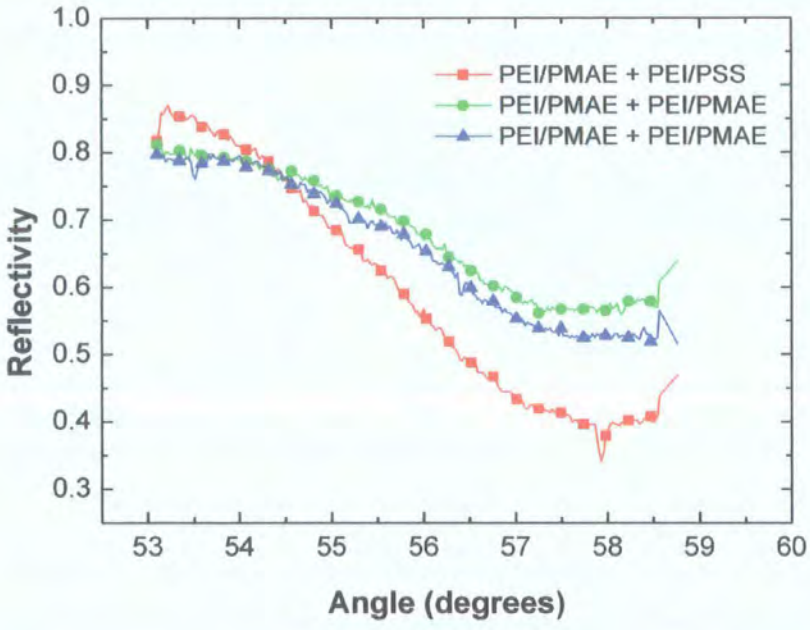

Figure 8.5 SPR curves for two different self-assembled polyelectrolyte multilayer architectures deposited on a four-channel sensor chip. One of the Au-coated channels has PSS as the outer layer while the two left have PMAE.

What is important to note is that two different LbL thin films were effectively deposited on the same chip and that it has been possible to identify their SPR profiles. This result is encouraging for the ability of the SPR system to read different channels simultaneously. Ideally, an alternative to Design 1 should be found in order to invert the dimensional gold/SF10 ratio, i.e. to have wider gold coating and reduce the area of the uncoated glass. This will reduce the influence of the reflected light from the glass on the SPR profiles of the gold stripes. Moreover, the deposition technique adopted has a limitation on the number of architectures that can be deposited. With the simple partial last layer dip coating method, the differences between the organic films are limited to the external layer only. Alternative deposition methods are necessary in the future to exploit fully the potential of this method.

8.3 Sensor chip: Design 2

In the next series of experiments, it was decided to simplify the design of the sensing chip. One of the gold patterns used to form the multi-channel sensor is shown in Fig. 8.6. This 'chip' was produced by e-beam evaporation of 2 nm of chromium followed by 50 nm of gold through a shadow mask onto SF10 glass.

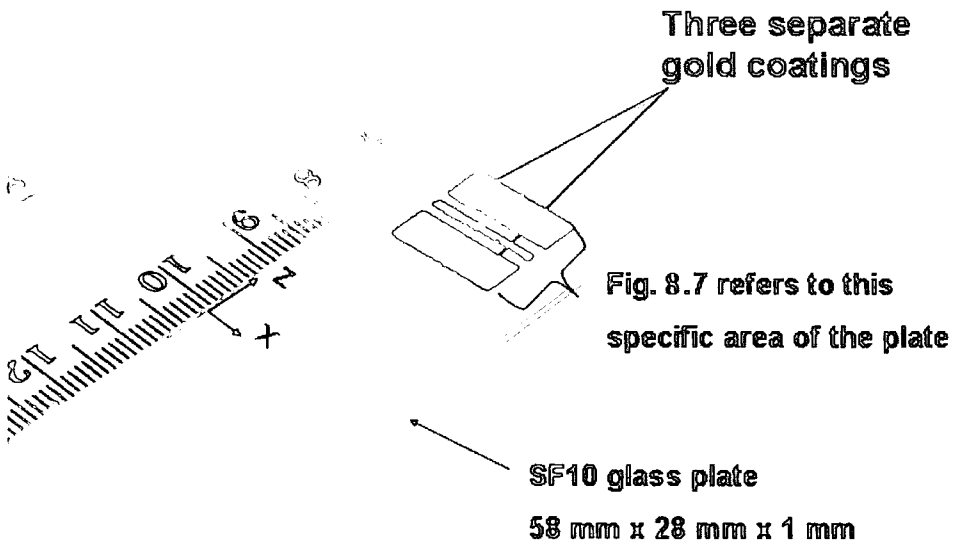

Figure 8.6 Large area single-chip incorporating several investigation channels. The gold pattern on an SF10 glass plate was deposited via e-beam evaporation using a shadow mask. The output from a commercial LED is first expanded and then focused with a range of incident angles along the Z direction indicated in figure. It is then possible to acquire data from a cross section in the X direction.

This design provided a clear physical distinction between the gold stripes (i.e. between the sensing channels) and allowed the acquisition of data from a cross sectional width of 15 mm (Z direction in Fig. 8.6). An appropriate lens system was placed in front of the CCD camera to detect the entire reflected beam.

Figure 8.7 shows an optical image captured using the SPR system with the chip surface exposed to air. Note the presence of the reflectivity minimum due to surface plasmon resonance in the areas coated with gold. For the two uncoated stripes (i.e. on the surfaces of the SF10 glass slide) a strong reflectivity variation near the critical angle (angle of total reflection) is evident. These features are as expected from theoretical

predictions: a thin metal surface is needed to excite the surface plasmons and the variation of reflectivity near the critical angle will be more marked for an uncoated glass surface than for one coated with metal. Given the actual optical configuration and angular range, the CCD camera is able to capture these images (i.e. as shown in Fig. 8.7) only if the sensing chip is in air. The critical angle and resonance minimum are much further apart when the chip is immersed in a liquid.

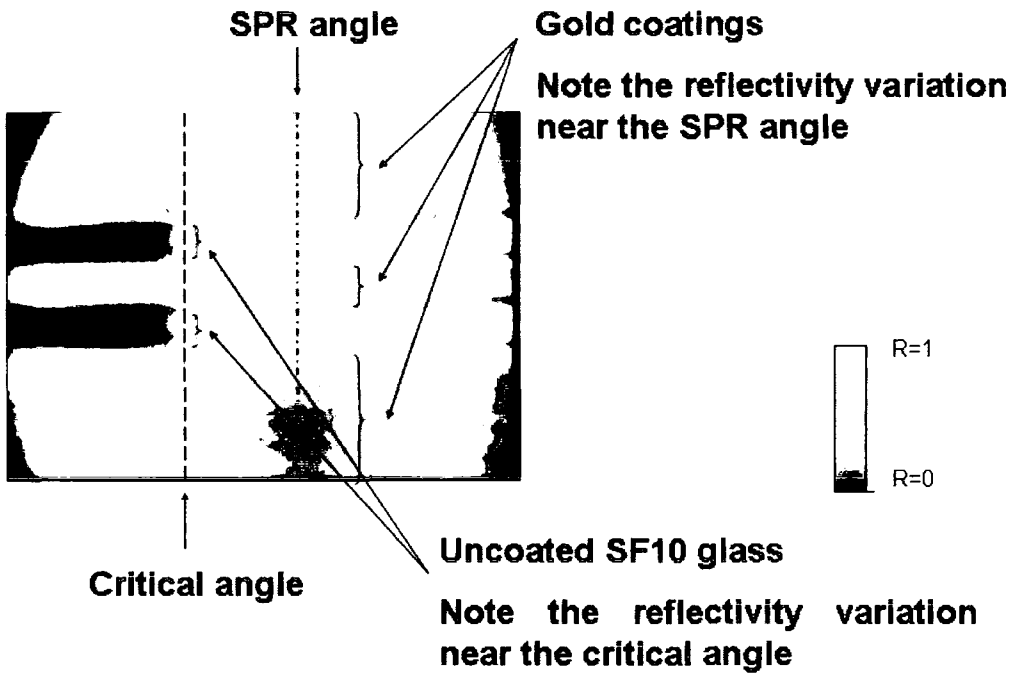

Figure 8.7 Optical image obtained from the SPR system with the sensing chip exposed to air. The reflectivity for the two regions of uncoated SF10 glass shows a sharp variation near the critical angle. The change in reflectivity near the surface plasmon resonance angle is evident for the three regions of the sensing chip coated with 50 nm of gold.

8.3.2 Multichannel sensing

The SPR curves corresponding to one bilayer of (PEI/PMAE) deposited on gold are shown in Figure 8.8. As expected, the addition of the organic bilayer shifts the resonance curve to a higher angle. The variation in the angular position of the reflectivity minimum is about 0.5° and is consistent with the experimental data obtained from a 'traditional' SPR set-up [5]. A further angular shift is apparent when the sensing film is exposed to 10^{-5} M of copper acetate. As noted previously [2, 5], the refractive index of the metal solution, within the range tested, is close to that of the buffer solution and its effect on the SPR curve can be neglected. The measured reflectivity change is,

therefore, a result of the adsorption of the metal cation on the active film. Because of this, an increase in thickness and/or change in the refractive index of the polymeric film will shift the SPR curve to higher angles. To detect the reflectivity variation in real time, the position of a reference line together with several independent scan lines along the Z direction (see Fig. 8.6) was fixed. The angular position of a time-drive line, along the X direction in Fig. 8.6, was set to the low angle side of the SPR minimum and a time scan was started. In this way, real time information on the change in reflectivity for both the reference and scan lines at a specific angle could be obtained.

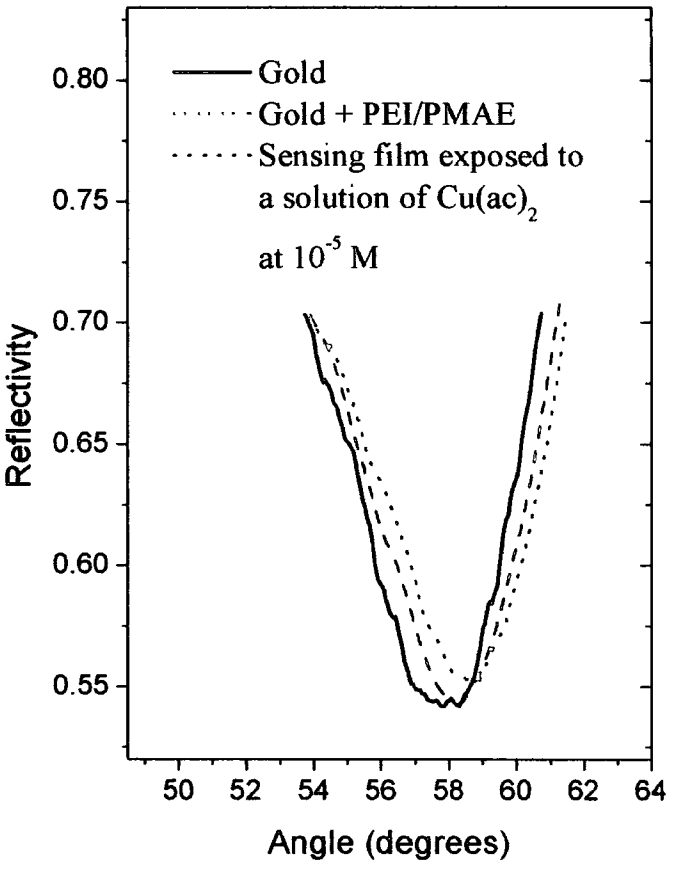

Figure 8.8 SPR curves for an uncoated gold surface, the same surface after deposition of one bilayer of (PEI/PMAE), and following exposure to a solution 10^{-5} M of copper acetate.

One area of concern is that, at the moment, the sensing chips, manufactured under seemingly identical conditions, exhibit variations in the depth of the resonance curve. This might affect the sensitivity of the system. However, the tests conducted in this work, using chips with different resonance mimina, showed a good consistency in sensitivity and selectivity for all the ions solution tested. This suggested that the devices possessed a good linearity when operated to the low angle side of the SPR minimum.

However, an enhancement in performance and improved reliability is expected through an optimization of the deposition condition and parameters. An alternative approach might also be used to detect the plasmon resonance shift and reduce the noise contribution in the signal received, for example analysis of the entire SPR spectra via data-processing algorithms [6, 7].

Sodium acetate Na(ac), copper(II) acetate $Cu(ac)_2$, iron(II) acetate $Fe(ac)_2$, nickel(II) acetate tetrahydrate $Ni(ac)_2$ and zinc acetate $Zn(ac)_2$ metal ion solutions were prepared at different concentrations in tris buffer solution and their pH was fixed at specific values by the addition of HCl. In all the sensing experiments, the sequence for the change of liquid in the sensing cell was performed via a peristaltic pump running continuously at 2 ml min^{-1}. The procedures and timings were strictly controlled.

The results of exposing the PEI/PMAE and PEI/PSS channels of the multisensor chip to a 10^{-4} M copper acetate solution, pH 6.2, are shown in Fig. 8.9. The initial part of the two reflectivity versus time curves (0 – 10 mins.) shows that both sensing films are relatively unresponsive to pH changes from 6.2 (for the tris buffer) to 3.4 (for the HCl). However, when a solution of copper acetate at 10^{-4} M at pH 6.2 was substituted for the HCl, both channels showed a clear increase in reflectivity. The saturation level for the reflectivity signal was generally reached after few minutes. This corresponds to a steady state during which there is equilibrium between the association and dissociation of the analyte with the ligand. This stage, together with the kinetics of the sensing reactions, is a function of the specific polymeric film/ metal ion interaction.

Figure 8.9 reveals a relatively high sensitivity of the PEI/PMAE bilayer to copper ions, confirming of our previous results [5]. The response to PEI/PSS is less, by a factor of about three. The formation of a PMAE/metal chelate via hydrogen exchange is expected to be an important sensing mechanism for Cu (II) ions (see Appendix A). PMAE has a pincer-like structure with two hydrogen atoms at the opposite extremes of a half ring and copper ions can become "trapped" in such structures. Physical adsorption of the metal ions (e.g. driven by electrostatic attraction between the negatively charged solid/liquid interface and positively charged copper ions) was also considered to be a significant process. From the chemical structure of PSS (see Fig. 7.8), chelate formation

with the metal ions is not expected because the sulfonic SO_3^- groups in the polymeric PSS do not form a comparable metal-receptive chelate structure. Hence, only a physical attraction with the metal driven by Coulombic forces can be considered. A further factor determining the sensitivity may be the morphology of the polyelectrolyte surface. In Chapter 6 a much rougher surface for the PEI/PMAE bilayer surface has been revealed. The larger surface area may thereby contribute to the enhanced sensitivity of this sensing surface over PEI/PSS.

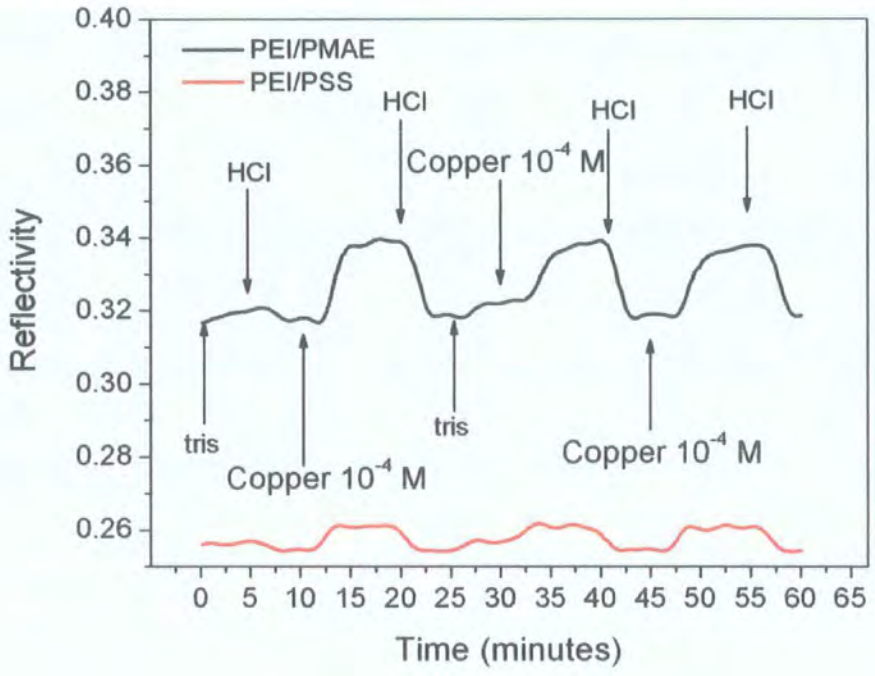

Figure 8.9 Response of the multichannel sensor chip to copper(II) acetate solution, pH 6.2 . The continuous line indicates the reflectivity signal registered from the PEI/PMAE active surface while the dashed line shows the signal from the PEI/PSS film. For clarity, the change in solution inside the sensing cell is indicated only for the PEI/PMAE channel.

As shown in Fig. 8.9, the process or regeneration using HCl proceeds with both types of bilayer with an almost complete recovery to the original signal level. Repeated exposure to copper and recovery using HCl produced repeatable responses. A figure of merit, F can be calculated considering the variation in reflectivity ΔR, the initial value of the reflectivity R_{in} and the response time t_r (see Fig. 2.4)

$$F = \frac{\Delta R / R_{in}}{t_r}$$

For the first sensing test in Fig. 8.9, the response time of the PEI/PMAE bilayer is of 1.34 minutes and F=0.05 min^{-1}, while the second and third response have a longer response time and lower figure of merit. The average figure of merit for the three responses is of 0.026 min^{-1}.

8.3.3 Response to different ions

In one of the experiments, several sensing routines were run one after the other using different metal acetate solutions. The results for solutions at 10^{-4} M are shown in Figs. 8.10(a), (b), 8.11(a), (b) and 8.12(a), (b). All the solutions were prepared at pH 6.2 (as in the case of the copper in Fig. 8.9). Starting from the experiment with copper acetate, a nickel solution was tested, followed by a sodium solution and then, zinc. An iron solution at the same pH was also tested, with no response (Fig. 8.12(a)). It was decided, then to use a slightly basic iron acetate solution at pH 7.6. According to the literature, the extremely pale bluish-green hexaaqua ion $[Fe(OH_2)_6]^{2+}$ will form more aggregated species as the pH of the solution increases [8]. To avoid the formation of hydrated iron oxide, i.e. the typical red-brown gelatinous precipitations that would give the solution a high degree of turbidity, only fresh acetate solutions were used when dealing with iron.

Figure 8.10 (a) is consistent with the result shown in Fig.8.9. PEI/PMAE seems to be more sensitive to copper acetate than PEI/PSS. A certain delay in the PSS response is also noted. Figure 8.10(b) shows that PMAE has a lower affinity to nickel. At this particular concentration the reflectivity change is approximately one half of that recorded with the organic film interacting with copper acetate ions. Again, PEI/PSS shows a quite small variation in reflectivity and a delay in response.

The result of the sensing experiment with a zinc acetate solution at concentration of 10^{-4} M is shown in Fig. 8.11. It is evident that the change in reflectivity is also larger for the PEI/PMAE film than for PEI/PSS. However, this time the recovery of the PEI/PMAE film via exposure to an HCl solution is not complete. PEI/PSS reacted with the zinc cations with a lower reflectivity change, a certain delay in response as in the previous case, but with almost a full recovery to the original signal when exposed to HCl. A stronger HCl solution is perhaps necessary for a full recovery. Also, it could be possible that the previous sensing routine has somehow modified the film structure making it

more receptive to the zinc ions. Eventually, after a continuous flow of tris buffer solution at pH 6.2, the reflectivity signal from the PEI/PMAE bilayer reached a stability plateau (although at a reflectivity value higher than that at the beginning of the sensing experiment).

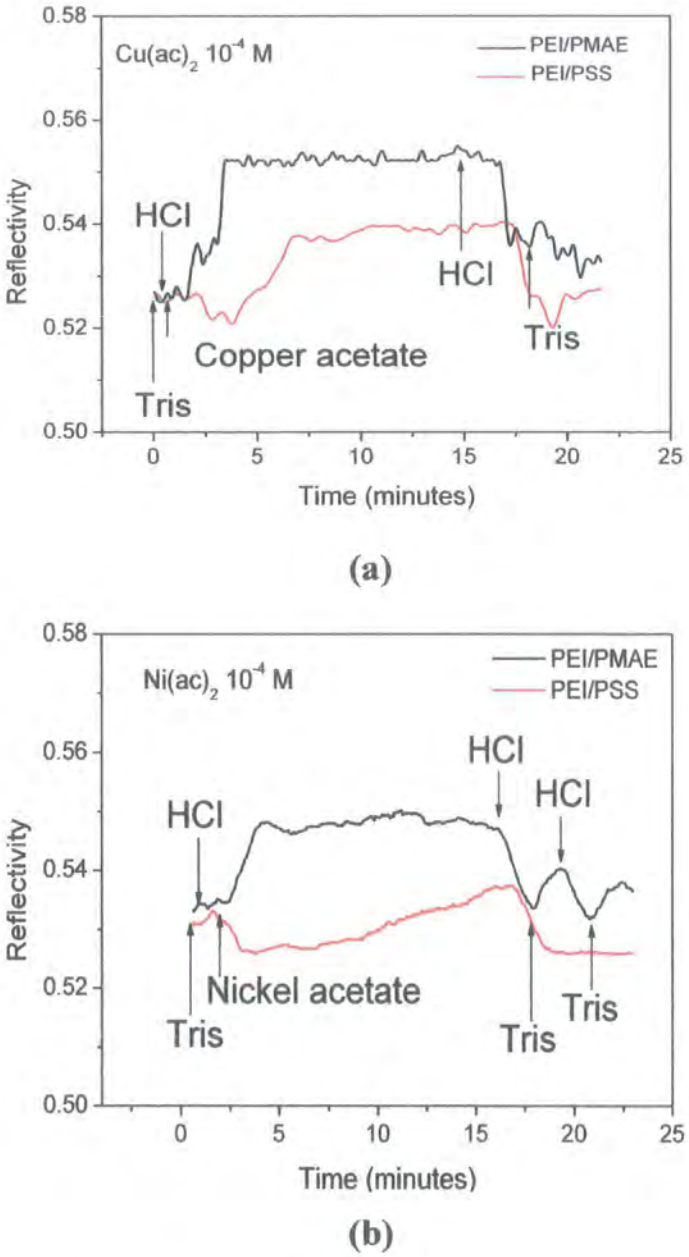

Figure 8.10 Response of the multichannel sensor chip to: (a) copper(II) acetate solution, pH 6.2; and (b) nickel(II) acetate tetrahydrate solution, pH 6.2. Both metallic ion solution concentrations 10^{-4} M. The black line indicates the reflectivity signal registered from the PEI/PMAE active surface while the red line shows the signal from the PEI/PSS film. For clarity, the change in solution inside the sensing cell is indicated only for the PEI/PMAE channel.

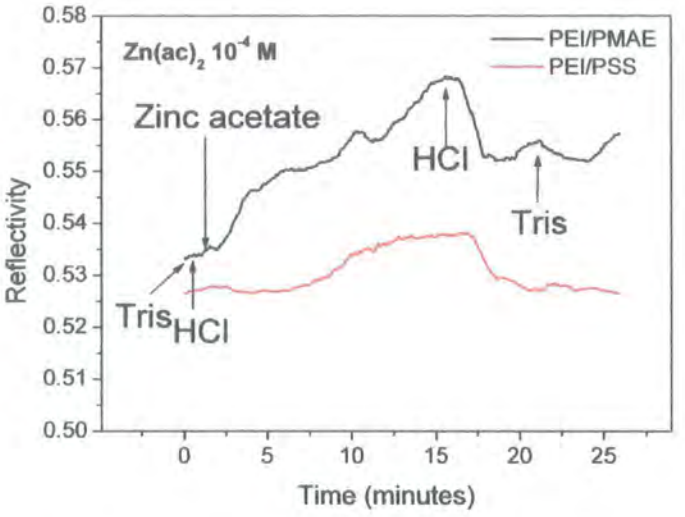

Figure 8.11 Response of the multichannel sensor chip to zinc(II) acetate solution, pH 6.2, concentration solution 10^{-4} M. The black line indicates the reflectivity signal registered from the PEI/PMAE active surface while the red line shows the signal from the PEI/PSS film. For clarity, the change in solution inside the sensing cell is indicated only for the PEI/PMAE channel.

It was decided, therefore, to try another test with a different metal acetate. An iron(II) acetate solution in tris buffer at pH 6.2, as in the previous cases), was then tested. Results from this experiment are shown in Fig. 8.12(a). Neither the PEI/PMAE nor PEI/PSS channels seemed to be responsive to Fe. Therefore, a slightly alkaline iron acetate solution at pH 7.6 was tested (Fig. 8.12(b)). This time the results were improved and it was possible to detect a consistent variation in reflectivity, especially for the channel with PMAE as outer surface. Tests with sodium acetate solution at 10^{-4} M were inconclusive and neither of the two channels seemed to have a particular interaction with the metal ions.

At the end of the series of sensing experiments, the full SPR profiles for the two channels were recorded and compared with those at the beginning of the session. In Figure 8.13, it is evident that while for the PEI/PSS channel the two profiles are almost coincident, for the PEI/PMAE channel instead there is a permanent shift of the SPR profiles. As explained previously this shift is probably due to a reaction of the organic film with zinc cations.

To understand the nature of the zinc-PMAE interaction, a new sensing chip was tested with a zinc acetate solution at concentration of 10^{-4} M. The results of this experiment are shown in Fig. 8.14. As shown, this time the response to zinc was less dramatic.

Comparing Figs. 8.11 and 8.14, it is possible that the sequence of exposure to different metal cations could have modified the PEI/PMAE film in such a way to make it more sensitive to zinc. Furthermore, the "quality" of the sensing film could have a strong influence on the sensitivity to zinc. Further studies are needed to clarify these points.

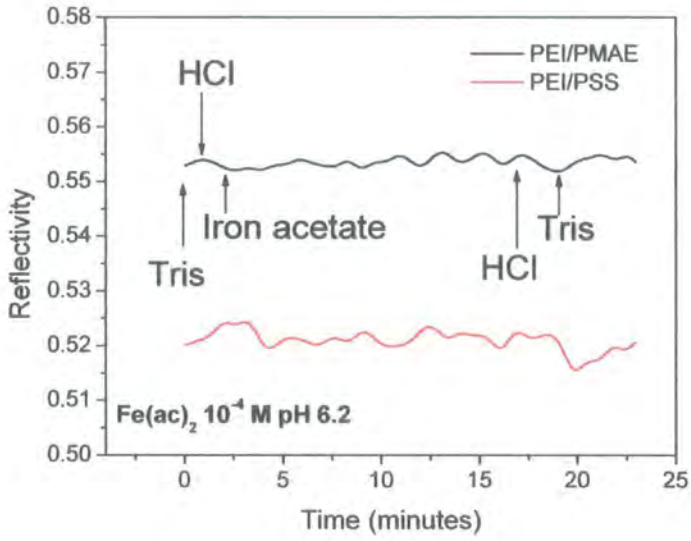

(a)

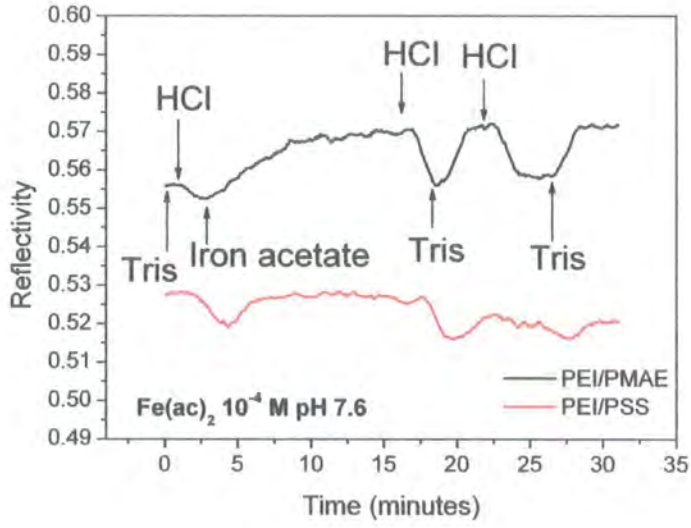

(b)

Figure 8.12 Response of the multichannel sensor chip to: (a) iron(II) acetate solution, pH 6.2; and (b) iron(II) acetate solution, pH 7.6.

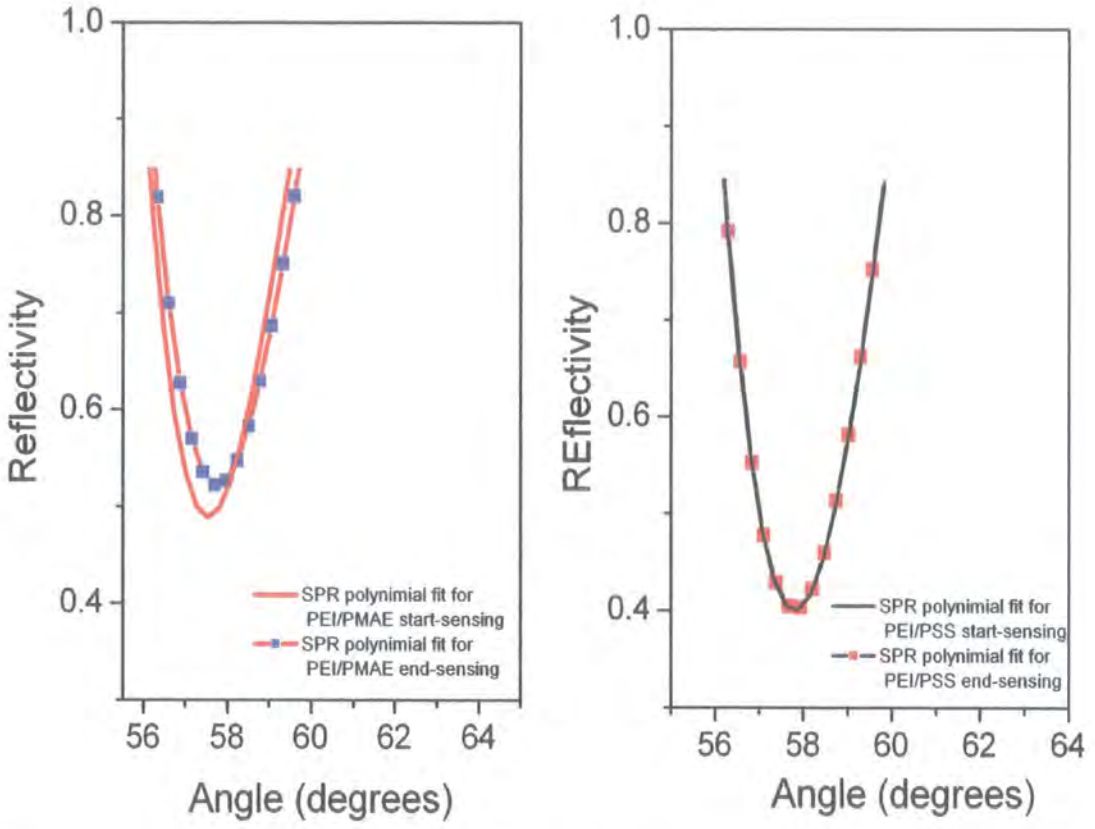

Figure 8.13 Polynomial fit for the SPR profiles of the two channels PEI/PMAE and PEI/PSS before and after the conclusion of the sensing experiments (see Fig. 8.10-12).

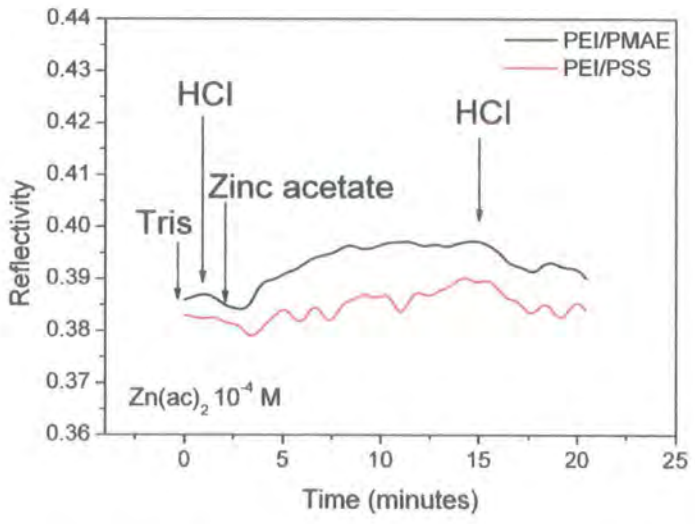

Figure 8.14 Response from a virgin multichannel sensor chip to a zinc(II) acetate solution, pH 6.2, concentration solution 10^{-4} M. The black line indicates the reflectivity signal registered from the PEI/PMAE active surface while the red line shows the signal from the PEI/PSS film.

The lower affinity of the PEI/PMAE bilayer for nickel and iron compared to the copper is apparent from Fig. 8.10(b) and Fig. 8.12(b). An even lower response occurs with PEI/PSS. The differences may be explained in terms of the different stability constants for the complexes. Moreover, the geometry of the complexes might play a significant role in this context, explaining why metals with similar characteristics, like copper, nickel and iron, have a different affinity with the same active surface [9].

In Chapter 7 it was noted that for particular active materials (e.g. EDTA) the geometry of the metal-aqua ions has an important impact on the stability constant for the interaction of the sensing material with metal cations. Once dissolved in solution, each metal cation is surrounded by water molecules. However, not all the metals have the water molecules distributed around them in the same fashion. Some have all the water molecules at the same distance, others have a more irregular distribution. Among the metals investigated (iron, nickel, copper and zinc) copper is the only one that, in solution forms a tetragonally distorted octahedral complex with the water molecules (the others form a more uniform octahedral field), Fig. 7.3. The main difference concerns the position of two of the six water molecules, which are more distant and interact weakly with the central copper ion (Jahn-Teller effect). Therefore, they tend to be more easily moved away and replaced from the active sites of the sensing materials. This peculiarity is reflected in a rapid increase of the stability constant for the complex with copper (Irvine-Williams effect, see Fig. 7.4). It might be thought that a similar mechanism occurs for PMAE, giving a stronger interaction with copper and a weaker one with nickel and iron.

One interesting feature in Fig. 8.10(b) and Fig. 8.12(b) is the oscillations in the reflectivity signal that appear to occur following iron or nickel exposure and on subsequent cycling between the tris buffer and HCl. This phenomenon was not apparent using copper (Fig. 8.9 and Fig. 8.10(a)), or before the sensing layer had been exposed to the metals. It is believed that interactions with Fe or Ni could have altered the architecture of the PEI/PMAE film (and, to a limited extent, that of the PEI/PSS film). Maybe, after such metals have dissociated from the polyelectrolyte films, they leave behind a more porous and less uniform surface with more electrostatic active sites. Before a process of self-annealing occurs, such modified architectures may be more sensitive to pH variations.

8.3.4 Sensing tests on an "aged" chip

The suggested modification to the film morphology following exposure to different metal cations described above could have an influence on the sensing performance. After a few days of storage in a bath of tris buffer solution, the same chip used for the sequential sensing experiment described above (with metal cation solutions of Cu, Ni, Zn, Na and Fe at 10^{-4} M), was retested in a similar exposure sequence. This time the two-channel sensor was exposed to the metal ion solutions, at a concentration of $2x10^{-5}$ M, close to what is thought to be the detection limit for the equipment.

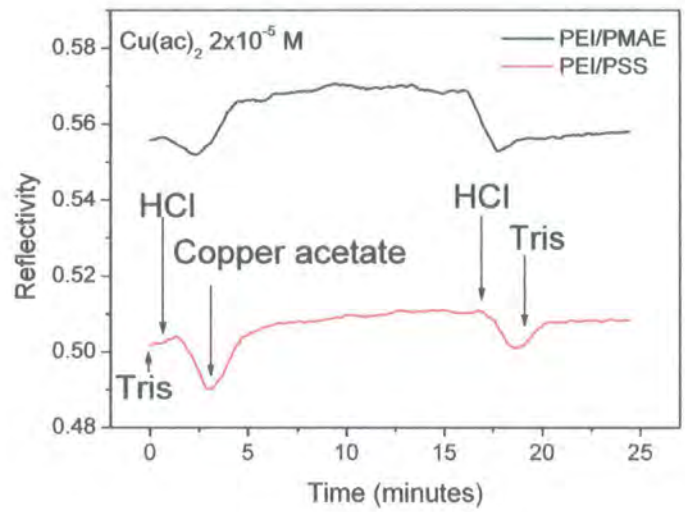

(a)

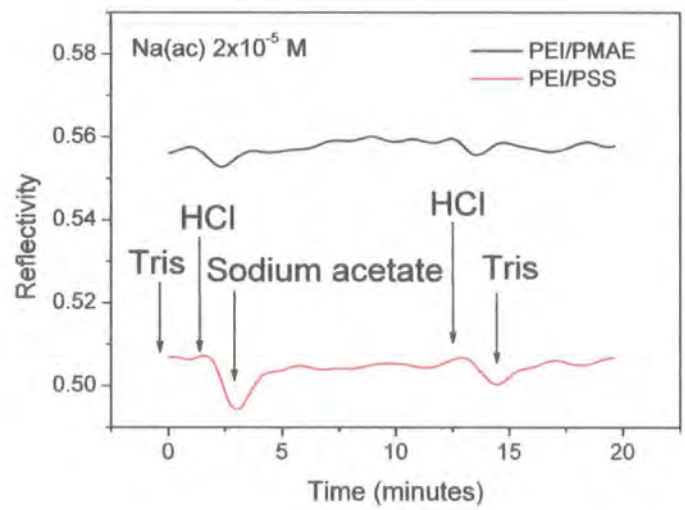

(b)

Figure 8.15 Response of the "aged" multichannel sensor chip to (a) copper(II) acetate solution, pH 6.2, concentration solution $2x10^{-5}$ M, (b) sodium acetate solution, pH 6.2, concentration solution $2x10^{-5}$ M The black line indicates the reflectivity signal registered from the PEI/PMAE active surface while the red line shows the signal from the PEI/PSS film. For clarity, the change in solution inside the sensing cell is indicated only for the PEI/PSS channel.

In Figure 8.15 and Fig. 8.16, the changes in real time of reflectivity for the two channels are shown. No response is evident for sodium on both channels, while a positive signal is obtained for copper, nickel and zinc on the PEI/PMAE channel. Interestingly, both films seem to have a certain ability to detect pH variations (buffer and metal solutions at pH 6.2, HCl solutions at pH 3.5).

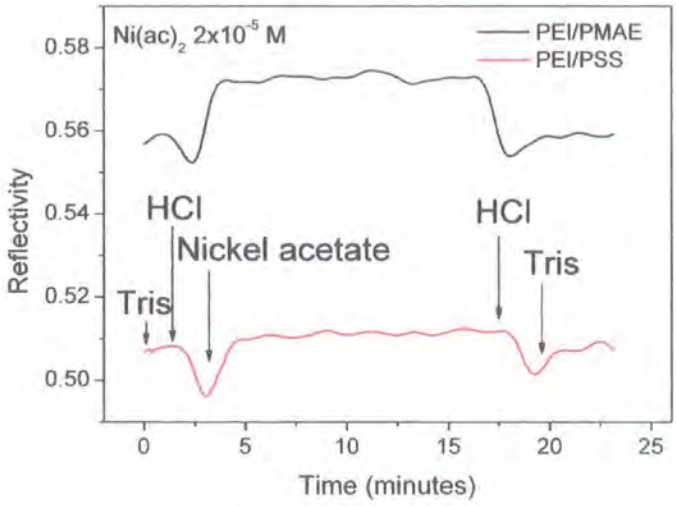

(a)

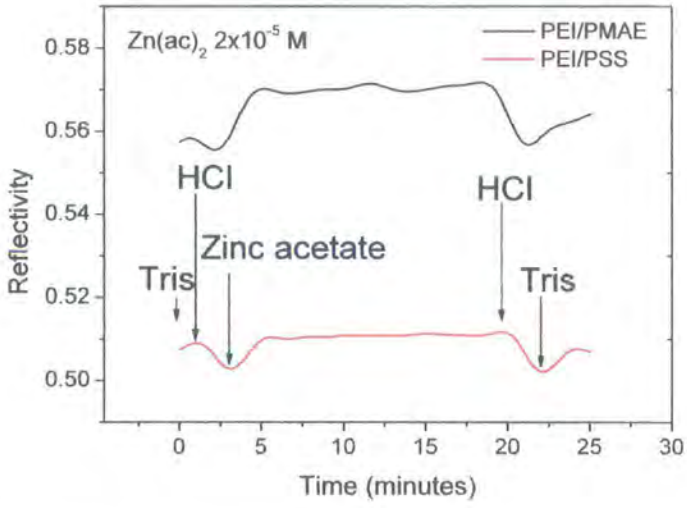

(b)

Figure 8.16 Response of the "aged" multichannel sensor chip to (a) nickel(II) acetate solution, pH 6.2, concentration solution $2x10^{-5}$ M, (b) zinc(II) acetate solution, pH 6.2, concentration solution $2x10^{-5}$ M The black line indicates the reflectivity signal registered from the PEI/PMAE active surface while the red line shows the signal from the PEI/PSS film. For clarity, the change in solution inside the sensing cell is indicated only for the PEI/PSS channel.

As in the previous experiments, positive responses come from the PEI/PMAE channel for copper, nickel and zinc, while the channel with PSS as outer layer seems to have a

lower affinity. In particular, at this molar concentration of $2x10^{-5}$ M, the reflectivity change is minimal. These results are similar to those with solutions at molar concentration of 10^{-4} M and indicate that the main PSS-metal cation interaction mechanism is charge compensation between the positive metal ions and the negative PSS surface. Such compensation is proportional to the molar concentration; the more cations in the cuvette, the more electrically charged sulfonate groups are involved in the interaction, giving a change in the reflectivity signal.

In Table 8.1, a summary of the results obtained in these series of experiment is presented.

Sensing Channel	Metal ion concentration: $2x10^{-5}$ M				pH variation (from pH 6.2 to 3.5)
	Copper acetate	Nickel acetate tetrahydrate	Zinc acetate	Sodium acetate	
PEI/PMAE	√	√	√	X	√
PEI/PSS	X	X	X	X	√

Table 8.1 Results of exposing PEI/PMAE and PEI/PSS bilayers to various metal ion solutions of concentration $2x10^{-5}$ M. A positive response is indicated by a tick and a negative by a cross.

A comparison of the SPR profiles for the two channels at the beginning and end of these set of experiments is shown in Fig. 8.17. Because no strong interaction between zinc and PMAE was observed, the SPR profiles from this channel are almost coincident. In contrast, the PEI/PSS channel seems to have been slightly affected due to the changes in pH rather then the metal ions. Such feature opens some interesting questions about the role that chemical interaction and aging of the organic film have on the pH sensitivity. Especially for PSS this might be worth future studies, considering that pH variations are generally thought to have very little effect on its charge density.

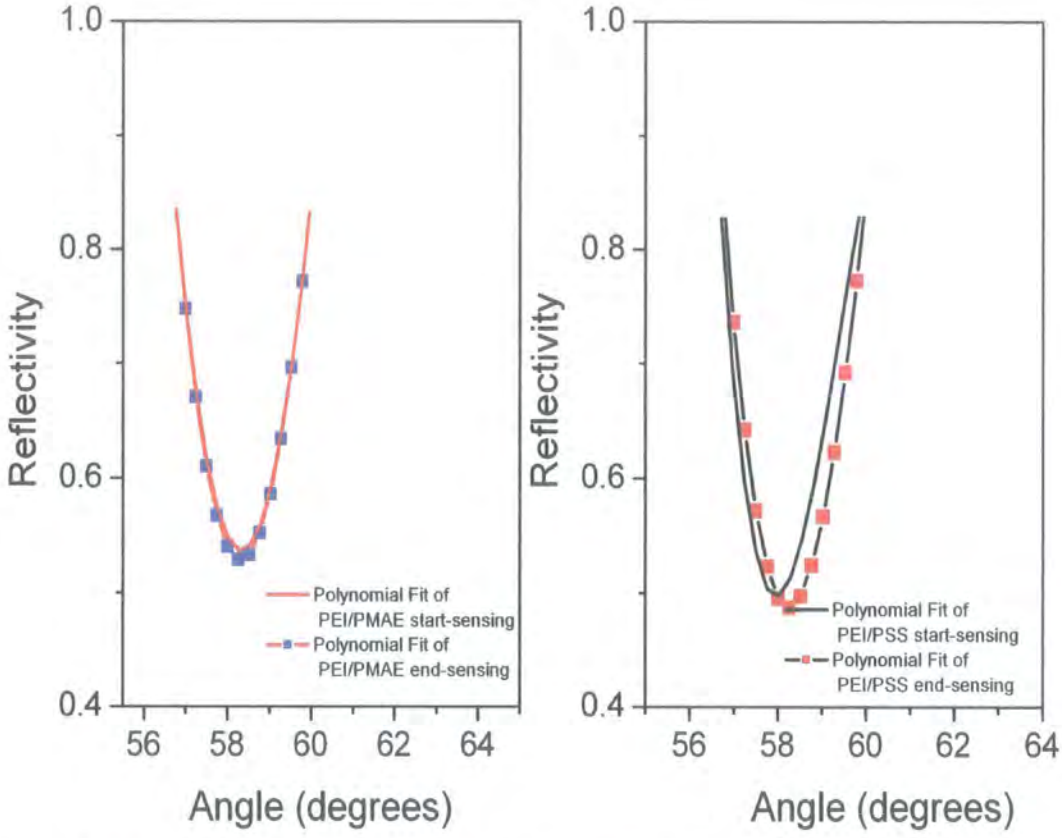

Figure 8.17 Polynomial fit for the SPR profiles of the two channels PEI/PMAE and PEI/PSS before and after the conclusion of the sensing experiments in Fig. 7.18 and Fig. 7.19.

In conclusion, this series of experiments have produced some reassuring data on the ability of "aged" LbL multilayer films to be responsive to metal cations even after a relatively long storage time.

8.4 Conclusions

Different designs of multichannel sensing chips have been fabricated. An arrangement of gold stripes has been prepared on a SF10 glass slide. Two LbL organic films (PEI/PSS and PEI/PMAE) were deposited and their SPR profiles have been identified. This result proved that it is possible for the SPR system to read different sensing channels at the same time. An improved version consisted of an arrangement of two large gold patterns covering a large portion of the area investigated and separated by a central uncoated glass stripe. Solutions containing metal ions at various molar concentrations were tested. Polyelectrolyte films, deposited by the layer-by-layer self-assembly technique, were used as the sensing layers (PEI/PSS and PEI/PMAE). The

two channels exhibited independent sensing responses to a range of metal ions. The results augur well for the development of commercial multichannel, single chip SPR sensors. Further work will focus on improvements to the sensitivity of the device and on a full understanding of the sensing dynamics. Moreover, systematic studies of the influence of the films thickness on the sensing behaviour, together with investigation of more LbL multilayer systems will be necessary. Alternative sensor data analysis techniques might improve the reliability and resolution of the overall sensing system.

References

1. Palumbo, M., Pearson, C., Nagel, J., and Petty, M.C., A single chip multi-channel surface plasmon resonance imaging system. Sensors and Actuators B: Chemical, 2003. 90(1-3): p. 264-270.

2. Palumbo, M., Pearson, C., Nagel, J., and Petty, M.C., Surface plasmon resonance sensing of liquids using polyelectrolyte thin films. Sensors and Actuators B: Chemical, 2003. 91(1-3): p. 291-297.

3. Homola, J., Yee, S.S., and Myszka, D., Surface plasmon resonance biosensors, in *Optical biosensors*, F.S. Ligler and C.A.R. Taitt, Editors. 2002, Elsevier.

4. Homola, J., Present and future of surface plasmon resonance biosensors. Analytical and Bioanalytical Chemistry, 2003. 377(3): p. 528-539.

5. Pearson, C., Nagel, J., and Petty, M.C., Metal ion sensing using ultrathin organic films prepared by the layer-by-layer adsorption technique. J. Phys. D: Appl. Phys, 2001. 34: p. 285-291.

6. Johansen, K., Stalberg, R., Lundstrom, I., and Liedberg, B., Surface plasmon resonance: instrumental resolution using photo diode arrays. Measurement Science & Technology, 2000. 11(11): p. 1630-1638.

7. Nenninger, G.G., Piliarik, M., and Homola, J., Data analysis for optical sensors based on spectroscopy of surface plasmons. Measurement Science & Technology, 2002. 13(12): p. 2038-2046.

8. Richens, D.T., *The Chemistry of Aqua Ions*. 2000, Chichester: John Wiley &Sons Ltd.

9. Congreve, A., Kataky, R., Knell, M., Parker, D., Puschmann, H., Senanayake, K., and Wylie, L., Examination of cobalt, nickel, copper and zinc(II) complex geometry and binding affinity in aqueous media using simple pyridylsulfonamide ligands. New Journal of Chemistry, 2003. 27(1): p. 98-106.

Chapter 9

Conclusions and suggestions for further work

9.1 Conclusions

Organic films were assembled following the layer-by-layer (LbL) method. Polyelectrolytes, i.e. polymers baring electrostatic charged groups along their chains, were used as components of the thin films. In particular, poly(ethylene imine), PEI, poly(ethylene-co-maleic acid), PMAE, and poly(styrene sulfonate), PSS, constituted the molecular bricks of the LbL architectures. In this work, an attempt was made to use polyelectrolyte multilayers as sensors and to investigate the possibility of using them within a multichannel system [1, 2]. A novel opto-chemical sensing device exploiting the surface plasmon principle was developed [3]. A multichannel approach, using a specially designed sensing chip, was demonstrated to be a practical route for the detection of metal ions in solution [2, 4]. Atomic force microscopy was used to elucidate the morphology of the organic films. Polyelectrolytes with different charge densities were shown to form dissimilar structures. This is believed to have an influence on the sensing performance of the LbL architectures [5].

The phases of design and realization of the multichannel SPR system have been described in Chapter 5. The device is able to interrogate and analyze data from a multi-channel single chip, i.e. a platform with several active materials. Alternative optical set-ups were tested and the final choice provided a SPR platform with no moving parts, exploiting a focused beam across a range of angles. Different light sources were investigated and the final choice resulted in the adoption of a commercial light emitting diode, a Toshiba TLRH190P. A CCD camera was used as the detector. A lens system allows the CCD camera to read several plasmon waves generated on the sensor surface. An in-house acquisition/processing programme has been specifically developed for the SPR system [6]. Fitting of the experimental data to theoretical curves is possible, although elements of uncertainty exist because the SPR technique does not allow an independent determination of the film thickness and optical constants. A calibration test using sucrose solutions showed a sensitivity of 4.3×10^{-4} refractive index units per pixel line-pair. The exact ratio pixel/angle was established from studies of the angular position of the critical angle as a function of the different dielectrics in contact with the metal surface. Therefore, it was possible to correlate the SPR reflectivity to the angular position.

In recent years, atomic force microscopy investigations of the outer surface of LbL self-assembled organic films have enhanced the level of understanding of their structure and behaviour [7, 8]. As described in Chapter 6, the *zone* model distinguishes, within the LbL film, three separated parts with specific characteristics and features according their distance from the solid interface. In this way, a description of the multilayer formation is possible. The *island* model is concerned with the adsorption of the first polymeric chains onto the solid template. Charged macromolecules tend to adsorb on selected defect sites of the solid support and form islands composed of polymer coils. On increasing the number of deposition steps, these islands coalesce until they achieve a full coverage of the surface. The LbL architectures investigated were composed of three PEI/PMAE bilayers or three PEI/PSS bilayers. Limited adsorption of the first polymer layers was discovered. Areas where the process is complete coexist with those where very few of the polyions have been successfully adsorbed. This behaviour of limited adsorption is, for the polymer architectures under study, independent on the electrostatic nature of the polyelectrolytes used. However, the charge density does have a role in determining the morphology of the multilayer outer surface. (PEI/PSS)x3 films showed a more uniform profile in comparison to (PEI/PMAE)x3 architectures. On the portions of the surface where the adsorption was limited, it was possible to image isolated polyelectrolyte complexes. These polyions appear to be kinetically trapped on the surface according to what is believed to be their conformation in solution. In some cases, it was possible to image a cluster of polymer chains. Examination of the surrounding surface around suggests that the coils were adsorbed on a relatively free part of the film. The stretched conformation of the chain suggests the possibility that they correspond to PSS coils on a PEI substrate.

Samples assembled in-beaker and in a sealed cell at high flow rate (2.5/5 ml min^{-1}) were compared. For the multilayers incorporating PMAE, the effect of the continuous flow was dramatic while the differences were less for those films containing PSS. For the latter architectures, an island-type adsorption was still recognisable by AFM while (PEI/PMAE)x3 self-assemblies were rougher and very irregular. For some experiments a single bilayer PEI/PMAE was self assembled on the AFM cantilever tip surface. AFM images of a three bilayer (PEI/PMAE)x3 film obtained by using this chemically modified tip were obtained. Electrostatic repulsive forces between the charged film outer surface and the LbL coated tip are believed to have had an effect, albeit small, on

the sample imaging. However, more experimental work is necessary to clarify the role of interaction forces between the functional groups present on the two surfaces.

The use of LbL polyelectrolyte multilayers as sensors for metals cations in solution has been described in Chapter 7. The polyelectrolyte-metal interaction and the behaviour of the metals in solution have been discussed. The nature and geometry of the conformation of the hydrated metal ions is believed to have an influence on the sensitivity of the polymeric films. A detection limit down one part per million (copper acetate concentration of 10^{-5} M) for Cu^{2+} ions was found using a two bilayer LbL film with PMAE as the outer surface. Notably, the maximum concentration level of copper in water is fixed at 20.5 x 10^{-6} M according the U.S. federal regulations and 31.5 x 10^{-6} M according the World Health Organization. The system performance for copper detection can be compared with that of some commercial devices exploiting ion selective electrodes or reflectance photometry. By comparing two complementary thin films it has been shown that the outer surface of the LbL architectures is mainly responsible for the ion detection. The first was composed of (in order from the solid support) PEI/PMAE and a cationic modified polyacrylic acid, PMADAMBQ. The second has a further PMAE layer adsorbed on top the PMADAMBQ. The detection of anionic species and pH was also demonstrated. Exact knowledge of the acidity level in liquids and the real-time monitoring of the dynamics of pH changes can be then achieved.

The adsorption characteristics of two alternative polyanions, PMAE and PSS, were compared together with those of the polycation PEI. Reflectivity changes in real-time were used to follow the adsorption steps during the deposition of the multilayer film. For the two negatively charged polymers, PMAE and PSS, it was found that a difference in electric charge density might have a direct influence not only on the outer surface morphology, as discussed in Chapter 6, but also on the film thickness and on the time required by the polymer to complete the adsorption.

In Chapter 8, the feasibility of multichannel detection was illustrated. Using a shadow mask, different arrangements of gold stripes on a SF10 glass slide were prepared. Polyelectrolyte films, deposited by the layer-by-layer self-assembly technique were used as the sensing layers (PEI/PSS and PEI/PMAE). Their distinctive SPR profiles

were clearly identified. This result proved that it is possible for the sensing system to read different sensing channels simultaneously. The most successful of the arrangements consisted of two gold patterns covering a large portion of the area investigated and separated by a central uncoated glass stripe. Solutions containing ions of copper, zinc, sodium, nickel and iron, at molar concentrations of 10^{-4} or $2x10^{-5}$ M were tested. The two channels showed independent sensing responses. The influence of the different possible sensing mechanisms has been discussed in detail. Relatively long storage times appear not to compromise the sensing performance of the materials. However, metal/film interactions seemed to have an effect on the modulating the pH sensitivity of the LbL architectures.

9.2 Suggestions for further work

The research presented in this thesis augurs well for the development of an even more refined multichannel, single-chip SPR sensor that could have commercial applications. Future work might focus on further improvements to the sensitivity and selectivity of the device and on a full understanding of the sensing dynamics.

Two different, but complementary, paths could be followed to improve the sensing system. The first concerns refining the components that "support" the sensing, i.e. light source, optical system, light detector, acquisition and processing systems. Because a sensing device is such a complex assembly of parts, every improvement will result in an improved performance of the overall system. In particular, the noise from the CCD camera (and, in general, the signal-to-noise ratio) needs to be reduced, as this currently limits the sensitivity of the SPR device. The use of a two-dimensional photodiode array should be considered. In addition, it could be worth investigating the use of a light sensor with an improved dynamic range to provide a more accurate reference of the input variation from the light source. At the moment, this is achieved by recording the beam reflected by the uncoated portions of the SF10 glass slide. However, the camera used (COSTAR SI-M350) has proved to be rather sensitive to high luminous power levels and, therefore, poor at distinguishing relative reflected beam intensity variations between 0.9 and 1 (a.u). Improved focusing of the light probe and a reduction of the wavelength range of the LED (via, for example, a suitable filter(s)) could also be important goals because these would reduce the superposition of SPR profiles that

affect the output signal. Finally, the sensing data are currently collected by recording, in real time, the change in reflectivity of a single band on the SPR curve. Therefore, in comparing data from different sets of experiments, it is important to ensure that parts of the curves with consistent slope variation are chosen. To accomplish this is not straightforward, given the arbitrary nature of this choice. Alternative data analysis techniques might improve the reliability and resolution of the overall sensing system. For example, it might be useful to analyze the entire SPR curve rather than just a portion of it [9, 10]. In this way, the information gathered would be more reliable.

On a second front, i.e. the research on the sensor materials, a systematic study of the influence of the films thickness on the sensing behaviour is necessary. Studies focused on the chemical and physical aspects of the interaction with the analytes are essential. In future, it will be necessary to address specifically if and how the interaction with the measurand introduces modifications to the internal organization of the sensing architectures and in the morphology of their outer surfaces. Thus, the duration of the working life of the sensing-chips and their long-term reliability could be examined. Investigation of further LbL multilayer systems is also needed. The specific metal/polymer interaction is essential in defining the sensitivity and selectivity of the sensing device. Further work should be focused on a search for novel materials with very specific selectivities. Multichannel detection (in the sense used in this thesis, i.e. without the use of neural networks) is only really useful if the active surfaces have distinct sensing behaviour, i.e. have a proper selectivity. Of course, neural networks might be used and therefore some concessions on the specific selectivity of each channel might be given. Ideally, it would be preferable to deposit a larger number of active materials on the sensing chip. The LbL and SAM methods offer a good operational flexibility and are the main candidates for such task. However, it is necessary to find alternative techniques to the last layer partial coating method for the patterning of the channels onto the chip surface. The use of flow channels or soft lithography techniques might provide useful ways forward [11, 12].

References

1. Palumbo, M., Pearson, C., Nagel, J., and Petty, M.C., Surface plasmon resonance sensing of liquids using polyelectrolyte thin films. Sensors and Actuators B: Chemical, 2003. 91(1-3): p. 291-297.

2. Palumbo, M. and Petty, M.C. Ultrathin polymer films:application to metal ion sensing. in *ACS New York Meeting, September 7-11*. 2003. New York: PMSE division, ACS.

3. Palumbo, M., Pearson, C., Nagel, J., and Petty, M.C., A single chip multi-channel surface plasmon resonance imaging system. Sensors and Actuators B: Chemical, 2003. 90(1-3): p. 264-270.

4. Palumbo, M., Nagel, J., and Petty, M.C., Surface plasmon resonance detection of metal ions: layer-by-layer assembly of polyelectrolytes sensing layers on a multichannel chip. IEEE Sensors Journal, 2003. submitted 3rd October 2003.

5. Palumbo, M., Pearson, C., and Petty, M.C., Atomic force microscope characterization of poly(ethyleneimine)/poly(ethylene-co-maleic acid) and poly(ethyleneimine)/poly(styrene sulfonate) multilayers. in preparation.

6. Nagel, J., SPR Images. 2001: Institute of Polymer Research Dresden e.V. , Dresden, Germany.

7. Tsukruk, V.V., Bliznyuk, V.N., Visser, D., Campbell, A.L., Bunning, T.J., and Adams, W.W., Electrostatic deposition of polyionic monolayers on charged surfaces. Macromolecules, 1997. 30(21): p. 6615-6625.

8. Picart, C., Lavalle, P., Hubert, P., Cuisinier, F.J.G., Decher, G., Schaaf, P., and Voegel, J.C., Buildup mechanism for poly(L-lysine)/hyaluronic acid films onto a solid surface. Langmuir, 2001. 17(23): p. 7414-7424.

9. Johansen, K., Stalberg, R., Lundstrom, I., and Liedberg, B., Surface plasmon resonance: instrumental resolution using photo diode arrays. Measurement Science & Technology, 2000. 11(11): p. 1630-1638.

10. Nenninger, G.G., Piliarik, M., and Homola, J., Data analysis for optical sensors based on spectroscopy of surface plasmons. Measurement Science & Technology, 2002. 13(12): p. 2038-2046.

11. Sapsford, K., Taitt, C.R., and Ligler, F.S., Planar waveguides for fluorescence biosensors, in *Optical Biosensors: Present and Future*, F.S. Ligler and C.A. Rowe Taitt, Editors. 2002, Elsevier: Amsterdam.

12. Kane, R.S., Stroock, A.D., Jeon, N.L., Ingber, D., and Whitesides, G.M., Soft lithography and microfluidics, in *Optical Biosensors: Present and Future*, F.S. Ligler and C.A. Rowe Taitt, Editors. 2002, Elsevier: Amsterdam.

Appendix

1. Metal complexes and stability constant

A metal complex is formed by association between a metal atom or ion and another species, known as ligand, which is either an anion or a polar molecule. A simple description of the nature of the bond between a ligand and a metal treats the ligand as an electron-pair donor and the metal as an electron-pair acceptor. The donation of a pair of electrons from ligand to metal establishes a coordinate bond. In the terminology of molecular orbitals, orbitals on the ligand and metal of σ-symmetry overlap to give σ-bonding. In some cases, where electrons and orbitals of appropriate symmetry are available in the metal and ligand, π-bonding makes an additional contribution. Where metal d-electrons interact with vacant ligand orbitals to form a π-bond, this represents a transfer of electronic charge from metal to ligand that is in the reverse direction to that resulting from σ-bonding [1].

In the case of ligands such as ammonium chloride, only one pair of electrons is involved in σ-bonding with a metal. This type of ligand is called *unidentate* (literally one-toothed). Many molecules or ions contain more than one donor atom and it may be sterically possible for them to coordinate one metal atom at two or more positions in its coordination shell, behaving in a *multidentate* fashion. For example, ethylene diammine, $NH_2CH_2CH_2NH_2$, *en* contains two donor nitrogens and acts as a bidentate ligand towards many metals, closing them in an heteroatomic ring. This process of ring formation is known as chelation. The word chelate, which describes the ring, is derived from the Greek *chele*, meaning a lobster's claw. Ligands like *en* are referred as chelating agents and the complexes they form as metal chelates.

In aqueous media, each metal ion M^{n+} is hydrated and its reaction with a ligand L involves replacement of water molecules in its coordination shell [2]. In solution, there is always the possibility of competing reactions which can affect the extent of the association of the metal ions with the ligand. For example, since hydrated metal ions behave as acids they can undergo hydrolysis by releasing one or more protons from the coordinated water molecules

$$M(H_20)_x^{n+} \rightleftharpoons M(H_2O)_{x-1}(OH)^{(n-1)+} + H^+(aq) \quad (A.1)$$

$$M(H_2O)_{x-1}(OH)^{(n-1)+} \rightleftharpoons M(H_2O)_{x-2}(OH)^{(n-2)+} + H^+(aq) \quad (A.2)$$

It is clear from equations (A.1) and (A.2) that this effect can be reduced by the addition of acid in solution. Although this may have the desired effect of ensuring that the metal ions are predominantly present as $M(H_20)_x^{n+}$, it may promote competing reactions, namely protonation, which involve the ligand, L

$$L + H_30^+ \rightleftharpoons LH^+ + H_2O \quad (A.3)$$

The amount of free ligand available for the association with the metal ion, and hence the extent to which the complex formation occurs, varies with the pH and the magnitude of the equilibrium constants.

The reaction between metal ions and the ligand is an equilibrium process and so an equilibrium constant may be defined in terms of the relative activities of the various species present, i.e. their effective concentrations [1, 3]. Thus for the reaction between a hydrated metal ion and a unidentate ligand, the equilibrium constant can be expressed as

$$K_1 = \frac{a(ML) \cdot a(H_2O)}{a(M) \cdot a(L)} \quad (A.4)$$

Similarly

$$K_2 = \frac{a(ML_2) \cdot a(H_2O)}{a(ML) \cdot a(L)}. \quad (A.5)$$

For brevity, coordinated water molecules and charges are omitted. If the metal electrostatic charge is n^+, for a complete coordination of the cation, n reactions with unidentate ligands are necessary (or 1 reaction with a n-dentate ligand and so on). For each of these reactions it is possible to define a stepwise equilibrium constant K (as in A.4 and A.5) and an overall $\beta = \prod_1^n K_n$ binding (equilibrium) constant [3].

For reactions in dilute aqueous solution, the activity of water is supposed to be equal to the unity and so, another constant K_1^T can be defined as

$$K_1^T = \frac{K_1}{a(H_2O)} = \frac{a(ML)}{a(M) \cdot a(L)} = \frac{[ML] \cdot \gamma(ML)}{[M][L]\gamma(M) \cdot \gamma(L)} \quad (A.6)$$

where K_1^T is the *thermodynamic stability* (or *formation*) *constant* of the complex ML, square brackets denote concentrations, and $\gamma(m)$, $\gamma(L)$ and $\gamma(ML)$ are the activity coefficients. K_1^T is a true thermodynamic constant and is independent of ionic strength. Another constant, K_1^C, can be defined in terms of concentrations of the species present

$$K_1^C = \frac{[ML]}{[M][L]} \quad (A.7)$$

K_1^C is known as the *concentration stability constant* and its value varies with the ionic strength of the medium. With increasing dilution, the activity coefficient quotient $\gamma(ML)/\gamma(M)\gamma(L)$ approaches unity and so $K_1^C \rightarrow K_1^T$.

2. The chelate effect

For chelation to occur, the ligand must contain at least two donor atoms capable of bonding to the same metal atom. Donor atoms may form part of a basic or acidic functional group. A basic group is one that contains an atom carrying a lone pair of electrons which may interact with a metal ion (or a proton) like: $-NH_2$ (amino), $-NH$ (imino), $-N=$ (tertiary acyclic or heterocyclic nitrogen), $=O$ (carbonyl), $-O-$ (ether, ester), $=OH$ (alcohol), $-S-$ (thioether), $-PR_2$ (substituted phosphine) and $-AsR_2$ (substituted arsine). An acidic group loses a proton and coordinates with a metal atom. These groups include: $-CO_2H$ (carboxylic), $-SO_3H$ (sulphonic), $-PO(OH)_2$ (phosphoric), $-OH$ (enolic or phenolic), $=N-OH$ (oxime) and $-SH$ (thioenolic and thiophenolic).

Another condition for chelation is that the functional group should be so located in the ligand that the formation of a ring including the metal atom is sterically possible. Even when the donor atoms appear to be appropriately situated for chelation, this may be rendered difficult or impossible by the presence of bulky groups substituted elsewhere

in the molecule so that close approach of the ligand to the metal is hindered or prevented altogether. The presence of functional groups and the fulfilment of steric requirements are necessary but not always sufficient conditions for chelation to occur. For example, in aqueous solutions of low pH, competitive protonation of the ligand maybe so extensive that some, if not all, of the donor atoms are unable to coordinate to metal ions [1].

Metal chelates have an extra stability compared with analogous complexes of the same metal which contains no chelate rings. The name *chelate effect* is given to this phenomenon. The origin and the nature of this effect are related to the changes in thermodynamic quantities accompanying complex formation.

The thermodynamic stability constant K_1^T can be expressed in terms of the Gibbs' free energy change ΔG^0, according equation (A.8). R is the gas constant and T the temperature expressed in Kelvin. Moreover, combining the First and Second Laws of Thermodynamics, it is possible to express ΔG^0 through the variation of enthalpy ΔH^0 and entropy ΔS^0.

$$\Delta G^0 = - RT \ln K^T \qquad (A.8)$$

$$\Delta G^0 = \Delta H^0 - T\Delta S^0 \qquad (A.9)$$

According to equation (A.8) a more stable complex is directly related to a more negative value of ΔG^0. From equation (A.9), it is evident that such a change in ΔG^0 can be associated with either a negative ΔH^0 value or a more positive ΔS^0 value, or with a combination of both these change. Comparing the reactions between the same Ni^{2+} hydrated ion in water and two different ligands, the unidentate ammonia, NH_3 and the bidentete, ethylene diammine, *en*, it is found that the constant stability for the latter is almost ten orders greater than for the former (see Fig. A.1) [3]. Thermodynamical considerations through equations (A.8) and (A.9) can help to understand why. In the reaction represented in (r.1) there are the same number (7) of independent species on the left and the right of the reaction, while for (r.2) there is an increase of independent species from the right to left (from 4 to 7) since ethylene diamine, *en* is bidentate and

therefore replace six molecules of water. That means that (r.2) results in a bigger gain in entropy than (r.1). Therefore, the stability constant will be larger for (r.2).

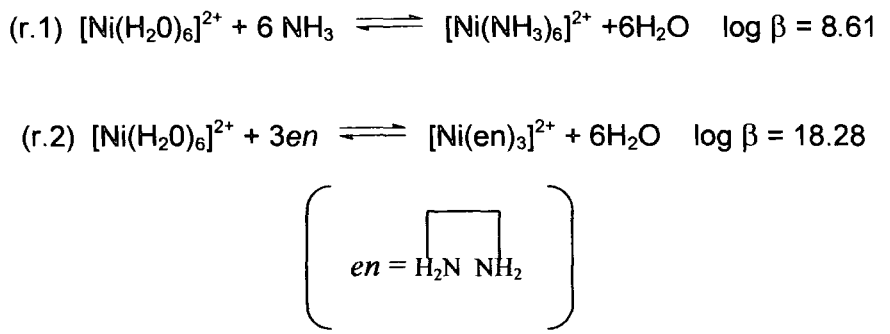

Figure A.1 Chelating ligands bind metals ion strongly.

Enthalpy factors also play a role. The polar amino groups, which are separated in ammonia, are covalently brought together in ethylene diamine overcoming part of their mutual repulsion and making coordination energetically more favourable. Another factor is the increase in basicity (and consequently metal binding ability) of the ethylene diamine amino groups resulting from the inductive effect of the alkyl bridge.

Interestingly, from five membered chelate rings upwards, the chelate effect decreases in magnitude with increasing ring size (four membered rings are unstable due to extreme ring strain). This can be explained by considering the configurational entropy of the chelate chain. The longer the chain, the higher the configurational entropy and so ring formation becomes increasingly improbable.

References

1. Bell, C.F., *Principles and Application of Metal Chelation.* Oxford Chemistry Series, ed. P.W. Atkins, J.S.E. Holker, and A.K. Holliday. 1977, Oxford: Oxford University Press.

2. Richens, D.T., *The Chemistry of Aqua Ions : Synthesis, Structure and Reactivity.* 1997, Chichester: John Wiley &Sons Ltd.

3. Beer, P.D., Gale, P.A., and D.K., S., *Supramolecular Chemistry.* Oxford Chemistry Primers, ed. J. Evans. 1999, Oxford: Oxford University Press.

Publications

1. Petty, M.C., Nagel, J., and **Palumbo, M.**, Surface plasmon resonance sensing of aqueous solutions using polyelectrolyte thin films, in *Encyclopaedia of Sensors*, C.A. Grimes, E.C. Dickey, and M.V. Pishko, Editors, American Scientific Publishers.

2. **Palumbo, M.**, Pearson, C., and Petty, M.C., Atomic force microscope characterization of poly(ethyleneimine)/poly(ethylene-co-maleic acid) and poly(ethyleneimine)/poly(styrene sulfonate) multilayers, Thin Solid Films, accepted for publication.

3. Paul, S., **Palumbo, M.**, Petty, M.C., Cant, N., and Evans, S.D., Deposition of functionalised gold nanoparticles by the layer-by-layer electrostatic technique, in *Quantum Dots, Nanoparticles and Nanowires-Fall 2003 MRS Proceedings*.

4. **Palumbo, M.**, Nagel, J., and Petty, M.C., Surface plasmon resonance detection of metal ions: layer-by-layer assembly of polyelectrolytes sensing layers on a multichannel chip, IEEE Sensors Journal, accepted for publication.

5. **Palumbo, M.** and Petty, M.C. Ultrathin polymer films:application to metal ion sensing. in *ACS New York Meeting, September 7-11*. 2003. New York: PMSE division, ACS.

6. **Palumbo, M.**, Pearson, C., Nagel, J., and Petty, M.C., Surface plasmon resonance sensing of liquids using polyelectrolyte thin films. Sensors and Actuators B: Chemical, 2003. 91(1-3): p. 291-297.

7. **Palumbo, M.**, Pearson, C., Nagel, J., and Petty, M.C., A single chip multi-channel surface plasmon resonance imaging system. Sensors and Actuators B: Chemical, 2003. 90(1-3): p. 264-270.